UNIVERSITY OF SOUTHAMPTON

FACULTY OF PHYSICAL AND APPLIED SCIENCES

Electronics and Computer Science

Design Considerations of Harvested-Energy Management

by

Mustafa Imran Ali

Thesis for the degree of Doctor of Philosophy

May 2012

UNIVERSITY OF SOUTHAMPTON

ABSTRACT

FACULTY OF PHYSICAL AND APPLIED SCIENCES
Electronics and Computer Science

Doctor of Philosophy

DESIGN CONSIDERATIONS OF HARVESTED-ENERGY MANAGEMENT

by Mustafa Imran Ali

Using energy harvesting for powering autonomous sensor systems can meet the goal of perpetual operation. However, the uncertainty in system supply coupled with the size constraints presents challenges in design of such systems. To address these challenges, this thesis is concerned with effective management of harvested-energy for matching supply and demand in order to operate perpetually with uniform performance. The thesis focuses on two fundamental design considerations in addressing these challenges: (i) managing variability of the energy harvesting source, and (ii) matching the demand with energy supply under the influence of non-ideal characteristics of the harvesting system.

To address the problem of variability of energy source, the thesis focuses on effective prediction of harvested-energy. An effective approach for evaluating the accuracy of solar energy prediction algorithm is proposed and optimised values of prediction algorithm parameters are determined to minimise prediction error. The problem of achieving uniform performance under the supply variability is addressed by proposing a new prediction-based energy management policy. The results of the proposed policy are compared with other recently reported policies and it is shown that the proposed policy achieves up to 41% lower variance in performance and 30% lower dead time of the system, which is important to achieve the goal of perpetual operation.

To address the problem of effective matching of supply and demand, the thesis considers the design of photovoltaic energy harvesting supply and storage subsystem in terms of its component's non-ideal characteristics. The influence of these characteristics on supply and demand is identified using modeling of losses and component interdependencies, and empirically validated using a reference system design. Using the proposed modeling, the performance of recently reported energy management policies is evaluated to show that these are ineffective in achieving the goal of perpetual operation, and optimisations are proposed to address this.

Declaration of Authorship

I, Mustafa Imran Ali , declare that the thesis entitled *Design Considerations of Harvested-Energy Management* and the work presented in the thesis are both my own, and have been generated by me as the result of my own original research. I confirm that:

- this work was done wholly or mainly while in candidature for a research degree at this University;
- where any part of this thesis has previously been submitted for a degree or any other qualification at this University or any other institution, this has been clearly stated;
- where I have consulted the published work of others, this is always clearly attributed;
- where I have quoted from the work of others, the source is always given. With the exception of such quotations, this thesis is entirely my own work;
- I have acknowledged all main sources of help;
- where the thesis is based on work done by myself jointly with others, I have made clear exactly what was done by others and what I have contributed myself;
- parts of this work have been published as: [2]

Signed:.....

Date:.....

Contents

List of Figures

List of Tables

Acknowledgements

Firstly, I would like to thank the School of Electronics and Computer Science at University of Southampton for providing a competitive environment, state-of-the-art research facilities, supporting peers and excellent supervisors, which was conducive to bringing out the best of my abilities.

I would like to extend sincerest gratitude to my supervisor, mentor and coach, Professor Bashir Al-Hashimi. This work would not have been possible without his vision, guidance and encouragement. I sought to learn how to conduct research and present it, but working with him I have ended up learning many more life-long skills. I would like to thank my second supervisor, Dr. Geoff Merrett, and my internal examiners, Dr. Kirk Martinez and Dr. Tom Kazmierski, for their invaluable advise.

This work has directly and indirectly benefitted from insightful discussions, helpful advise and guidance from numerous colleagues and friends to whom I would like to greatly acknowledge. To Amit Acharrya, Saqib Khursheed, Sheng Yang, Evangelos Mazomenos, Rishad Shafik, Shida Zhong, Jatin Mistry, Urban Ingelsson, Anton Kulakov, and Hamed Shahidipour, thank you very much for the helpful discussions and friendly advise. I would like to extend special thanks to Dirk De Jager for his generous help in implementation of validation system by providing code libraries and sharing his technical expertise, and to Alex Weddell for numerous insightful discussions, sharing his technical experience, and providing code and data.

This research has benefitted from generous contributions of fellow researchers. I would like to thank Christopher Vigorito (University of Massachusetts, Amherst), Jaein Jeong (UC Berkeley), and Christian Renner (TU Harburg) for generously sharing simulation code, and Jay Taneja (UC Berkeley) for providing Hydro Watch board design details.

Last but not at all the least, I would like to thank my family: my caring wife Ummehani and lovely daughter Rashida for their love, patience, sacrifices and support, to whom I lovingly dedicate this thesis, and my parents who imbued in me the drive to undertake everything I have accomplished.

To my wife Ummehani and daughter Rashida...

List of Abbreviations

AC	Alternating Current
ADC	Analog-to-Digital Converter
A/D	Analog-to-Digital
CC	Constant Current
CV	Constant Voltage
DC	Direct Current
EWMA	Exponentially Weighted Moving Average
I-V	Current-Voltage
LQ	Linear Quadratic
MAPE	Mean Absolute Percentage Error
MCU	Microcontroller Unit
MPPT	Maximum Power POint Tracking
NiMH	Nickel Metal Hydride
NREL	National Renewable Energy Laboratory
NWTC	National Wind Technology Center
PF	Progressive Filling
PV	Photovoltaic
SoC	State-of-Charge
STC	Standard Test Conditions
WCMA	Weather Conditioned Moving Average

Chapter 1

Introduction

Energy harvesting is defined as the conversion of some form of environmental energy into electrical energy. Using energy harvesting to power devices such as autonomous wireless sensors is highly desirable since these devices are deployed in places where use of wires for communication or power supply is very costly or even unfeasible. In many cases these devices also need to have very small physical dimensions to be conveniently deployed at targeted locations or even carried around [70]. The contemporary choice of power source for wireless devices are some type of batteries [7]. Since battery replacement is undesirable due to its cost or even inaccessibility to deployed systems [70], low-power design [66] and energy conservation techniques [7] are employed in order to maximise operating lifetime. Even though the power consumption of electronic devices has been steadily minimised using various techniques over the past years [66], the advancements in battery technology have not kept pace, thus becoming the major bottleneck in realisation of long-life wireless sensing applications [70]. Therefore, being able to operate perpetually without a tethered source of power can greatly increase the utility of wireless sensing devices.

Energy harvesting [40] is a promising approach to realising the goal of near perpetual operation [62] if there is the possibility to harvest energy from the deployment environment. The design of optimised energy harvesting powered systems can be simple if a certain power availability is guaranteed from the harvesting source at all times [65]. In this case, the design will mostly involve optimising the harvester (supply) to deliver the required power depending on the consumption demands of the device. However, this is not the common scenario since most energy harvesting sources or environments are dynamic, supplying variable amounts of stimuli with time [133]. This variability of energy harvesting source leads to design challenges and optimisation opportunities that are different than those of battery powered systems design. For example, the selection/design of the harvester needs be optimised based on the expected environmental energy supply and the average demand of the application workload [146, 59], but due to the variability of energy harvesting source this is not sufficient to ensure perpetual

operation. The energy storage capacity also needs to be selected appropriately to allow a certain amount of energy to be buffered for times of energy unavailability [59, 10]. In addition to optimising the harvesting supply subsystem for a given application demand, the variability of the energy source makes the case for adapting the application energy consumption to maximise the consumption of harvested energy while preventing the system from being completely shut down [65, 154, 102, 103, 39]. This can be achieved by using harvesting-aware (adaptive) energy management that determines the energy consumption budgets of the application according to the available energy and harvesting capability. Investigating the design considerations of harvested-energy management is the topic of this thesis.

This chapter introduces the preliminary concepts needed for understanding the contributions of this thesis and presents its aims and objectives. The chapter is organised as follows. Section 1.1 introduces energy management in the context of the energy harvesting system design to motivate the aims and objectives of this thesis. Sections 1.2-1.4 discuss the individual parts of the energy harvesting system and related works while Section 1.5 focuses on harvested-energy management and its state-of-the-art. Section 1.6 presents the aims and objectives of this thesis, Section 1.7 outlines its chapters and Section 1.8 presents the contributions.

1.1 Energy Harvesting System Design with Energy Management

This section outlines the structure of an energy harvesting system, and discusses the fundamental problems in the design of such systems. It explains the general objectives of harvested-energy management, its position in context of the complete system and interdependencies with other system components. This section serves as a road map for rest of this chapter and sets the stage for discussing the aims and objectives of this thesis in Section 1.6.

Figure 1.1 depicts the organisation of an energy harvesting system as conceived in this thesis. It consists of an energy source within a deployment environment, and an energy harvesting supply and storage subsystem for capturing and delivering environmental energy to a wireless sensor device. The wireless sensor device implements an application workload which is the consumer of harvested-energy, as well as harvested-energy management to determine the energy budgets for application workload based on the monitored energy resources. The overall design objective is to match the average power supply rate with the average power demand of the application workload to achieve long-term perpetual system operation. The main challenges in achieving this goal is the variability of energy harvesting source and practical constraints on the power output of the energy harvesting supply and storage subsystem. To address the objective of

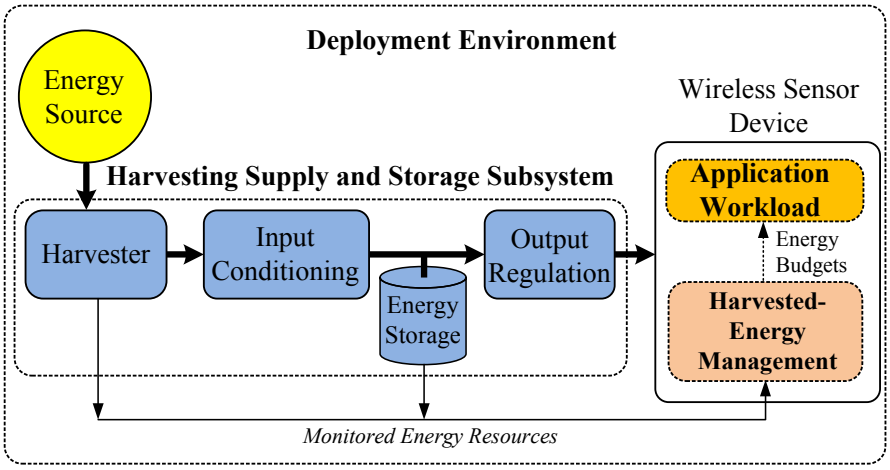

Figure 1.1: Organisation of a typical energy harvesting powered system with harvested-energy management as conceived in this thesis.

matching the supply and demand under the variability of the energy harvesting source, two aspects of system design need to be considered:

1. The energy harvesting supply and storage subsystem needs to be engineered to deliver a certain supply (depending on the environmental energy available).
2. According to this available supply, harvested-energy management needs to determine the energy budgets for the application workload.

Based on these two aspects, Figure 1.2 identifies the problem specification and the system design space of energy harvesting systems. The problem specification includes selection of the type of energy harvester depending on the deployment environment and the given application workload energy demand. The system design space includes the design of harvesting supply and storage subsystem and harvested-energy management. A harvesting supply and storage subsystem is needed to extract useful power output from the harvester. Its design involves selection of energy harvester output power and capacity of energy storage, which determines the average power delivery to the load. Furthermore, the operating voltage/current range of the harvester, the energy storage and the application workload may not be compatible, therefore requiring the addition of appropriate input and output power conditioning circuitry (Figure 1.1). The energy losses between these components due to the non-ideal characteristics of system components also have to be taken into account since they reduce the net energy available. The two main considerations are supply efficiency and capacity. Chapter 2 discusses in detail the design of harvesting supply and storage subsystem.

Given the harvesting supply and storage subsystem design, harvested-energy management (Figure 1.2) determines the allocation of harvested-energy to the application workload to ensure maximum utilisation of harvested-energy while not exceeding the supply

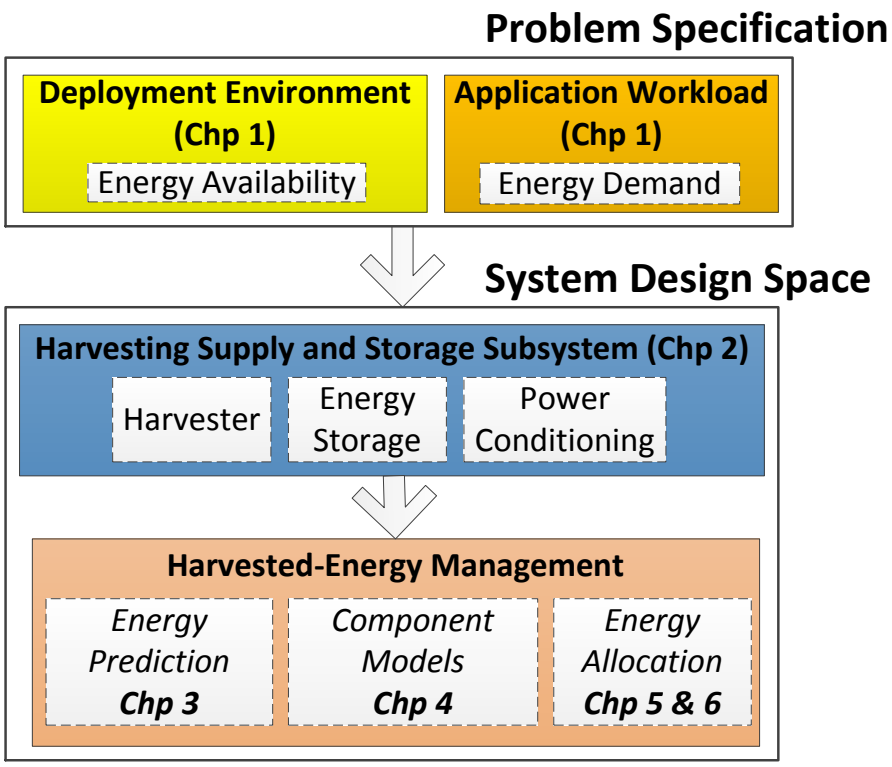

Figure 1.2: Problem specification and design space of energy harvesting systems.

and storage capability. To meet this goal effectively, harvested-energy management has to account for the characteristics of the energy source, the power delivery and storage subsystem and the application workload. Knowledge of energy source variations is needed to determine the amounts of energy to be consumed during different time intervals, with the overall goal of maximising its utilisation. Chapter 3 discusses prediction of harvested-energy to enable the determination of energy consumption budgets. Awareness of losses of and non-ideal characteristics of harvesting system components is needed to achieve the desired match between supply and demand. Chapter 4 discusses system modeling that allows harvested-energy management to take into account these characteristics of harvesting supply and storage subsystem. Using the knowledge of supply thus determined, the energy budget allocation is performed by using an algorithm or policy that aims to achieve the general objectives of energy management while accounting for any application-specific constraints. Chapters 5 and 6 discuss the energy management policies and their effective realisation. Figure 1.3 indicates the factors influencing the design of the harvested-energy management.

The next sections of this chapter discuss the different parts of an energy harvesting system (Figure 1.1). First the characteristics of wireless sensor applications to be powered by energy harvesting are discussed in Section 1.2. Section 1.3 discusses the main types of energy harvesters and their range of power outputs. Section 1.4 discusses the energy harvesting supply and storage subsystem designs and Section 1.5 surveys the state-of-the-art in harvested-energy management. The identification of choices that define the

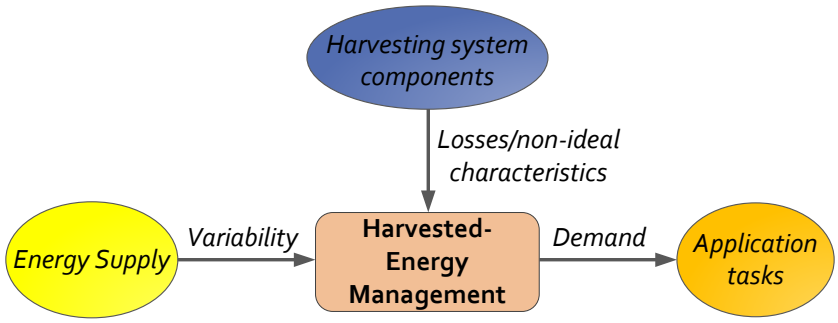

Figure 1.3: Factors influencing the implementation of harvested-energy management.

scope of this thesis is also discussed where applicable.

1.2 Energy Harvesting Powered Applications

This section describes the typical devices and their applications that need to be powered using energy harvesting. This thesis focuses on maximising performance and operating times of very low-power wireless sensor devices using energy management. The usage of these devices demands autonomy from tethered means of communication and power supply. Using wireless communications allows freedom from communication wires and the next evolutionary step is the ability to operate perpetually without the constraint of tethered power supply. The contemporary solution is to rely on either primary or rechargeable batteries, however, the need to replace or recharge batteries limits the usability and/or wider applications of these systems by varying degrees [125]. Note that the qualification of the term 'very low-power' is not absolute since decreasing manufacturing cost, increasing miniaturisation and computing power has helped to create a range of low-power devices with varying hardware complexity, power consumption and applications. The contemporary variety of wireless devices range from smartphones with a typical power consumption close to 1 Watt in active mode to roughly 100 mW in idle mode [18], to wireless sensor nodes (also called motes [34]) having an active mode consumption of tens of mW and idle mode consumption of few μW [120] or even nW [8]. Limited battery capacity is a bottleneck for all wireless computing, however, the limited lifetime problem is nowhere near as severe as in case of remote and wireless sensing applications where replenishing batteries is inherently unfeasible due to the large number of deployed nodes and difficulty of access after deployment [70]. In the case of personal mobile devices, recharging of a battery by the user is not a major issue since there is usually a single device to maintain, whereas in the case of wireless sensor networks there can be many devices. Furthermore, even a single battery replacement can be prohibitive depending upon deployment, e.g., at an oil rig [70].

A more focused definition of the low-power systems of interest in this thesis is: those applications for which replacement of depleted batteries or manual recharging is infeasible, and their supply requirements can be fulfilled (to a practical extent) by state-of-the-art small scale energy harvesters. The contemporary devices that fall under this category can be classified as wireless sensors. This section discusses examples of typical wireless sensor applications under consideration, their system components and power consumption. A brief survey of approaches used to maximise operation lifetime specific to these applications is also presented, followed by a discussion of design considerations from the perspective of harvested-energy management.

1.2.1 Wireless Sensor Network Applications

This section briefly reviews applications of wireless sensor systems that are required to operate for very long periods (many months) from the available energy source. Wireless sensors are perceived as an enabling technology for pervasive or ubiquitous computing [160]. The potential of wireless networked sensors to permit interaction with the physical world has opened up a vast number of applications. Contemporary wireless sensors have been deployed in a variety of applications that include military, industrial, agriculture, environmental monitoring, structural health monitoring, and smart buildings [162]. The general functionality of these applications involves collection of data samples of some physical phenomenon, pre-processing the collected data and transmitting it to a base station. Other applications include event detection and tracking movement of mobile entities. A number of detailed surveys [16, 5] have been published that cover these applications and classify them according to their key attributes [132]. A few examples of these applications (Figure 1.4) are mentioned in this section to motivate the energy management considerations discussed later. Wireless sensors used for observing the breeding season of birds lasting seven months by measuring the humidity, pressure, temperature, and ambient light level of the burrows is described by Mainwaring et al. [87]. Juang et al. [64] attached sensor nodes to the bodies of Zebras for sampling of physical location and movement. Morais et al. [100] describe a network of sensors that are powered by combination of solar, wind and water flow, for monitoring the conditions that influence growth of crops, e.g., temperature, soil moisture, light and humidity. Simon et al. [142] implemented a system of locating the position of snipers by measuring the time of arrival of muzzle blast and its shockwaves using acoustic sensors. Wireless sensors deployed at different positions on a bridge were used to monitor its structural health using time-synchronised high frequency sampling of accelerometer signals [68], while Dondi et al. [31] describe a solar energy harvesting custom designed sensor node for active ultrasonic structural health monitoring. A network of solar energy harvesting sensors were deployed to monitor the microclimate of a watershed [146].

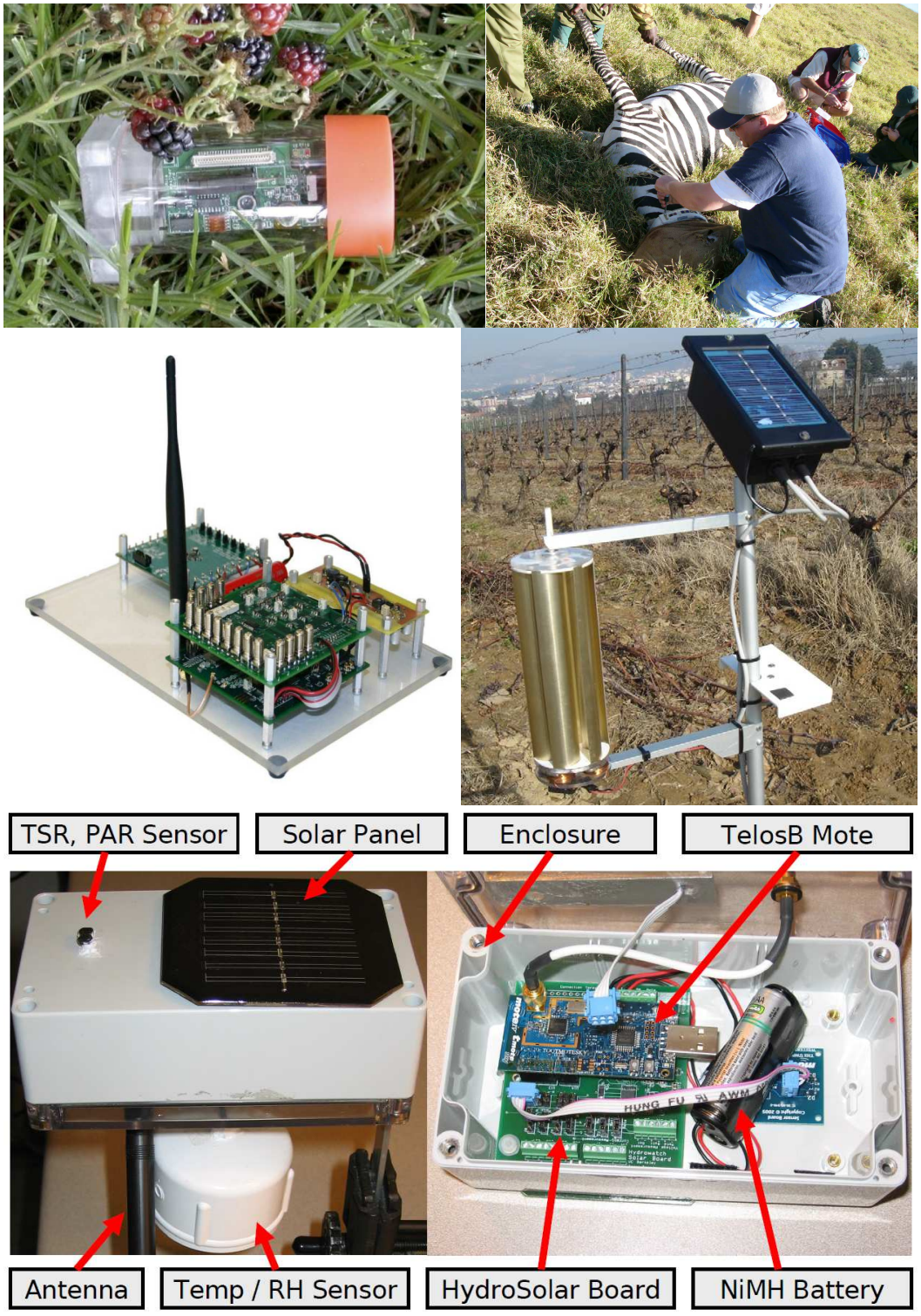

Figure 1.4: A few examples of wireless sensor applications (reproduced from cited sources): (top left) wireless sensors used to observe the breeding season of birds [87], (top right) sensor nodes attached to the body of animals for monitoring movement [64], (middle left) solar harvesting active ultrasonic structural health monitoring node [31], (middle right) precision agriculture using sensors powered by a combination of solar, wind and water flow [100], and (bottom) HydroWatch node for monitoring microclimate of watershed [146].

In the various application examples considered in this section, for increasing the fidelity of data collection or event-detection/target-tracking accuracy, a corresponding increase in the frequency of sampling the sensor(s), data processing and communication activity is required. In this thesis this is called the application workload, which determines the energy consumption of the overall system. One of the common requirements among these applications is the demand for long operating lifetimes while satisfying some application workload requirements. The difficulty in achieving this requirement using batteries alone is widely acknowledged as a critical barrier that limits the realisation of more ambitious applications. The next section discusses the system components and power consumption of typical wireless sensor systems.

1.2.2 System Components and Power Consumption

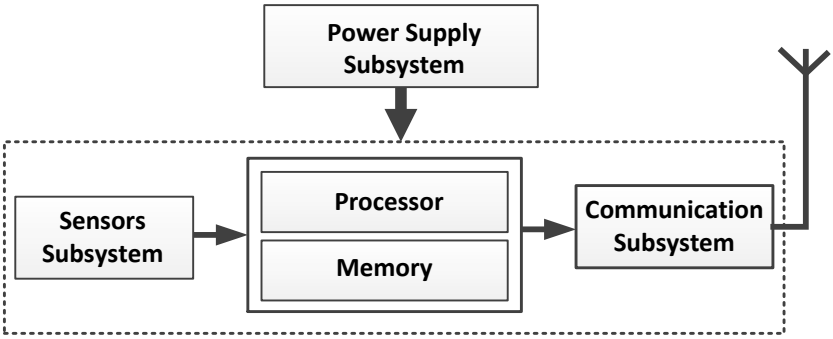

Figure 1.5: A generic structure of wireless sensing nodes.

The present generation of wireless sensor nodes (called motes) has been inspired by research efforts started a decade ago such as Networked Embedded Systems Technology (NEST), Smart Dust and Wireless Integrated Networked Sensors (WINS) [121, 132, 34]. A variety of mote systems/platforms have been proposed in the last decade both academically and commercially [43, 34]. A wireless sensor node can be generalized as being composed of sensing, computing and memory, and communication subsystems (Fig. 1.5). A widely used mote called the Telos developed by UC Berkeley and later commercialised [120] is shown in Fig. 1.6. The labels indicate the common components of the system. The power can be supplied via a USB interface when connected to a host PC or via expansion headers from a battery (regulated or unregulated) or an energy harvesting supply. The power supply subsystem may also provide facilities for querying the state of energy of the node to implement energy aware algorithms and communication protocols as discussed in the next section.

Table 1.1 [34] gives a comparison of low-power processors used in wireless sensors and their active and deep sleep mode current draw (at 3V and 1MHz). The release year provides a sense of the underlying technology trends. Similarly, Table 1.2 [34] gives a list of radio modules and their receive and transmit mode power consumptions. Table

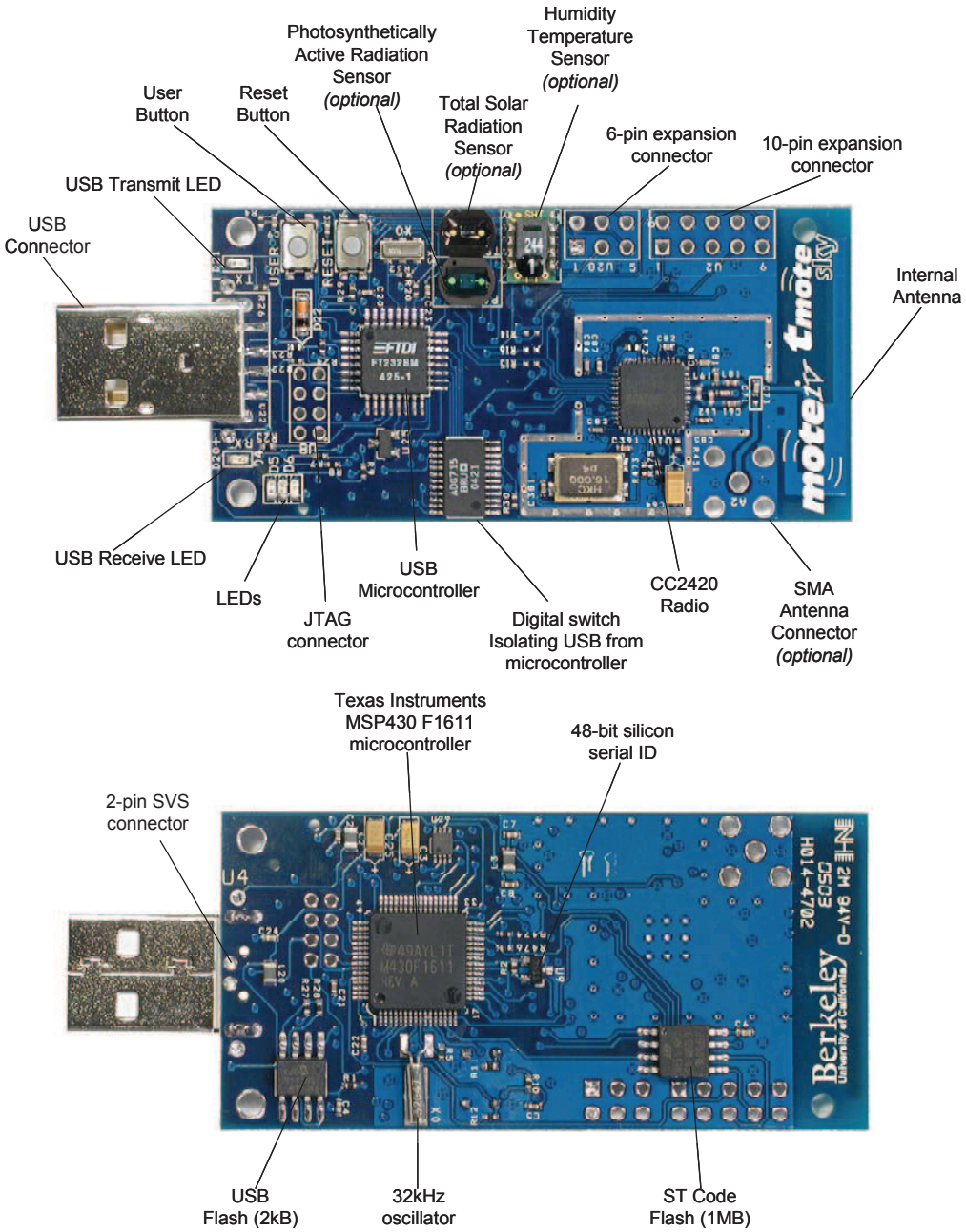

Figure 1.6: A commercial Tmote Sky wireless sensor node with labels indicating typical components (reproduced from [27]).

1.3 lists the power consumption of typical activities and modes of three commonly used wireless sensor platforms [120]. It may be noted that wireless transmission and reception have the highest power draw among the other activities, while the sleep mode power consumption is three orders of magnitude smaller. For this reason, the most common energy conservation technique in wireless sensing applications is duty cycling between active and sleep modes by shutting down the radio and MCU during periods of inactivity. Figure 1.7 (top) shows the typical long-term current draw profile of a duty-cycled system [61], which is dominantly a flat profile during sleep mode and spikes of high current draw

Table 1.1: Comparison of power consumption of microcontrollers used in wireless sensor platforms (adapted from [34]).

Mfg	**Device**	**Year**	**Arch**	**VCC** (V)	**Active** (mA)	**Sleep** (μA)
Atmel	ATmega128L	2002	RISC/8	2.7-5.5	0.95	5
	ATmega1281	2005	RISC/8	1.8-5.5	0.9	1
	ATmega2561	2005	RISC/8	1.8-5.5	0.9	1
Ember	EM250	2006	XAP2b/16	2.1-3.6	8.5	1.5
Freescale	HC05	1988	8-bit	3.0-5.5	1	1
	HC08	1993	8-bit	4.5-5.5	1	20
	HCS08	2003	8-bit	2.7-5.5	7.4	1
	MC13213	2007	HCS08	2.0-3.4	6.5	35
Jennic	JN5121	2005	RISC/32	2.2-3.6	4.2	5
	JN5139	2007	RISC/32	2.2-3.6	3	3.3
TI	MSP430F149	2000	RISC/16	1.8-3.6	0.42	1.6
	MSP430F1611	2004	RISC/16	1.8-3.6	0.5	2.6
	MSP430F2618	2007	RISC/16	1.8-3.6	0.5	1.1
	MSP430F5437	2008	RISC/16	1.8-3.6	0.28	1.7
	CC2430	2007	8051	2.0-3.6	5.1	0.5
ZiLOG	eZ80F91	2004	ez80/16	3.0-3.6	50	50

Table 1.2: Comparison of power consumption of IEEE 802.15.4-compatible radios used in wireless sensor systems (adapted from [34]).

Mfg	**Device**	**Year**	**VCC** (V)	**Rx** (mA)	**Tx** (mA)	**Sleep** (μA)
Atmel	RF230	2006	1.8-3.6	15.5	16.5	0.02
Ember	EM260	2006	2.1-3.6	28	28	1
Freescale	MC13192	2004	2.0-3.4	37	30	1
	MC13202	2007	2.0-3.4	37	30	1
	MC13212	2005	2.0-3.4	37	30	1
Jennic	JN5121	2005	2.2-3.6	38	28	<5.0
	JN5139	2007	2.2-3.6	37	37	2.8
TI	CC2420	2003	2.1-3.6	18.8	17.4	1
	CC2430	2005	2.0-3.6	17.2	17.4	0.5
	CC2520	2008	1.8-3.8	18.5	25.8	0.03

during active mode. A magnified view of current draw during the active mode (Figure 1.7 bottom) shows the varying current drawn during the different activities such as switching to active mode, sampling the sensor, turning the radio on, transmitting and receiving, and finally switching to idle mode. The next section discusses the various energy conservation techniques for wireless sensing applications.

Table 1.3: Measured current consumption of Telos mote compared to MicaZ and Mica2 motes (reproduced from [120]).

Operation	**Telos**	**Mica2**	**MicaZ**
Minimum Voltage	1.8V	2.7V	2.7V
Mote Standby (RTC on)	5.1 μA	19.0 μA	27.0 μA
MCU Idle (DCO on)	54.5 μA	3.2 mA	3.2 mA
MCU Active	1.8 mA	8.0 mA	8.0 mA
MCU + Radio RX	21.8 mA	15.1 mA	23.3 mA
MCU + Radio TX (0dBm)	19.5 mA	25.4 mA	21.0 mA
MCU + Flash Read	4.1 mA	9.4 mA	9.4 mA
MCU + Flash Write	15.1 mA	21.6 mA	21.6 mA
MCU Wakeup	6 μs	180 μs	180 μs
Radio Wakeup	580 μs	1800 μs	860 μs

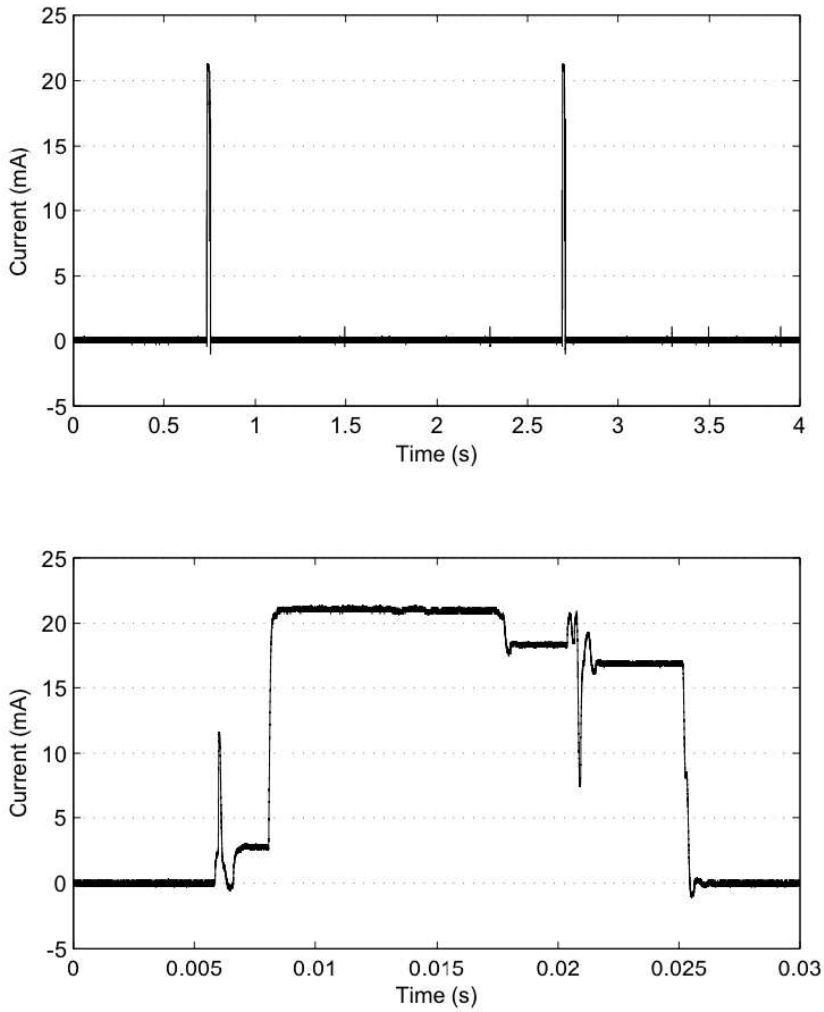

Figure 1.7: A typical current profile of wireless sensor systems: (top) long periods of sleep punctuated by short, periodic bursts of high-current activity, (bottom) detailed view of current drawn during active period (reproduced from [61]). Note that the time-scales shown are relative to start of each measurement.

1.2.3 Energy Conservation Techniques

Until recently, the choice of power source for wireless sensor systems have been small light weight batteries. The advancements in battery technologies have not been able to keep pace with demands of providing increased operating lifetimes under the constraints of small weight and volume. This section reviews techniques proposed to prolong the operating lifetime of wireless sensor systems under constraints of a finite supply of battery energy. When using energy harvesting, these techniques can be adapted to work in a harvesting-aware mode.

The state-of-the-art low-power systems rely on a combination of techniques to maximize their lifetime within a given battery energy budget. These include reducing power consumption of digital and analogue components by using low voltage for analog and voltage/frequency scaling (DVFS) for digital circuits, shutting down unused blocks with power gating [66, 110], and clock gating for digital circuits. On top of these techniques lie the operating system, application and network level power management approaches. Low-power processors optimised for wireless sensors have been proposed in [44, 138]. Techniques to minimise energy consumption of sensor and communication subsystems are discussed in [3, 75, 73, 161], which also include a number of strategies at the application and network level. These approaches to energy conservation attempt to maximise the time spent in deep-sleep mode of the processor and radio, while intelligently deciding how to best allocate the active time to achieve the application goals. This is generally termed as duty cycling. Furthermore, to conserve energy during active periods, the focus is on minimizing the need for communication since it consumes the bulk of energy (Table 1.2) compared to computations. A comprehensive survey of approaches to minimize communications is presented in [7]. The following summarises the major approaches [7] for optimizing the communications duty cycle:

Network Topology Control [135]: By exploiting node redundancy, which is typical in sensor networks, and adaptively selecting only a minimum subset of nodes to remain active for maintaining connectivity. Nodes that are not currently needed for ensuring connectivity can go to sleep and save energy. Finding the optimal subset of nodes that guarantee connectivity is referred to as topology control. Therefore, the basic idea behind topology control is to exploit the network redundancy to prolong the network longevity.

System Sleep/Wakeup Protocols [67]: These strategies decide at what time the nodes should wake-up for relaying messages so that they need to remain active for minimum durations.

MAC Protocols with Low Duty Cycle [30]: These protocols try to minimize the energy wasted due to collisions in the network while at the same time minimizing the active time of radio subsystem.

Another subset of techniques focus on minimizing the amount of data transmitted or the need to transmit the sensed data by using data compression [89], in-network processing [29] and data prediction [13]. These techniques tradeoff communication at the expense of increased computation by relying on the fact that communication is much more expensive than computation. A class of approaches attempt to minimize the power consumption of sensing by adjusting the sampling frequency or using multiple sensors with different power consumptions according to sensing fidelity needed [4].

1.2.4 Discussion

Wireless sensing applications have inherent characteristics that can take advantage of energy harvesting to achieve near perpetual operation such as the availability of various energy harvesting sources in the deployment environment. Most of the applications discussed in Section 1.2.1 operate in a conservative mode to prolong system life while satisfying the minimum application demands, possibly incorporating some of the energy conservation techniques discussed in Section 1.2.3. Note that the usage model of many of these applications allows for some flexibility in their operation depending on the energy resources available. For instance, the user may prefer the highest possible rate of sampling of data but if this is not possible while achieving the desired operating lifetime, it may be acceptable to use a low sampling and reporting rate as long as the system operation lifetime is maximised. This is an important aspect from the perspective of harvested-energy management because it allows scaling of an application's energy consumption according to the available energy (Section 1.1). Energy conservation and (dynamic or runtime) energy management are not the same, since energy management involves monitoring the energy resources and adjusting system operation accordingly. As an example of how harvested-energy management can benefit, consider the case of watershed microclimate monitoring application [146] powered by solar energy harvesting. The authors note that even after careful engineering of the harvesting supply and storage subsystem according to the average application workload demand, most of the wireless sensor nodes did not meet the lifetime requirement due to the unexpected shortages of harvested-energy in the deployment environment. The main reason quoted was the difference in harvested-energy between the environment used for system design evaluation and the actual deployment environment. However, if some form of harvested-energy management was used, it would have allowed the wireless nodes to adjust their energy consumption to maximise their lifetime.

In [63], the concept of operation priorities is introduced (Figure 1.8) to enable a wireless sensing application to degrade gracefully when faced with an energy shortage. The concept takes advantage of the fact that most practical applications are already designed for a 'best effort' operation because of battery constraints while meeting the minimum acceptable performance. The concept of priority enables a system that is unable to

```
1. Network lifetime of at least one year.
2. Sample all sensors at 1Hz.
3. a. Communicate readings on multihop tree.
   b. Store readings locally.
4. Maximize sampling rate.
```

```
1. Network lifetime of at least 1 month.
2. Sample all sensors every 5 minutes and
   a. Send readings to base station.
   b. Log readings to local storage.
```

Figure 1.8: Operating priorities for system-level energy management. Line numbers indicate priority (Reproduced from [63]).

meet all the goals of the user, due to shortage of energy, to degrade gracefully by at least satisfying the most important goals. This is achieved by using a policy such those shown in Figure 1.8. Consider the first policy shown in Figure 1.8 (top), the line item numbers indicate the priority of a directive and the sub-numbering (e.g., 3.a, 3.b) implies selection between either one of these, with the higher ones having priority, i.e. 'a' before 'b'. According to this policy, the first priority is to guarantee a lifetime of one year, then a minimum sampling rate of 1 Hz, followed by either communicating readings on the network or storing them locally, depending on whether there is enough energy for sending. Finally, if all these directives are achieved and there is more energy, the sampling rate is increased. On the other hand, if the available energy is insufficient to meet all of the directives, the system degrades in the reverse pattern: first, the sampling rate is reduced until it reaches 1 Hz. Then, if the energy is not sufficient to satisfy directives 1, 2, and 3.a, energy management attempts to satisfy 1, 2, and 3.b. and so on.

This concept of energy-driven operation is a natural fit to the variability of most energy harvesting sources as discussed in the next section. The priority-driven policy discussed in this section is an example of fine-grained application-level energy management. In Chapters 5 and 6 of this thesis, generic harvested-energy management policies are discussed that allocate the harvested energy such that the energy consumption can be adaptively controlled to prevent the system from shutting down due to shortages, while maximising the consumption of available energy. It should be noted that if the application workload demand is completely inflexible, energy management cannot benefit in this case. The only way to guarantee the required lifetime under a variable energy supply is to select the harvesting supply and storage subsystem capacities according to the worst-case energy availability.

1.3 Energy Harvesting Sources and Harvester Types

This section describes the different types of energy harvesters. The deployment environment for wireless sensors determines the types of energy sources available for harvesting. Since development of efficient or new harvesters is not the aim of this work, from the perspective of energy management, we are concerned with the following aspects of energy harvesting environments and harvesters:

Harvester Technology Can the harvester provide enough usable energy to fulfill the minimum consumption demand of the application workload? For a given energy availability, this also depends on the physical dimension of the harvester. A variety of transducers have been developed such as photovoltaic, thermoelectric, electromechanical, electroacoustic, electromagnetic etc., but only a limited of these can be used as energy harvesters, generating sufficient power output with practically acceptable physical dimensions for embedded system applications such as wireless sensors. For example, sound energy harvesting is still in a very early stage of development [45] while the current state of radio frequency harvesting requires large size antennae [117], which may not be feasible use with small sized systems.

Harvesting Environment In what manner or pattern is the energy provided by the environment or source? More specifically, is the energy source controllable or uncontrollable, and does the supplied energy follow a predictable, partially-predictable or stochastic pattern? Some combination of these possibilities can obviate the need for any energy management while others can make energy management trivial, such as when the harvested energy can be generated when needed in a fixed pattern. For example, consider the special case in which the energy source is controllable and predictable, such as when the energy is harvested from machinery which generates a certain fixed pattern of vibrations when turned on. In this case, there is no real need for harvested-energy management if the harvested-energy is only needed when the machinery is on or the pattern in which machinery will be turned on is completely predictable. The predictability of supplied energy determines the type of energy management policy that should be used [39, 154].

This section reviews the main harvesting technologies that are commercially available, which include energy harvesting from light, kinetic energy (vibrations and wind), and thermal differences. Design considerations for energy harvesting powered applications such as realistic levels of power that can be derived and the variability of energy source are also referred to. A comprehensive review of harvesting technologies is beyond the scope of this work. A number of reviews of energy harvesting techniques have been published [19, 37, 99, 156, 40], with the most recent survey in [40].

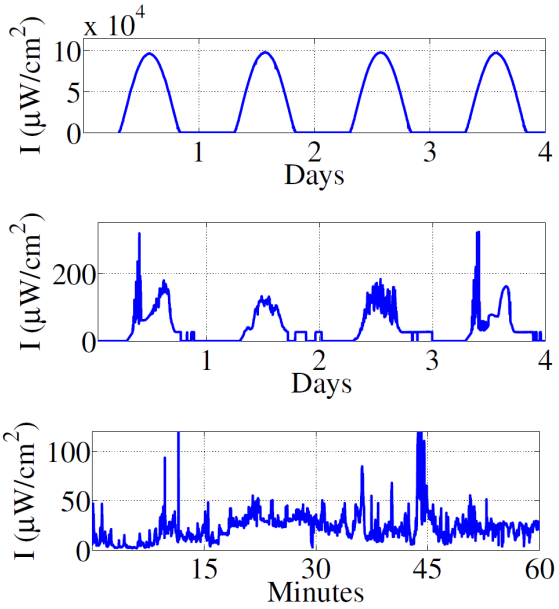

Figure 1.9: Examples of different light energy harvesting environments: (top) an example of predictable solar energy profile of Las Vegas, US, (middle) partially-predictable profile measured on an office window, and (bottom) stochastic behaviour measured from a mobile device at New York, US at nighttime (reproduced from [39]).

1.3.1 Photovoltaic Energy Harvesting

A photovoltaic (PV) cell is fundamentally a semiconductor diode whose p-n junction is exposed to light [155]. Several types of semiconductors, including amorphous, monocrystalline and polycrystalline silicon, are used to commercially manufacture PV cells. The technology behind silicon based PV panels is relatively mature and a number of deployments of autonomous sensors powered by natural (solar) [65, 164, 146] or artificial lighting (or a mix) [39] have been reported.

Light energy is measured in watts per square meter or smaller units derived from this and is termed as irradiance. Another common way of measuring the intensity of light as perceived by the human eye is called Lux. Figure 1.9 [39] show the measured illumination power (irradiance) under different conditions both outdoor and indoors. Note that the difference in light power levels between outdoors (top), indoors (middle) and night time artificial light (bottom) ranges across three orders of magnitude. Furthermore, the pattern of available energy varies from predictable, partially predictable to stochastic.

Figure 1.10 shows an amorphous silicon photovoltaic module with dimensions 97mm x 57mm from Sanyo, along with its measured power curves at various light levels under a 40W tungsten lamp. This cell is optimised for indoor use and at lower light levels it has higher efficiency levels than a cell optimised for outdoor use. It has a peak power of 600μW at 300 Lux and 1.8mW at 1,000 Lux. Figure 1.11 shows a monocrystalline 60mm x 60mm outdoor solar panel and its measured output power at summer mid-day

(a) Sanyo AM1816 amorphous silicon 97mm x 57mm PV panel (reproduced from [26]).

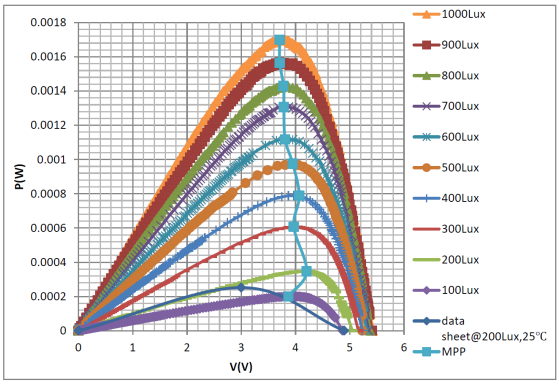

(b) Measured power output versus voltage curves under different light levels of a tungsten lamp.

Figure 1.10: An indoor photovoltaic panel and its measured power under different light levels.

(a) A monocrystalline silicon 60mm x 60mm PV panel (reproduced from [116]).

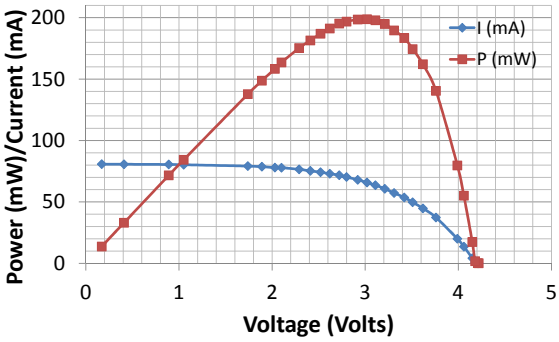

(b) Measured power output versus voltage curve under clear summer mid-day conditions.

Figure 1.11: An outdoor photovoltaic panel and its measured power.

in Southampton. The peak power is 200mW, which is more than 100 times that of the indoor panel of similar size. Photovoltaic cells behave as voltage controlled current sources, and are characterised by their open-circuit voltage (V_{oc}) and short-circuit current (I_{sc}), along with other parameters. As incident light levels drop, short-circuit current decreases, while open-circuit voltage remains fairly constant as shown in Figure 1.10b. Furthermore, Figures 1.10b and 1.11b show that the power output varies with the operating voltage and to maximise the power output the PV panel should be operated at its optimal operating point (V_{opt} and I_{opt}) as discussed further in Section 1.4.

Table 1.4: List of vibration sources with their maximum acceleration magnitude and frequency of peak acceleration (reproduced from [133]).

Vibration Source	Peak Acc. (m/s^2)	Frequency of Peak (Hz)
Base of 5 HP 3-axis machine tool with 36" bed	10	70
Kitchen blender casing	6.4	121
Clothes dryer	3.5	121
Door frame just after door closes	3	125
Small microwave oven	2.25	121
HVAC vents in office building	0.2 – 1.5	60
Wooden deck with people walking	1.3	385
Breadmaker	1.03	121
External windows (size 2 ft X 3 ft) next to a busy street	0.7	100
Notebook computer while CD is being read	0.6	75
Washing Machine	0.5	109
Second story floor of a wood frame office building	0.2	100
Refrigerator	0.1	240

1.3.2 Vibration Energy Harvesting

Vibration energy harvesting uses different types of mechanisms such as electromagnetic, piezoelectric and electrostatic to convert ambient vibrations to electrical energy. The key attribute of most vibration energy harvesters is that these are 'tuned' to specific frequencies, called the resonant frequency, and the output of harvester degrades beyond this frequency [133]. Techniques for adapting this resonant frequency of the harvester have recently been proposed [20].

Vibration energy is measured in terms of its acceleration and frequency in units of gravity (g) and Hertz (H), respectively. Table 1.4 shows the results of a survey [133] of peak accelerations and frequencies of vibration of a range of objects; it may be noted that a number of electrical devices in this table exhibit twice of mains-frequency (60Hz, US) vibrations. This observation is important because a vibration energy harvester is 'tuned' to specific frequency and the output power degrades beyond this frequency. Figure 1.12 shows the measurement of accelerations and peak acceleration frequencies along three axes from a heating pump and car body. Note that the frequency and amplitude of vibrations from the heat pump along the Y-axis can be considered as fairly uniform with a single dominant frequency which can used to tune the harvester. On the other hand, the car's vibration along the X-axis exhibit a random pattern that can be considered as stochastic, with changing dominant frequencies which make a case for adapting the resonant frequency of the harvester according to the dominant frequency to maximise the harvester output.

Vibration energy generators fall under three main types [156]: electromagnetic, piezoelectric, and electrostatic. Only the first two of these types are commercially available [82, 36, 28, 1] and are considered in some detail in the following sections.

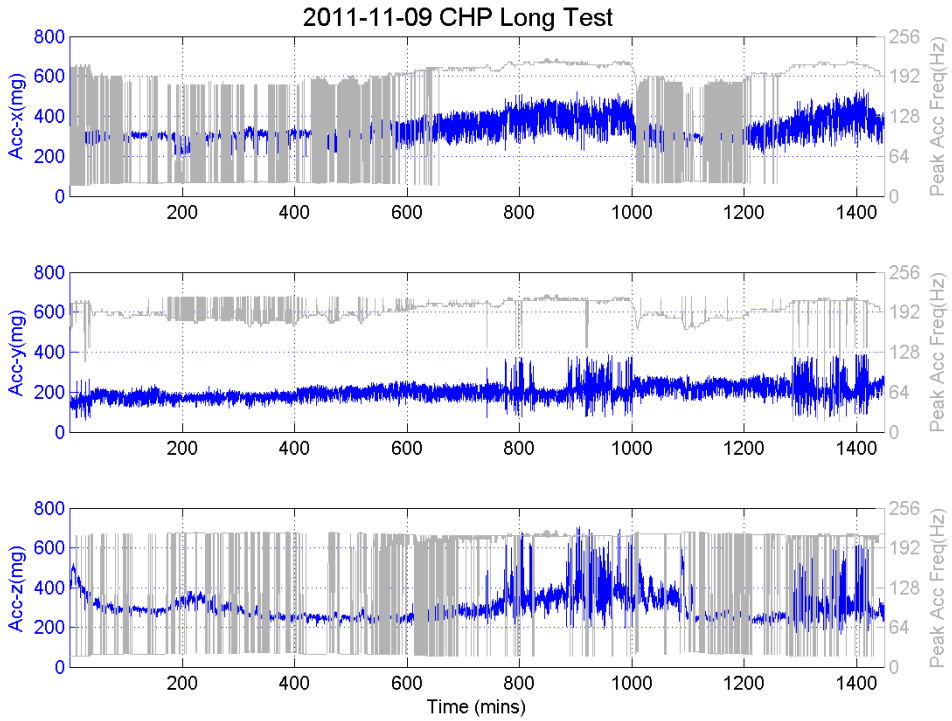

(a) Measurement of vibrations and peak frequencies of a heat pump (reproduced from [42]).

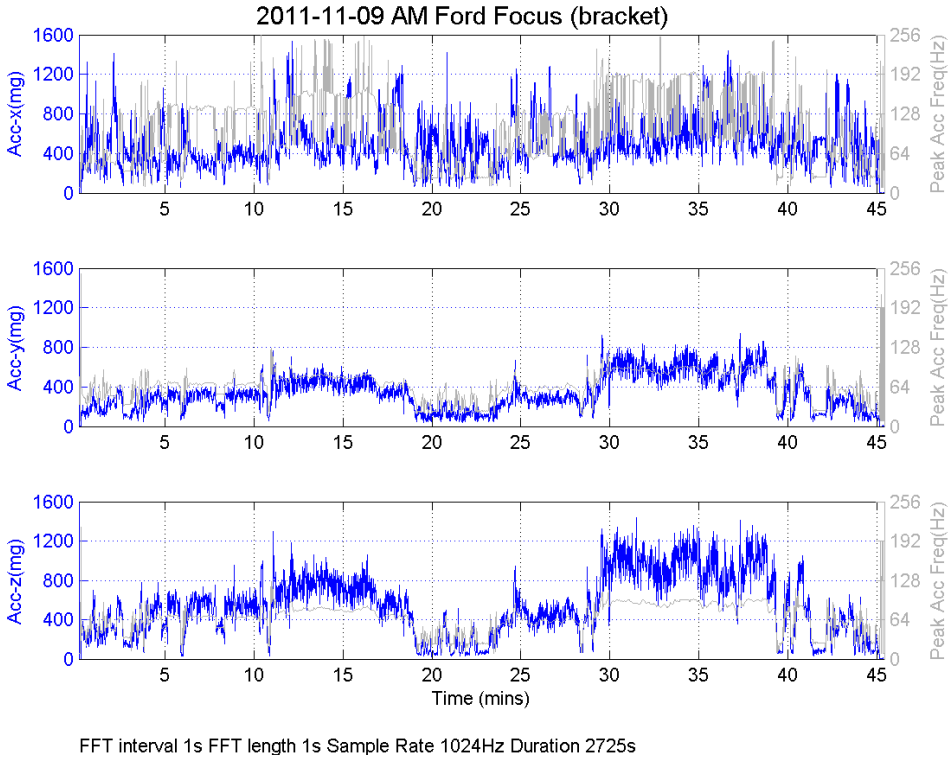

(b) Measurement of vibrations and peak frequencies from a car engine (reproduced from [41]).

Figure 1.12: Measurement of vibrations and peak acceleration frequencies of vibrations from a heat pump and car engine.

(a) Free-Standing Vibration Energy Harvester (PMG FSH) by Perpetuum Inc (reproduced from [82]).

(b) Vibration energy harvester from Ferro Solutions (reproduced from [36]).

Figure 1.13: Different varieties of commercially available electromagnetic vibration energy harvesters.

1.3.2.1 Electromagnetic

Electromagnetic generators are based on the principle that movement of a magnet relative to a coil induces an electrical current in the coil. The disadvantage of electromechanical generators is their high cost [82] but compared to piezoelectric based generators they are relatively low-impedance sources that produce moderate voltages that can be efficiently rectified and used to power electronic devices [157]. Commercial electromagnetic generators have been developed targeting energy harvesting from vibrating machinery. PMG Perpetuum has developed one such generator, the PMG FSH (Free-Standing Vibration Energy Harvester) [82] in two versions tuned to 100Hz and 120Hz (Figure 1.13a) capable of generating peak output of 4mA (0.5g) up to 5 VDC, with the current drive output independent of load voltage up to 5 V. It has with a height of 63mm and diameter of 68mm. Ferro Solutions manufacture a similar device, the VEH-360 [36], with a height of 39mm and diameter of 53mm which is tuned to 60Hz (Figure 1.13b). Its reported output is 0.3mA (50mg) to 1.6mA (100mg) at 3.3VDC.

1.3.2.2 Piezoelectric

The basis of electric power generation from piezoelectric materials is mechanical deformation of these materials using some source of vibrations. Piezoelectric generators benefit from straightforward fabrication, but their drawback is that they generate high AC voltages but low current, which can be difficult to convert efficiently to DC [157]. Piezoelectric-based vibration energy harvesting technology has been commercialised by

(a) AdaptivEnergy piezoelectric vibration energy harvester inside casing.

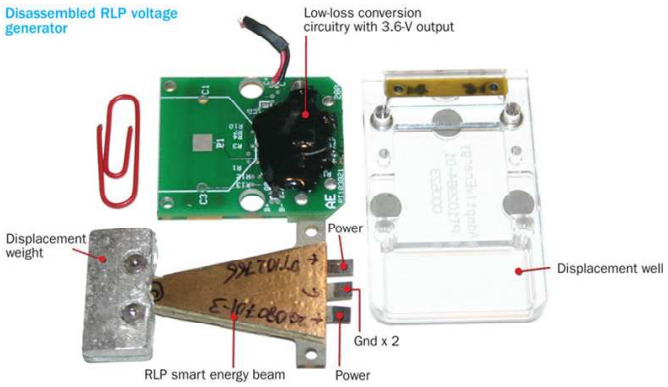

(b) Disassembled device showing its components.

Figure 1.14: JouleTheif piezoelectric vibration energy harvester from AdaptivEnergy (Reproduced from [1] and [88]).

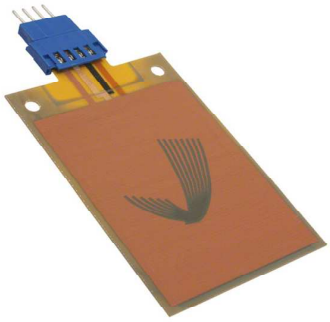

(a) Structure of Mide piezoelectric harvester.

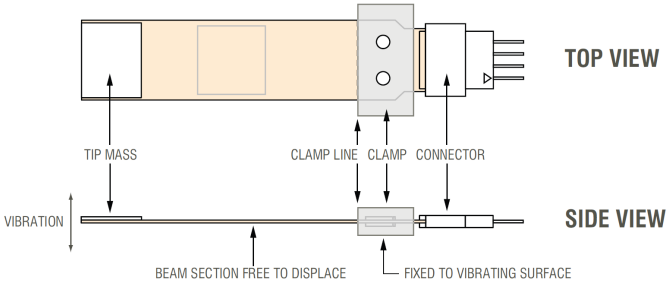

(b) Diagram showing different parts of the harvester. (reproduced from [36]).

Figure 1.15: Volture piezoelectric vibration energy harvester from Mide (Reproduced from [28]).

AdaptivEnergy with their 'JouleTheif' [1] (Figure 1.14) and Mide with their 'Volture' generator range [28] (Figure 1.15). The JouleTheif by AdaptivEnergy is reported to generate output of 3.9mJ in 1.4 seconds (2.78mW) from 1g vibration at 60 Hz [88] while the Mide Volture generator is available in a variety of dimensions and Figure 1.16 shows the output of PEH20w model (designed for 80-175 Hz) at different amplitudes using a resistive load of 20KΩ.

1.3.3 Thermoelectric Energy Harvesting

A thermoelectric energy harvester converts thermal energy in the form of temperature differences into electrical energy. Thermoelectric energy harvesting is based on the Seebeck effect [40, 127]. A thermoelectric harvester is constructed by using many thermocouple elements and each thermocouple is composed of an n-type material electrically

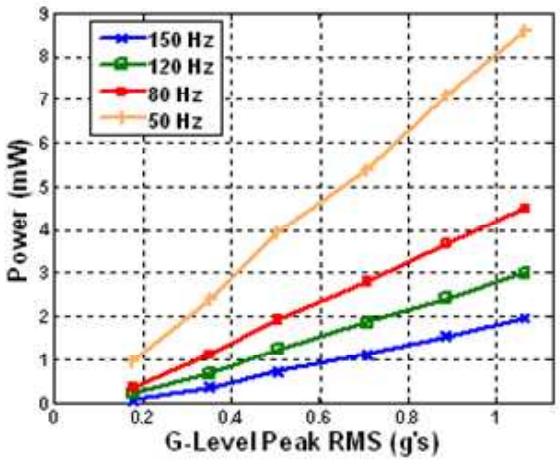

Figure 1.16: The performance data of Mide Volture PEH20WG (Reproduced from [28]).

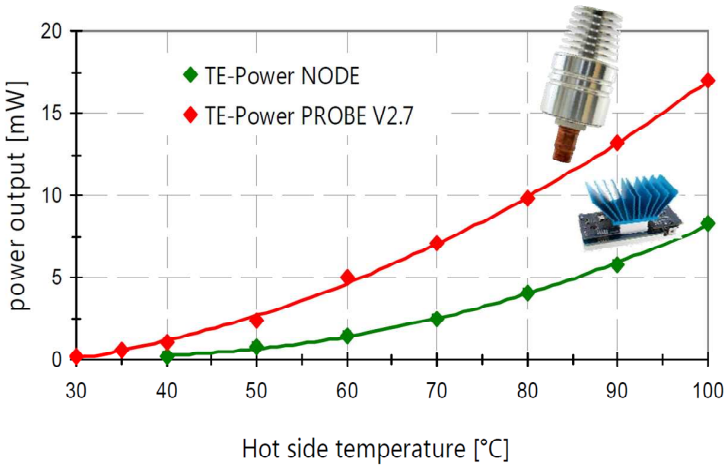

Figure 1.17: Output power of Micropelt thermoelectric generators versus hot side temperature (reproduced from [38]).

in series with a p-type material. When a temperature difference is applied across this material, heat begins to flow from the hotter to the cooler side. Thus, the heat energy causes the free electrons and holes to move and form an electric potential, resulting in current flow if the circuit is closed. The voltage obtained at the output of the thermoelectric harvester is proportional to the temperature difference across the thermoelectric element [127]. Thermoelectric harvesters have been commercialised by Micropelt, which has developed a range of thermoelectric harvesters in different form factors suited to different applications and two types of these are shown in Figure 1.17. The figure also shows the output power versus hot side temperature at an ambient temperature of 25 degree Celsius and using natural convection.

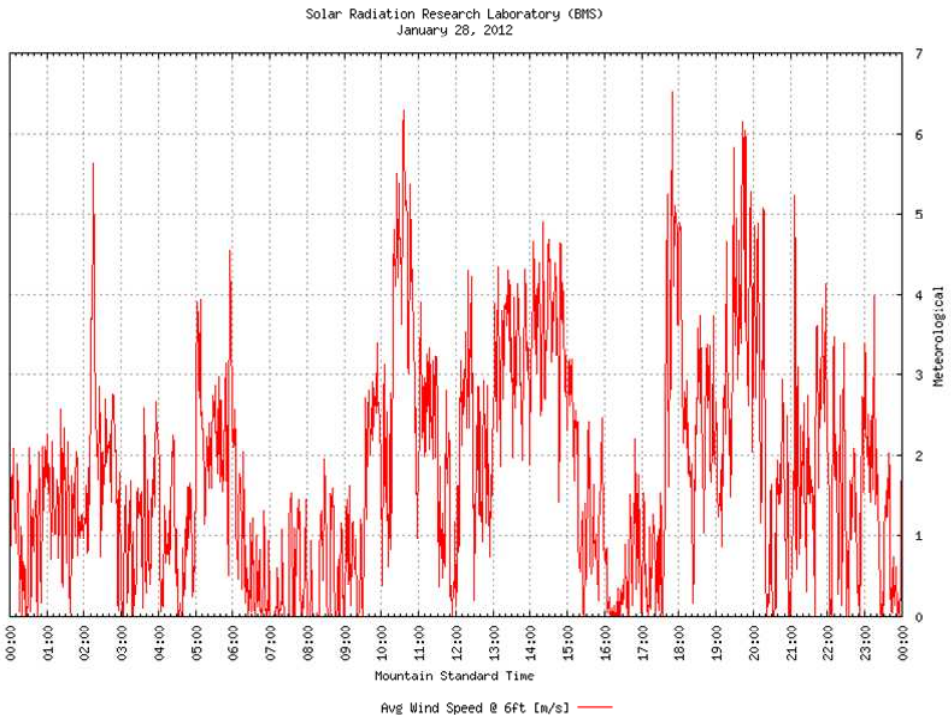

Figure 1.18: Profile of wind speed measured over a single day at height of 6 feet above ground (reproduced from [114]).

1.3.4 Wind Energy Harvesting

Wind-energy harvesting on a micro-scale for powering wireless sensors has been demonstrated using various prototypes systems using small scale turbines and piezoelectric windmill (Figure 1.19). Figure 1.18 shows the profile of wind energy over a day [114]. As can be seen, the pattern of wind energy can exhibit a very high variability over a short period and can be considered as practically stochastic. Based on the design of the energy harvesting device, the amount of wind energy that can be harvested ranges from a few microwatts to 500 mW. The authors of [145] demonstrated a platform for wind energy harvesting using a small size wind turbine with maximum power point tracking. The maximum output power ranged from 2 to 100 mW for wind speeds of 2.3 to 8.5 meters per second. The authors of [123, 122] propose a piezoelectric windmill (Figure 1.19 left) that converts air current into electrical energy by vibrating piezoelectric benders, with a reported maximum output power of 7.5 mW at a wind speed of 10 miles per hour. In [118], a wind harvesting system with maximum power tracking is described and the authors reported that the wind turbine used can output a maximum power of 500 mW (Figure 1.19 middle). Similar to [118], the authors of [100] also used a wind turbine to harvest wind energy (Figure 1.19 right). The authors reported that their wind turbine can output 45 mW at wind speed of 5 meters per second and 210 mW at wind speed of 9 meters per second.

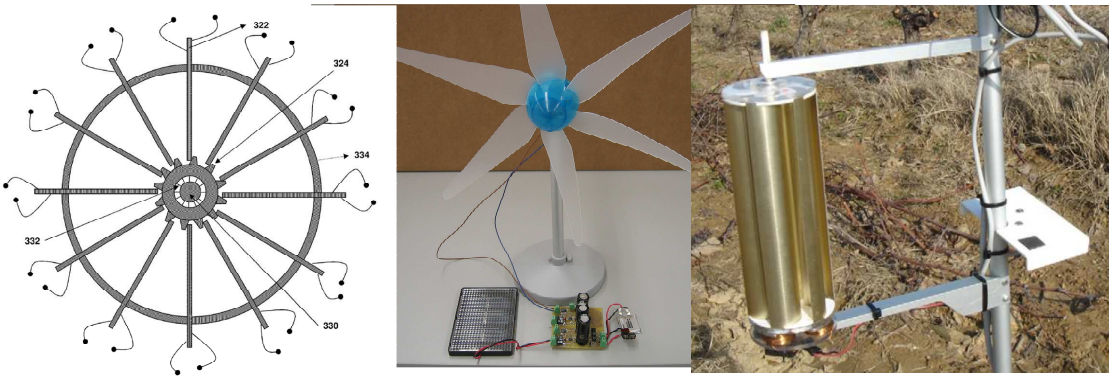

Figure 1.19: Different types of wind energy harvesters (left to right): piezo windmill [123, 122], horizontal turbine [118], and vertical axis turbine [100] (reproduced from cited sources).

Table 1.5: Power output comparison of different types of harvesters.

Type	Subcategory	Stimuli	Power	Cost
Photovoltaic	Sanyo Amorphous Si	1000 Lux	1.8mW	£9.35
Photovoltaic	Monocrystalline Si	Sunny Day	200mW	£3.90
Electromagnetic	PMG FSH	100/120Hz@0.5g	20mW	£150-180†
Electromagnetic	FerroSolutions VEH-360	60Hz@0.1g	5.28mW	n/a
Piezoelectric	AdaptivEnergy JouleTheif	60Hz@1g	2.78mW	$49
Piezoelectric	Mide Volture (tuned)	50Hz@1g	8mW	$399
Thermoelectric	Micropelt TE-Power Node	80 elcius	10mW	£70.53
Wind	Small turbine [145]	2.3-8.5 metre/sec.	2-100 mW	£12‡
Wind	Piezoelectric Windmill [122]	10 mph	7.5mW	n/a
Wind	Horizontal Turbine [100]	5-9 metre/sec.	50-210 mW	n/a

† Based on price quote obtained via sales enquiry.
‡ For a similar turbine as used in [145].

1.3.5 Discussion

The choice of energy harvester is dictated by the working environment of the embedded system and the aim of this section is to give an overview of state-of-the-art in commercially-oriented and relatively mature energy harvesting technologies. Table 1.5 summarises the output power of different types of harvesters considered in this chapter. Besides the power output achievable from these harvesters, cost is an important practical concern in design of embedded applications. In this respect, PV technology is currently the most affordable means of energy harvesting available since the cost of commercially available vibration and thermoelectric solutions are well above the price of small PV panels (Table 1.5). Furthermore, with respect to the output harvested power, PV harvesting is capable of powering a range of contemporary wireless sensing systems depending on the size of PV panel permissible and available illumination, however, the selection of the appropriate type of PV panel is important especially in low-light or artificially lit environments. On the other hand, vibration and thermoelectric technologies not only have a limited power output, but also require a specific operating threshold to provide any useful output at all. For example, present technologies for vibration energy harvesting are sensitive to specific vibration frequencies, so the technologies are typically

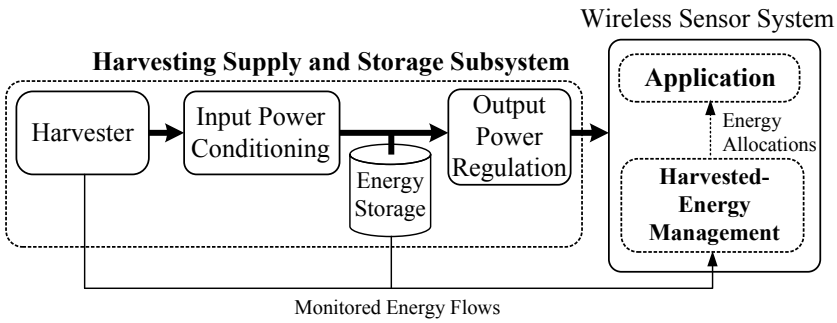

Figure 1.20: Generic model of an energy harvesting supply and storage system along with the wireless sensor application workload.

applicable to deployment on machines working from a mains power supply or at a fixed frequency (Table 1.4). Similarly, thermoelectric devices require maintaining a suitable temperature difference across the thermocouple (Figure 1.17), which can only be a satisfied in a limited number of working environments. Wind energy is relatively promising in terms of its availability and output power but it also requires comparatively large sized generator and the pattern of wind speed shows a very high degree of fluctuation making the useful output of wind generator smaller than outdoor PV panels [118].

Considering the relative benefits of photovoltaic harvesting mentioned above, this work has selected photovoltaic harvesting systems as a concrete instance for investigating design consideration for harvested-energy management. Small size PV panels deployed outdoors are capable of powering a variety of application workload demands, nevertheless, there is need to intelligently manage the time-varying supply of harvested-energy. Chapter 3 discusses prediction of solar harvested-energy to assist an energy management policy (Chapter 6) to adapt an application workload's energy consumption to dynamically match the supplied energy. The next section discusses the required system components to efficiently extract, store and deliver energy from a given harvester to the application workload.

1.4 Energy Harvesting Supply and Storage Subsystem

The energy harvesting supply and storage subsystem captures the energy required to meet the application workload demand. The main components in this subsystem are shown in Figure 1.20 and their purpose is explained in this section.

Since the output of the harvester varies depending upon harvesting source fluctuations, the energy storage is an important part of this subsystem so that the non-uniform output of the energy harvester can be smoothed for delivery to the load. The power conditioning elements are required because the operating voltage/current range of the harvester is constrained by its construction/type and may not match the operating range of the energy storage or load. Similar constraints apply to energy storage and load and hence

voltage converters are required to enable power flow from harvester to energy storage and the load. In addition to matching the harvester, energy storage and load characteristics, another needed functionality is to ensure that the maximum power is delivered from the harvester for any given environmental stimulus. This is achieved by using maximum power point tracking (MPPT) circuits that manipulate operating point to improve the converted power output of the harvester.

The key issues in the design of the power delivery subsystem are (i) the selection of appropriate sizes of harvester and energy storage capacities and (ii) minimize the wasted energy in the stages during power delivery from harvester to the load. Since the supply chain is made up of harvester, power converters and storage stages, to maximize the power delivered multiple challenges need to be addressed.

Harvester Maintaining the harvester conversion efficiency across variations in environmental conditions (illumination intensity, vibration frequency, temperature etc.) [139, 84]. For example, the conventional MPPT approaches used for outdoor solar panels are not suitable due to their power consumption requirements and for this reason 'micro' solar MPPT approaches have been proposed [6, 14, 69, 22]. MPPT techniques for wind energy harvesting [118, 145], and thermoelectric energy harvesting [127] have also been proposed.

Power Conversion Minimizing the losses in voltage conversion circuitry at sub-watt power levels and across the variable range of inputs. For high efficiency DC-DC conversion at sub-milliwatt levels, circuits optimised for energy harvesting applications have been proposed [146, 21, 126, 74]. Harvesters such as thermoelectric generators produce very low voltage and additional circuits are needed to kick-start operation of the DC-DC converter [74, 127].

Storage Desirable properties include high charging efficiency, low leakage, very large number of cycles, low recharge circuit complexity and ability to accurately measure remaining energy. These properties are conflicting in real storage technologies such as different battery types and supercapacitors [59, 157]. For instance, rechargeable batteries have limited charge cycles and lower charging efficiency than supercapacitors, while supercapacitors have higher self-discharge [131, 164, 158].

The specific configuration of components used in the design of power delivery and energy storage depends on the type of energy harvester used as well as the desired characteristics of a energy storage. For instance, Figure 1.21 shows the generic configuration of photovoltaic energy harvesting subsystem. Besides the PV panel, energy storage and load, the input regulation can be used to ensure the proper charging of energy storage and MPPT, while the output regulator delivers a constant voltage to the load. This configuration is discussed in more detail in Chapter 2 of the thesis. Similarly, Figures 1.22 and 1.23 show the configuration used in wind and vibration energy harvesting systems. Compared to

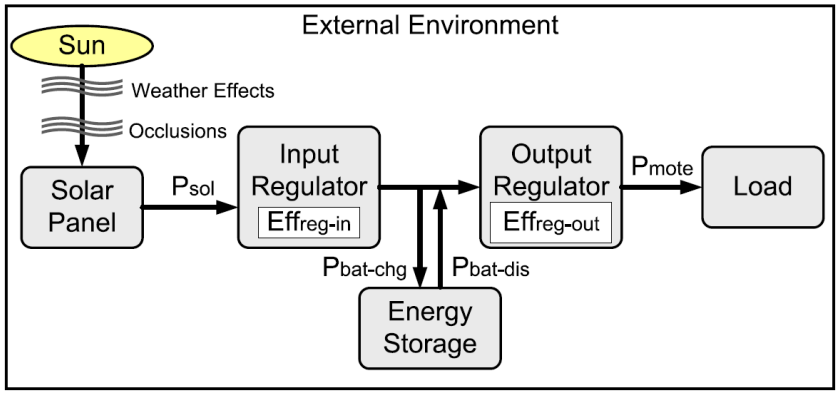

Figure 1.21: Generic model of a PV energy harvesting system (reproduced from [59]).

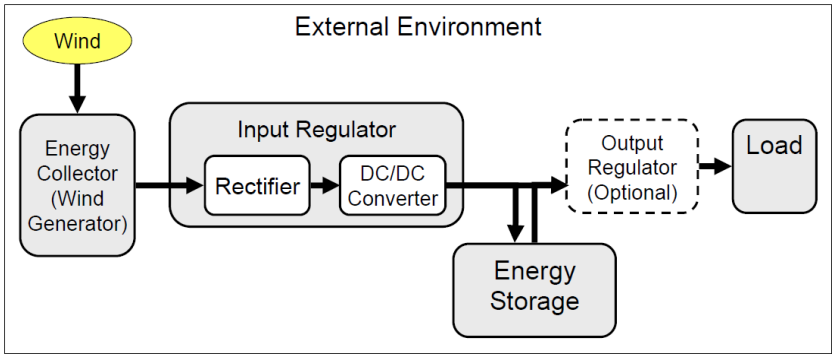

Figure 1.22: Generic model of a wind energy harvesting system (reproduced from [59]).

a PV harvesting system, since the electricity generated from the wind generator or a vibration energy harvester is AC, it needs to be converted to DC before it is stored in the energy storage. The input regulator, which consists of a rectifier and a DC-DC converter, does the following: first, the rectifier converts the AC output to DC, and second, the DC-DC converter adjusts the voltage level of the rectifier output to be within the charging range of the energy storage. To address the start-up and efficiency problems with rectifier circuits, [72] discusses switched-inductor regulation. Figure 1.24 shows the structure of PV harvesting system using a hierarchical energy storage [62] composed of a supercapacitor and rechargeable battery to benefit from individual strengths of each type of storage. A switch is used to select between the two energy storage devices to supply the load, and a DC-DC converter is used as a charger for the batteries.

From the perspective of energy management, the energy harvesting supply and storage subsystem influences the operation of energy management in two ways:

1. For a given energy source, the harvester size determines how much energy can be captured and the capacity of energy storage influences the uniformity of consumption achievable with respect to harvesting source variations.

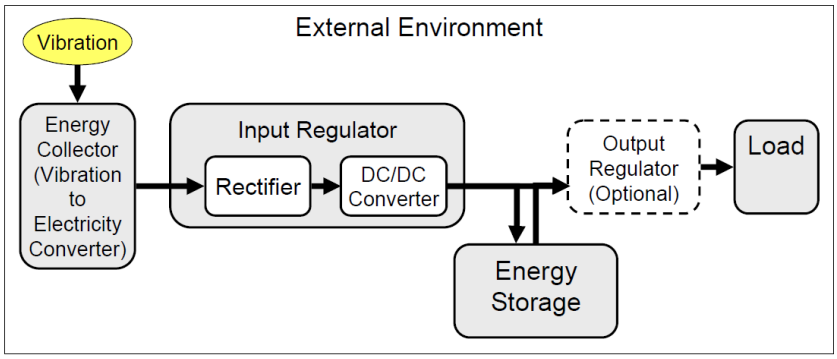

Figure 1.23: Generic model of a vibration energy harvesting system (reproduced from [59]).

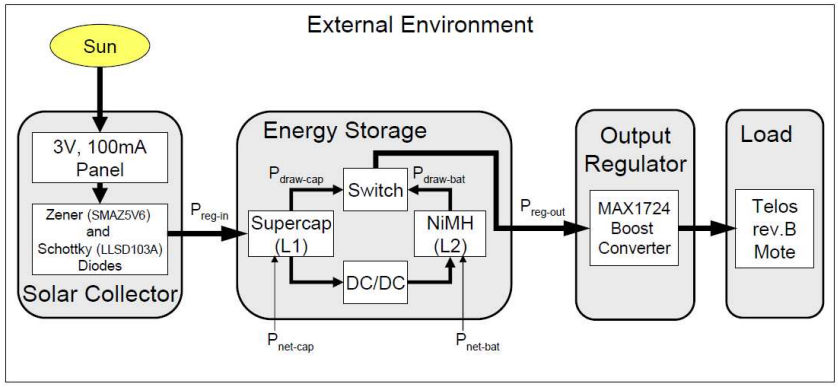

Figure 1.24: An instance of PV harvesting system with multi-level energy storage (reproduced from [59]).

2. The characteristics of system components such as input regulation, energy storage, and output regulation determine the losses in the system and the actual energy available to be consumed or stored. Furthermore, due to the non-ideal characteristics of system components, the amount of losses are also dependent on the value of input power, stored energy and power consumed.

Since the purpose of energy management is to manipulate the amount of energy being consumed, it needs an awareness of the correct values of energy flows or the model of underlying system. Thus, the specific configuration of the harvesting subsystem has to be taken into account for the practical realisation of energy management. Furthermore, support for monitoring of system energy flows such as harvested-power, stored energy and energy consumption [34, 63, 159] is also required. Figure 1.25 shows the implementation of a PV energy harvesting supply and storage subsystem with support for monitoring of PV panel current and various voltages. Chapter 2 focuses on the design of PV energy harvesting and supply subsystem with respect to supply and demand considerations and efficiency of design, while Chapter 4 discusses non-ideal behaviour of system components to enable the design and evaluation of energy management based on the underlying system configuration.

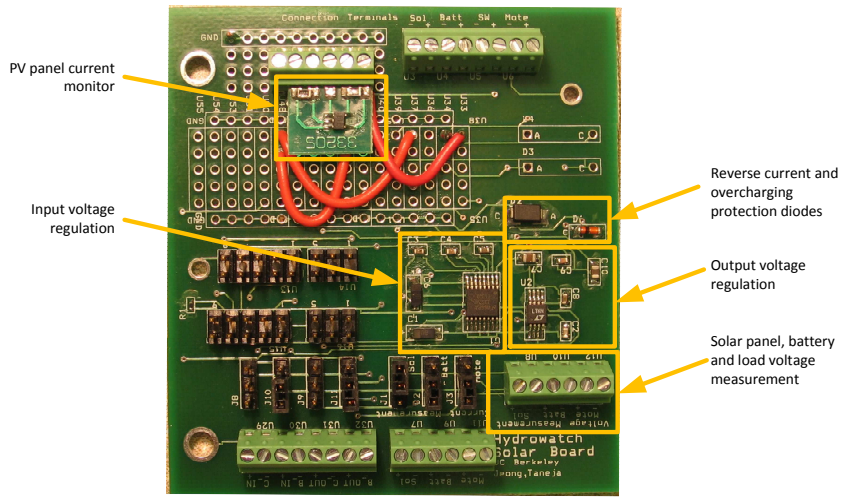

Figure 1.25: Design of a PV energy harvesting and storage subsystem showing the power conditioning and power measurement components (adapted from [146]).

1.5 Harvesting-Aware Energy Management

Techniques for operating lifetime maximisation in case of (primary) battery powered systems focus on energy conservation (Section 1.2.3), since this is the only way to maximise the lifetime of applications while achieving the desired performance, as the total energy budget is dictated by the battery capacity. In energy harvesting powered applications, the same approach can be used but this by itself cannot guarantee uninterrupted operation at all times because of the variability of harvested energy. On the other hand, it is also possible that using a conservative mode of consumption results in wasted energy that could be used to increase the application workload, e.g., to achieve a higher sampling rate or higher rate of message transmission, resulting in a more responsive system in the case of a wireless sensor application as described in Section 1.2.1. The general concept of harvested-energy management is to allocate energy to the application workload with the aim of maximising the utilisation of available energy while not exceeding it, a concept aptly termed as 'energy-neutral operation' [65, 154]. To achieve this, the system energy consumption needs to be adapted according to the output of the supply subsystem (Section 1.4). This implies that, depending on the energy availability, the system can increase its energy consumption (if desirable) rather than operating in energy conservation mode (as usually desirable in a battery powered systems) and consume energy that otherwise cannot be stored in limited energy storage. In case of reduced energy supply, it can also decrease the application workload to prevent undesirable shutdown. This section reviews recent works on harvesting-aware energy management by identifying the main approaches, and places the work undertaken in this thesis in context. The common theme in all work undertaken on harvesting aware energy management is the recognition of the variability of the energy supply and the need to dynamically

adjust the application operation according to supply while achieving application goals. Different models of applications [105] have been targeted for adaptation.

One category of works aim at real-time scheduling of tasks under the variable supply of harvested-energy while minimising the number of deadline misses. In [102], Moser et al. investigate 'lazy' scheduling algorithms as compared to 'earliest deadline first' scheduling for optimal scheduling of real-time tasks under the joint constraints of energy and time on a single processor. To handle the uncertainty in energy availability, the authors introduce the concept of energy variability characterisation curves (EVCC) based on the maximum and minimum energy produced in any time interval. The authors note that the performance of algorithms are highly sensitive to the accuracy of the prediction achieved by EVCC. The model of the energy harvesting system is simplistic and the energy source is modeled synthetically. In [80, 81], the authors propose energy aware dynamic voltage and frequency (EA-DVFS) scheduling that improves upon the lazy scheduling by assuming a dynamic voltage frequency scaling capable processing unit to more efficiently use the tasks slack to further minimise the deadline miss rate. Liu et al. [79, 78] investigate variation of the technique in [81] by assuming a more realistic model of the system that considers the efficiency of energy storage and various prediction techniques to show the impact of these on earlier results that were based on perfect knowledge of harvested-energy. In [86], the DVFS based real-time scheduling is extended to multi-core processors. Task scheduling for structural health monitoring (SHM) applications is discussed in [119] called Head-of-Line Low-Overhead Wide-priority Service (HOLLOWS). It uses an energy-constrained prioritised queue model to describe the residence time of tasks entering the system and dynamically selects the set of tasks to execute, according to system accuracy requirements and expected energy. A prediction algorithm is also proposed to estimate energy expected, as required by the scheduling algorithm. For the same SHM application [31], a DVFS based task scheduler based on a linear regression model is proposed in [128] that relates the energy consumption, execution time and data accuracy to the number of tasks and their complexity. This work is further improved in [32] to achieve consistent performance under the variability of solar harvested-energy. Zhang et al. [163] propose harvesting-aware speed selection algorithms for time-critical and performance-intensive monitoring and control activities, based on Dynamic Voltage Scaling (DVS) for CPUs and Dynamic Modulation Scaling (DMS) for wireless radios. The purpose is to maximise energy reserves while meeting application performance requirements of wireless sensors in a network under spatiotemporal energy variability to achieve resilience to network-wide workload burst or shortage in amount of energy harvested.

Another model of application is one that consists of a set of repetitive tasks with different costs in terms of energy consumption, which may be dependent on each other, and the aim is to decide the rate of task execution in a given interval based on energy available in the interval and the application performance constraints on tasks execution. Based

on this model, [107, 103] present a multi-parametric linear programming based policy to determine the rates of tasks execution based on prediction of future energy. Since the online solution can be computationally prohibitive in terms of both runtime and energy consumption, the solution is based on off-line computation based on different possible system states and environmental conditions. The authors note that the performance of the policy is sensitive to prediction errors and a worst-case long-term energy prediction technique is used to prevent the system from depleting the energy storage because of mis-prediction. The system model used takes into account the energy storage efficiency and the possibility of consuming energy directly depending on supply and demand. A simpler model of application with duty cycling of one task is considered in [65] and the goal is to maximise the average duty cycle of application. The system model considers energy storage efficiency and possibility to consume energy directly without discharging the energy storage depending on energy available. Using prediction of future energy, the policy determines the times in future when energy can be consumed directly and allocates maximum possible duty cycle during these time slots to maximise utilisation harvested-energy and thus the average duty cycle. [164, 165] and [154] also consider an harvesting adaptive duty cycling control. [154] propose a Linear Quadratic Tracking based controller to adapt the duty cycle based on monitoring of stored energy in a rechargeable battery and also consider reducing the variability of energy consumption as an optimisation objective. [164, 165] consider the leakage in supercapacitors and the aim is to minimise the wasted energy by allocating higher duty cycles when leakage is higher, using a proportional gain controller.

In [106, 104, 39], an optimisation problem based on utility maximisation framework is considered, which is based on maximising the allocation of available energy to an application while achieving smoothness of energy consumption under a variable supply of energy. Utilising the knowledge of future harvested energy, [106, 104] propose a polynomial time heuristic that allocates energy as uniformly as possible within the constraints of finite energy storage while [39] propose a max-min time-fair allocation policy to achieve the same goal. In [76, 77], the problems of energy harvesting aware sensing, routing and data dissemination in wireless sensor networks is considered under the time-varying profile of harvested-energy. Similarly, a number of other works which are too numerous to mention here consider harvested-energy management in context of energy source variability and some wireless sensor network application specific optimisation objective. Some of these works require knowledge of energy source to manage variability and to this end many of the works discussed above with few exceptions [65, 128, 32] assume perfect knowledge of future energy. On the other hand, energy source model-free approaches are described in [154, 164, 165], while Gorlatova et al. [39] discuss various energy allocation approaches based on a stochastic model of the energy source. With the exception of considering the energy storage efficiency, the model of energy harvesting system assumed in majority of these works is highly simplified, with energy source modeled as a series of values that determine the energy stored in an ideal buffer.

The focus of this thesis is on energy management design considerations, mainly the variability of harvested-energy and the non-ideal characteristics of various system components. Considering this, the goal is to uniformly allocate harvested-energy that can be utilised by any application to achieve consistent performance. In Chapter 5, some of these energy management policies are evaluated using detailed system modeling (Chapter 4) to identify the shortcomings in the original system model and propose improvements, while Chapter 6 considers the problem of time-uniform energy allocation under a variable energy harvesting supply.

1.6 Project Aims and Objectives

As discussed in previous sections, the choice of a suitable harvester depends on the available environmental energy sources and the capability of the harvester to deliver sufficient power within any imposed constraints on its selection. The power delivery and storage subsystem needs to be designed to optimise the power extracted from the harvester and it determines the amount of energy that can be harvested and buffered. The embedded applications under consideration can vary their energy consumption within certain limits by increasing or decreasing their workload. This can be exploited by harvested-energy management to optimise the utilisation of available energy by maximising the energy consumption while not exceeding the available supply capacity. Effective implementation of energy management requires awareness of the energy source variations to optimise long-term operation, while also accounting for the non-ideal characteristics of harvesting system components. There has been a significant amount of work covering different aspects of energy harvesting powered applications in the last few years as discussed in this chapter. These works have addressed different problems in this domain such as the validation of different energy harvesting system designs, optimisation of the harvesting supply subsystem, and adapting application parameters accordingly to the spatiotemporal variability of the harvesting source using some form of energy management. With few exceptions [65, 165], harvested-energy management and harvesting subsystem design are considered together; in most of the works, methods of harvested-energy management are discussed and evaluated while abstracting the details of harvesting subsystem [154] and focusing mainly on the specifics of a given application [76], even assuming complete knowledge of the energy source variations [103, 39].

The aim of this thesis is to investigate design considerations for harvested-energy management with particular emphasis on variability of energy supply and the non-ideal characteristics associated with harvested-energy supply and consumption. Figure 1.26 shows the topics of this thesis and the links between these to address the project aims and objectives, which are as follows:

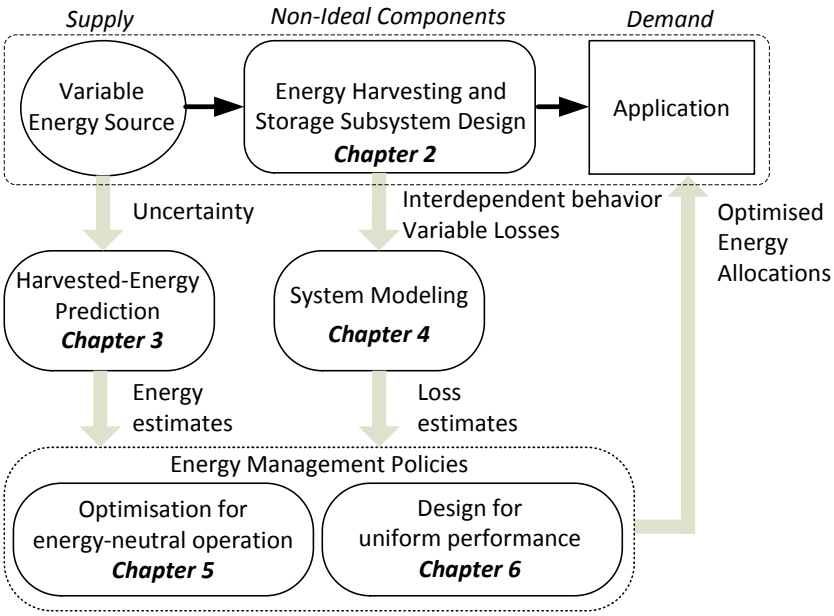

Figure 1.26: Overview of thesis topics in context of design considerations for harvested-energy management.

- To manage variability of energy harvesting supply using suitable harvested-energy prediction technique. This is addressed in Chapter 3.
- To study the energy harvesting system designs to identify necessary components and their characteristics such as interdependency and losses, which influence energy supply and consumption. This is addressed in Chapter 2.
- To better manage supply and demand, determine the various parameters that affect these using suitable modeling and validate it empirically. This is addressed in Chapter 4.
- To demonstrate the utility of modeling in achieving energy-neutral operation, evaluate and optimise existing energy management policies. This is addressed in Chapter 5.
- To achieve uniform operation of application under supply variability, propose practical energy management policy for optimised allocation of energy budgets using harvested-energy prediction. This is addressed in Chapter 6.

As a concrete instance of problem specification (Figure 1.2), this thesis focuses on photovoltaic harvesting systems using solar energy due to its widespread applications, relatively high power output and maturity of harvester technology compared to other means of harvesting since harvester development is beyond the scope of this work. As the target workload, a single wireless node is considered instead of a network because the principles discussed are applicable to each node in a network. For adaptation of application

parameters, a generic model of energy budget allocation is considered since the allocated budget can be used to decide duty cycles, sampling rates, transmission rate, etc. depending on application specific functionality.

1.7 Thesis Outline

The thesis is organised as seven chapters.

Chapter 1 outlined the complete system within which harvested-energy management needs to function. The goal was to explain the major components in an energy harvesting powered application, such as the embedded application, the harvesting sources and harvesters, and the power supply subsystem. Furthermore, the possible choices amongst the different types of these major components and their relevance to the problem of harvested-energy management was discussed.

Chapter 2 discusses the design of energy harvesting supply and storage subsystems. The aim is to identify the required components, their characteristics, and their selection from the aspect of efficient realisation of the energy harvesting system. This chapter explains the interdependency between system components and the losses associated with supply and consumption, which are modeled in Chapter 4. It also describes a reference system implementation that is referred in Chapters 4 to validate the system modeling, and in Chapters 5 and 6 to optimise and evaluate energy management policies.

The variability of harvested energy is a key challenge in harvested-energy management since it makes it difficult to determine the energy spending budget that will guarantee that the utilisation of all available energy is maximised without exceeding the total harvested-energy. In addition, the knowledge of energy to be harvested in future can be used to determine the energy budgets that result in uniform performance of the application workload in the long-term. Chapter 3 considers the problem of prediction of harvested-energy with low computation and energy consumption overheads, and focuses on prediction of solar energy for low-power and resource constrained wireless sensor devices. The main contribution of this chapter is an effective short-term prediction technique through systematic evaluation of the prediction algorithm parameters. The obtained results are used in Chapter 6 for evaluation of the proposed energy allocation policy.

The common objectives of harvested-energy management are to ensure a dynamic balance between energy supplied and consumed. A better correlation between supply and demand can be achieved if the non-ideal behaviour of each system component is considered, and its variation (if any) based on component's input/output (or inter component dependency). The contribution of Chapter 4 is to address this by identifying the contribution of individual system component on supply or demand through modeling. The

proposed approach to modeling the system and its individual components is validated against empirical measurements using the reference system configuration described in Chapter 2.

Chapter 5 applies the modeling concepts discussed in Chapter 4 to show that existing energy management policies need to reconsider their underlying system model to operate in an effective manner. This chapter evaluates three energy management policies and the contribution of this chapter is the identification of changes to the system model of these policies to correctly achieve energy neutral operation and/or maximise harvested energy utilisation. Chapter 6 considers the problem of uniformity of energy budget allocations under the variable supply of harvested energy. Using knowledge of future harvested energy, it is possible to allocate energy as uniformly as possible while achieving energy neutral consumption. A prediction based energy budget allocation policy is proposed and using the system model considered in Chapter 4, the results are compared with close variants and a prediction-less policy. It is shown that proposed policy achieves lower variance of allocated energy at comparable energy utilisation and system dead times. The chapter also applies the system modeling in Chapter 4 to determine the size of PV panel and energy storage to meet a given minimum consumption demand of application workload. Chapter 7 presents the conclusions and discusses directions for future work.

1.8 Thesis Contributions

The contributions of this thesis are:

1. This thesis defines the goals of harvested-energy, identifies the two fundamental challenges in its realisation, i.e., uncertainty in supply and non-ideal system components, and establishes the dependence of harvested-energy management on different parts of an energy harvesting system such as the energy source, harvesting system components and application workload demand.

2. To address uncertainty in energy supply the thesis focuses on prediction of harvested-energy and proposes a systematic approach for evaluation of solar energy prediction algorithm accuracy and simplifies determination of prediction algorithm parameters for minimising the average prediction error across multiple profiles of input energy.

3. The thesis identifies the interdependencies of harvesting system components and their non-ideal characteristics, proposes appropriate modeling to quantify these, and optimises recently proposed harvested-energy management policies to achieve effective match of application workload demand with energy supply.

4. To achieve uniform performance under supply uncertainty, the thesis proposes a prediction based energy management policy that achieves lower variance in performance and lower system dead-time at comparable utilisation of harvested-energy compared to recently proposed approaches.

The contributions discussed in Chapter 3 of this thesis have been published as:

- Mustafa Imran Ali, Bashir M. Al-Hashimi, Joaquín Recas, David Atienza, "Evaluation and Design Exploration of Solar Harvested-Energy Prediction Algorithm," Design, Automation and Test in Europe Conference and Exhibition (DATE), 2010, page 142-147, 8-12 March 2010

Chapter 2

Photovoltaic Harvesting Supply and Storage Subsystem Design Considerations

As discussed in Chapter 1 (Section 1.3), photovoltaic energy harvesting has been chosen in this thesis to investigate the harvested-energy management design considerations. This was because of lower cost, higher power output per unit area, and applicability to many wireless sensor applications. For a given deployment location, the amount of energy available to the workload is dictated by the capability of the harvesting subsystem to capture, store and supply energy. As discussed in Section 1.1, the aim of energy management is to allocate energy budgets for application workload consumption according to harvested-energy availability. Furthermore, it was discussed that effective energy management has to account for the characteristics of the energy source (harvesting environment), harvesting subsystem and demand of application workload. Unlike the harvesting environment characteristics that cannot be controlled but only estimated to minimise uncertainty (Chapter 3), the harvesting subsystem needs to be carefully engineered by appropriate selection of components to ensure sufficient energy supply to the application workload. This chapter considers the design choices for photovoltaic harvesting supply and storage subsystems in detail. This is important since energy management policies need to consider the non-ideal behaviour of the chosen system components for energy budget allocations to effectively adapt the demand according to supply. Chapter 4 discusses the modeling of system components' non-ideal behaviour such as losses and inter-component dependencies. Figure 2.1 depicts a generic architecture of a photovoltaic energy harvesting system, showing the system components and their interconnections. The environmental energy (irradiation) is captured by the photovoltaic (PV) panel and this is made available through the input power conditioning block for replenishing the energy storage and consumption by the application workload.

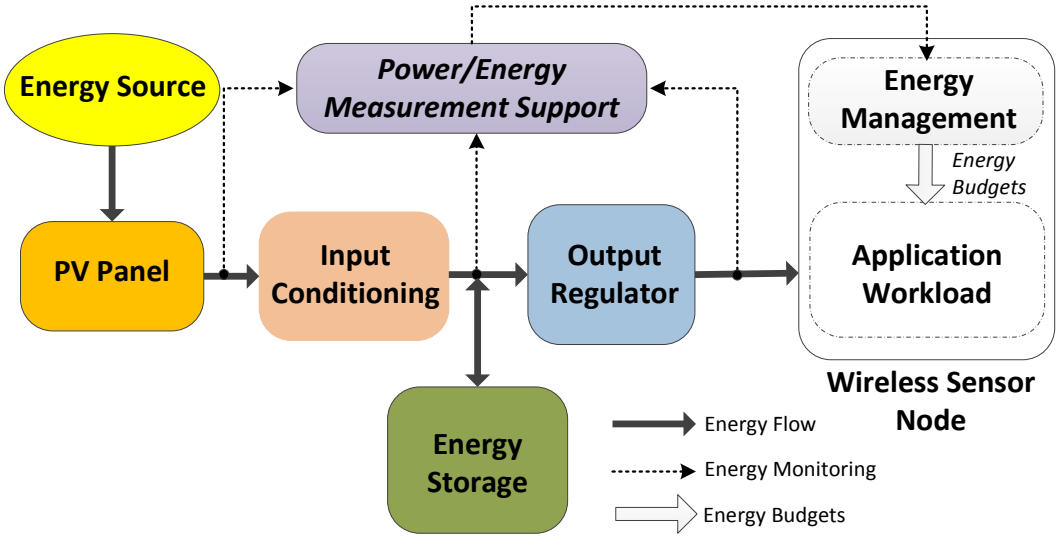

Figure 2.1: Architecture of a photovoltaic energy harvesting sensor node.

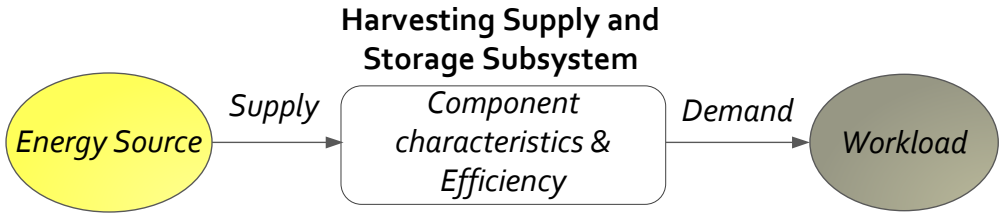

Figure 2.2: Factors influencing the design of harvesting supply and storage subsystem.

The application workload is connected through the output regulation block to the harvester output and energy storage. Depending on the load demand and energy supplied, the load demand can be supplied from the output of PV panel, the energy storage, or both. The harvested-energy management is implemented on a processing unit that is part of the wireless sensor node. To allocate energy budgets, energy management policy requires measurement of energy harvested, stored, and consumption. To obtain these values, measurement circuits may be used.

Figure 2.2 broadly depicts the factors influencing the design of the harvesting supply and storage subsystem. These factors can be categorised into two main design considerations:

Matching Supply and Demand Given the deployment environment, the required energy supply from the PV panel and energy storage capacity needs to be decided to meet a given (average) application workload demand. In most practical energy harvesting powered applications (Section 1.2), there is a desired minimum operating demand of the application that must be met to obtain results while operating perpetually. The harvesting subsystem has to be engineered for sustaining this minimum acceptable demand. This involves selecting the power output of PV panel and capacity of energy storage accordingly. It may be non-trivial to achieve

this in an exact manner since it is not always possible to accurately characterise the environment's energy supply and fluctuations completely over the long-term [59]. Furthermore, the selection of PV panel and energy storage is also constrained by physical dimensions, mainly due to the need for miniaturisation, and possibly cost.

Maximising System Efficiency At an abstract level, the sensor node is the consumer of energy, the photovoltaic panel caters to this demand by extracting energy from the environment and energy storage buffers this energy. In an ideal system, the harvester (PV panel) output would be independent of the state of energy storage or the load. However, real system components are interdependent and their current-voltage (I-V) characteristics are non-linear and need to be matched to realise a functioning harvesting subsystem and enable efficient operation. High efficiency of energy transfer is an important factor since the harvested energy is invariably constrained by the small size of PV panels. Although there can be multiple choices of components to design a harvesting subsystem with a given supply rate and storage capacity, the inflexibility in choice of a component due to its desired properties, e.g., supercapacitor vs. rechargeable batteries, may constrain the choice of other system components such as PV panel, input/output power conditioning elements etc.

The aim of this chapter is to present harvesting supply and storage subsystem design with respect to the above two considerations. Given a harvesting subsystem design, energy management needs to account for system losses for balancing supply and demand to achieve energy-neutral operation. Chapter 4 discusses modeling of system components to identify the non-ideal characteristics and a reference system design is used to validate the modeling. This chapter also discusses the selection of this reference system design. The chapter is organised as follows. Section 2.1 discusses related work, Section 2.2 presents the design considerations for the photovoltaic energy harvesting system, Section 2.3 gives the details of the reference system design and Section 2.4 concludes the chapter.

2.1 Related Work

A number of previous works have touched upon design considerations for energy harvesting systems [10, 59, 83, 24] and a variety of photovoltaic energy harvesting system designs have been proposed in the literature [124, 62, 146, 164, 141] covering different points in the design space [59]. These designs are driven by different objectives such as design simplicity [65, 146], long life of energy storage [141, 62], and maximum power point tracking [141, 118, 15]. Recently, the use of supercapacitors as energy storage and the resulting challenges in maximum point point tracking [141, 14, 15], cold booting a system with an empty supercapacitor [164, 22, 24] and leakage management [164, 131]

have received much attention. Considerations in maximising system energy efficiency [83] and application driven design of systems has also been discussed [146]. Based on the study of these different designs of photovoltaic energy harvesting and storage subsystems, this chapter summarises the design choices and identifies the behaviour of each system component in terms of losses and the interdependency between system components. Based on the general structure of these systems, the aim is to identify parameters that influence harvested-energy management in adapting demand according to supply. Chapter 4 builds upon these concepts and discusses the modeling of these parameters, and validates it using a reference system design described in this chapter (which is based on the principle of design simplicity).

2.2 Design Considerations

This section discusses the underlying issues in the design of an optimised harvesting subsystem. First, the matching of supply with the energy consumption demand of the application workload is considered. Next, the requirements for interfacing the PV panel, energy storage and load for efficient design is explained. Then each system component is discussed along with its associated design considerations.

2.2.1 Dimensioning Energy Supply and Storage

Dimensioning involves selecting the PV panel nominal output power and the energy storage capacity to cater to a certain demand. Consider a simple case of a PV harvesting system deployed in a predictable setting where the lights are illuminated for a certain fixed time per day and the application workload needs to operate at a constant demand throughout. Assuming that there are no constraints on sizes of PV panel and energy storage, the PV panel can be selected such that it is capable of capturing the energy required for a complete day's demand while the energy storage should be large enough to meet the energy demand under periods of no supply. This simplistic scenario can be generalised to more realistic cases in which the energy available varies from day-to-day due to changes in magnitude or periods of availability. Therefore, selecting an optimised harvesting capacity is complicated by variations in the deployment environment. A possible approach is to select the PV panel according to worst case supply and the energy storage for buffering worst case shortages. However, this may not be possible due to the practical constraints on permitted physical dimensions of these components, besides costs. The planning for supply and demand also needs to account for the non-ideal factors or losses in energy transfer between the energy harvester and the application workload. The focus of this thesis is on the adaptive allocation of energy budgets using energy management policies, rather than simply the design of supply capacity to meet a static demand. Nevertheless, energy management policies can only allocate energy

within the energy resources provided by the harvesting supply and storage subsystem. Chapter 6 considers the influence of PV panel size and energy storage capacity on performance of energy management policy.

2.2.2 Efficiency Considerations in Energy Harvesting Supplies

2.2.2.1 Voltage Conversions Overhead

The terminal I-V (current-voltage) characteristics of the PV panel, energy storage and the required supply voltage of the application workload (processor, radio, ADC etc.) can be incompatible. For example, the wireless sensor node may require a 3.3V supply, the rechargeable battery (NiMH) terminal voltage can range from 0.9-1.4V from fully discharged to charged, while the PV panel's maximum power voltage lies in the range of 3.6-4.0V for nominal illumination conditions. In this case power conditioning circuitry is required to harvest energy from PV panel and power the wireless sensor node, which inevitably introduces losses in the supply path. The need for voltage regulation and conversion to supply multiple voltages to different subsystems is not uncommon in low-power battery operated embedded systems [51]. However, the scarce and intermittent supply of harvested-energy and the desire for perpetual operation makes it critical to achieve high efficiency. A possible solution is to use components with closely matching I-V characteristics, such as a PV panel with (near) maximum output power voltage that is matched with voltage range of the battery [59, 146, 85], since the voltage range of battery is fixed based on their chemistry (e.g., NiMH or Lithium-ion). If voltage regulation must be used, the efficiency of the regulator should be as high as possible under a given operating range of input voltages and output currents (Section 2.2.7.1).

2.2.2.2 Requirements for Energy Storage

In contemporary rechargeable battery powered electronics devices (e.g., mobile phones), the battery is recharged while the application workload receives its supply power simultaneously when connected to a tethered power supply [147]. An energy harvesting supply has some similarity with these rechargeable battery powered devices since a harvester powers the workload and also charges the energy storage (battery or supercapacitor) when the harvested-energy exceeds the demand of application workload [65, 59]. On the other hand, the energy storage fulfills the demand when the power output of harvester alone cannot supply the required load. The key difference between an energy harvesting supply and contemporary rechargeable battery devices is the variable supply of harvested-power which leads to variable and intermittent charging of the energy storage. This is not the case in contemporary rechargeable battery power supplies since a dedicated charging path is used while supplying the load. The implication of this for the energy harvesting supply and storage subsystem is that it should be capable

of storing a variable amount of energy while sustaining intermittent charge/discharge cycles. Rechargeable batteries such as NiMH and Lithium-ion/polymer are not capable of optimal energy storage in this manner and to maintain their lifetime recommended charging ranges need to be used [11, 150, 149, 148, 152]. Another problem with irregular charging of batteries is the difficulty in determining when these have been fully charged leading to damaged batteries, which can be catastrophic in Lithium batteries, or wasted capacity due to undercharging. A related implication for energy management is that the exact amount of stored energy cannot be reliably determined even by using advanced battery monitors or fuel-gauges, since these are designed to monitor battery parameters under regular charging and discharging conditions [50]. These factors make supercapacitors more suited to energy harvesting supplies as they are more flexible in accepting a range of charging rates [35], however, supercapacitors have a wide voltage range and the self-discharge of supercapacitors is higher [131, 158, 164] and not straightforward to quantify [158], and therefore needs consideration in both harvesting subsystem design and energy management. Section 2.2.5 discusses the energy storage characteristics in more detail.

2.2.3 Estimation of Deployment Environment

Estimation of harvesting capability of a given deployment environment involves determining the expected energy a PV panel will harvest. This can be used to decide the size of PV panel that can be sufficient to ensure a certain average supply. Although, the focus of this thesis is not to optimise the harvesting subsystem based on such estimation, for the sake of completeness this section briefly discusses the related works on this topic.

The PV panel datasheet specifies its nominal power output P_{panel} at standard test conditions (STC), which implies input light energy of 1 kW/m^2 of air mass (AM) 1.5 radiation [108]. Therefore, to calculate the PV panel output power or energy, an estimation of the amount of solar radiation power is needed. In [59], a software suite called Meteonorm [94] is mentioned, which uses meteorological database of more than 30 years of solar radiation measurements from a number of locations around the world. For locations not available in the database, the software estimates its approximate solar radiation based on its geographic characteristics (latitude, longitude and altitude), and matches it to the data of previously known locations. The estimates of solar energy radiation are output as a monthly solar radiation E_{month} in kWh/m^2. Using E_{month}, the peak solar hours (PSH) can be calculated, which implies the equivalent number of solar radiation hours per day assuming that solar energy is received at an uniform intensity of 1 kW/m^2. From this value the available energy from a specific solar panel for one day, $E_{sol-day}$, can be estimated as the product of the PSH and the solar panel output power P_{panel} at 1 kW/m^2 as usually provided by manufacturer datasheets:

$$E_{sol-day} = PSH \times P_{panel} = \frac{E_{month}}{1kW/m^2 \times days} \times P_{panel} \tag{2.1}$$

Another approach taken in [71] does not use the panel output power but expresses the available energy in terms of area of PV panel (A), panel efficiency (e_{panel}), the loss due to angular deviation from the incident solar radiation (a), the losses in power transfer circuitry (e_{el}), and a temperature exceedance loss (L):

$$E_{sol-day} = (1 - L) \cdot e_{el} \cdot e_{panel} \cdot A \cdot a \cdot \frac{E_{month}}{days} \tag{2.2}$$

Note that these estimates are very coarse-grained and the aim is to guide PV panel selection. These cannot be used for management of short-term variability of harvested-energy. Chapter 3 discusses short-term harvested-energy prediction techniques to achieve this purpose.

2.2.4 Application Workload Demand

The application workload is the consumer of harvested energy and it includes all digital and analogue modules that constitute a wireless sensor node [34, 43] such as a microcontroller, wireless radio, sensors, supporting peripherals and specialised processing unit such as a digital signal processor [31] or FPGA [109] (Section 1.2.2). The application workload usually has different power consumption states corresponding to the different activities or tasks that make up the application functionality such as sensing, data processing, data transmission, and data reception. Also, various energy conserving idle/inactive modes in processor and radio are available, in which certain modules are shutdown or put in standby mode [55, 49]. A commonly used method of conserving energy in many wireless sensor applications is duty cycling, in which the application workload alternates between idle and active states (Section 1.2.3). Based on the energy consumption of these different activities and application functionality, a given energy budget will dictate the performance that can be achieved by the application workload. For example, given an energy budget for a certain interval, a data collection application can decide its sensor sampling rate, duty cycle of radio to transmit its sampled data and participate in routing other packets in a multi-hop wireless network (Section 1.2.1). Furthermore, there is also potential for dynamic voltage scaling [95] since the processing element and some peripherals can operate within a range of supply voltages, with lower voltages providing greater power savings at the cost of reduced clock frequency, although the cut-off voltages can be different among different components. For example, the flash memory can have a cut-off voltage of 2.2V [55] while the microprocessor core can work down to 1.8V [55]. Although, different elements in a wireless sensor system may be able operate within a range of input voltage, a fixed supply voltage is required for

Table 2.1: Description of different activities in application active mode shown in Figure 2.3 (bottom) (derived from data in [101]).

Activity Label	Description	Time Elapsed
A	Sample temperature sensor	78 μs
B	Sample V_{CC}	37 μs
C	Calculate temperature and V_{CC} from ADC sample results (MSP430 active and radio idle)	140 μs
D	Oscillator startup time	300 μs
E	Timeout before chip ready goes high tolow	150 μs
F	Transmit message to TX FIFO and prepare message TX (MSP430 active and radio idle)	140 μs
G	PLL calibration of radio frequency synthesizer	809 μs
H	RX mode (clear channel assessment)	180 μs
I	Switch between RX and TX mode	30 μs
J	TX mode (message transmission)	800 μs
K	Radio prepares for sleep (MSP430 active and radio idle)	70 μs

deterministic operation of the clocking subsystem and A/D converter, the latter needs a fixed supply voltage for use as a voltage reference. Depending on the required supply voltage values of the wireless sensor system and the voltage range of energy storage, some suitable voltage regulation can be used as discussed in Section 2.2.7.1. The cost of using this voltage regulation is that the efficiency of the output regulator influences the energy consumed by the workload.

To determine the required energy supply to support a given application workload, or conversely to determine the application performance within an energy budget allocated by energy management, consider a simple application example of a periodic temperature sensing application using Texas Instruments ez430-RF2500 wireless sensor node [101]. To conserve energy, the application duty cycles between idle and active states of the microprocessor (TI MSP430) and radio (CC2500). Figure 2.3 (top) shows a five seconds profile of current drawn with one data transmission per second, where the spikes indicate the active mode. Due to the different power consumptions depending on the activity, the instantaneous power during the active mode can vary. Figure 2.3 (bottom) shows the current profile during the active mode for the application task involving sampling and transmission of temperature sensor value to a receiving node. Table 2.1 gives brief description of different activities during the active mode shown in Figure 2.3 (bottom). The total energy consumed during active mode is 35.508μAs lasting for 2.838ms (Table 2.2), resulting in an average current of 12.511μA, while the total current drawn in sleep mode (processor+radio) is 1.3μA [101]. For the purpose of quantifying the application demand, the average power consumption can be used, which is determined by power consumption during the active and idle modes, and the number of tasks per unit time. For one transmission per second, the average power consumption is given by:

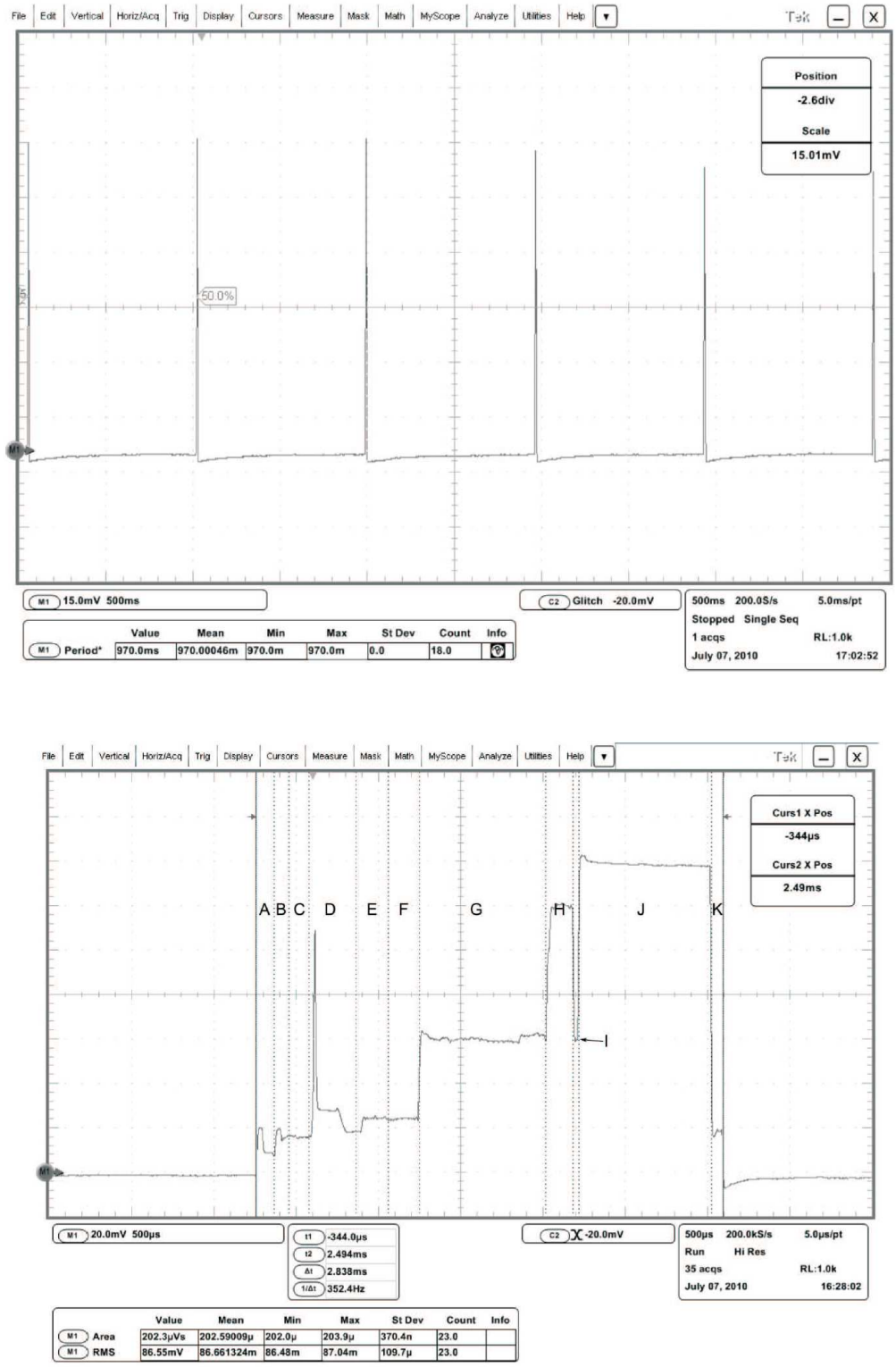

Figure 2.3: (top) Profile of application current drawn for five seconds, (bottom) current profile during a single application task (reproduced from [101]).

Table 2.2: Current consumption of different activities in application active mode shown in Figure 2.3 (bottom) (reproduced from [101]).

Radio Event	Current Consumed	Time Executed	Amps * Seconds Consumed
XOSC startup	2.7 mA[(1)]	300 µs [(1)]	810 nA*s
Ripple counter timeout	1.75 mA	150 µs	262 nA*s
Idle mode	1.5 mA	375 µs	563 nA*s
PLL calibration	7.5 mA	809 µs	6067 nA*s
RX mode	18.8 mA	180 µs [(1)]	3384 nA*s
TX mode	21.2 mA	800 µs [(1)]	16 960 nA*s
		Total	**28 047 nA*s**
MSP430 Event	**Current Consumed**	**Time Executed**	**Amps * Seconds Consumed**
MSP430 active current	2.7 mA	2.705 ms	7304 nA*s
MSP430 LPM0 current	1.1 mA	55 µs	61 nA*s
ADC10 active	850 µA	115 µs	98 nA*s
		Total	**7463 nA*s**
		Transmission Total	**35 508 nA*s**

(1) Estimated from oscilloscope measurement

$$3V \times \frac{1.3\mu A \times (1s - 2.838ms) + 12.511\mu A \times 2.838ms}{1s} = 3V \times 36.80\mu A = 110.4\mu W \tag{2.3}$$

In the given example, the average power consumption will increase if more sample transmissions are performed in a given interval. Depending on the desired application workload (sampling and transmission frequency), the resulting average power consumption can be used for the purpose of planning the supply and storage capacity of the harvesting subsystem [146, 59]. Using energy management, the knowledge of each application task's energy consumption can be used to decide the number of task executions within a given energy budget. The energy management policies discussed in Chapters 5 and 6 use the duty cycling approach for adapting the application workload energy consumption.

2.2.5 Energy Storage

The selection of the PV panel's nominal output power is an important consideration in the design since the long-term application demand can only be met with an appropriate supply capability. The role of energy storage is to smooth the fluctuations in supply by buffering excess energy and supplying it when PV panel output cannot meet the demand. The characteristics of the selected energy storage influences the overall design of the harvesting subsystem, especially the design of input and output power processing because of the constraints imposed by charging and discharging characteristics. On the other hand, energy harvesting systems also impose certain requirements on energy storage performance, as discussed in Section 2.2.2.2, which makes some storage types more suitable for use in energy harvesting systems. The commonly used types of energy storage applicable to design of compact and low-power energy harvesting subsystems can be broadly classified as rechargeable batteries and supercapacitors. Among the types of rechargeable battery chemistries, Nickelmetal hydride (NiMH), Lithium-ion

(Li-ion), Lithium-ion Polymer (Li-poly) and thin-film or solid-state Li-ion batteries are the most commonly used types of batteries for low-power portable devices [59, 53, 151, 157]. The following sections discuss the constraints and requirements according to the characteristics of interest for design of the energy harvesting subsystem and energy management.

2.2.5.1 Operating Voltage Range

This refers to the terminal voltage range of energy storage during charging and discharging states. Since the energy storage connects to both the PV panel and the load, the operating voltage range has to be matched with both the PV panel output and load. If this range falls outside the operating range of PV panel, the panel will not output any power while the load can be damaged or will not operate if the energy storage voltage exceeds or lies below its supply range. As mentioned in Section 2.2.2.1, this is an important consideration in efficient design of supply subsystem because matching the operating voltage involves using power converters (Section 2.2.7) which consume energy and add to system design complexity and cost. The operating voltage of rechargeable batteries is constrained by their chemistries, with NiMH cells having a range of 0.9-1.45V and 3.7-4.2V for Lithium cells from fully discharged to full charged states [11, 150, 149, 148, 152]. In case of supercapacitors, they can discharge down to 0V and can have a maximum voltage of 2.1-3V for a variety of different capacities [17, 35, 25]. Since a wireless sensor workload may demand a stable supply voltage, a high efficiency voltage regulator can be used to interface the workload to the energy storage. In case of the PV panel, it is possible to select a PV panel that eliminates the need for input power processing as explained in Section 2.2.6, however the very wide voltage range of supercapacitors require special considerations for input power interface design which are discussed in Section 2.2.7.2.

2.2.5.2 Capacity vs Physical Size

The physical size of the energy storage is a major constraint for a compact low-power system. The energy stored per unit weight is called the energy density and among the three main types of energy storages, Lithium batteries have the highest energy density followed by NiMH, while supercapacitors have the lowest as shown in Figure 2.4. The capacities of batteries, commonly denoted by C, are indicated in milli or micro Ampere hours (mAh or μAh). This rated capacity is obtained at a recommended nominal discharge current (Section 2.2.5.3) and at higher currents, the capacity usually decreases. NiMH cells are available in capacities up to 4000 mAh [98] while Li-poly are available in 2600 mAh [97] with dimensions close to standard AA sized batteries. Thin-film or solid-state Lithium batteries are currently available in very small capacities of less than 100μAh [53] and are only suitable for very low duty cycle operation. To obtain

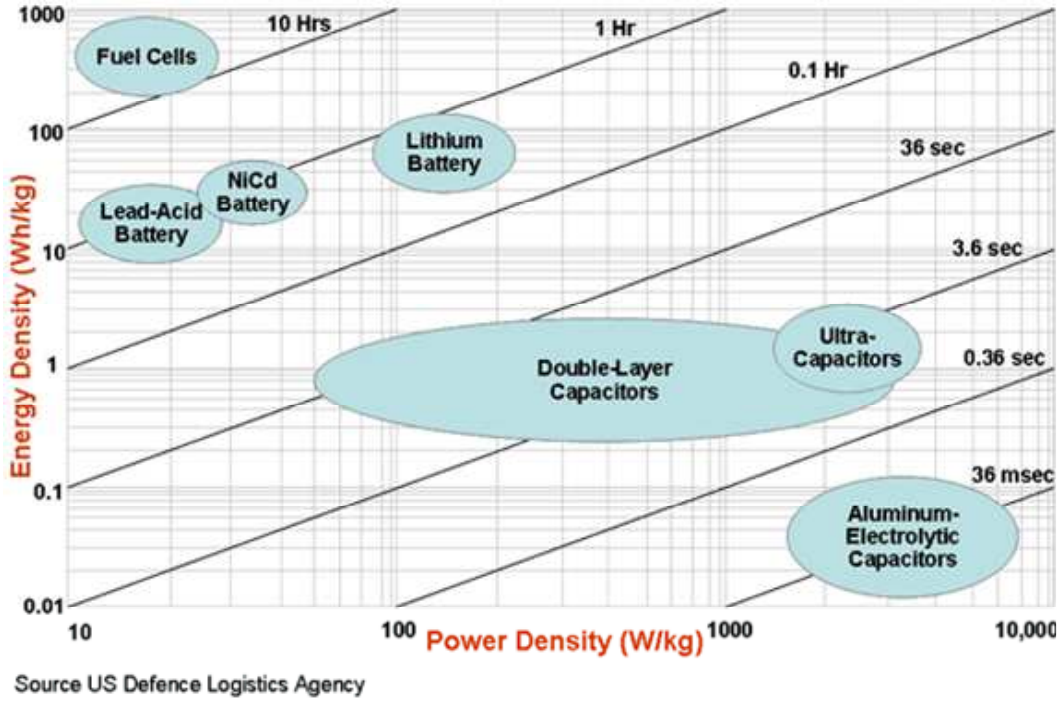

Figure 2.4: Comparison of energy and power densities of different energy storage types (reproduced from [115]).

the total energy in Joules or Watts-Hours, the capacity is multiplied by the nominal voltage:

$$E_{batt} = V_{nom} * C_{batt} \tag{2.4}$$

Note that due to the higher nominal voltage of Lithium batteries than NiMH for a given mAh capacity, Li-poly holds roughly 3 times more energy than NiMH. Supercapacitor energy capacities are specified in terms of their capacitance (C) values (Farads) and their maximum voltage (V) using the capacitor energy equation $E = 1/2CV^2$. For comparison, a Maxwell Technologies 3000F 2.7V supercapacitor weighs 0.51 Kg [164] and holds energy equivalent to a 2531mAh NiMH AA cell.

2.2.5.3 Charging and Discharging Characteristics

Energy storage devices have recommended charging and discharging current and voltage ranges which should be met for correct operation and preventing damage. These charging and discharging currents are usually a function of total capacity. For batteries, these are specified in terms of percent of the maximum capacity (C) in mAh. For example, for a 1000mAh battery, a 100mA charge or discharge current will be specified as 0.1CA. For NiMH and Lithium batteries, there is a normal and fast charging current [148, 152], with full charging times determined by the rate of current and indicated by the upper voltage

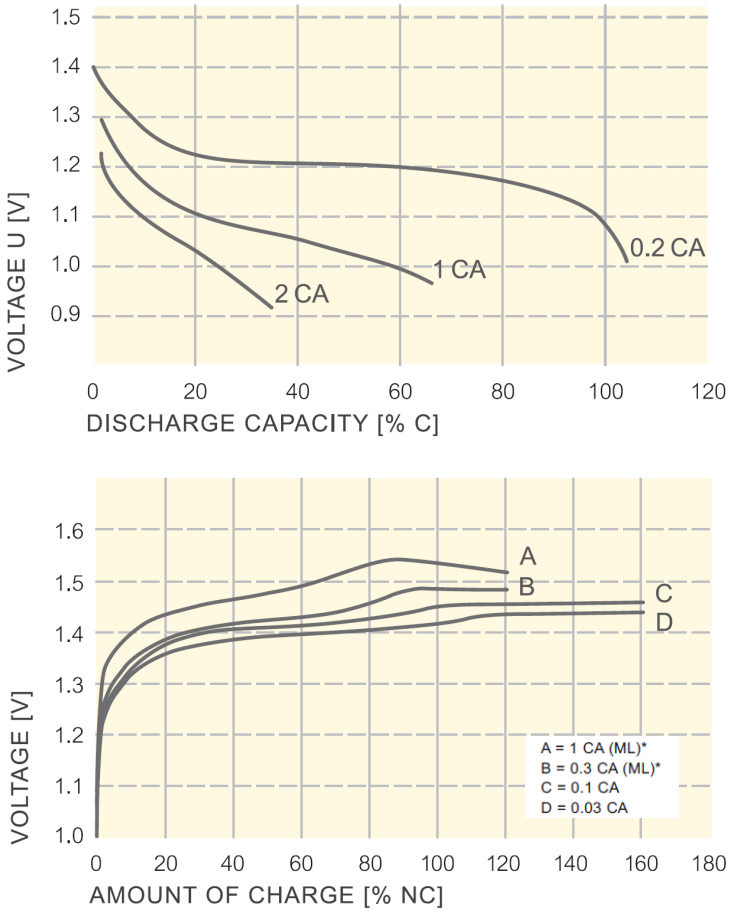

Figure 2.5: (Top) Typical discharge curves of NiMH Button Cells at various continuous loads at room temperature. (Bottom) Typical charging curves at various charging currents of NiMH High Rate Button Cells at room temperature (Reproduced from [96]).

limit [96]. The end of discharge condition is similarly indicated by a lower voltage cut-off beyond which batteries can be damaged. Commonly, the full capacity of the battery is obtained by using 0.2C discharge rate, and achievable capacity decreases at higher discharge currents. Figure 2.5 show the charging and discharging curves for Varta NiMH button batteries at different rates at room temperature. In case of supercapacitors, the allowed currents are much higher [35]. Lithium batteries have different charging requirements than NiMH requiring initial charge using constant current (CC) followed by a constant voltage (CV) as shown in Figure 2.6.

For the design of the harvesting subsystem, the maximum discharge current of the battery is not a major issue due to the small current draw (less than 100mA) of the load, which translates to 0.2CA rate for a 500mAh battery. The maximum charging currents are determined by the PV panel specification and varies according to the environmental conditions. The maximum current output of the PV panel should not exceed the recommended fast charging current of the battery to prevent damage. On the other hand, if the current output of the panel is less than C/50 or 0.033CA, called the trickle

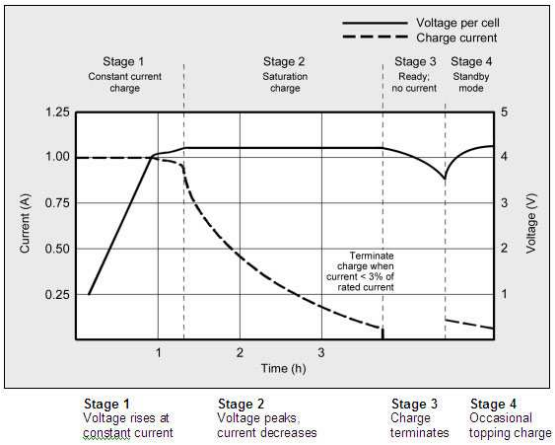

Figure 2.6: Different stages in fully charging a Lithium-ion battery (Reproduced from [152]).

charging rate, the batteries will not charge. Efficient design of energy harvesting systems demands that the variable harvested-energy inputs should be captured. Therefore, the energy storage should be matched to the PV panel current supply and vice versa to ensure high efficiency of energy capture. Supercapacitors can be charged at variable currents and thus do not have strict charging requirements of batteries. On the other hand, Lithium batteries are highly sensitive to both under and overcharge conditions and designing with Lithium batteries requires that these conditions should be carefully detected, mainly to prevent battery explosion risks due to overcharge.

2.2.5.4 Efficiency, Leakage, Lifetime and Stored Charge Measurement

The efficiency of charging determines how harvested energy is captured by the energy storage. A high efficiency is highly desirable since it implies that the energy storage can be replenished with less harvested energy. Lithium batteries and supercapacitors have reported charging efficiencies of greater than 90% while NiMH batteries have a 66% charging efficiency [157]. The leakage rate of stored charge is major factor if the stored energy has to be conserved for long periods, e.g., when harvested-energy input is scarce due to prolonged shortage. Lithium and NiMH batteries have low leakages [96, 97] while supercapacitors have relatively high self-discharge rate, which increases with both capacity and charged voltage [164, 131, 158]. The number of allowed recharge cycles is a major factor limiting the operational life of an energy harvesting subsystem. Rechargeable batteries typically have less than 1000 cycles while supercapacitors can endure a million cycles [17].

Accurate determination of the State of Charge (SoC) of energy storage is critical for practical realisation of energy management policies, however, this appears to be one of the fundamental challenges in energy harvesting systems for multiple reasons. Determining the SoC using battery voltage is a simple technique commonly used in low-cost

primary battery operated devices. This technique is not accurate because the battery voltage alone is not a sufficient indicator, as it is influenced by rate of discharge, relaxation effects, temperature, and aging effects [91]. In case of rechargeable batteries, voltage based determination of the SoC is further complicated by different profiles of voltage depending on charging or discharging states (Figure 2.5). An accurate method of determining the SoC is by tracking of energy charged in or discharged from the battery, commonly known as Coulomb counting [91]. The state-of-the-art off-the-shelf SoC determination ICs, called battery fuel gauges, use Coulomb counters along with other sophisticated algorithms to learn the battery capacity over multiple charge/discharge cycles and also compensate for different battery chemistries, aging effects and other factors in order to give an accurate estimate of SoC. However, as mentioned in Section 2.2.2.2, these fuel gauges are designed to measure the battery state under controlled charging and discharging conditions, while in energy harvesting supplies intermittent charging and discharging are quite common. Another problem is the low-power operating range of application workload in which case the current drawn between the sleep mode and radio transmission can vary as much as four orders of magnitude (Section 2.2.4) in a very short burst of activity lasting a few milliseconds [63]. This requires both a high rate of sampling the variations in current drawn as well as a high dynamic range of sampling [61, 34]. This requires high accuracy Coulomb counters, most of which are designed for Lithium-ion batteries commonly used in mobile and embedded devices. Supercapacitors are widely perceived [164, 131] as much simpler compared to batteries in their stored charge determination based on voltage monitoring and use of ideal capacitor formula. However, recent works [15, 158] have shown that supercapacitors exhibit non-ideal charging and discharging characteristics similar to batteries, and determination of stored energy and actual leakage is influenced by the recent history and pattern of charging and discharging. Despite of these issues in determination of SoC in energy harvesting storage subsystems, the commonly used approach is to rely on Coulomb counters in the case of batteries to monitor the charging and discharging [124], and terminal voltage in the case of supercapacitors to estimate their stored energy [164, 131].

2.2.6 PV Panel

For a given environmental energy, the size of PV panel determines the amount of harvested power as discussed in Section 2.2.3. A PV panel is constructed using series and/or parallel combination of individual PV cells [155]. The maximum (open circuit) voltage of each cell is determined by the type of cell and varies from 0.5-0.6V [58]. The maximum (short circuit) current is proportional to the area of cell. The series combination of PV cells increases the total terminal voltage while parallel combination adds up the currents of the individual PV cells.

(a) 60mm x 60mm PV panel with V_{MP}:1.92V, I_{MP}:200mA, V_{OC}:2.20V and I_{SC}:220mA (reproduced from [111]).

(b) 80mm x 45mm PV panel with V_{MP}:3.84V, I_{MP}:100mA, V_{OC}:4.40V and I_{SC}:110mA (reproduced from [112]).

Figure 2.7: Two PV panels with same area of 3600 mm^2 and maximum power output (384 mW) but different configurations of cells.

The output power of the panel depends on both environmental stimuli and its terminal voltage. The peak power output of a PV panel under a given irradiance level is specified in terms of optimal voltage and current, called the maximum power point. The I-V relationship is non-linear and shown in Figures 2.16 and 2.17 for two small size panels used in the design of the reference system. Different PV panels can provide the same maximum power but at different combinations of terminal voltage and current. For example, Figure 2.7 shows two PV panels with one on the left having a maximum power voltage V_{MP} of 1.92V and current I_{MP} of 200mA. It provides the same maximum power (400mW) as the panel on the right with V_{MP} of 3.84V and current I_{MP} of 100mA. One of these panels can be selected based on which has I-V characteristics that have a better match with the type of energy storage connected to the panel output. For example, if the PV panel on the left, with an open-circuit voltage of (V_{OC}) 2.2V, is connected directly with two series NiMH batteries (2.0-2.6V) via a reverse protection diode, the PV panel will not be able to supply any power since its output current is zero at 2.2V (V_{OC}). Even if the batteries are completely discharged to near 2.0V, the forward voltage drop of reverse protection diode will need to be overcome. On the other hand, if the 3.84V panel is used it will work across the whole voltage range of batteries, but the operating range of the panel will be below the maximum power point. It should be noted that these specified maximum power outputs of the PV panel and corresponding operating points are specified under standard test conditions (STC) which implies 1000 Watts per square meter of radiation; in practice, the output power is usually smaller and operating points shift to the left of I-V curve, depending on the input light conditions (Figures 2.16 and 2.17).

2.2.7 Input Conditioning and Output Voltage Regulation

Sections 2.2.5 and 2.2.6 discussed the selection of an energy storage device and PV panel for matched operation to ensure high efficiency while meeting the required demand. However, it may not be possible to completely match the I-V characteristics of workload, energy storage and PV panel, e.g., if the application workload components such as microprocessors and radio operating at 2.2V are connected to a Lithium battery with operating range of 3-4.2V, the energy storage voltage needs to be stepped-down over the full voltage range of Lithium batteries. As another example, since supercapacitors have a wide voltage range, the PV panel voltage may need to be restricted to ensure useful power output that is independent of the supercapacitor voltage. The following sections discuss the design considerations of power conversion circuits between energy storage and application load, and PV panel and energy storage.

2.2.7.1 Energy Storage - Load Interface

A voltage regulator is commonly used to supply a fixed voltage to the workload independent of the operating voltage range of the energy storage. A buck, boost or buck-boost converter is required depending on the type of energy storage used and the required workload voltage. For example, a Texas Instrument ez430-RF2500 wireless board requires 3.3V to operate at 16 MHz clock. If two series NiMH batteries are used for energy storage with possible voltage range of 1.8-2.9V, then a boost converter is needed with a minimum input voltage of 1.8V to output 3.3V. If a supercapacitor with maximum voltage of 2.7V is used as energy storage, then a boost converter with lower cut-off voltage (e.g., 0.3V) will allow maximum utilisation of supercapacitor stored energy. On the other hand, use of Lithium battery (3.6-4.2V) will require a buck or buck-boost converter, depending on exact type of Lithium battery. The cost of using the output regulator is the sub-unity efficiency that is a function of input voltage and output currents as shown in Figures 2.8 and 2.9 for two different 3.3V boost converters by Texas Instruments. Note that the variations in efficiency of power conversion in terms of input voltage and output current differs with the type of regulator used and can be highly non-linear. In the efficiency relationships shown in Figures 2.8 and 2.9, the efficiency increases with increase in input voltage and output current, however, a sudden drop in efficiency is observed with increase in output current beyond a certain value, especially with low input voltage. Since the efficiency of output regulation influences the energy consumed by the application for a given energy budget, this must be taken in to account during energy management to ensure that demand and supply are matched. Chapter 4 considers the modeling of this efficiency and in Chapter 5 the influence of this is shown on energy management policies.

The battery over-discharge protection circuit may also be considered part of energy storage load interface since it can be used to shut down the output voltage regulator

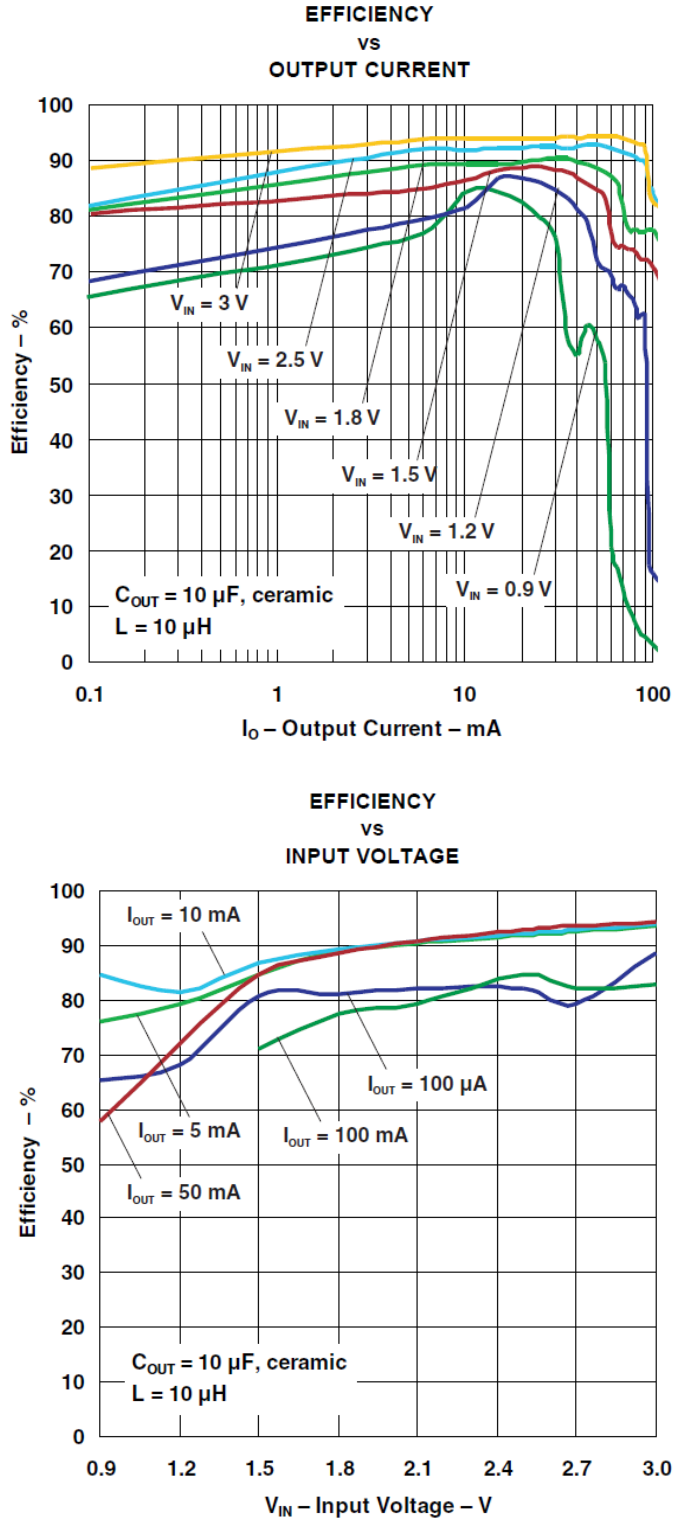

Figure 2.8: Efficiency of TI TPS61097 3.3V boost converter as functions of input voltage and output current (reproduced from [56]).

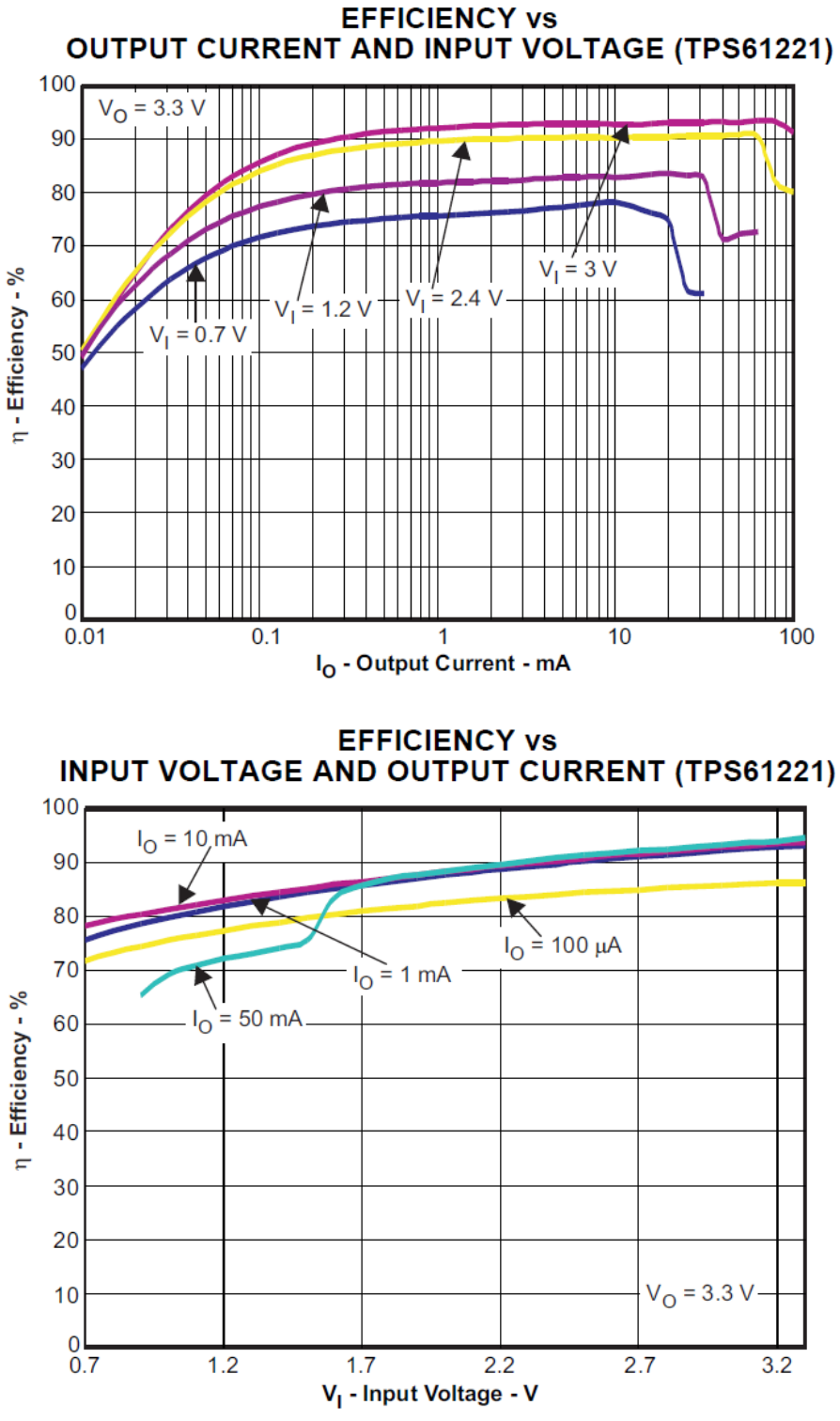

Figure 2.9: Efficiency of TI TPS61221 3.3V boost converter as functions of input voltage and output current (reproduced from [57]).

or put the load in suspended (very low-power) state depending on the cut-off voltage limit for over-discharge protection. Similar arrangement is also needed to cold start from a depleted supercapacitor since the output regulator can draw a large current to start-up causing the supercapacitor voltage to fall below the threshold, thus preventing the regulator from starting up at all. Cold start designs are proposed in [164, 22].

2.2.7.2 PV Panel - Energy Storage Interface

The PV panel and energy storage (rechargeable battery or supercapacitor) interface can typically include reverse current flow protection, charging controller and maximum power point tracking circuits. The simplest of this interface includes a reverse current protection diode, which prevents energy storage from forcing current into the PV panel under low illumination conditions but adds a diode voltage drop (exact value depends on diode type) between the PV panel and energy storage. This simple interface can be sufficient and even efficient in the case where the PV panel nominal operating voltage range falls a diode drop above the operating voltage range of energy storage. On the other hand, the PV panel will not be able to output any power in the limiting case if the PV panel nominal voltage range falls completely below the voltage range of energy storage plus the diode drop. Hence, this arrangement is suitable for systems that are able to select a PV panel or energy storage accordingly. As discussed in Section 2.2.5.1, the voltage range of energy storage devices, especially batteries is fixed and depends on the chemistry of battery. Supercapacitors have some flexibility in this regard since they have a wide operation range. On the other hand, a PV panel voltage range is determined by the number of PV cells in series and PV panels are available in a larger variety for similar output power as discussed in Section 2.2.6. The PV panel can be selected to satisfy the condition of voltage range match. If this is not possible, then some type of voltage conversion circuitry is required, which increases the design complexity and introduces losses in the path, that are inherent in power conversion circuits.

Another circuit block that can be part of the PV panel and energy storage interface is charging control or current/voltage limiting to prevent overcharge or to supply a constant current or voltage for charging, if the energy storage requires it. For example, the proper charging of Lithium-ion (polymer) battery requires a constant current and later constant voltage charging arrangement. On the other hand, NiMH batteries can be charged with a range of currents ranging from 0.033CA to 0.3CA [96], but overcharge detection and termination is required to prevent battery damage. In this regard, supercapacitor have the maximum flexibility in terms of charging currents while Lithium batteries need a careful charging arrangement to prevent risk of explosion due to overcharge [152].

Besides the blocks mentioned, the maximum power point tracking (MPPT) block can also be part of this interface. In case of low-power harvesting supplies, the main concern is the efficiency of this block and a number of implementations have been proposed. It

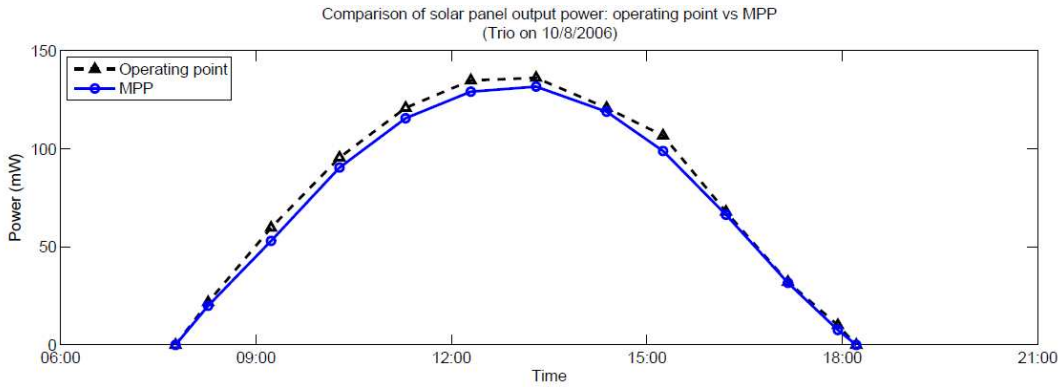

Figure 2.10: Comparison of solar panel output power: operating point vs MPP (reproduced from [59]).

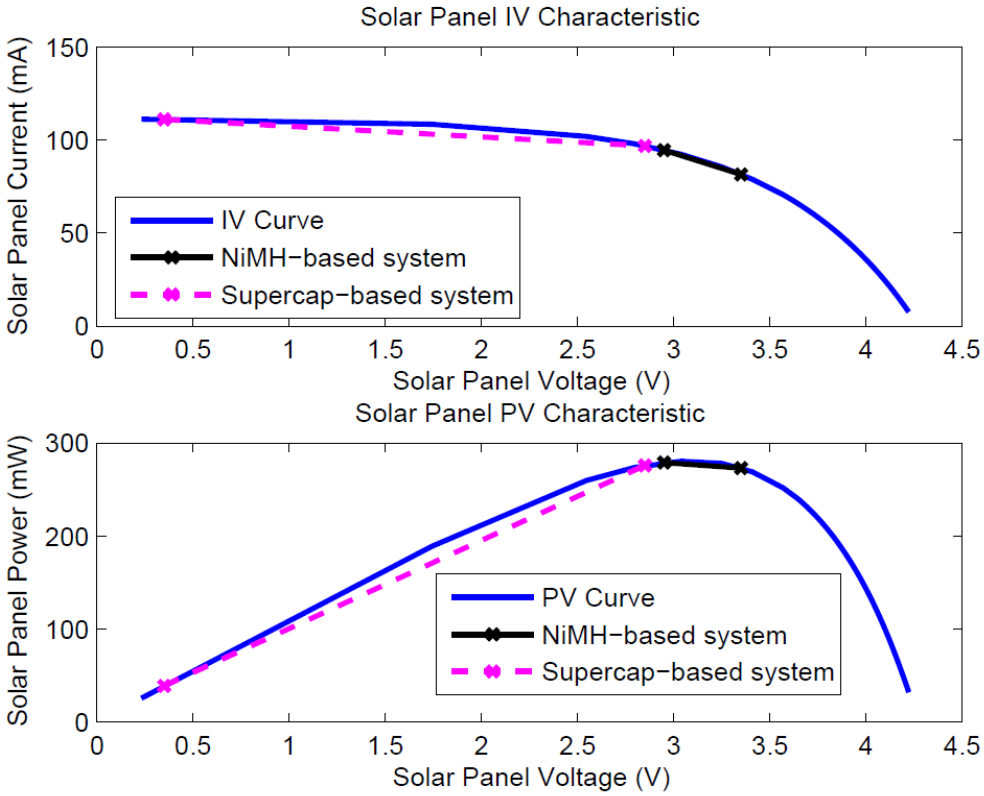

	2AA NiMH	**22F supercap**
V_{stor}	2.6V to 3.0V	0V to 2.5V
V_{sol}	2.95V to 3.35V	0.35V to 2.85V
P_{sol}	272.9mW to 280.4mW (97.3% to 100% of MPP)	38.8mW to 275.7mW (13.9% to 98.3% of MPP)

Figure 2.11: Operating range of PV panel: a system with direct connection between PV panel and energy storage (reproduced from [59]). V_{stor} is energy storage voltage, V_{sol} is PV panel voltage, and P_{sol} is the output power of PV panel.

has also been shown that in some cases, the benefit gained from MPPT is marginal as shown in Figure 2.10 especially if the PV panel can operate near to its maximum power point by using a matched connection as discussed in Section 2.2.6. In this case, the use of MPPT is only beneficial if the gain achieved is greater than power consumed by the MPPT circuit [59]. On the other hand, when using a supercapacitor the resulting voltage swing as a supercapacitor fully discharges or charges can make the PV panel deviate greatly from its near maximum power operating point as shown in Figure 2.11. In this case the MPPT block can ensure that PV panel operates close to its maximum. A number of MPPT blocks specifically designed for supercapacitor based harvesting systems have been proposed [141, 15]. With a fully discharged supercapacitor, another issue is 'cold-booting' where the depleted supercapacitor doesn't allow the PV panel to charge up the supercapacitor. A pulse based charging circuit is proposed in [141] that allows the rapid charging of a supercapacitor compared to direct charging.

2.2.8 Measurement of System Energy Flows

Besides the energy supply and storage components, support for measurement of various energy values is required by harvested-energy management to adapt consumption according to supply. This includes measurement of harvested energy being supplied to the energy storage and load, stored energy in battery or supercapacitor, and energy consumption. This can be achieved using measurements of currents and voltages associated with supplied and consumed energy flows, and by monitoring the terminal voltage and/or charge drawn from energy storage. For obtaining the energy value over an interval, the power needs to be measured periodically and averaged. The on-board ADC of the sensor node can be used to sample voltages such as the PV panel output voltage and the energy store voltage. Since the voltage and current can both vary, current measurement is also required to calculate the power or energy. The common approach [124, 146, 165] is to use a small value current sense resistor and measure the voltage drop across it to obtain the current flow. In case of small voltages, a current sense amplifier may be used [146, 137]. Furthermore, measurement of this voltage drop may be done with high-side or low-side sensing which implies either a differential voltage is measured or the sense resistor is connected between negative terminal and ground (single ended voltage). Accuracy of measurement is an important issue and slow changing currents such as PV panel currents can be measured easily using this approach. However, the current consumption of application workload can have high a dynamic range [61, 33] since the difference between active currents (0.5-20 mA) and sleep mode currents (few μA) can easily be 10^4 (Section 2.2.4). Furthermore, the application activity can involve fast changing current draws in a short burst as shown by example in Section 2.2.4. This requires use of a high sampling rate and high dynamic range of ADC. Use of dedicated ICs is a possible solution [61] but these ICs can consume quiescent current which can be higher than the sleep mode current of application workload, thus resulting in noticeable

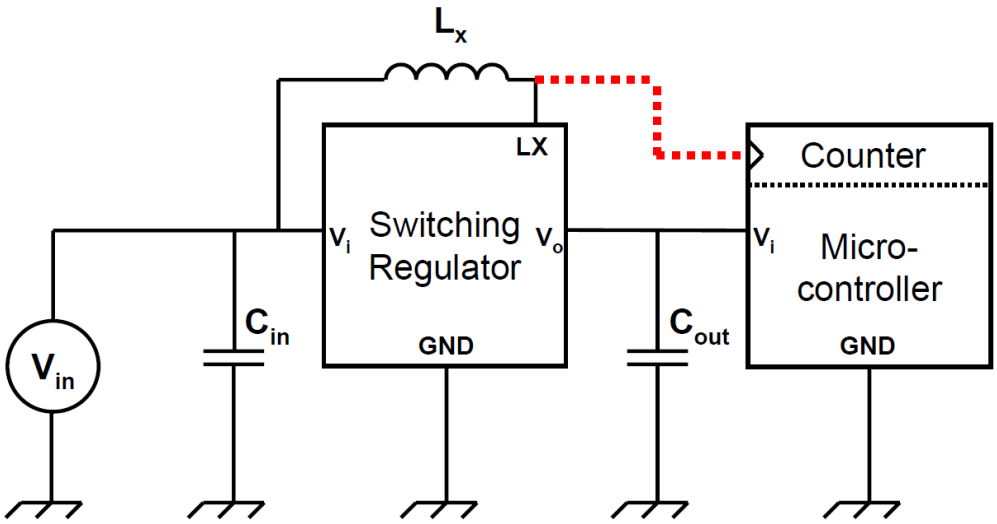

Figure 2.12: Implementing load current measurement by measuring the switching pulses of regulator (reproduced from [33]).

overheads [61]. Dutta et al. [33] proposed a low-overhead method of monitoring the workload current consumption based on counting the switching frequency of a Pulse Frequency Mode (PFM) switching regulator using the integrated timers of wireless sensor node microcontroller as shown in Figure 2.12. However, this method has a strong dependency on the input voltage changes of the switching regulator [33] as shown in Figure 2.13. This makes it ineffective to use in energy harvesting systems because the continuous fluctuations in energy storage voltage due to intermittent charging and discharging makes it difficult to correlate the measured frequency and input voltage. A simple but low-accuracy alternative is to use models of application workload activity, such as duty cycling [154, 165, 131, 59], to approximate its power consumption.

2.3 Design of Reference Photovoltaic Energy Harvesting System

In this section, the design of the reference PV energy harvesting and storage subsystem is discussed in light of design considerations and choices discussed in Section 2.2. This reference system configuration (Figure 2.14) is used in Chapter 4 for obtaining empirical results for validation of system modeling. The system model based on this configuration is referenced in Chapters 5 and 6 for evaluation of energy management policies. This selected system configuration focuses on design simplicity while optimising the transfer of power from the photovoltaic panel to the application workload. Measurement support of key power flows is also provided. The detailed schematic and component data are given in Appendix A. Figure 2.15 shows the PCB with a wireless sensor node attached. The following sections describe the design details in terms of power supply (PV panel,

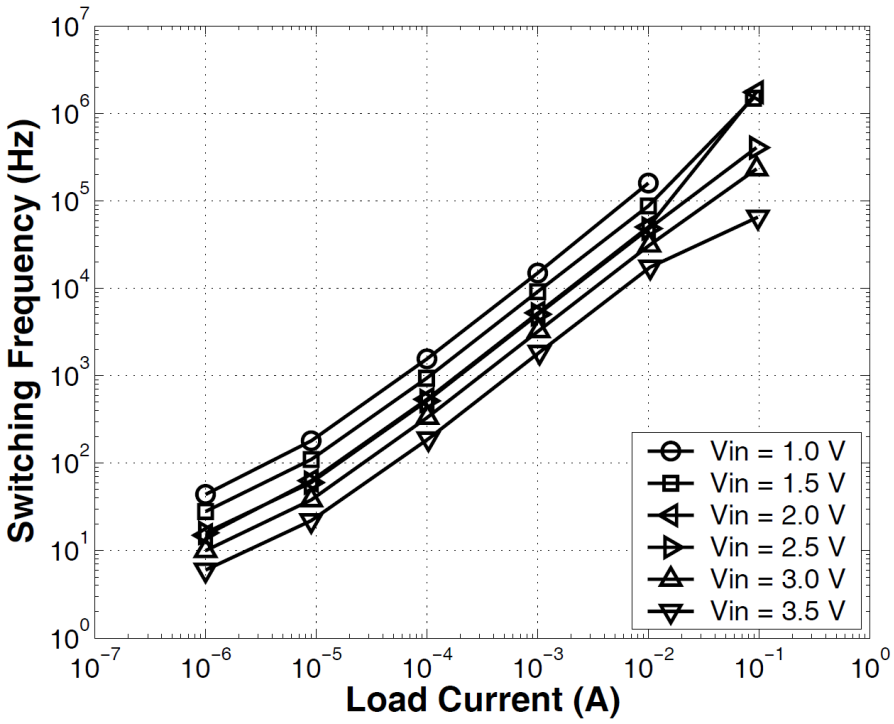

Figure 2.13: The relationship between switching frequency and load current for MAX1724 regulator according to different input voltages (reproduced from [33]).

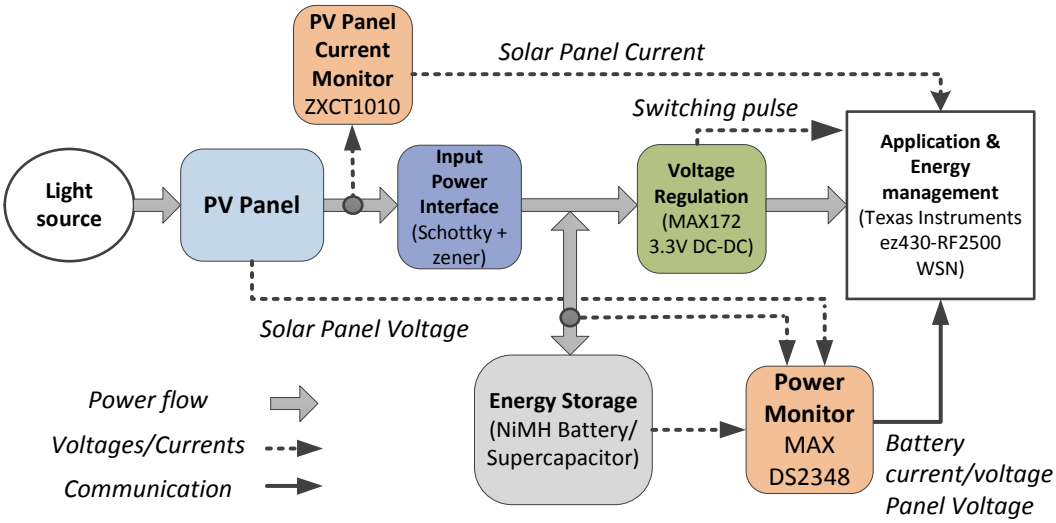

Figure 2.14: System implementation for validating case studies.

input power interface and energy storage), power consumption (voltage regulation and application workload) and power measurement support.

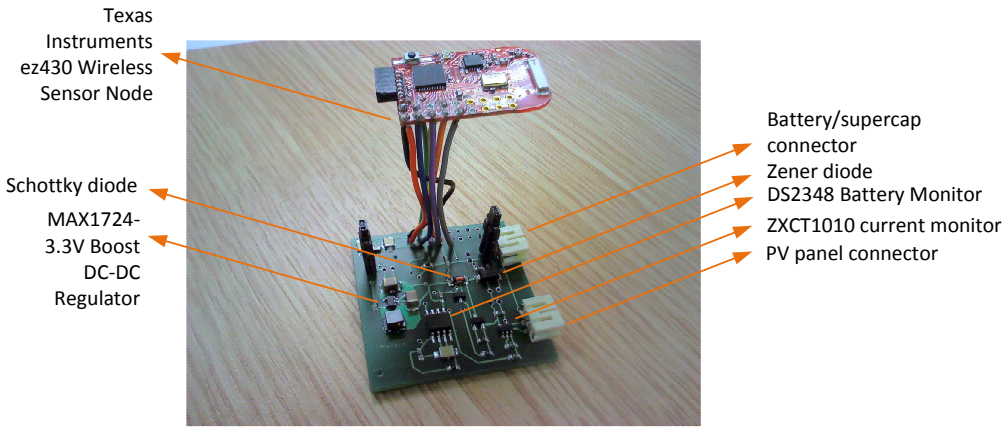

Figure 2.15: Reference energy harvesting system with labels indicating main components.

(a) A monocrystalline silicon 60mm x 60mm PV panel supplied by MUTR (reproduced from [116]).

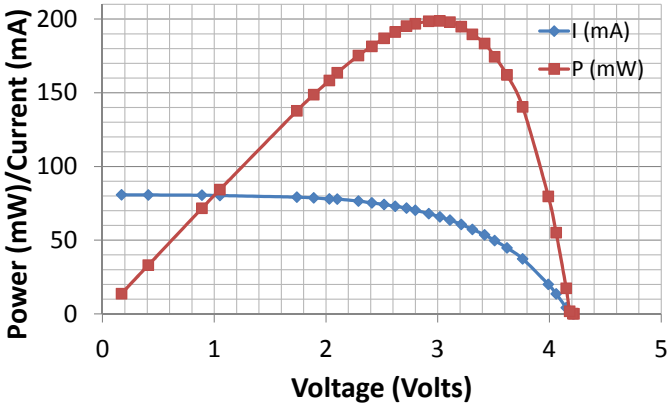

(b) Measured power output versus voltage curve under clear summer mid-day conditions at Southampton.

Figure 2.16: Smaller of the two panels selected for reference system configuration.

2.3.1 PV Panel, Input Power Interface and Energy Storage

The PV panel, energy storage and the power transfer interface in between are considered together due to the interdependency between selection of these parts of the design. As discussed in Section 2.2.7.2, the role of input power processing depends on the selected energy storage charging requirements, PV panel and energy storage I-V characteristics and the need for maximum power point tracking. Therefore, if the PV panel and energy storage are selected so that the I-V characteristics are matched to a large extent and the energy storage has simple charging requirements, then the complexity of input power interface can be reduced as well as the associated losses. This principle motivates the selection of PV panel and energy storage device for the reference system configuration. As discussed in Section 2.2.5, the energy storage terminal characteristics can guide the

(a) A BP SOLAR - MSX-005F polycrystalline silicon 80mm x 148mm PV panel (reproduced from [143]).

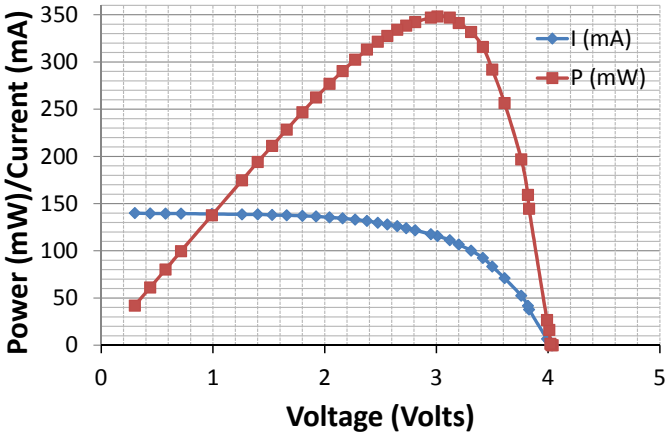

(b) Measured power output versus voltage curve under clear summer mid-day conditions at Southampton.

Figure 2.17: Larger of the two panels selected for reference system configuration.

selection of suitable PV panels. Therefore, instead of using maximum power point tracking circuit, the power transfer from PV panel is maximised by matching the nominal operating ranges of PV panel and energy storage [60, 83]. This simplifies the design and bypasses input power conditioning inefficiency, which is a function of circuit design, energy storage voltage and output power of the solar panel (illumination conditions) [141]. Use of an MPPT circuit was avoided because off-the-shelf solutions are not available. Most MPPT circuit designs proposed in the literature are highly customised for the particular PV panel used [141, 15], so implementing these and ensuring their correct operation would have been time consuming.

For energy storage, two options are selected: either two NiMH batteries in series with a combined voltage in the range of 1.8 (fully discharged) to 2.9V (fully charged), or a 2.7V 100F supercapacitor [35]. Both NiMH batteries and supercapacitors have relatively simple charging requirements. In case of NiMH batteries, the main consideration is that the charging current should not be higher than the fast charging current to prevent damage, which is typically 0.3C of rated maximum capacity [153]. For example, for a 1000mAh battery this value is 300mA while for a 250mAh battery this is 75mA. Overcharge protection is also needed, which is implemented based on a maximum voltage threshold using a Zener diode in parallel with energy storage with breakdown voltage of 2.9V. Protection of reverse current flow from the energy storage to the PV panel under low light conditions is required and is implemented using a Schottky diode (Figure 4.6), which adds a diode voltage drop of 0.37-0.6V between the energy storage and battery depending on the current transferred (20mA-200mA).

Based on the voltage ranges of the energy storage, two PV panels were selected and their

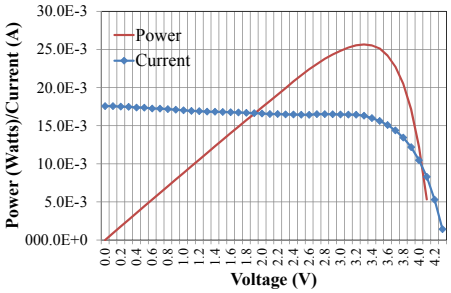

(a) 60mm x 60mm PV panel output.

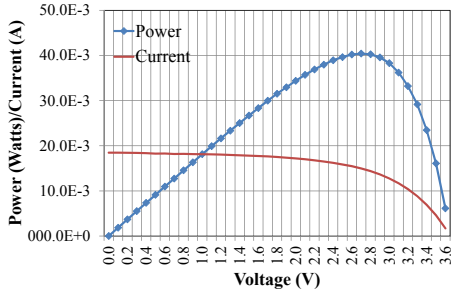

(b) 80mm x 148mm PV panel output.

Figure 2.18: P-V and I-V curves of two tested panels under well lit indoor conditions.

I-V and P-V curves are shown in Figures 2.16 and 2.17 under sunny outdoor conditions (in Southampton). The smaller panel (60mm x 60mm) delivers 200mW (3V@66mA) of maximum power while and larger panel can deliver 350mW (3V@116mA). Note that the maximum power voltages of these panels are close to 3V under these conditions, while up to 20% reduction in output power occurs as the operating voltage is decreased from 3V to 2V. Thus, the selected PV panels can operate within 20% of their MPP with 2 NiMH batteries in series, with the exact output determined by the voltage of battery. It should be noted that under lower illumination conditions, the MPP shifts to the left (i.e., less than 3V). In the extreme case of low illumination, the panel operating voltage can fall below the energy storage voltage, resulting in no energy harvested. However, it was found that these panels were still able to harvest power under well lit indoor conditions under the given range of voltages as shown in Figure 2.18.

The design of this input stage involves two tradeoffs. First, the elimination of MPPT circuitry decreases the complexity of prototype system development and eliminates any associated losses, however, when using supercapacitor as energy store the wide range of supercapacitor voltage change with stored energy change can lead to wide fluctuation in harvested-power from PV panel (Figure 2.11). This implies that the harvested power for a given input light intensity can vary depending on the supercapacitor voltage. One consequence of this for energy management is that the accuracy of harvested-energy prediction is affected (Chapter 3) since the actual harvested-power is no longer a function of input light intensity. The effect of this behaviour is discussed in Chapter 5 and 6 when evaluating energy management policies. The next tradeoff is selection of NiMH batteries instead of more efficient Lithium-ion batteries. While this reduces the complexity of PV panel-energy storage interface design because of the use of simple variable rate charging, the losses in the system are increased due to the lower efficiency of NiMH batteries. These losses need to be considered in energy management policy design. This tradeoff was considered reasonable in light of safety issues in case of improper charging of Lithium-ion batteries as compared to NiMH batteries. Furthermore, the dedicated charging circuitry involve power conversion circuits which clearly have sub-unity efficiencies.

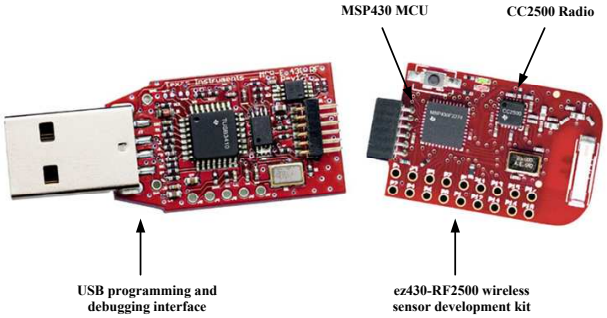

Figure 2.19: Texas Instruments ez430-RF2500 wireless sensor kit with USB debugging interface attached (adapted from [136]) The MSP430 microcontroller unit (MCU) has an on-chip 10-bit ADC.

2.3.2 Application Workload and Voltage Regulation

A Texas Instruments ez430-RF2500 wireless sensor node (Figure 2.19) [52] containing a Texas Instruments MSP430F2274 microcontroller and Chipcon CC2500 RF transceiver is used as the application workload due the to ease of programming in the C language and the availability of library of common routines. The MSP430 MCU has a multichannel 10-bit ADC which can be used to sample voltages for monitoring of power as discussed in the next section.

The voltage supply to the sensor node is fixed to 3.3V by using a Maxim 1724 boost DC-DC converter [48] (Figure 2.14) in the supply subsystem. The efficiency of the regulator is a function of both current drawn and supply voltage and it has efficiencies of greater than 50% over the range of typical currents drawn by ez430-RF2500 as shown in Figure 2.20. Also, it can operate at lowest input voltage of 0.91V, which is an important feature when using supercapacitors since supercapacitors can be discharged down to 0V and but the useable energy of supercapacitors is limited by lowest input voltage of the regulator. Although, other regulators could have been selected such as those discussed in Section 2.2.7.1, the choice of this regulator was also driven by the need to experiment with low-overhead power monitoring of application workload as described in [33]. This is discussed further in the next section.

2.3.3 Power Measurement Support

This reference system design caters to power monitoring requirements for implementing harvested-energy management by using additional components besides the harvesting subsystem. A ZXCT1010 high-side current monitor [137] is used to monitor PV panel's output current by converting the current flow to a single-ended voltage drop across a 2Ω sense resistor. The on-board 10-bit ADC of the ez430-RF2500 is used to sample this voltage to measure the PV panel current. The battery and PV panel voltages can also be monitored using the on-board ADC. A Maxim DS2438 battery monitor [90] is

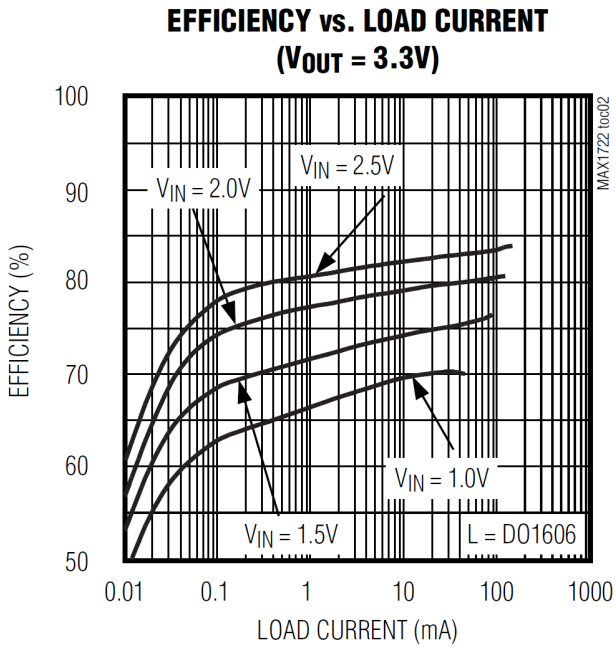

Figure 2.20: Efficiency of MAX1724 regulator from datasheet with output voltage 3.3V (reproduced from [48]).

used as a Coulomb counter to measure the net charge going in/out of the NiMH battery besides other variables, as indicated in Fig. 2.14. With the aim of measuring the average current drawn by the application workload using the low-overhead technique in [33], the switching pulse output of MAX1724 is connected to the Timer A input of MSP430. However, this technique was found to be impractical for measuring the application's energy consumption because of the difficulty in continuously correlating the fluctuating energy storage voltage (input voltage of the MAX1724) with the measured switching frequency. To estimate the application energy consumption, the model of application activity is used with corresponding values of current draws measured off-line using an oscilloscope or high-fidelity multimeter, such as the average current drawn in idle and active modes of the ez430-RF2500 wireless sensor node.

2.4 Concluding Remarks

Since the energy management implementation is dependent on the characteristics of harvesting system components, Chapter 2 discussed the design consideration in selection and integration of these components from the aspect of the efficient realisation of a harvesting subsystem. The concepts of harvesting supply subsystem design discussed in this chapter are referenced in Chapter 4 that discusses modeling of system components, and in Chapters 5 and 6 which consider effective design of harvested-energy management policies. This chapter also described a reference photovoltaic energy harvesting system

implementation that is used as a concrete example for system modeling validation in Chapter 4 and evaluating harvested-energy management policies in Chapters 5 and 6.

Chapter 3

Effective Short-Term Solar Harvested-Energy Prediction

As outlined in Chapter 1, energy harvesting presents different set of system design choices than battery powered electronic systems. Compared to a battery powered supply the amount of energy available is not limited, but unlike a tethered power supply, the amount of energy available at different times can vary and may not be completely predictable. The variability in harvested-energy supply is a challenge in system design since it is difficult to guarantee that the system's energy consumption demand is matched with harvested-energy supply at all times to achieve perpetual operation with maximum performance. An energy buffer (battery or a supercapacitor) can only smooth the effect of these variations on the application workload [146] but to match consumption with supply requires that consumption should be adapted according to available energy [102, 65, 113, 103, 154, 39]. The capability to predict future energy incomes enables designing energy management policies that can schedule energy consumption of the application workload in such a manner that utilisation of incoming energy can be maximised while ensuring that total consumption does not exceed the supply [102, 65, 113, 103, 39]. Such policies can prevent wasted energy due to undesirable overflow of energy storage and also prevent unexpected depletion of stored energy resulting in complete shutdown of the system. This has been termed in literature as 'energy neutral' mode of operation [65, 154].

The purpose of harvested-energy prediction is to know how much energy will be harvested in a certain period in future. This is different from knowing how much energy is stored at present, as commonly used in battery powered systems to determine system lifetime. In general, the combined knowledge of future energy harvesting and stored energy can be used to adaptively schedule an application workload and this will be discussed in Chapter 5 and 6. The manner in which the predicted energy knowledge is utilised in an energy harvesting application depends upon the optimisation objective.

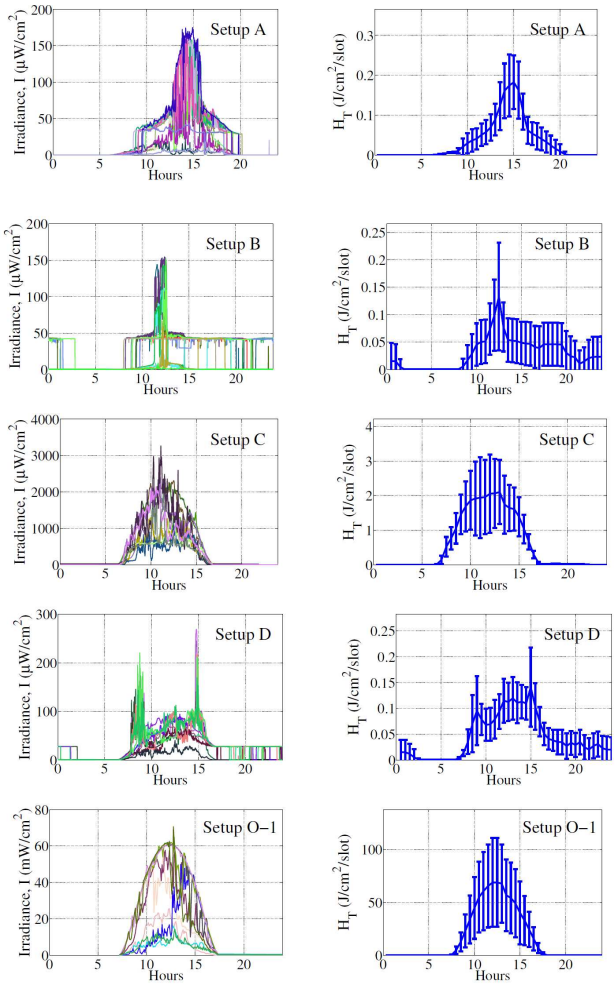

Figure 3.1: Sample profiles for outdoors (Setup O-1) and indoors (Setups A-D) locations receiving solar energy. The graphs on left show measurements from different days overlayed, while graphs on right show average and standard deviation (Reproduced from [39]).

For example, in [65] the knowledge of total expected energy in a day is used to calculate the maximum budget while the knowledge of specific time slots in a day is used to increase efficiency of energy utilisation in a system with lossy energy storage. In [129, 119], the expected time to harvest a given amount of energy is used to decide when to schedule tasks having a certain consumption requirement. In [103, 39], the knowledge of future energy is used to allocate energy in uniform manner while preventing underflow.

As discussed in Chapter 1 (Section 1.3), this thesis focuses on solar energy harvesting systems. The amount of solar energy received at different times in a day and across days can vary significantly as shown in Figure 3.1. To manage this variability, this chapter focuses on effective short-term prediction of solar harvested-energy within a day based on historical data. State-of-the-art research in solar energy prediction with low resource requirements is considered in detail and the best approach is identified. The main contribution of this chapter is a systematic approach for parameters evaluation of solar

energy prediction algorithm to empirically determine the achievable accuracy and implementation overhead. This is achieved by using an effective error evaluation technique to evaluate the algorithm performance with different sizes of prediction intervals. Based on evaluation results, guidelines are given for prediction algorithm parameter selection to ensure high accuracy across different real solar energy profiles. The prediction algorithm computation overhead is determined using measurements on the reference wireless sensor platform (Chapter 2). Harvested-energy management can also utilise long-term prediction (a day or more ahead) depending on the approach [106]. However, accurate long-term prediction is not achievable using historical harvested-energy data only due to the influence of multiple weather effects [59]. Appendix B reviews possible approaches to long-term solar energy prediction for wireless sensors based on weather forecasts [140] and history of weather effects [59]. Also, a low-overhead generic prediction approach that can be used for prediction of other energy sources is reviewed in Appendix B.

The chapter is organised as follows. Section 3.1 mentions key considerations for implementation of harvested-energy prediction, Section 3.2 discusses characteristics of solar radiation, and Section 3.3 discusses low-overhead prediction approaches for solar energy harvesting. Section 3.4 discusses parameters evaluation of short-term solar harvested-energy prediction algorithm and Section 3.5 concludes the chapter.

3.1 Key Considerations for Harvested-Energy Prediction

Prediction Error The utility of any energy management decision making is dependent upon the accuracy of prediction outcomes. In context of energy harvesting, an over estimation of future energy can lead to depleted energy storage and ultimately disruption of system activity. On the other hand, an underestimation can result in poor utilization of harvested-energy once the energy store is full and further energy cannot be stored.

Although a large average error will in general lead to poor performance, the requirement of an acceptable average error depends upon an application's objectives. For example, if the the prediction algorithm is able to track the energy source in a manner that the effect of under and over estimation are neutralised over a short interval of time, it is possible that the application load can utilise the harvested energy without incurring shortages or overflow of energy stored.

Length of Prediction Slot and Horizon The interval over which the energy is being predicted is termed as the prediction slot. The distance of this slot from current time is called the prediction horizon. For example, if the energy is being predicted over one hour then the prediction slot is 1 hour, and if this is two hours ahead from current time then the horizon is two hours. In short-term prediction, the energy is predicted over the next slot (horizon is zero). In general, the accuracy becomes

poor as the prediction slot increases as shown in Section 3.4. The simple techniques discussed in Section 3.3 can achieve reasonable accuracy for short predictions slots, while long-term prediction requires different approach to obtain acceptable error as discussed in Appendix B.

Implementation Cost Most energy harvesting applications are wireless sensor nodes that have limited computational resources, specially memory. Even if the available memory is not a limitation, the overhead in terms of energy consumed for prediction computations can be an issue if the prediction activity significantly increases an application's energy budget. Hence, it is highly desirable that these overheads should be minimised.

Measurement Support and Prediction Error Feedback The predicted value uses history of measurements of actual energy received. Any error in measurements carries over to prediction outcomes. Depending upon harvester type, accurate measurement of incoming energy can require sampling of harvester's voltage and/or current at a certain resolution that is sufficient to capture the variations in harvester's output. This requires dedicated circuitry and analog-to-digital conversion of sampled values of current and voltages. Furthermore, to implement closed loop control, the prediction error needs to be tracked [65]. The ability to do this is also dependent on fidelity of energy measurement support. Chapter 2 (Section 2.2.8) details the system support for measurement of harvested-energy.

3.2 Characteristics of Solar Energy

Solar radiation follows a well defined diurnal cycle and under clear sky (sunny) conditions the amount of radiation during a day can be predicted accurately using models such as the scaled astronomical model described in [59] based on angle of inclination of the PV panel with respect to sunlight, the time of the day, day of the year, location (latitude) and attenuation factor. Figure 3.2 shows the trends of solar radiations at a fixed location at four different times of the year under ideal conditions. It is evident that the maximum amount of solar radiation and its duration during a day depends on time of the year. The weather effects such as the movement of cloud, atmospheric turbidity etc. [59] affect the actual radiation conditions at different times of the day and across days. Figure 3.3 shows the measured radiation values at 10am for nearly 1200 consecutive days. It can be seen that besides the slowly changing trend due to seasonal changes over a year, as also shown in Figure 3.2, there is a significant random variation across consecutive days due to atmospheric factors, which makes it difficult to accurately predict the future harvested-energy based just on the knowledge of ideal conditions. Since these atmospheric factors depend on current local weather, the prediction accuracy can be improved by taking

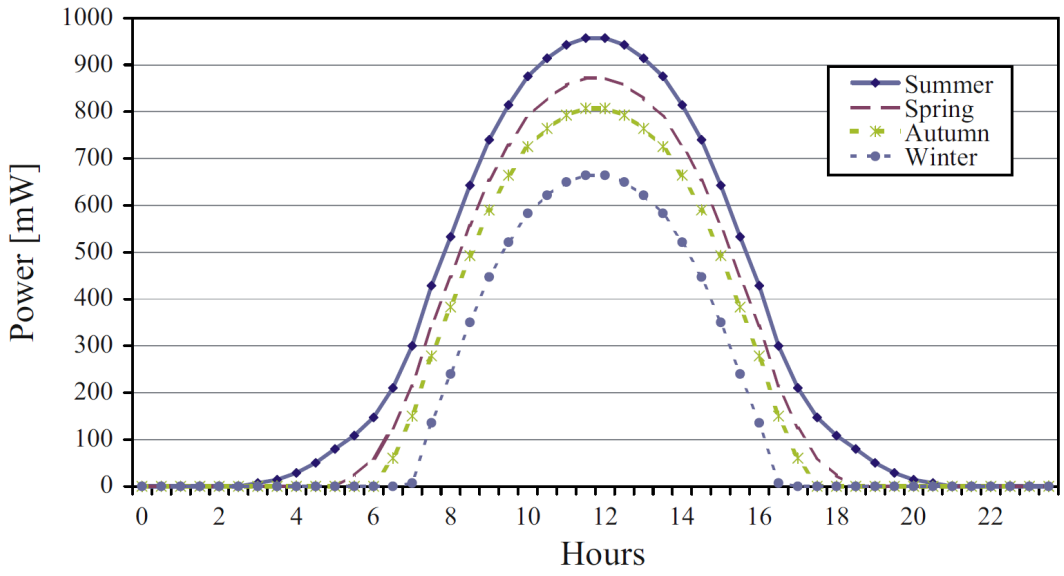

Figure 3.2: Power output of solar panel over a day under clear (ideal) conditions during different seasons in a year (Reproduced from [12]).

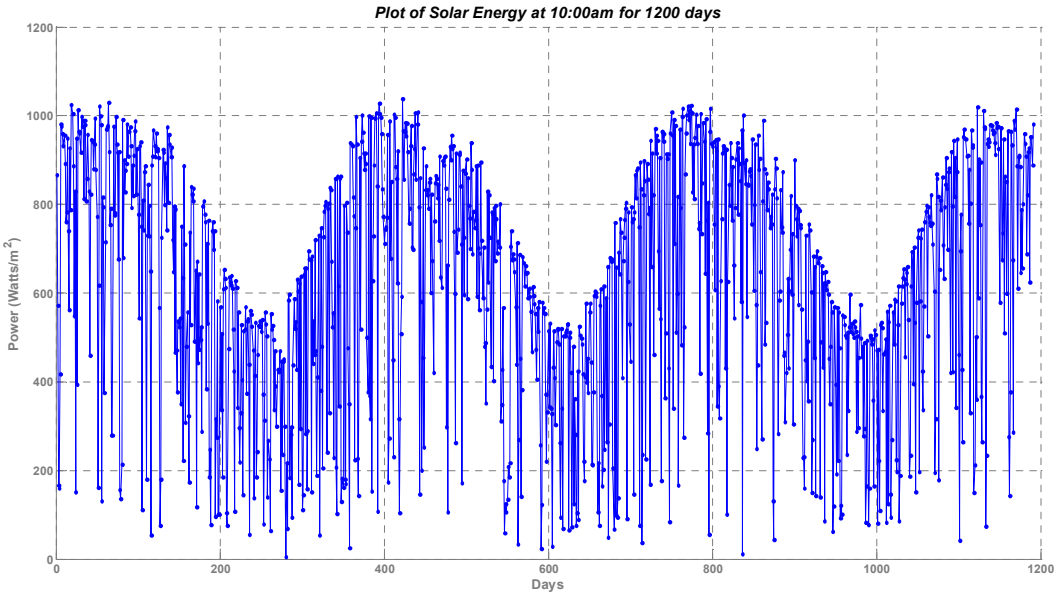

Figure 3.3: Plot of solar radiation value at the same time of the day over 1200 days using data available from [114].

in to account the observed or forecasted local conditions. The prediction techniques described in the next section attempt to correlate the most recent conditions with past averages in order to increase the prediction accuracy.

3.3 Short-term Solar Energy Prediction

This section discusses solar energy prediction algorithms proposed in the literature for predicting within a day (short-term). The techniques are compared to identify the most

effective approach.

3.3.1 Exponentially Weighted Moving Average (EMWA)

Kansal et al. [65] were the first to propose this simple solar energy prediction algorithm to support their harvested-energy management approach. Moser et al. [106] used similar prediction in their proposed adaptive power management framework, among others. The method exploits the diurnal cycle of solar energy and can adapt to the slow changing seasonal variations (Figure 3.2). The predictor is based on the observation that energy generation during a given time slot of day is similar to that generated at the same time period on previous days. A historical summary (weighted average) of the energy generation profile during the day is maintained by dividing a day into (N) discrete time slots of duration T minutes. The value of the current harvested-energy in a given slot is added to a weighted average of the energy received at that time of the day during all previous days. The weights are exponential, resulting in decaying weights for older data. Let $E_i(d)$ denote the value of energy generated in slot i as observed at the end of that slot in current day d. The historical average $EWMA_i$ maintained for slot i is given by:

$$EWMA_i(d+1) = \alpha E_i(d) + (1-\alpha) EWMA_i(d) \tag{3.1}$$

Thus, for predicting the harvested-energy value of future slot in the next day $(d+1)$, EWMA sums the currently measured harvested energy to the previous predicted value, weighted with α and $1-\alpha$, respectively. The value of α determines the contribution of current measured value. If the value of α is high (close to 1), the current measured value maintains more importance in the sum and vice versa.

3.3.2 Weather Conditioned Moving Average (WCMA)

The EWMA approach predicts the value of energy to be harvested during a particular time slot of the day as a weighted average of the energy received during the same time slot over previous days. This approach can give accurate predictions for consistent weather conditions, however, changing weather effects resulting in a mix of cloudy and sunny days (Figure 3.3) can introduce significant prediction errors. For instance, a sudden cloudy day can occur after a number of sunny days and the EWMA approach will not be able to account for this change resulting in over-prediction. Similarly, a partially cloudy (or sunny) day will also result in large prediction errors. Recas et al. [129] proposed an improved solar energy predictor that not only takes into account the historical conditions at a certain time of the day but also adjusts the prediction for the changing weather conditions throughout a day. Noh et al. [113] use a variant of this

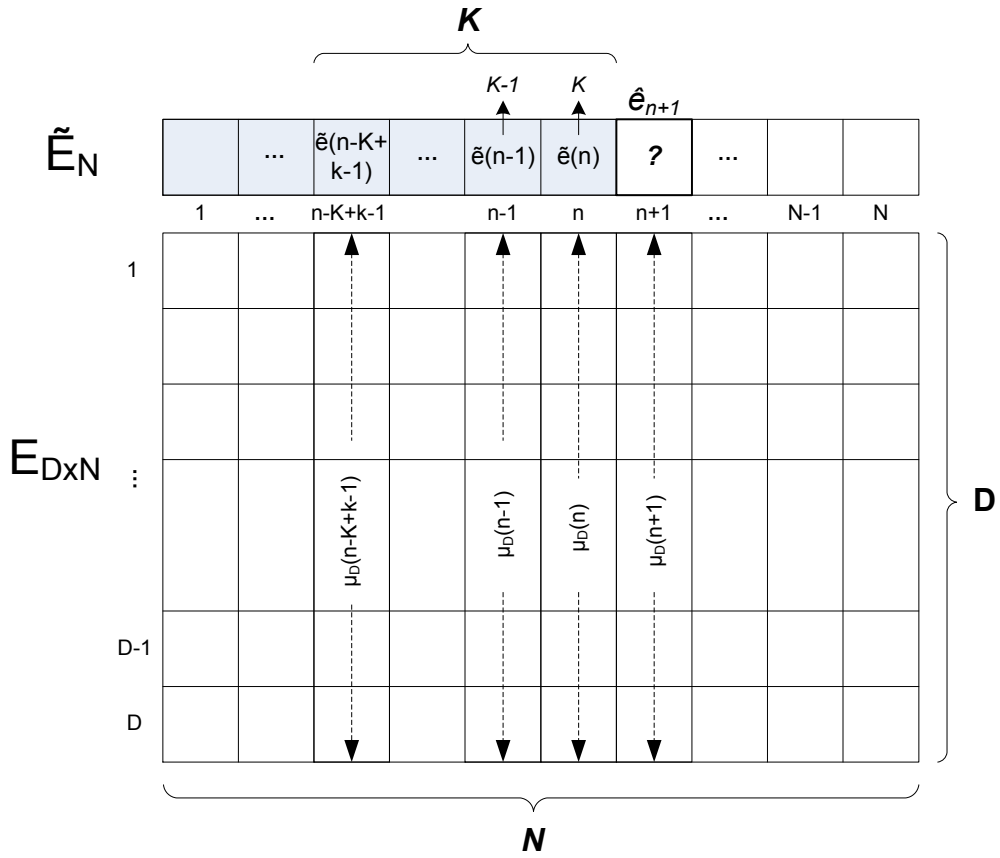

Figure 3.4: Graphical depiction of the WCMA prediction algorithm.

approach for prediction in their minimum variance energy allocation. The algorithm is described in Figure 3.4 and explained next.

As in case of EWMA, a day is discretized into N equal duration time slots. Incoming power sampling and prediction are performed once per slot and the slot's length is the prediction interval. The algorithm [129] maintains a matrix $\mathbf{E}_{D\times N}$ of historical measured power values $e(i,j) \in \mathbf{E}_{D\times N}$ of the last $D \in \mathbb{Z}^+$ days' slots. It also stores a vector of measured power values $\widetilde{e}(j) \in \widetilde{\mathbf{E}}_N$ of the current day's elapsed slots. The matrix $\mathbf{E}_{D\times N}$ and the vector $\widetilde{\mathbf{E}}_N$ are shown in Fig. 3.4. Suppose that at present $n \in N$ slots have elapsed on the current day shown shaded in Fig. 3.4 and $\widetilde{e}(n)$ is the measured energy at the end of slot n. The energy $\hat{e}_{n+1}$ during slot $n+1$ (marked with a '?', Fig. 3.4) needs to be predicted. In Fig. 3.4, $\mu_D(n+1)$ denotes mean of measured energies of $n+1$ slots in the past D days. The predicted power is a combination of present slot power $\widetilde{e}(n)$ and the average $\mu_D(n+1)$ of predicted slot $(n+1)$:

$$\hat{e}_{n+1} = \alpha \cdot \widetilde{e}(n) + (1-\alpha) \cdot \mu_D(n+1) \cdot \Phi_K \tag{3.2}$$

In Equation 3.2, α is a weighting parameter with value $0 \leq \alpha \leq 1$. The determination of α and other algorithm parameters is explained in Section 3.4. $\mu_D(j)$ is the average of

power measured at the beginning of slots $j \in N$ in the past D days:

$$\mu_D(j) = \frac{\sum_{i=1}^{D} e(i,j)}{D} \tag{3.3}$$

Φ_K is a conditioning factor for $\mu_D(n+1)$ and it quantifies the current day's conditions relative to the previous days. It is a function of parameter $K \in \mathbb{Z}^+$, which is the number of slots considered before slot $(n+1)$ of the current day (Fig. 3.4). Φ_K is a measure of how much brighter or cloudier the current day is compared to previous days [129]. It is evaluated using Equation 3.4, which is a weighted average of ratios $\eta(k) \in H_K$ (Equation 3.5), where each ratio $\eta(k)$ compares the current day's measured power (of a slot) to past days' average. The weights $\theta(k) \in \Theta_K$ (Equation 3.6) decrease from 1, $\frac{K-1}{K}$, $\frac{K-2}{K}$ and so on to $\frac{1}{K}$ starting from slot n, since slots earlier than n are assumed to be less correlated to the future slot $(n+1)$ [129]. A value of Φ_K greater that one implies that the measured values of last K slots of the current day are greater than the mean of past D day values, which represents a sunny day and vice versa.

$$\Phi_K = \frac{(\Theta_K)^T \cdot H_K}{\sum_{k=1}^{K} \theta(k)} \tag{3.4}$$

$$\eta(k) = \frac{\widetilde{e}(n-K+k)}{\mu_D(n-K+k)} \tag{3.5}$$

$$\theta(k) = \frac{k}{K} \tag{3.6}$$

To motivate the contribution of this chapter, the role of algorithm parameters needs has to be understood. Note that the predicted value (Equation 3.2) is obtained from two terms: the first of these terms is labeled the persistence term in this discussion and the second one is the conditioned average term. The persistence term determines how much slot n power value contributes directly to the predicted value, while the conditioned average term is the contribution of average of past $(n+1)$th slots scaled by the conditioning factor Φ_K. The parameter α weighs these two contributions. As shown in Fig. 3.4, the parameter D controls how many past days influence the predicted value, while the parameter K determines the influence of previous slots of the current day. Thus, the predicted value and its accuracy depends on the values of these parameters' (α, D, K). The values of parameters α, D, and K that minimise the average error is termed as the 'optimised set'. This is determined by evaluating Equation 3.2 using different values of each parameter over a target solar power data set to find the minimum value of an error function. The contribution of this chapter is determination of this optimised set by selecting an error function and simplifying the parameter determination across

Table 3.1: An illustrative example of WCMA prediction. '?' indicates the future value to be predicted.

Day	**slot** $n-2$	**slot** $n-1$	**slot** n	**slot** $n+1$
4	277	272	221	263
3	350	353	347	347
2	345	346	349	353
1	249	255	314	289
Current	342	256	230	?
μ_D	305	306	307	313
H_K	1.12	0.84	0.75	
Θ_K	0.33	0.67	1.00	

different data sets. Section 3.4 presents the details of the proposed parameter evaluation approach.

To illustrate the steps in the WCMA prediction algorithm an example is presented in Table 3.1, which gives a snapshot of the measured energy values of four consecutive slots of the past four days. Suppose that the values of algorithm parameters are: $\alpha = 0.7$, $D = 4$ and $K = 3$. The current day's measured energy values for three slots are also given and the value of the fourth slot '?' needs to be predicted. Based on these past days values, the means μ_D of each slot are given. The next row gives the ratios $\eta(k)$ using the values of current day's measured energy and past mean. The required values of weights $\theta(k)$ are 1, 0.67 and 0.33. The value of Φ_K using vector Θ_K and H_K is calculated as:

$$\Phi_K = \frac{(1.12, 0.83, 0.75) \times (0.33, 0.67, 1.00)}{\Sigma(0.33, 0.67, 1)} = 0.84 \tag{3.7}$$

Finally, the predicted value is calculated to be:

$$\hat{e}_{n+1} = 0.7 \cdot 230 + (1 - 0.7) \cdot 313 \cdot 0.84 = 240 \tag{3.8}$$

3.3.3 Other Prediction Approaches

A number of techniques have been proposed in the literature for forecasting of short-term solar radiation based on time-series forecasting using Autoregressive models and its variants [130, 9], artificial neural networks (ANN) [93, 92], and using combination of two dimensional linear filters and ANN [46]. These are powerful general purpose techniques, however, which require a large amount of historical data and/or are computationally intensive, thus not suitable for implementation in resource constrained low-power energy harvesting systems. The two approaches discussed in Sections 3.3.1 and 3.3.2 are simple techniques that exploit smart observations regarding the solar energy generation model.

In [12], the authors investigate the use of neural networks and 2-D linear prediction filter for forecasting of short-term solar harvested-energy for low-power applications and compare it to the WCMA method. The reported results indicate that both 2D linear filter and neural network approaches achieve less accuracy than the WCMA algorithm at a much higher computation cost. Appendix B reviews long-term prediction/modeling of solar energy and a generic prediction approach for other energy sources.

3.4 Evaluation and Parameters Optimisation of WCMA Prediction Algorithm

In Section 3.3.2, an effective short-term solar harvested-energy prediction approach was described. The accuracy of the prediction algorithm is dependent upon parameters such as the length of prediction interval and window sizes of historical energy source data samples used. At the same time, these parameters also determine the overhead of performing prediction algorithm operations and memory requirement for storing historical power samples. Since harvested power is often limited, it is important to minimize the energy consumption overhead of harvested-energy management activity, including prediction. The effectiveness of harvested-energy management is sensitive to the accuracy of prediction algorithm. This has been acknowledged in previous works [65, 106, 113, 129], nevertheless, there is a lack of clear justification how the prediction accuracy should be best quantified. In previous works, the choice of prediction parameters have been based largely on specific cases, and no comprehensive evaluation has been presented across multiple data sets.

This section presents a systematic approach for evaluation of prediction accuracy of solar harvested-energy and applies this to evaluate achievable accuracy of WCMA algorithm described in Section 3.3.2 using multiple real solar energy data sets. The algorithm performance is measured by varying the energy harvesting source sampling rates (or prediction slots) and trade-off in prediction accuracy and cost is obtained based on implementing prediction algorithm on actual hardware. The results are compared across different data sets to give guidelines to simplify prediction algorithm's parameters selection, which ensures that high accuracies can be achieved without the need to determine parameters for different profiles. Finally, the case for dynamic parameters selection is motivated and it is shown that on average greater than 10% higher accuracies can be achieved compared to the static selection of parameters.

3.4.1 Prediction Error Measurement

This section discusses an error evaluation technique that accurately models the prediction error and is intuitive to allow comparison of prediction algorithm across different

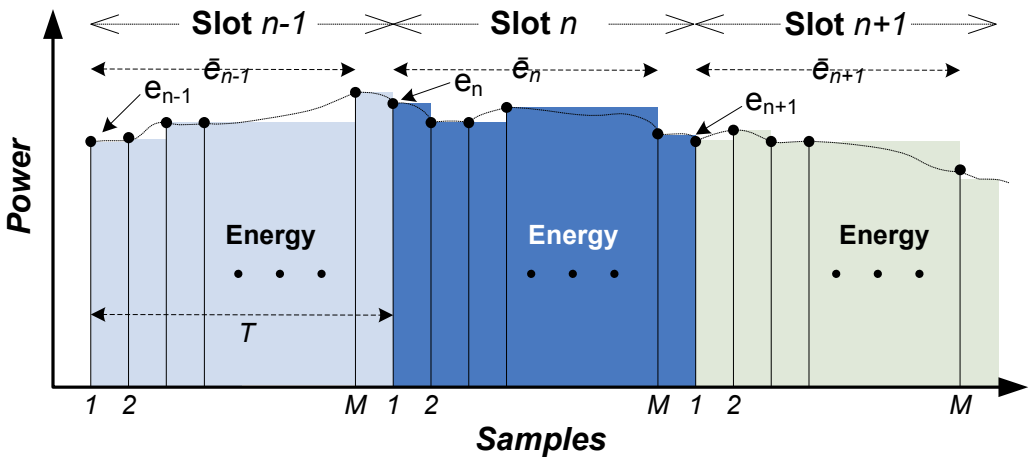

Figure 3.5: A section of solar power samples profile showing slot boundaries, samples per slot, slot energy calculation, and mean slot power

solar power data sets. It is suggested how predicted output should be compared so that the result is representative of the actual error and which error function to use for computing averaged error to model the overall losses in prediction. To motivate the error calculation technique described in this section, Figure 3.5 shows a section of measured solar power profile of a day. Slot boundaries are indicated and in each slot M power samples are available. For instance, if slot length is $T = 30$ minutes ($N = 48$) and sampling resolution of available data is 5 minutes then $M = 6$. Power samples at start of each slot are indicated and these are used by prediction algorithm (Section 3.3.2) to predict future slot power. The energy received during a slot n can be obtained from its mean power $\bar{e}_n$ by $\bar{e}_n \times T$. Harvested-energy management system estimates the energy of slot n by using the predicted power value $\hat{e}_{n+1}$ as $\hat{e}_{n+1} \times T$.

In previous works [65, 129], the prediction error of a slot n ($error'_n$) is expressed as:

$$error'_n = e_{n+1} - \hat{e}_{n+1} \tag{3.9}$$

Since predicted power is used to estimate a slot's energy, it is intuitive to compare the predicted power to mean power of a slot to express prediction error:

$$error_n = \bar{e}_n - \hat{e}_{n+1} \tag{3.10}$$

The value of $\bar{e}_n$ will be more accurate if solar power samples data is available at a high resolution (e.g., 1 minute resolution compared to 5 minutes). This leads to realistic modeling of prediction error when using Equation 3.10.

Since determination of prediction accuracy needs to account for prediction error outcomes of a large number of sample points, a suitable average error function is required.

Root Mean Squared Error (RMSE) is a commonly used measure of determining estimation accuracy [47], however, RMSE is sensitive to large outliers and its value is dependent on scale of data. This makes use of RMSE non-intuitive for evaluating harvested-energy prediction since sudden large fluctuations in solar energy profile are difficult to model with simplistic (heuristic) prediction algorithms and may give large error values (outliers) that can bias the average results. Mean Absolute Error (MAE) does not suffer from this aspect but it is also data scale dependent, making comparison of prediction performance across different solar power data sets non-intuitive. In this work, the Mean Absolute Percentage Error (MAPE) function is used (Equation 3.11) since it is independent of data scale.

$$MAPE = \frac{1}{T} \sum \left| \frac{error_n}{\bar{e}_n} \right| \tag{3.11}$$

In Equation 3.11, T is the the total number of predicted values. Similarly, $MAPE'$ is defined as used in [129] based on $error'_n$ instead of $error_n$ (see Equation 3.9 and 3.10) and it will be used to compare prediction algorithm's parameters optimisation results (Section 3.4.3). Since solar energy arrives in large bursts mainly during mid day, for harvested-energy management it is relevant to measure accuracy of prediction during this time. Therefore, night-time values (zero) where prediction is accurate but not useful, and small values at start/end of a day where prediction errors are not meaningful for evaluating prediction performance, should not be included in average prediction error calculation (Equation 3.11). This prevents the average prediction error to be influenced by values outside region of interest. This is achieved by only including those sample values in the average error calculation that are at least 10% of the peak value.

3.4.2 Evaluation Setup

The prediction algorithm (Section 3.3.2) is evaluated using publicly available solar irradiance data of ten different sites [114], out of which six sites (Table 3.2) are selected that demonstrate variety in solar energy profile variations. The use of multiple sites with large of number of recorded observations (365 days) attempts to validate the proposed algorithm over long term deployment conditions (different number and distribution of sunny and cloudy days in each irradiance trace) and independent of the deployment location.

To present the algorithm evaluation results, the range of values used for the algorithm parameters are: $N = \{288, 96, 72, 48, 24\}$, $0 \leq \alpha \leq 1$, $2 \leq D \leq 20$ and $1 \leq K \leq 6$. These values are exhaustive to capture the main trends as shown by results in the following sections. For a given N, the objective is to find the optimised set of prediction algorithm parameters α (weighing factor), K (previous slots) and D (number of past days) for each solar power data set, which minimizes the average prediction error, $MAPE$. The

Table 3.2: Details of the data sets used.

Data Set	Location	Observations	$DAYS$	Resolution
SPMD	CO	105,120	365	5 minutes
ECSU	NC	105,120	365	5 minutes
ORNL	TN	525,600	365	1 minute
HSU	CA	525,600	365	1 minute
NPCS	NV	525,600	365	1 minute
PFCI	AZ	525,600	365	1 minute

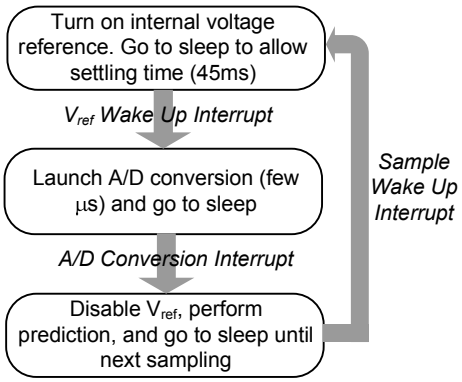

Figure 3.6: Description of power value sampling and prediction sequence.

evaluation is performed for days 21 to 365 as this allows matrix of past days samples $\mathbf{E}_{D\times N}$ used in the prediction algorithm to be filled for $D = 20$, and it also ensures that an equal number and same sample values are used for average error calculation irrespective of number of past days (D).

To evaluate the prediction algorithm on actual hardware, the following set-up has been used [55]:

- Test board: MSP-TS430PM64.
- Microcontroller: TI MSP430F1611 (3V@5MHz).
- Compiler: TI Code Composer Essentials version 3.2.

Fig. 3.6 shows the steps in computation of prediction algorithm in hardware. Most of the time, micro-controller remains in deep sleep mode in which only the Wake-Up timer is running. The MSP430 wakes up according to the number of predictions per day (N), enables the voltage reference used in Analog-to-Digital (A/D) conversion and waits in sleep mode until the voltage settles. It then launches the A/D conversion and waits for it to complete (again in sleep mode). When A/D conversion is complete, it shuts down the voltage regulator, executes the prediction algorithm and re-enters in deep sleep mode.

Table 3.3: Prediction error and parameter values using different error evaluations at $N = 48$ for six solar power data sets.

Data set	α	D	K	$MAPE'$	$MAPE$	α	D	K	$MAPE$
SPMD	0.2	19	1	42.07%	17.77%	0.7	20	1	15.80%
ECSU	0.2	20	2	32.89%	15.36%	0.7	20	3	13.45%
ORNL	0.4	20	3	36.61%	18.04%	0.7	20	3	17.22%
HSU	0.4	20	3	26.90%	14.99%	0.7	18	3	14.01%
NPCS	0.0	15	1	17.17%	11.43%	0.6	20	2	8.06%
PFCI	0.2	20	3	13.93%	8.22%	0.6	20	3	6.59%

3.4.3 Evaluation Outcomes

Having proposed the error evaluation function in Section 3.4.1, the difference in results is presented between average prediction error measurement using $MAPE$ (Equation 3.11), which uses average slot power to calculate error, compared to $MAPE'$, which uses error between estimated and actual sampled power at the beginning of slot. Table 3.3 shows two sets of optimisation results for α, D and K with $N = 48$ samples per day for different solar power data sets. In the first set, $MAPE'$ has been used as the cost function ($MAPE$ value is also calculated for these configurations), the second set has been obtained by minimizing $MAPE$ function. Note that the values of average prediction errors for $MAPE$ are significantly lower compared to $MAPE'$. Also, the obtained values of prediction algorithm parameters (α, D, and K) differ between the two error evaluations, especially the value of α. Furthermore, it can be seen that if $MAPE$ is calculated with set of parameters obtained using $MAPE'$, $MAPE$ values are higher than those obtained in the second set, indicating that the obtained set of parameters using $MAPE'$ are not optimised.

Next, the prediction algorithm is evaluated using different values of prediction slots. The aim is to address the following two issues:

1. How much influence does varying prediction slot or sampling rate per day (N) have on prediction accuracy and associated overhead?

2. Based on analysis across multiple solar power data sets, can some guidelines be determined to simplify tuning of parameters α, K and D independent of specific data set?

To address the first issue, Table 3.4 shows prediction error for five values of N and the optimised values of parameters K, α and D for each of six data sets. As can be seen for all data sets, prediction accuracy increases with increase in N, with predictions errors less than 9% in all cases at $N = 288$, a gain of up to 9% compared to $N = 48$. Fig. 3.7 graphically depicts the trends in $MAPE$ with N for all data sets.

Table 3.4: Prediction results at different values of N for six solar power data sets.

Data Set	N	α	D	K	$MAPE$	$MAPE@K=2$
SPMD	288	1	n/a	n/a	0†	0†
	96	0.8	20	1	10.2668%	10.39%
	72	0.8	20	1	12.3556%	12.47%
	48	0.7	20	1	15.7999%	16.10%
	24	0.6	12	2	20.35%	n/a
ECSU	288	1	n/a	n/a	0†	0†
	96	0.8	20	2	9.39%	n/a
	72	0.8	20	3	11.11%	11.19%
	48	0.7	20	3	13.45%	13.51%
	24	0.6	19	1	18.24%	18.51%
ORNL	288	1	n/a	n/a	8.31%	n/a
	96	0.8	20	3	14.42%	14.47%
	72	0.8	20	4	15.72%	15.88%
	48	0.7	20	3	17.22%	17.43%
	24	0.6	12	2	21.43%	n/a
HSU	288	0.9	20	1	6.00%	6.01%
	96	0.8	20	4	10.80%	10.88%
	72	0.8	20	5	12.11%	12.30%
	48	0.7	18	3	14.01%	14.11%
	24	0.7	12	2	19.19%	n/a
NPCS	288	0.9	20	1	3.91%	3.92%
	96	0.7	20	3	6.78%	6.80%
	72	0.6	20	2	7.40%	n/a
	48	0.6	20	2	8.06%	n/a
	24	0.5	20	1	8.88%	9.11%
PFCI	288	0.9	20	4	3.45%	3.46%
	96	0.7	20	5	5.64%	5.77%
	72	0.6	20	4	5.92%	6.08%
	48	0.6	20	3	6.59%	6.68%
	24	0.5	10	2	8.97%	n/a

n/a: not applicable
†N=288 is not defined for this data set since the resolution of data set samples is 5 minutes

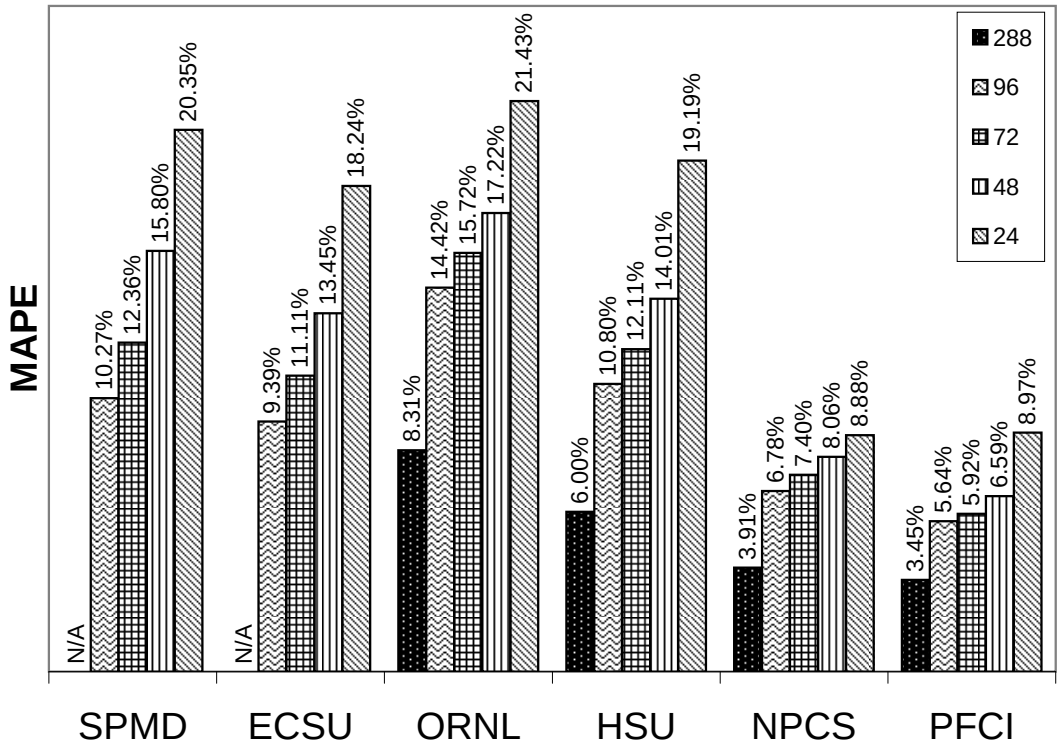

Figure 3.7: Performance of prediction algorithm using different values of N

Table 3.5 gives the energy consumption of power sampling (A/D conversion) and prediction algorithm execution at some parameters' configurations. The energy consumption during system sleep mode per day is also given. As can be seen, the A/D conversion for sampling the power consumes the bulk of energy and prediction algorithm uses an additional 4μJ to 9μJ depending upon its parameters' values. Taking 5μJ as roughly the typical energy consumption of prediction algorithm, the total energy consumption per day of prediction activity is given in last row of Table 3.5. If this is compared in context of energy consumption of sleep mode, it is interesting to note that the total energy consumption of the sampling and prediction activity combined for $N = 48$ (2.880mJ per day) is still small compared to the total energy consumption of sleep mode (356mJ per day), indeed just 0.8%. Considering the extreme of $N = 288$ (17.28mJ per day), it is 4.85% of sleep mode energy consumption. Comparing the increase in overhead with increase in accuracy, it can be seen that using $N = 288$ achieves an average error of less than 9%, or an improvement of 7-10% in average error compared to N=48 in high variability data sets (Table 3.4). Fig. 3.8 gives the total energy consumption at different values of N per day as a percentage of the sleep mode energy consumption.

Table 3.4 shows that as value of N approaches 288, the value of α tends to 1. Value of $\alpha \approx 1$ implies that prediction algorithm is mainly relying on the currently sampled power value to determine the predicted value, and $\alpha = 1$ essentially means that current value can be used to predict the energy. These results show that using high values of N, need

Table 3.5: Energy consumption of power sampling and prediction algorithm.

Hardware Activity	**Energy/Cycle**
A/D conversion	55μJ
A/D conversion + Prediction (K=1, α=0.7)	58.6μJ
A/D conversion + Prediction (K=7, α=0.7)	63.4μJ
A/D conversion + Prediction (K=7, α=0.0)	61.5μJ
Low power (sleep) mode 1.4μA@3V	356mJ per day
A/D conversion 48 samples per day@55μJ	2640μJ per day
A/D conversion + prediction 48 times per day@60μJ	2880μJ per day

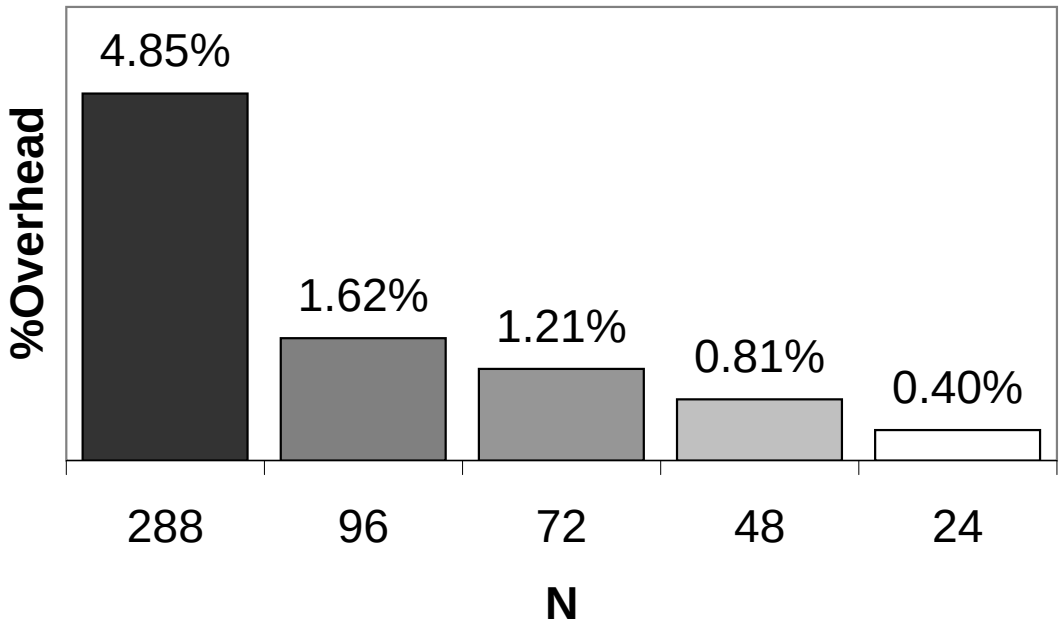

Figure 3.8: Overhead of prediction algorithm at different values of N as a percentage of sleep mode power consumption per day

for using the prediction algorithm is reduced but at the same time energy consumption overhead is dominated by power sampling of ADC and not by prediction activity.

Next, the issue of simplifying tuning of prediction algorithm parameters across different solar power profiles is addressed to achieve low average errors across different data sets:

- D: Fig. 3.9 shows the values of $MAPE$ versus D at $N = 48$ using values of α and K obtained in Table 3.4. It can be seen that beyond a certain D value, further gains in accuracy are small. D can be set to value of 10-11 irrespective of the data set used to obtain low $MAPE$ while conserving samples storage memory requirement of prediction algorithm.

- α: Table 3.4 indicates that $\alpha = 0.5$ to 0.6 gives minimum average error at $N = 24$, and for $N = 288$ $\alpha \approx 1$ is desirable. For other values of N in between, $0.7 \leq \alpha \leq 0.8$ with $48 \leq N \leq 96$ gives the minimum average error. These trends are graphically summarised in Figure 3.10.

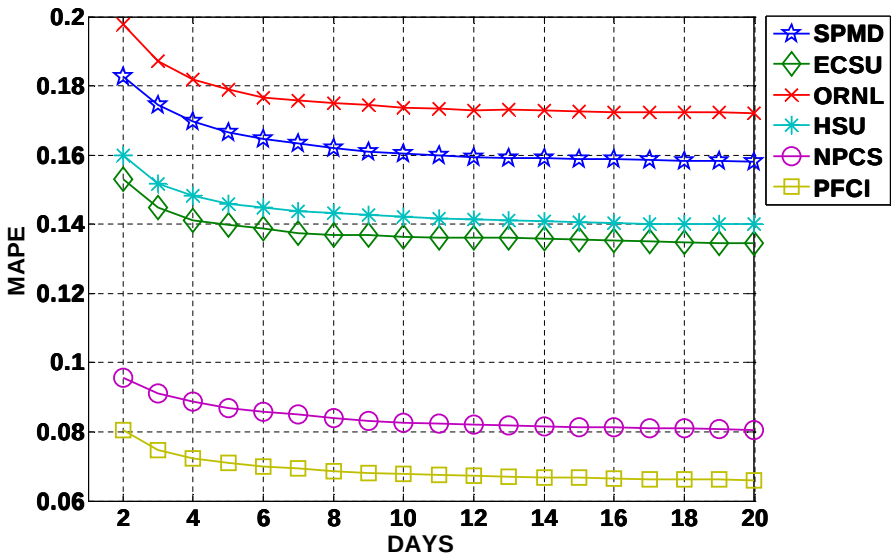

Figure 3.9: Trends in $MAPE$ with increasing D for different solar power data sets

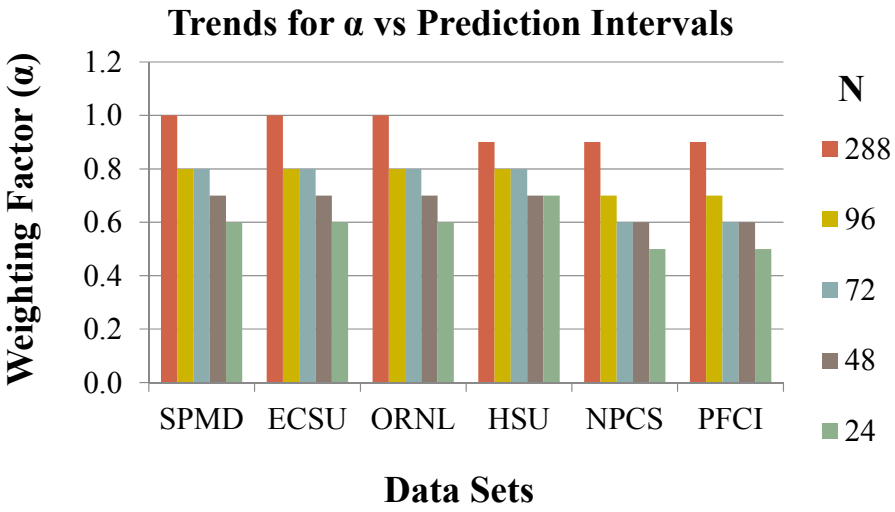

Figure 3.10: Trends in α for different solar power data sets for minimum MAPE

- K: The last column of Table 3.4 show that $K = 2$ gives an average error that is very close to minimum error value obtained for all data sets as graphically depicted in Figure 3.11.

3.4.4 Prediction with Dynamic Parameters Selection

In Section 3.4.3 it was shown that increasing the harvested-power sampling rate (N) always results in higher prediction accuracy at a higher energy consumption overhead. It was also shown that as more number of past days (D) are considered, the average prediction error decreases noticeably initially, with the rate of decrease soon becoming

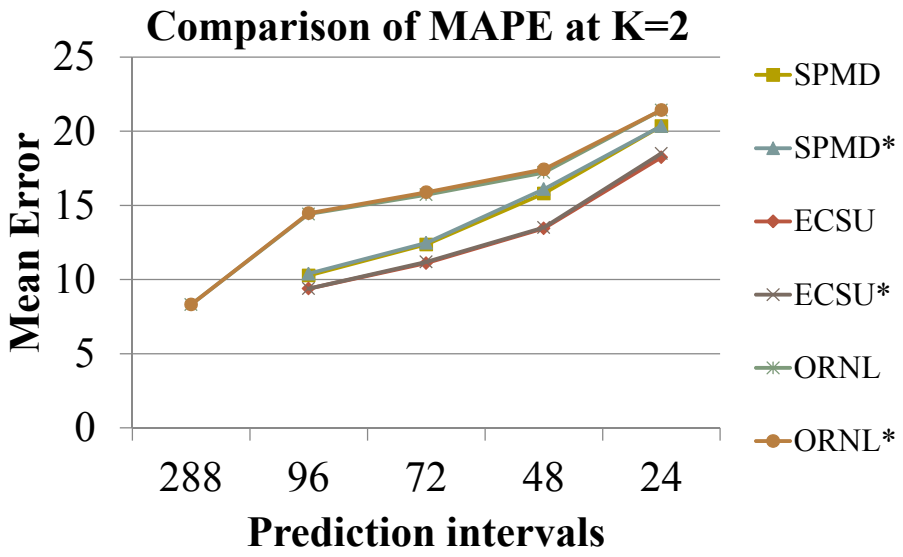

Figure 3.11: Comparison of $MAPE$ for $K = 2$ for different solar power data sets

Table 3.6: Results for dynamic parameters selection varying both α and K, only K at a fixed α and vice versa.

		Static	K+α	K only		α only	
Data Set	N	MAPE	MAPE	α	MAPE	K	MAPE
SPMD	96	10.27%	4.25%	0.4	7.31%	6	5.48%
	72	12.36%	5.13%	0.3	8.54%	6	6.47%
	48	15.80%	6.43%	0.3	10.63%	6	8.21%
	24	20.35%	6.95%	0.3	13.08%	3	11.21%
ECSU	96	9.39%	3.76%	0.3	6.32%	6	4.85%
	72	11.11%	4.44%	0.3	7.40%	6	5.68%
	48	13.45%	5.37%	0.3	8.92%	6	6.93%
	24	18.24%	6.16%	0.3	11.25%	3	10.37%
ORNL	288	8.31%	3.85%	0.2	6.07%	6	4.68%
	96	14.42%	6.40%	0	9.35%	6	7.69%
	72	15.72%	6.72%	0	10.09%	6	8.10%
	48	17.22%	7.38%	0.1	11.34%	6	9.26%
	24	21.43%	7.30%	0.2	12.94%	3	12.03%
HSU	288	6.00%	2.75%	0.3	4.46%	6	3.43%
	96	10.80%	4.60%	0.1	7.19%	6	5.76%
	72	12.11%	5.15%	0.2	8.14%	6	6.49%
	48	14.01%	5.52%	0.2	9.32%	6	7.36%
	24	19.19%	5.92%	0.3	11.21%	3	10.11%

insignificant. It can also be noted that across different data sets as well as at different values of N for a given data set, the average prediction error was minimized for combination of parameters α and K that varied for these different cases. From these observations, it can be concluded that although there is a fixed trend in average error values when N or D are varied, the average error value with a given K and/or α depends on variations in solar power profile. In other words, for a given value of N and D, values of K and α may be varied at different points in a profile to minimize error at these points compared to using certain fixed values that minimize the average error across the whole profile (Section 3.4.3).

To demonstrate the potential gains in prediction accuracy by dynamically varying α and K, Table 3.6 gives the values of average errors with dynamically changing both α and K, changing only K at a given α and vice versa. These error values are obtained by minimizing the error obtained at each prediction by dynamically selecting the value of adjustable parameter(s). Average error obtained using static parameters setting is also given (from Table 3.4) for comparison. When K is dynamically changing, a fixed value of α has been chosen for which average error is minimum among other values of α. The same consideration has been made when α is changed. Note that maximum gains in average error as compared to average error of static parameters selection are achieved when both K and α are adapted, followed by adapting only α at a given K. Furthermore, these gains of dynamic algorithms compared to static algorithm increase as N is decreased. This is a useful outcome since the implementation overhead of dynamic adjustment will be minimized at a smaller N. It is interesting to note that the dynamic algorithm accuracy at $N = 48$ is higher than the accuracy of static algorithm at $N = 288$. It should be noted that the indicated error values with dynamic parameters' selection are minimum achievable since an ideal approach to select best parameters at every point is used. These results indicate that it is promising to develop a dynamic parameters selection algorithm that can achieve less than 10% average error without the need to use higher sampling rates to minimize overhead.

3.5 Concluding Remarks

Harvested energy prediction is an important component for realisation of harvested-energy management because of the variable supply of harvested-energy. This chapter discussed low computation and energy overhead prediction approaches suitable for low-power wireless sensor systems. The chapter focused on solar energy prediction and possible approaches for both short-term and long-term prediction are discussed. A problem with application of prediction algorithm is the determination of best values of associated parameters. The contribution of this chapter was parameters optimisation of short-term solar energy prediction to minimise the average prediction error and guidelines for determination of parameters across different input profiles. It was shown that values of

parameters D, K and α can be chosen according to N independent of the specific solar energy data set. This allows the algorithm to be used under different input conditions without the need to evaluate the required parameters. The solar energy prediction algorithm presented in this chapter is used in Chapter 6 to propose an energy-management policy to achieve uniform performance of energy harvesting systems under the variability of solar energy supply.

Chapter 4

Modeling of Photovoltaic Energy Harvesting Systems

As outlined in Chapter 1 (Section 1.1), the energy management determines the allocation of harvested-energy to the application workload such that the energy supply and consumption are matched to achieve perpetual operation under a variable supply of harvested-energy. This is also referred as 'energy neutral' mode of operation [65]. Chapter 3 focused on harvested-energy prediction to minimise uncertainty in the supply to enable application workload to be adapted according to expected energy supply. Chapter 2 discussed the design of photovoltaic energy harvesting supply and storage subsystem, identifying the system components and their design considerations, such as maximising the energy transfer efficiency between supply and consumption. Given a certain configuration of the harvesting supply and storage subsystem, this chapter considers the problem of how to achieve the desired match between supply and consumption under the non-ideal characteristics or losses of system components. As a motivating example, consider the general architecture of a photovoltaic energy harvesting system in Figure 4.1. Now consider an energy management policy with the objective of matching application workload energy consumption with harvested-energy. If this policy measures harvested-energy as output of the PV panel, it will fail to achieve the desired objective as it does not consider non-ideal characteristics (or losses) of system components such as input regulator, energy storage and output regulator (Figure 4.1) that affect supply of PV panel and application workload demand. Furthermore, a fixed value of system efficiency may not be sufficient due to the varying efficiency of a specific component as a function of its input and output as mentioned in Chapter 2 (Section 2.2.7). Hence, a better correlation between supply and demand can be achieved if the non-ideal behaviour of each system component is considered, and its variation (if any) based on component's input/output (or inter component dependency). This chapter addresses this by identifying the contribution of individual system component on supply or demand through modeling. The intention is not to propose novel models for different components, but to

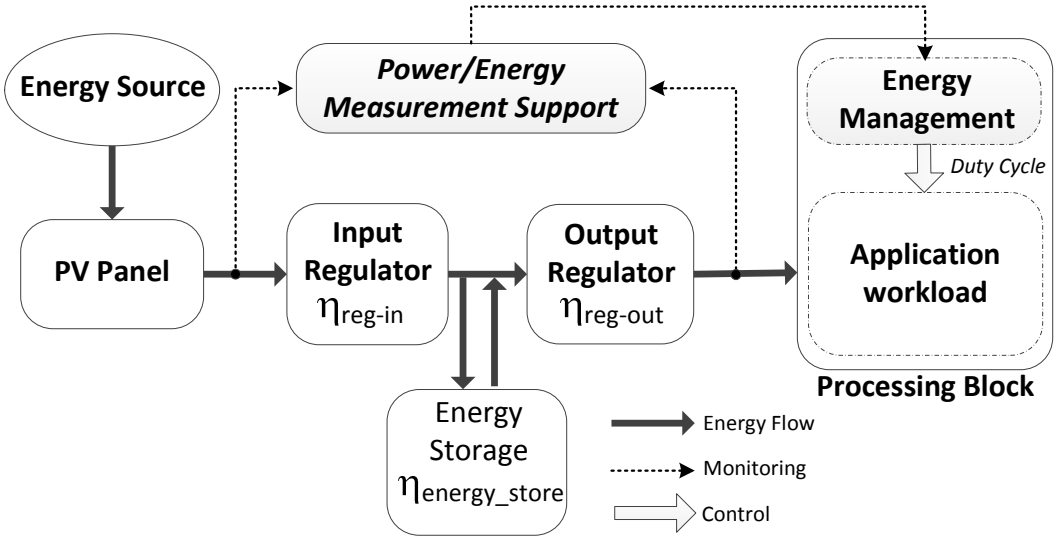

Figure 4.1: A naive attempt at matching supply and demand by considering only PV panel output and application workload consumption.

identify the characteristics that influence the supply or demand and selection of suitable models that achieve this purpose. The proposed approach to modeling the system and its individual components is validated against empirical measurements using the reference system configuration described in Chapter 2 (Section 2.3). The applicability of this modeling to optimising harvested-energy management is discussed in Chapter 5.

This chapter is organised as follows. Section 4.1 discusses the related work and places this work in context of previous works. Section 4.2 discusses the role of each component in the system model from the perspective of energy management and describe the selected modeling approach. In Section 4.3, the complete system model is validated using the reference system configuration by considering a case of matching supply and demand. Section 4.4 concludes the chapter.

4.1 Related Work and Contributions

A number of works [102, 103, 76, 39] on energy management abstract the details of energy harvesting system and focus mainly on the spatio-temporal variability of energy supply and application specific optimisation objectives [77, 76, 103, 102, 80, 81]. In these cases the system model consists of an energy supply modeled as a series of values representing the available energy at different times, which replenishes an ideal buffer of a given size, while the application depletes the buffer according to its activity costs. Other works model the inefficiency in the system as single parameter by acknowledging that the energy available to be buffered is less than harvested, and that the modeled input energy already accounts for this factor [154]. The limitation of this abstract system

model is that it cannot assist an energy management policy to correctly manage demand and supply in a real system. This is because practical management of supply and demand requires knowing what constitutes supply and demand, and given a specific realisation of an energy harvesting subsystem as discussed in Chapter 2, the contribution of individual components needs to be determined. Furthermore, the system (component) losses can be dynamic and this has been considered in case of energy storage in [65], which presents a more realistic system model that accounts for charge/discharge efficiency of rechargeable batteries and observe that energy supplied by PV panel can be consumed directly without discharging the battery if supplied power is greater than demand. Based on this system model, an energy management policy is proposed in [65] to minimise battery discharge and therefore the cost to replenish battery for maintaining energy neutral operation. For systems using supercapacitors as energy storage, leakage models have been presented in [131, 164] and leakage-aware energy management has been presented in [164] to counter its effect.

As mentioned in Section 4, the aim of this chapter is not to propose novel models of system components but to identify the required parameters and their possible variations for each system component through modeling to better match the demand and supply using energy management. This is necessary because certain parameters can have a dominating influence compared to others depending on the choice of components that make up the system (Chapter 2). For example, in case of energy storage rechargeable batteries have very small self-discharge while self-discharge of a supercapacitor cannot be neglected (Section 2.2.5). Furthermore, this chapter also focuses on how to obtain the value(s) of identified parameters given the specific components selected. This is important because the values of parameters and their variation can be different amongst different instances of the same system component, e.g., the specific type of voltage regulation used to supply power to the application workload. The next sections discuss the modeling of each system component and the interdependency between components that describes the overall relationship between supply and demand.

4.2 System Modeling

In Chapter 2 (Section 2.2), the role of each system component to be modeled was discussed. In this section, the requirements of modeling from energy management perspective and the selected modeling approach for each component is discussed. Results are presented to validate the modeling using specific instances of the component. Figure 4.2 shows the complete system and key energy flows between different components. Table 4.1 gives the description of these energy flows. The energy input P_{rad} (irradiation) is converted by the photovoltaic (PV) panel output (P_{panel}) and this is made available through the input regulator block (P_{reg_in}) for replenishing the energy storage (P_{chg}) and consumption of application workload (P_{load}). The application load is connected through

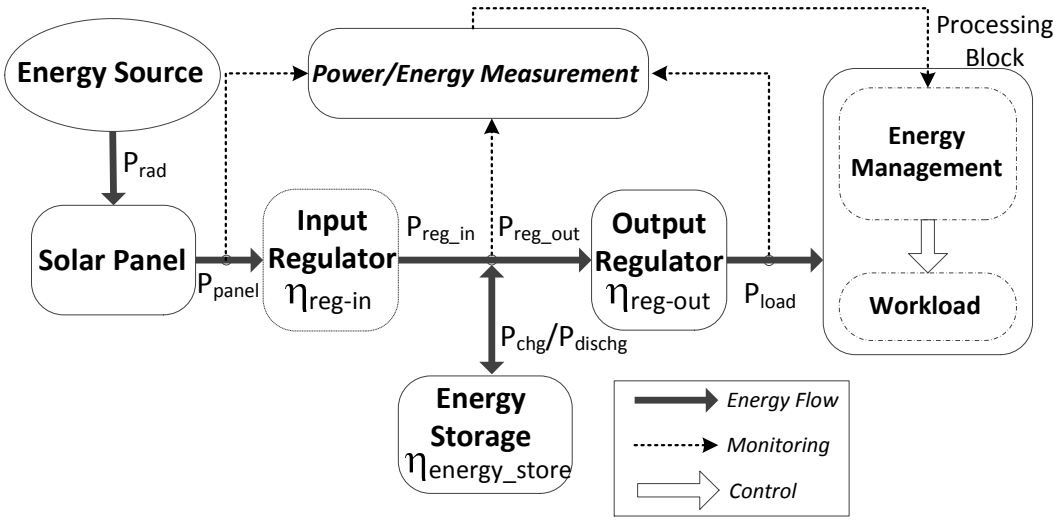

Figure 4.2: System model showing the input/output power flow between different components.

Table 4.1: System energy flows and efficiencies.

Metric	Description
P_{rad}	Power of incident irradiation
P_{panel}	Power produced by PV panel
P_{reg_in}	Power produced by input regulator
P_{reg_out}	Power demand of output regulator
P_{chg}	Power stored in energy storage
P_{dischg}	Power extracted from energy storage
P_{load}	Energy consumed by load
η_{energy_store}	Efficiency of energy storage
η_{reg_in}	Efficiency of input regulator
η_{reg_out}	Efficiency of output regulator

the output regulation block (P_{reg_out}) to input regulator and energy storage. Depending on the load demand and harvested-energy, the load can be supplied from the input regulator P_{reg_in}, the energy storage P_{dischg} or both. Harvested-energy management policy is implemented on a processing unit that is part of the workload block and it adjusts the power consumption of load (P_{load}) by monitoring energy harvested, energy stored, and energy consumption. Using this complete system model, the simulation evaluates system states in discrete time steps in terms of the energy flow of each component. The next section describes the simulation environment followed by details of modeling of each system block.

4.2.1 Simulation Environment

The system modeling has been implemented using MATLAB due to its ease of data types handling, visualisation support and rich library of functions for commonly needed

```
initializations()
.
.
for each simulation step
  get_energy_store_voltage()
  determine_solar_panel_state()
  calculate_supply_power()
  calculate_output regulator_power()
  determine_net_charge_discharge()
  update_energy_storage_state()
  invoke_energy_management_policy()
end for
```

Figure 4.3: Simulation outline of system blocks shown in Figure 4.2.

modeling tasks. Fig. 4.3 gives an outline of system simulation using interconnection of system components shown in Fig. 4.2. The modeling approach is inspired by a recent work by Jeong [59] in which the system is modeled at the level of abstraction of energy flows between system components based on their transfer characteristics. This also suits the aim of this chapter, which is to model the influence of each component characteristics on supply and demand. Each system component is modeled using a modular approach by encapsulating functionality within functions or scripts. A specific instance of a given component such as photovoltaic panel, voltage regulator etc. is implemented in a separate file so that different instances of a given component can be interchanged according to chosen system configuration. The interconnection of components with each other is implemented using function calls and a sequence of statements for interdependency checks. The simulator uses a specific configuration of an energy harvesting system along with user-defined components data to model the system behavior. The overall system configuration and interconnection between system components is realised using a separate system module file. This file coordinates the event driven execution of system state updates according to the steps given in Section 4.2.9. The resolution used for time-steps dictates the computation interval and consequently the estimation accuracy. Appendix C gives the MATLAB code for the top-level simulation scripts and components of the system, which are discussed in the following sections.

4.2.2 Energy Source

For evaluating energy management policies, it is critical that the modeling of environmental energy can capture the variations of the targeted deployment environment. For photovoltaic energy harvesting, the input light energy is called irradiance, expressed in $Watts/m^2$ or smaller units. The energy available at a location can be modeled as a series of irradiance values over time. These values be given as input to the PV panel model (Section 4.2.3) to determine the output power. Historical irradiance data sets

with 1 minute interval samples for many locations around the world are publicly available such as from US NREL [114] website. Another approach to modeling solar energy is to use a generic model of solar radiation, with location and time of the year as input [59]. However, this approach only models ideal weather conditions and doesn't account for random weather effects or variability. Jeong [59] has discussed how these effects can be included to make this model closer to real conditions. It should be noted that the output of this model has to be scaled according to the specific PV panel being used.

4.2.3 PV Panel

A PV panel output power is a function of the incident light conditions, temperature and terminal voltage. The operating point at a given light intensity and temperature is defined by the terminal voltage and current. This operating point of panel is determined by configuration used to connect the panel to rest of the system as explained in Section 4.2.4. This is important from viewpoint of energy management since change in terminal state of connected component(s) such as energy storage can change the operating point and thus amount of energy harvested, even under constant illumination conditions. The power output of panel dictates how much energy is available to energy management for manipulating consumption and energy store recharge. For an accurate reproduction of a PV panel behaviour, the change of operating points according to change in illumination conditions and panel terminal characteristics needs to be modeled.

The PV panel output is modeled according to the following: (1) input irradiance, (2) PV-panel characteristics (IV-curve), (3) the operating point of the panel (terminal voltage). To obtain the PV panel output power, the IV-curve at the given illumination is needed and the operating point needs to be determined. The IV-curve is a non-linear relationship between a panel's terminal voltage V_{panel} and its current output I_{panel}:

$$I_{panel} = IV\_Curve(V_{panel}) \tag{4.1}$$

Given this IV-curve, a solar panel's output power P_{panel} is given by:

$$P_{panel} = V_{panel} \cdot I_{panel} \tag{4.2}$$

The operating voltage V_{panel} of the solar panel connected to rest of the system is obtained by modeling the solar panel as a voltage controlled current source. The V_{panel} is determined by the output connection of the PV panel. This is either a regulating diode connected to energy storage or an input power regulator block such as a maximum power point tracker (refer to Section 4.2.4).

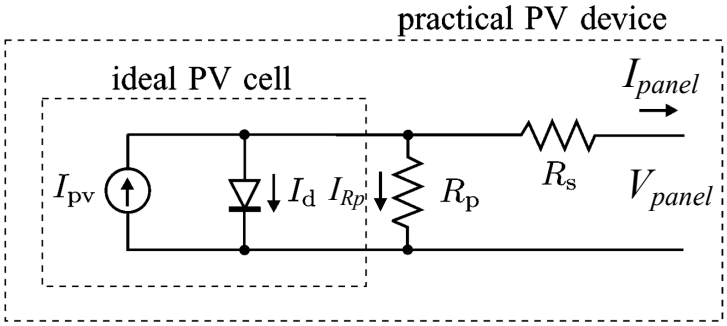

Figure 4.4: Single-diode model of the theoretical PV cell and equivalent circuit of a practical PV device including the series and parallel resistances (adapted from [155]).

To model the IV-curve of the PV panel, the single-diode model [155] with shunt (R_P) and series (R_S) resistances (Figure 4.4) is used as it achieves good fit with the empirical IV-curve [155]. Using this model, the IV relationship can be expressed by using the formula:

$$I_{panel} = I_{pv} - \overbrace{I_0 \left[\exp\left(\frac{V_{panel} + R_S I_{panel}}{V_t a}\right) - 1\right]}^{I_d} - \overbrace{\frac{V_{panel} + R_S I_{panel}}{R_P}}^{I_{Rp}} \tag{4.3}$$

where, I_{pv} and I_0 are the photovoltaic and saturation currents, respectively, of the array and $V_t = N_s kT/q$ is the thermal voltage of the array with N_s cells connected in series, k is the Boltzmann constant, q is the electron charge constant, T (in Kelvin) is the temperature of the $p-n$ junction, and a is the diode ideality constant. To obtain the I-V curve of a specific panel using this formula, the parameter values (R_P, R_S, I_{pv} and I_0) need to be determined. A number of different approaches have been proposed in the literature to determine these parameters. The approach proposed by Villalva et al. [155] is selected due to its practicality as it requires only four parameters to obtain the IV-curve: the open circuit and maximum power voltages (V_{oc} and V_{mp}), and short circuit and maximum power currents (I_{sc} and I_{mp}). These four parameters are commonly available in most PV panel datasheets or can be easily determined empirically at a given irradiance level. This approach also models the shift in maximum power point according to different input conditions, which is important for modeling losses from shift in maximum power operating point. The authors have made the modeling code written in MATLAB publicly available for download [155] and is reproduced in Appendix C.

Figure 4.5 show the IV and PV-curves of a Solarex MSX-005F PV panel using measured and modeled values. It can be seen that the modeled curve fits the measured data with a maximum error within 5%. Thus, compared to the simple approach that models the PV panel as its maximum power scaled by the input irradiance [154], the selected modeling

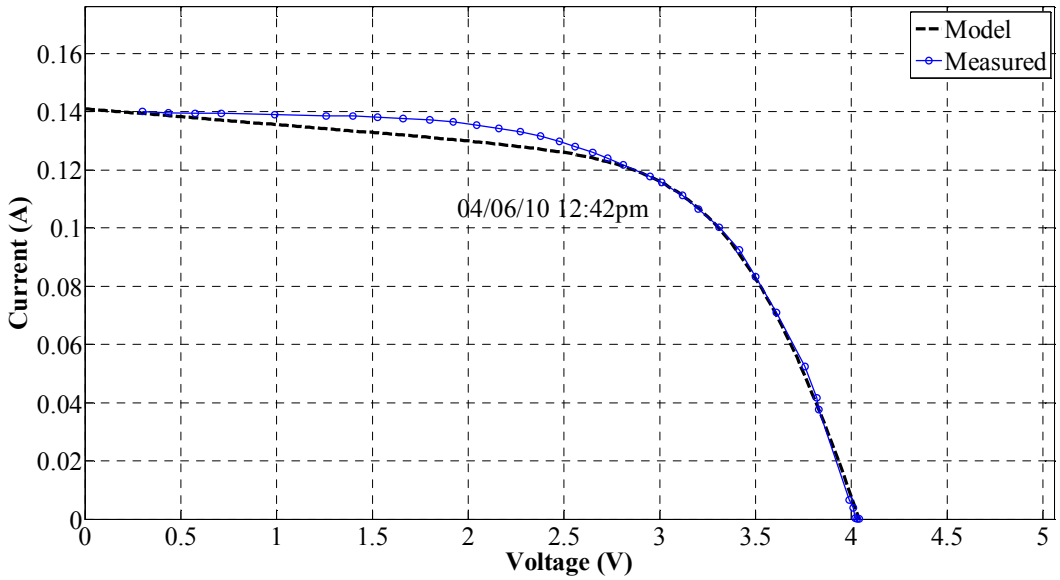

(a) Modeled and measured IV curves.

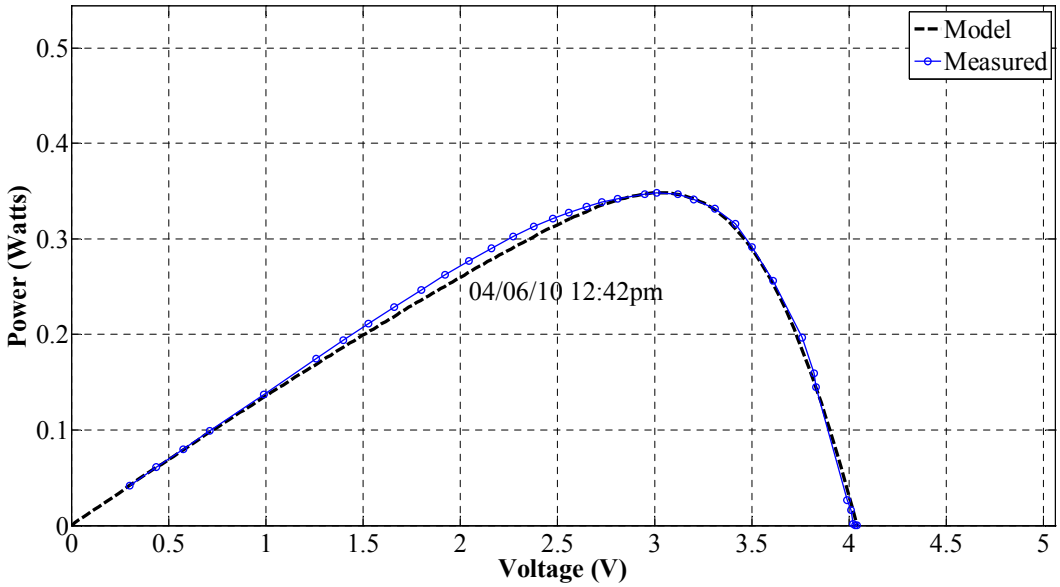

(b) Modeled and measured PV curves.

Figure 4.5: Solarex MSX-005F PV panel characterisation.

approach accounts for both the influence of external environment and system state on PV panel output.

4.2.4 Input Power Regulation/Conditioning

With respect to energy management, it is important to note that harvested power is determined by the configuration of this block. Modeling of input regulator should consider how it controls the PV panel operating voltage and take into account the efficiency of power transfer of input regulator to determine the actual power delivered from the

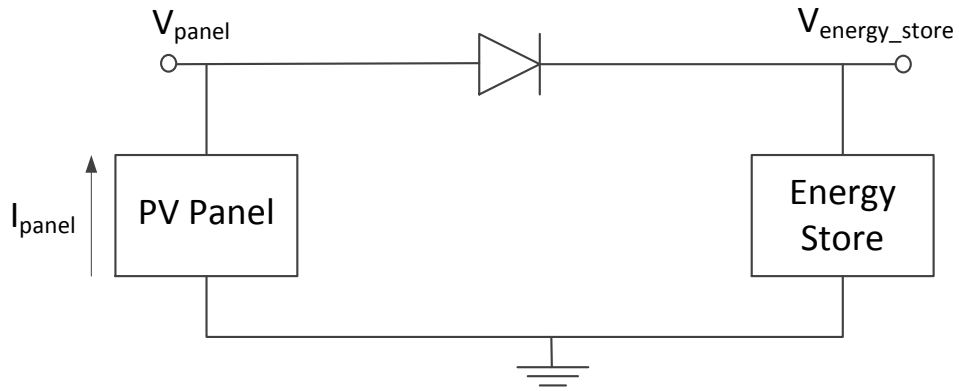

Figure 4.6: Connection of solar panel to energy storage through a Schottky diode.

PV panel. Since the input regulator is an interface between the PV panel and the energy storage, its modeling has to formulate the power transfer relationship depending on the operating point of PV panel and voltage of energy storage. As mentioned in Chapter 2 (Section 2.2.7.2), this transfer relationship depends on what configuration is used between the PV panel and energy storage.

The simplest case to model is that of a direct connection through a diode to prevent reverse current flow in to the panel (Figure 4.6). In this case, the solar panel voltage (V_{panel}) is determined by the voltage of the energy storage (V_{energy_store}) and the threshold voltage of the diode ($V_{threshold\_schottky}$) with the following equation [59]:

$$V_{panel} = V_{energy\_store} + V_{threshold\_schottky} \tag{4.4}$$

If the panel output current I_{panel} is greater than the diode conduction threshold, then the harvested power supplied to energy storage (P_{reg_in}) is given by:

$$P_{reg\_in} = V_{energy\_store} \cdot I_{panel} \tag{4.5}$$

For other cases in which the input regulator consists of either a fixed voltage regulator (buck/boost converter) for fixing the PV panel voltage or a dynamic power point tracking circuit, the modeling needs to consider:

(1) How the operating point of the PV panel is determined, as a function of regulator construction, environmental energy being received, and voltage of energy storage [59, 141]:

$$V_{panel} = f\,(\text{Regulation type}, P_{rad}, V_{energy\_store}) \tag{4.6}$$

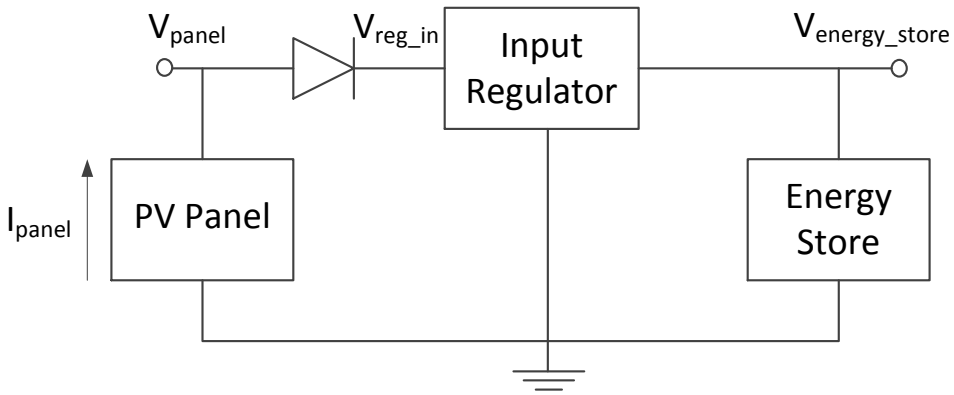

Figure 4.7: Connection of solar panel to energy storage via an input regulator.

(2) The efficiency of power delivered, usually as a function of input (PV panel) to output (energy store) voltage difference and PV panel current [141]:

$$\eta_{reg\_in} = f\left(V_{panel}, V_{energy\_store}, I_{panel}\right) \tag{4.7}$$

Different approaches are possible for modeling these characteristics. A very detailed circuit level model using SPICE or Simulink [144] can be used to simulate the detailed behaviour such as transients at start-up, load changes, and feedback of switching controller. However, from the perspective of matching supply and demand, the focus is on modeling of steady-state changes in power transfer efficiency (Equation 4.7) and how the PV panel terminal voltage can be determined (Equation 4.6) given the energy store voltage and other inputs depending on the regulator type. To achieve this, some relationship can be constructed that expresses these values in terms of the inputs. Since a variety of input regulator configurations are possible as discussed in Section 2.2.7.2 (Chapter 2), some examples are used to illustrate this. To model the efficiency of the regulator η_{reg_in}, a relationship can be constructed from the efficiency data measured empirically or derived from curves provided in the manufacturer data sheet. For example, consider a maximum power point tracking regulator described in [141]. For this regulator the voltage of the PV panel is determined using a maximum power point tracking circuit. The efficiency of this regulator can be obtained from the transfer curves as a function of PV panel output power and supercapacitor voltage as shown in Figure 4.8. As can be seen since these curves are non-linear, it is not easy to express these using a formula. To address this, piecewise linear interpolation can be used [59]. Next, another example is used to illustrate the modeling of Equation 4.6. Suppose that a step-down converter and Schottky diode constitute the input regulator (Figure 4.7) to fix the PV panel operating point to a certain voltage with supercapacitor as energy storage. Now, depending on the voltage of energy store V_{energy_store}, the following two cases determine the PV panel voltage [59]:

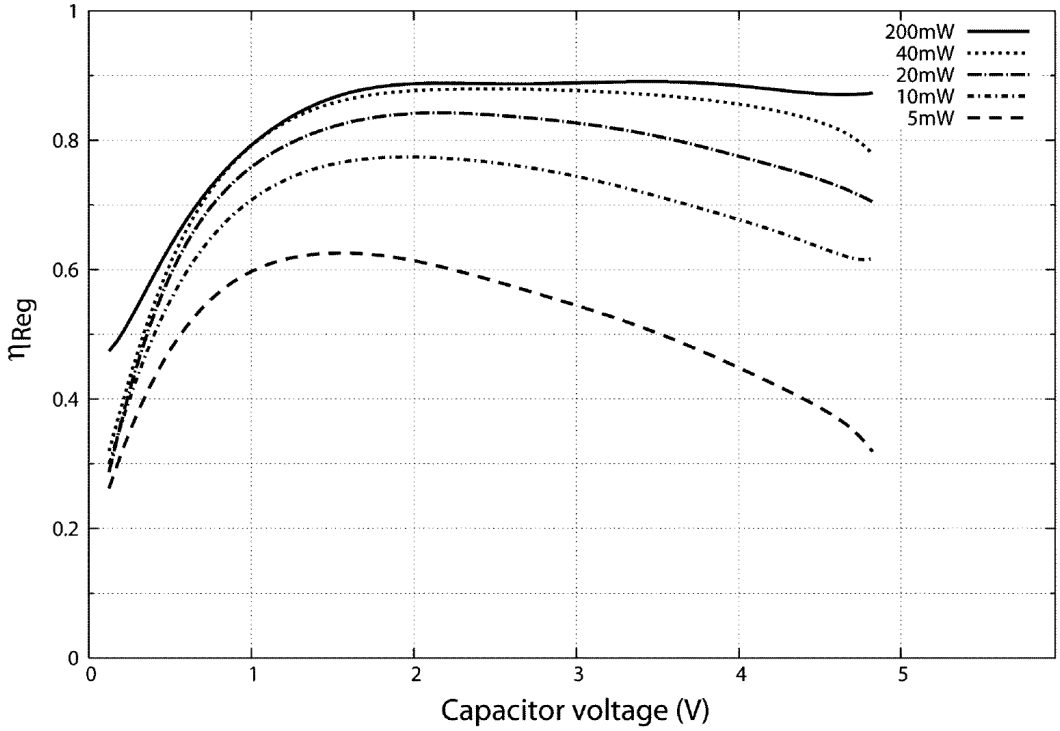

Figure 4.8: Efficiency curves of a MPPT input regulator [141] versus supercapacitor voltage and panel output power (Reproduced from [141]).

1. Constant input-voltage mode: When the output voltage of the input regulator V_{energy_store} is below a certain level $V_{reg\_in\_thres}$, the PV panel voltage V_{panel} remains constant irrespective of the voltage of the supercapacitor:

$$V_{panel} = V_{reg\_in\_on} + V_{threshold\_schottky} = const, \text{ if } V_{energy\_store} \leq V_{reg\_in\_thres} \tag{4.8}$$

where, $V_{reg\_in\_on}$ represents the constant voltage value. $V_{reg\_in\_on}$ and $V_{reg\_in\_thres}$ depends on the specifics of step-down converter used.

2. Pass-through mode: When the output voltage of the input regulator V_{energy_store} exceeds the threshold $V_{reg\_in\_thres}$, the PV panel voltage begins following the voltage of energy store (V_{energy_store}):

$$V_{panel} = V_{energy\_store} + V_{threshold\_schottky}, \; V_{energy\_store} > V_{reg\_in\_thres} \tag{4.9}$$

The reference system design used in this thesis uses a direct connection of PV panel through a diode for reasons discussed in Section 2.3. In this case, the behaviour is simple to model and is governed by Equations 4.4 and 4.5.

4.2.5 Energy Storage

For modeling of energy storage from viewpoint of energy management, it is important to consider the following:

1. **Losses in energy transfer (η_{energy_store})**: For energy neutral operation, these losses have to be included in the total energy that needs to be replenished.

$$E_{dischg} = \eta_{energy\_store} \cdot E_{chg} \tag{4.10}$$

2. **Terminal voltage characteristics (V_{energy_store})**: The change in terminal voltage of the energy storage during charging and discharging influences both the efficiency of output voltage regulator (Section 4.2.6) and the energy output from the PV panel (Section 4.2.4). Hence, energy management needs to account for these changes in input and output energies according to state of energy storage. The voltage-to-energy relationship (V_to_E), or vice verse, describes the relationship between the voltage and the energy level of the energy storage.

$$V_{energy\_store} = E\_to\_V(E_{energy\_store}) \Leftrightarrow E_{energy\_store} = V\_to\_E(V_{energy\_store}) \tag{4.11}$$

3. **Estimation of stored energy (E_{energy_store}) and leakages ($E_{leakage}$)**: Besides knowing what is currently available, it is also important to know how much of this can be available for consumption in future according to a given consumption rate. This is also affected by leakage over time-scale of interest.

These characteristics depend upon the type of energy storage. Energy storages can be classified into two main categories with respect to modeling requirements: supercapacitors and rechargeable batteries.

4.2.5.1 Supercapacitors

Supercapacitors are commonly modeled using the ideal supercapacitor relationship of stored energy and voltage:

$$E_{energy\_store} = \frac{1}{2} C \cdot V^2_{energy\_store} \tag{4.12}$$

Supercapacitors are generally characterised as having relatively high self-discharge compared to rechargeable batteries [131, 164]. In this regard, the leakage rate modeling

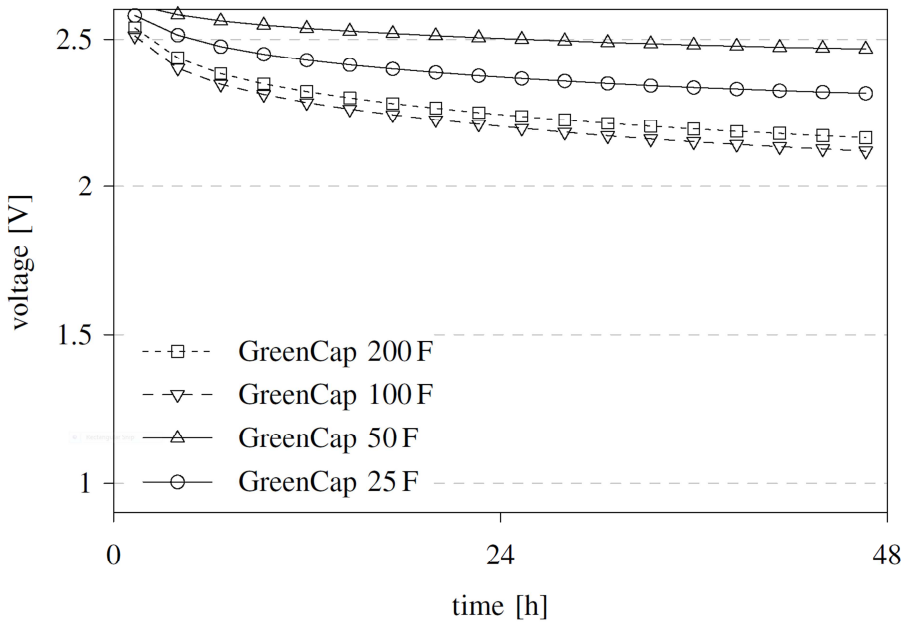

Figure 4.9: Self discharge of supercapacitors showing changing voltage vs time (Reproduced from [131]).

approach of [131] is used, using measured voltage-time data provided by authors of [131]. Based on the empirically observed behaviour of self-discharge as shown in Figure 4.9 for SAMWHA Green Cap supercapacitor [35], the leakage of supercapacitors is modeled as a non-linear (exponential) function of voltage [131, 164]. The voltage-time graph for supercaps of different capacities is given in Figure 4.9. This method is based on the observation that the energy level of a supercapacitor monotonically decreases and that self-discharge is highly correlated with the voltage. From the data plotted in Figure 4.9, the leakage power of the supercapacitors can be approximated numerically from:

$$E(V_C) = \frac{CV^2}{2} \Rightarrow P_{leak}(V_C) \approx \frac{\Delta E(V_C)}{\Delta t} = \frac{C\Delta V_C^2}{2\Delta t} \tag{4.13}$$

where ΔV_C^2 is the difference of supercapacitor voltages V_C^2 at time t and V_C^2 at time $t + \Delta t$. The corresponding results are shown in Figure 4.10. The noise in the lower voltage regions is due to the noisy measurement of the slowly decreasing voltage. Note that power is shown in logarithmic scale, leading to an exponential behavior of leakage power:

$$P_{leak} = P0 \cdot \exp^{\alpha \cdot V_C} \tag{4.14}$$

where, $P0$ and α are constants and their values are obtained from exponential least squares curve fitting [131]. The authors in [131] determined estimations according to Equation 4.14 for supercapacitor of various capacities. The results are shown in Figure 4.11. Appendix C gives the model for estimating the leakage using this approach.

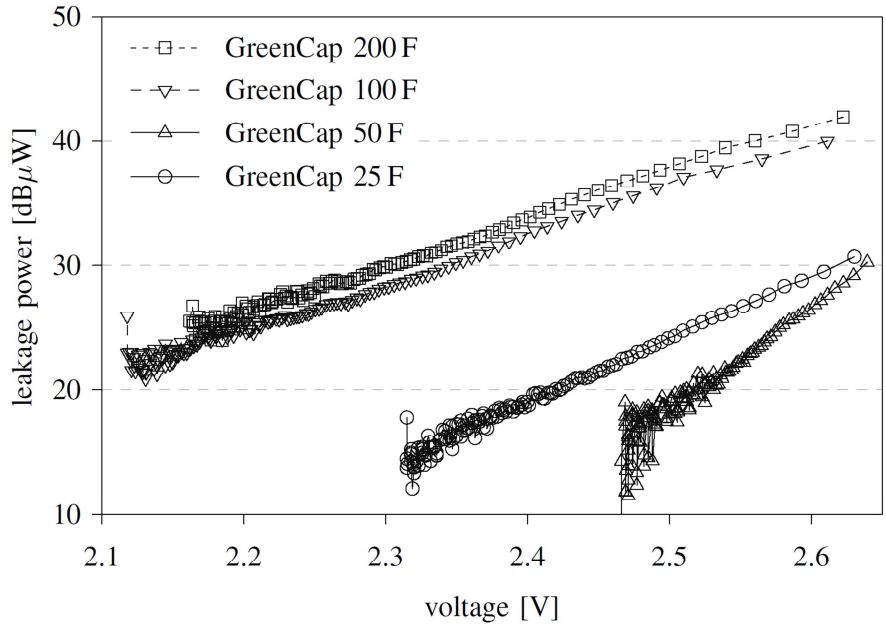

Figure 4.10: Measured leakage power of different sizes of supercapacitors (Reproduced from [131]).

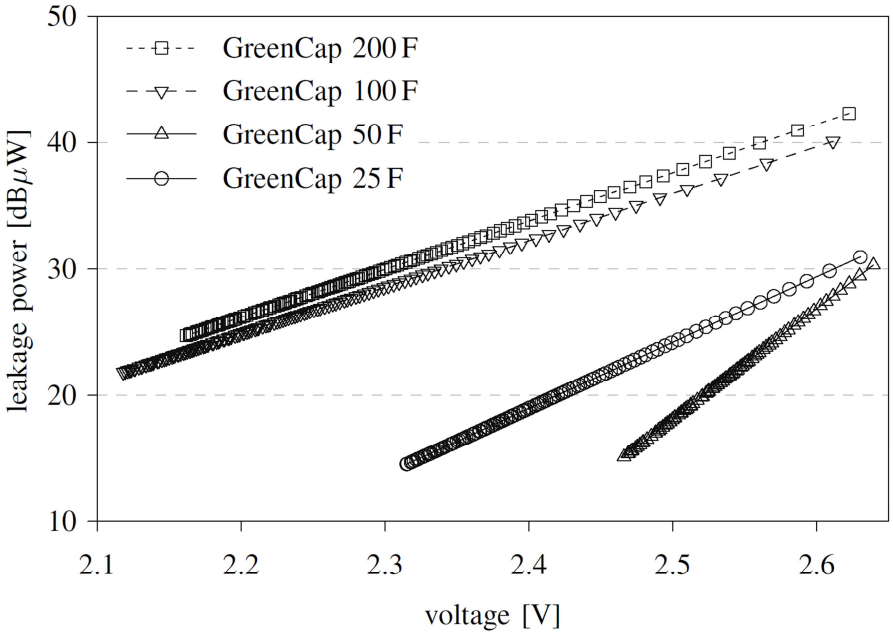

Figure 4.11: Estimated leakage power of different sizes of supercapacitors according to Equation 4.14 (Reproduced from [131]).

Figure 4.12 shows that the self-discharge rate can also vary according to how long the supercapacitor is held at a given voltage level [158]. Furthermore, it has been shown that the supercapacitor stored energy and voltage relationship cannot be accurately determined by using the ideal capacitor relationship [158, 15]. In [158], the supercapacitor behaviour is modelled using a RC ladder circuit with a voltage-dependent capacitance in its first branch. Based on this model, it is shown the supercapacitor terminal voltage and stored energy characteristics depend on the previous charge and discharge history. In [15], the authors show that over a large number of charge-discharge cycles, deviation of supercapacitor voltage-energy behaviour from the ideal capacitor equation becomes negligible. Based on this, the modeling approach selected in this work uses the ideal capacitor equation for voltage-to-energy relationship. Self-discharge is more difficult to quantify under the random level of charging and discharging experienced by a typical harvesting system. Accurate modeling of supercapacitor leakage and stored energy is an area of active research. However, from energy management perspective it is important to consider that all recent works [131, 164, 15, 158] note that leakage is only noticeable when the supercapacitor is charged up close to its maximum voltage, and can be ignored practically at lower voltages, which depends on the specific capacity and voltage range of supercapacitor. In this thesis, the exponential model [131] of leakage is used due to its ease of implementation, low complexity and ability to capture the general trend of observed self discharge as shown in Figures 4.9 and 4.12. Based on practical validations discussed in Section 4.3, this model was found to give higher self-discharge than observed under the conditions of experiment. Supercapacitors have a high average efficiency (greater than 95%) and can be practically ignored for modeling.

4.2.5.2 NiMH Rechargeable Batteries

For modeling energy management, a battery model capable of modeling the stored charge and voltage-capacity relationship is desired. Since NiMH batteries are most commonly used, this section focuses on modeling this type of battery. Accurate modeling of voltage-capacity relationship of rechargeable batteries is complicated by the fact that this relationship is non-linear and cannot be simply modeled by a single formula. Furthermore, it is dependent upon whether the battery is being charged or discharged as well as the rate of charging/discharging current. Figure 4.13 shows the capacity-to-voltage profiles for a Varta 150H NiMH battery. A number of battery models have been discussed in literature out of which the battery model proposed by Chen and Rincon-Mora [23] fulfils the modeling requirements mentioned. The authors present characterisation of Lithium-ion and NiMH battery and determine the equations for model parameters as a function of state-of-charge (SoC) and current. They note that NiMH batteries have a significant dependence on current and the model parameters are a function of both SoC and current. Although this model demonstrates a high accuracy, it is a circuit level model using variable resistors and capacitances and thus complex to simulate over

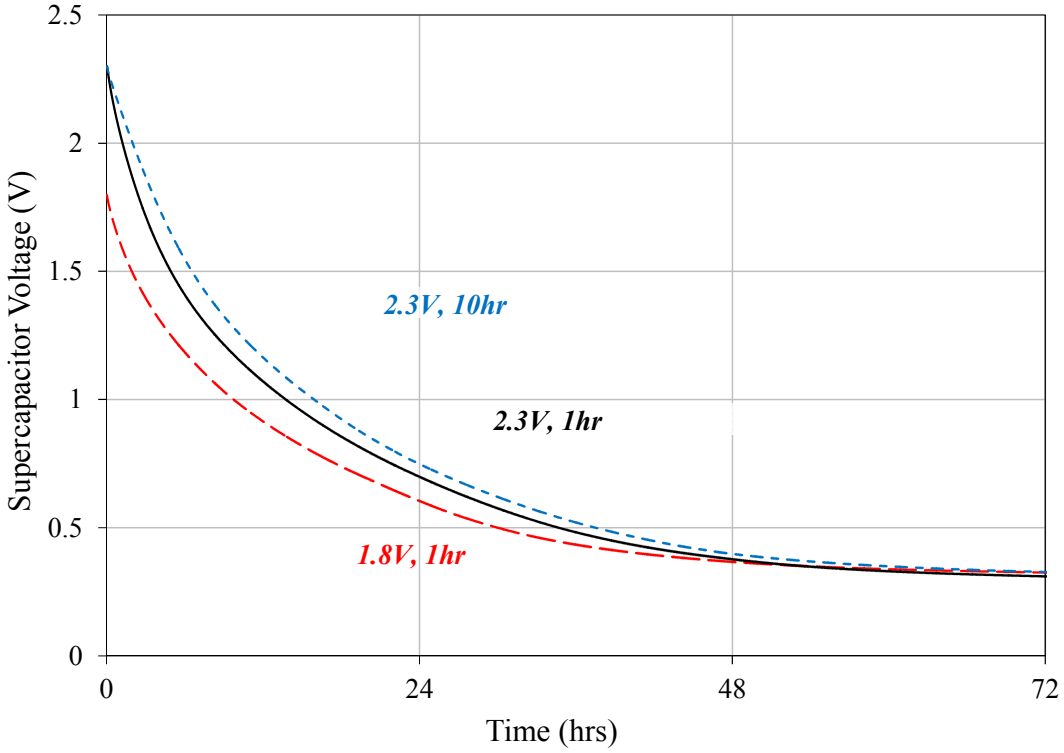

Figure 4.12: Measured self-discharge of Panasonic 4.7F 2.3V supercapacitor showing different rates of discharge according to charging conditions (Reproduced from [158]).

time scales of interest. An alternate approach is to use the empirically derived voltage-capacity curves (Figure 4.13) for typical values of charge and discharge currents. For example, voltage curves for discharge currents corresponding to sleep, active and radio transmission modes of sensor nodes workload can be obtained as these represent the typical loads. Similarly, charging curves within 0.1CA-0.3CA (safe limit) charging rate can be used. Based on these curves and piecewise linear interpolation, the voltage and capacity at any point can be approximated.

The average charge-discharge efficiency of NiMH batteries is taken as 66% based on datasheet and self-discharge is assumed to be negligible under typical dynamic charging and discharging conditions. Note that since the battery can have different voltage depending on whether it is being charged or discharged at any given time, the exact state needs to be determined based on the net current (supply vs demand). The details of this are given in Section 4.2.9 that discusses the overall interdependence between components.

4.2.6 Output Regulator Modeling

With reference to energy management, it is necessary to know how much losses are incurred depending on regulator input voltage for a given load power consumption.

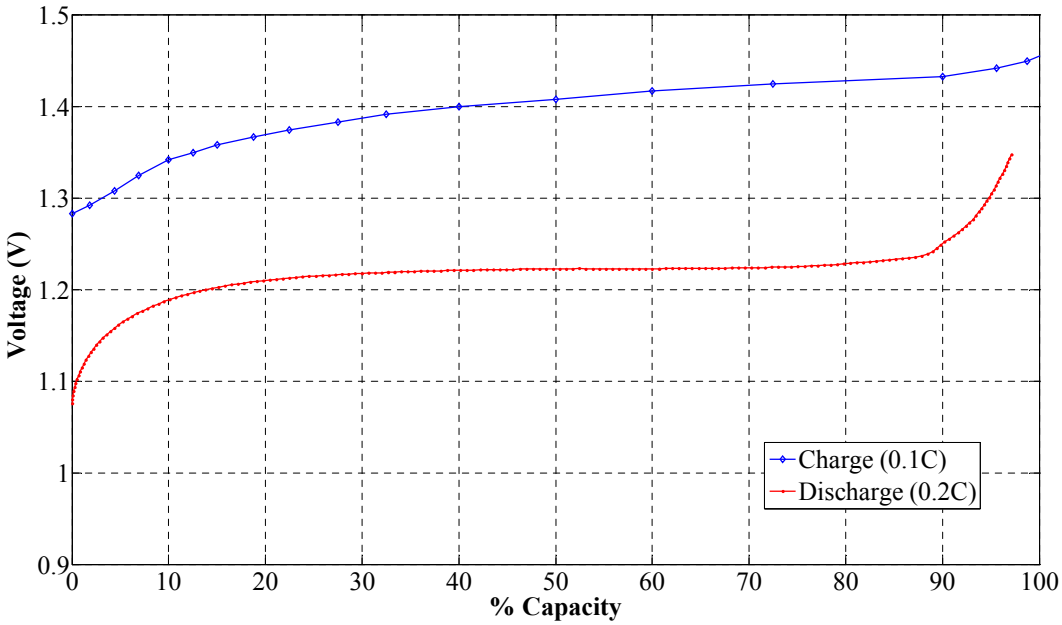

Figure 4.13: Empirically observed NiMH battery charging (0.1C) and discharging (0.2C) state voltage curves against capacity.

These losses are usually variable and must be accounted in energy budgeting to ensure correct energy neutral system operation. For instance, energy management may need to reduce consumption in low efficiency operating regions to avoid poor utilisation of harvested energy. Furthermore, some stored energy cannot be utilised when the energy storage voltage falls outside the regulator operating threshold and this needs to be modeled.

The modeling of output voltage regulator considers the following two issues, given the values of voltage input to the regulator and the output load current:

- **Power Efficiency**: What is the efficiency of power transfer?
- **Operating Range**: Is the regulator operational under the given the input voltage and current demand?

As mentioned in the case of input regulator modeling (Section 4.2.4), detailed performance modeling of the output regulator is not the aim here. Instead a relationship and set of conditions that expresses the power transfer efficiency and operating conditions of the regulator are needed. These are commonly available in manufacturer data sheets in the form of various graphs and can be used to build a model. These are mostly non-linear and have different forms among different parts as shown in Section 2.2.7.1. The piecewise linear interpolation method is used to capture these relationships for modeling [59]. The model is given in Appendix C.

4.2.6.1 Modeling Power Efficiency

The power efficiency of an output regulator η_{reg_out} is a function of the energy storage voltage V_{energy_store} and the output load current I_{load}.

$$\eta_{reg\_out} = f\left(V_{energy\_store}, I_{load}\right) \tag{4.15}$$

Figure 4.14 shows the estimation of efficiency of a MAX1724 regulator (Section 2.3 using piecewise linear interpolation based on the manufacturer-provided data. It can be observed that the efficiency of the MAX1724 increases as the load current increases. Furthermore, the efficiency of this regulator also increases with voltage and it reaches the saturation point at around 2.5V.

The power drawn by the output regulator is obtained by power consumption of the load P_{load} and output regulator efficiency η_{reg_out}.

$$P_{reg\_out} = \frac{1}{\eta_{reg\_out}} \cdot P_{load} \tag{4.16}$$

4.2.6.2 Modeling Operating Range

The operating range of the regulator can be modeled using the input voltage and maximum output current limits specified in the datasheet. First, the input voltage is checked to confirm whether it lies in the manufacturer-provided input voltage range. The maximum load current of an output regulator varies depending on its input voltage. This can also be modeled using interpolation when the maximum load current is provided for a sampling of input voltages.

4.2.6.3 Validation

Table 4.2 shows empirically obtained values for MAX1724 output regulator for wireless sensor load current values of 0.590mA (idle) and 20.06mA (active) for a range of input voltages. In a system using a supercapacitor, the input voltage will vary according to stored energy in the supercapacitor. Note that efficiencies are higher for active current compared to idle current, except at low voltages. Furthermore, the efficiency changes by more than 15% as the input voltage is reduced, thus decreasing the energy utilisation efficiency of harvested-energy.

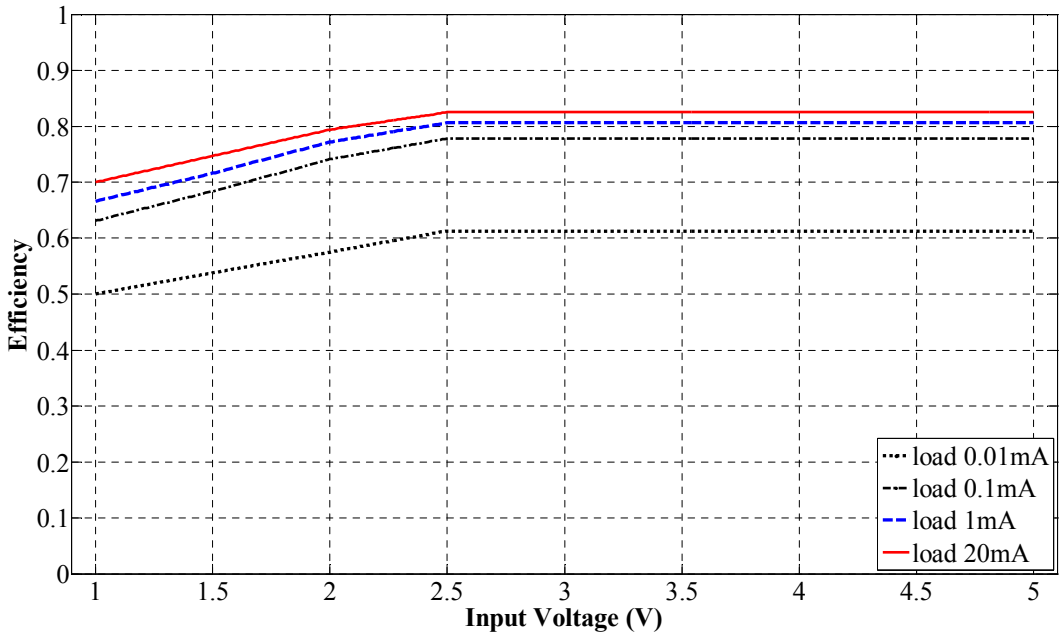

(a) Efficiency as a function of input voltage.

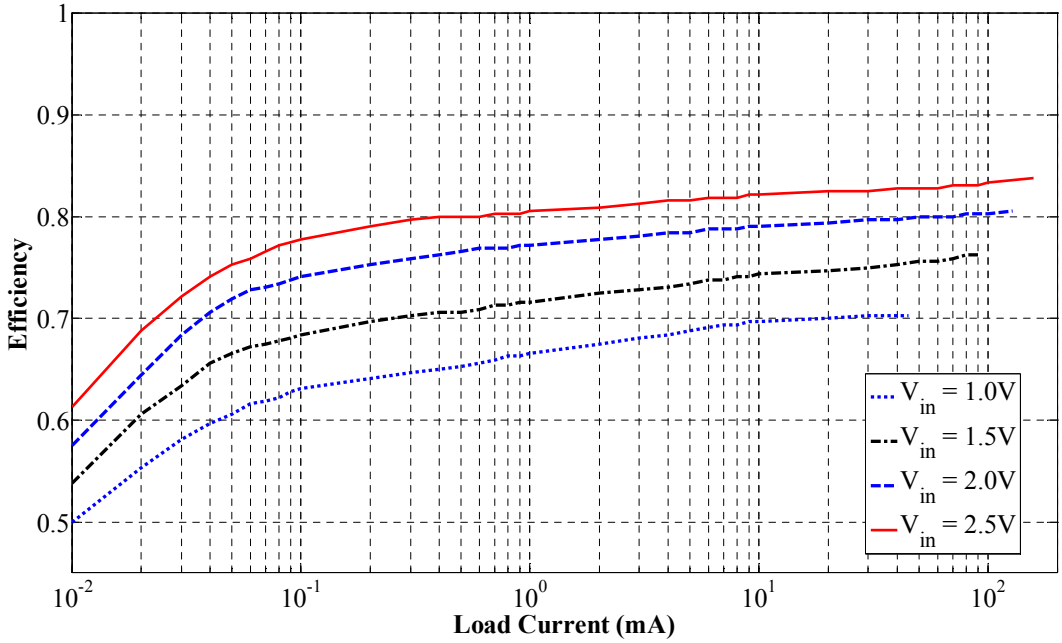

(b) Efficiency as a function of load current.

Figure 4.14: Piecewise linear modeling of efficiency of MAX1724 regulator from datasheet (Reproduced from [59]).

Table 4.2: Measured output regulator efficiencies for different input voltages for two load currents.

	Input Current (mA)				**E**fficiency %	
Input	Ideal		Measured			
Voltage (V)	Idle	Active	Idle	Active	Idle	Active
2.6	0.749	25.461	1.113	31.9	67.28	79.81
2.5	0.779	26.479	1.162	33.6	67.02	78.81
2.4	0.811	27.583	1.222	35.3	66.39	78.14
2.3	0.847	28.782	1.273	37.45	66.50	76.85
2.2	0.885	30.090	1.346	39.6	65.75	75.98
2.1	0.927	31.523	1.442	42.25	64.30	74.61
2	0.974	33.099	1.536	45.2	63.38	73.23
1.9	1.025	34.841	1.65	48.63	62.11	71.65
1.8	1.082	36.777	1.758	52.03	61.53	70.68
1.7	1.145	38.940	1.889	55.79	60.63	69.80
1.6	1.217	41.374	1.99	60.15	61.15	68.78
1.5	1.298	44.132	2.125	65.39	61.08	67.49
1.4	1.391	47.284	2.17	72.06	64.09	65.62
1.3	1.498	50.922	2.24	80.39	66.86	63.34
1.2	1.623	55.165	2.32	88.57	69.94	62.28
1.1	1.770	60.180	2.439	92.62	72.57	64.98
1	1.947	66.198	2.6	96.55	74.88	68.56
0.9	2.163	73.553	2.83	97.86	76.44	75.16

4.2.7 Workload and Energy Management

The application workload is the consumer of harvested energy and it includes all modules that constitute a wireless sensor node (Chapter 1, Section 1.2) such as a microcontroller, wireless radio, sensors, supporting peripherals and dedicated processing unit such as a digital signal processor. An application consists of different tasks or activities, having a number of power consumption levels. A simple approach for modeling application workload power is to average the power demand of different activities throughout the system operation. For example, for the common case of an application workload duty cycled between an active and idle state, the average current consumption I_{load} is calculated using the value of duty cycle (DC) and the current demands of active I_{active} and idle I_{idle} states.

$$I_{load} = DC \cdot I_{active} + (1 - DC) \cdot I_{idle} \quad (4.17)$$

$$V_{load} = V_{reg\_out} \quad (4.18)$$

$$P_{load} = V_{load} \cdot I_{load} \quad (4.19)$$

The shortcoming of this modeling is that it cannot accurately account for changes in operating characteristics of the output voltage regulator and rechargeable battery because they vary with the load current demand. For example, as discussed in Section 4.2.6 the regulator efficiency can be quite different for idle (uA) and active (mA) currents. Also, in case of modeling rechargeable battery, its terminal voltage is also a function of current drawn (Section 4.2.5). Hence, accurate modeling of load needs to account for different load currents drawn at different times. Instead of averaging, load power is calculated using per activity current demand I_{state}:

$$P_{load} = V_{load} \cdot I_{state} \tag{4.20}$$

This introduces the problem of managing the simulation time step since a wireless sensor node usually operates at many different current levels for short time intervals in its active state, whereas it can spend a large proportion of time in idle state. If the lowest time step is used, it will be inefficient to model the long term (multiple days) trends. A solution to this is to implement discrete event driven simulation, as explained in Section 4.2.10. Furthermore, only order of magnitude changes in current drawn by load are considered as different activities, e.g., change from μA to mA, or 10s of mA.

The functionality of application workload is modeled in terms of different activities in a given time interval and the time spent per activity, e.g, the time spent in acitve mode or in sleep mode. The implementation of energy management policy is modeled behaviourally, based on specific policy being used. The outcome of energy management can be an energy budget that is translated by the workload in its activity levels. It can also be a parameter that directly decides the activity levels, e.g., a duty cycle.

4.2.8 Energy Monitoring Components

Modeling of energy monitoring components needs to consider parasitic energy overheads and accuracy issues. The overheads introduced can me modeled in the following ways depending on the placement of monitoring circuitry:

- Loss in power harvested from PV panel.
- Additional power drawn from energy storage.
- Additional power drawn via output regulator.

Furthermore, these losses can be constant over time or variable, varying according to amount of power harvested or whether the monitoring circuit is idle or active. To illustrate these with an example, consider some typical monitoring circuits such as the current sense monitors used to calculate PV panel current output and battery monitor

to measure battery parameters. During active state, a current sense amplifier will draw some current from PV panel output for it's operation, which depends on the amount of current output from the panel. For example ZXCT1010 high side current monitor can draw up to 0.1-1 mA, depending on voltage drop across the sense resistor. Similarly, a DS2438 battery monitor IC has a quiescent current draw of 50-100 μA from the battery being monitored during active state.

The accuracy modeling should consider the physical limitation of monitoring hardware. For example, a ZXCT1010 current monitor will not be able to measure the PV panel current, if the panel voltage drops below 2.5V (the minimum operating voltage). Similarly, the DS2438 battery monitor cannot function if the battery voltage falls below 2.4V. In case of A/D converters used for sampling the voltages, errors due to offsets and quantization may also be modeled.

4.2.9 Overall System Behaviour

Given the behaviour of each system component and their interconnections, the overall system behaviour based on the interdependencies can be described as follows (also refer to Figure 4.3 and Appendix C.1):

1. Given the current state of energy storage (V_{energy_store}) and irradiance being received by PV panel, the input regulator determines the PV panel operating point V_{panel}.

```
supercap_vol_temp = calc_supercap_mJ_to_V(supercap_energy_mJ(i,1),
                                          supercap_capacitance);
panel_vol_temp = supercap_vol_temp + vf_schottky_init;
```

2. Using V_{panel}, the PV panel output current I_{panel} is determined from the IV-curve.

```
% interpolate for the given panel voltage from modeled I-V curve
panel_cur_temp = (interp1(V_panel,I_panel,panel_vol_temp))*1e3;
% turn off the Schottky diode if the forward-direction current
% is smaller than if_min_mA
if (panel_cur_temp < if_min_mA)
    panel_vol_temp = 0;
end

% solar panel output power
panel_pow_temp = panel_vol_temp * panel_cur_temp;
```

```
% power after Schottky diode and input regulator
reg_in_pow_temp = radiation_cur_temp * (panel_vol_temp -
                                        vf_schottky_init);
```

3. Based on efficiency of input regulator η_{reg_in}, the power delivered from input regulator (P_{reg_in}) is calculated.

```
% power after Schottky diode and input regulator
reg_in_pow_temp = radiation_cur_temp * (panel_vol_temp -
                                        vf_schottky_init);
```

4. Given the current load current demand I_{load}, and input voltage V_{energy_store}, the output regulator efficiency η_{reg_out} is determined to calculate the output power P_{reg_out}.

```
% set the load current as the average value.
load_cur(i,1) = current_duty_cycle * load_active_mA +
                (1-current_duty_cycle) * load_sleep_mA;

% determine the operating point of MAX1724 output regulator.
reg_out_vol_temp = calc_vout_MAX1724(supercap_vol_temp);
eff_reg_out_temp = calc_efficiency_MAX1724(supercap_vol_temp,
                                           load_cur(i,1));

% load seen by output regulator
reg_out_pow_temp = load_cur(i,1) * reg_out_vol_temp / eff_reg_out_temp;
```

5. Difference of power delivered from the solar radiation and used by the load is determined: $P_{net} = P_{reg\_in} - P_{reg\_out}$

6. If the surplus is positive ($P_{net} > 0$), System is in recharge state with energy of $P_{net} \cdot \Delta t$ being charged to energy storage.

7. If the surplus is non-positive ($P_{net} < 0$), System is in discharge state with energy of $-P_{net} \cdot \Delta t$ being discharged from energy storage.

```
% available power from the solar panel
avail_pow_temp = max (0, reg_in_pow_temp - reg_out_pow_temp);

% power discharge from supercap
supercap_draw_temp = max (0, reg_out_pow_temp - reg_in_pow_temp);
```

```
% net power from solar panel excluding load
net_temp = avail_pow_temp * eff_supercap -
            supercap_draw_temp;
```

8. The next energy level and voltage of the energy storage is calculated:

$$E_{energy\_store} = E_{energy\_store} + P_{net} \cdot \Delta t$$
$$V_{energy\_store} = E\_to\_V(E_{energy\_store}) \tag{4.21}$$

```
supercap_leakage_mJ(i,1) = min(supercap_max_mJ, ...
calc_100F_supercap_leakage_tuh(supercap_energy_mJ(i,1) / 1000,
                               delta_t) * 1000);

% calculate the supercap energy in the next step considering leakage
next_supercap_energy_mJ = min(supercap_max_mJ, supercap_energy_mJ(i,1) -
                          supercap_leakage_mJ(i,1) + delta_t * net_temp);
```

Since batteries can have different terminal voltage depending on charging or discharging state, the above steps are calculated for using both charging and discharging states and if either of these states result in net charge, then the charge state is selected.

4.2.10 Simulation Time-Step

The simulation time-step size influences the accuracy in modeling the effects of changing harvesting supply, load power and computation of non-linear characteristics of system components, e.g., voltage profile of battery, efficiency of regulator etc. However, using small time steps can drastically increase the simulation time. The solution is to use discrete event-driven simulation, such that the simulation time steps are decided based on changes in states of various components. The time steps can be defined in terms of events, which can be any of the following:

1. Change in harvester output power
2. Invocation of energy management policy to determine the load power consumption
3. Changes in power drawn by load (Section 4.2.7)
4. Crossing a knee point in piecewise linear model of a components

In practice it was found that using a simulation time step size of 30 seconds achieved reasonable accuracy between measured and simulated output as shown in Section 4.3.

4.3 System Model Validation

The selected modeling approach for each component and the interdependency between components that define the various system energy flows was discussed in Section 4.2. This section focuses on integrated validation of the complete system model to highlight the impact of state-dependent losses and component interdependency on energy neutral operation and energy utilisation. This is done by considering a system operation scenario and comparing the measured values obtained from the reference system with its simulated output. The reference photovoltaic energy harvesting system configuration described in Chapter 2 (Figure 2.14) is used for obtaining experimental results and model validation. Figure 4.15 shows the setup used for experiments and the energy harvesting supply attached to the sensor node. The PV panel is connected to a heat sink and a fan is used to keep the temperature from rising during experiments and panel characterization to avoid effects of temperature dependency. The intensity of input radiation is controlled by varying distance of 40W incandescent bulb from the panel. Fluke 8846A and Keithley 2002 high precision digital multimeters are used for measurements.

As a motivating case for validation and analysis, suppose that energy neutral system operation is required. Two cases are considered to show how this requirement can be violated by not accounting for factors that influence the energy flow (and vice versa). Consider a given workload demand that needs to be met with harvested-energy. When using energy management, the workload demand is normally decided based on the available energy. In this analysis, considering a fixed load demand and working backwards to determine the required energy supply makes it simpler to focus on changes in factors of interest without loss of generality. Suppose that the workload is operating at 50% duty cycle (30 seconds active and idle periods) and the load current demands for idle and active states (Section 4.2.6) are 0.590 and 20.06 mA, respectively. At an operating voltage of 3.3V supplied by the output regulator, the average power consumption is given by:

$$\begin{aligned} P_{load} &= V_{reg\_out} \cdot I_{load\_avg} \\ &= 3.3 \times (0.590 \times 0.5 + 20.06 \times 0.5) \\ &= 3.3 \times 10.325 = 34.0725mW \end{aligned} \tag{4.22}$$

Next, we consider the energy input required to match this load demand. Suppose that the energy management policy which decides the load demand does not account for the output regulator efficiency. Under this assumption, to meet the given load demand the required supply (P_{reg_out}) is determined as:

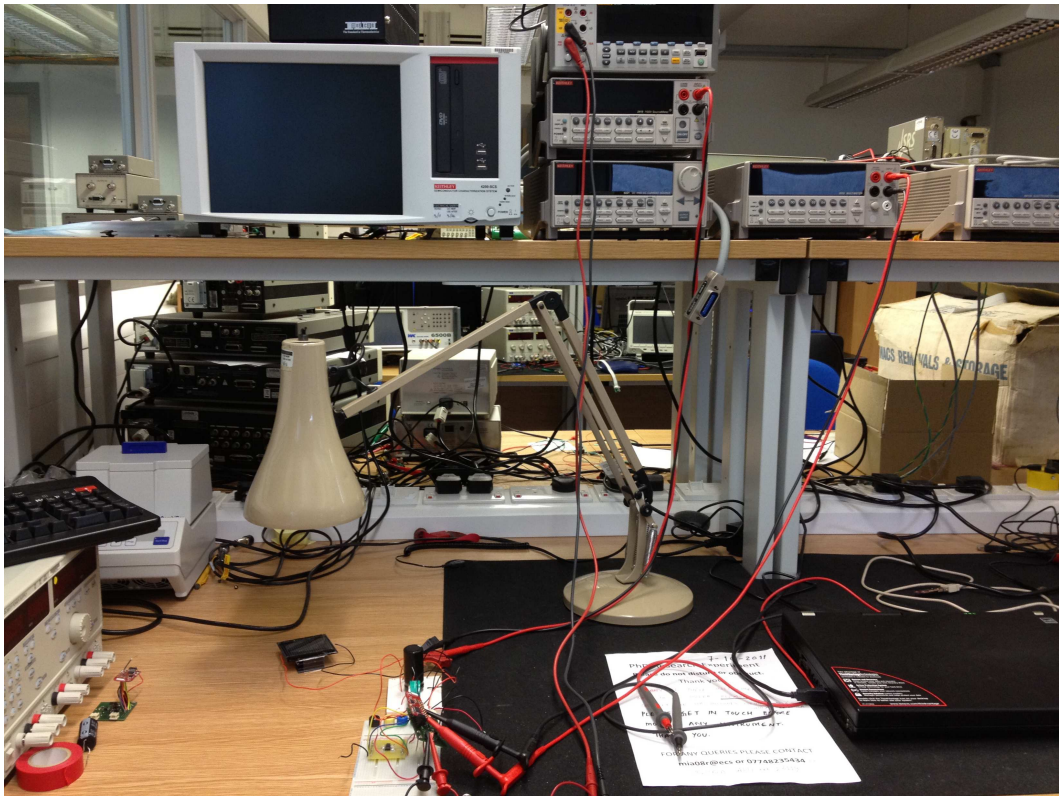

(a) Experimental Setup and instruments used.

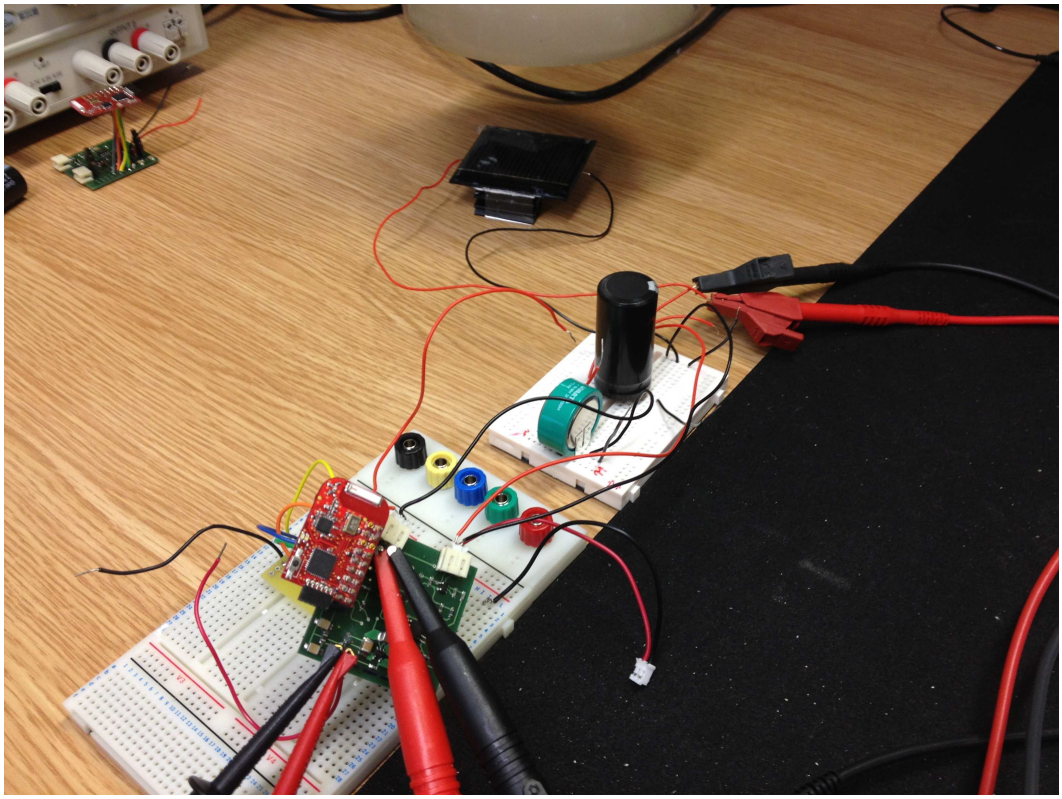

(b) Reference energy harvesting system.

Figure 4.15: Validation setup.

$$P_{load} = P_{reg\_out} = V_{energy\_store} \cdot I_{reg\_out} \tag{4.23}$$

This is the input power to the output regulator, determined by the energy store voltage V_{energy_store} (Section 4.2.6). The energy storage in this case is a supercapacitor, and suppose that its terminal voltage V_{energy_store} is 2.6V. Thus, for the required input power, the average value of input current I_{reg_out} is given by:

$$I_{reg\_out} = \frac{P_{reg\_out}}{V_{energy\_store}} = \frac{34.0725}{2.6} = 13.1048mA \tag{4.24}$$

This input current is supplied by the PV panel (via input regulator) and/or energy storage (Section 4.2.4). Under energy neutral operation, the harvested power P_{reg_in} meets this demand and the average power (charged and discharged) through energy storage should be zero:

$$P_{chg} = P_{dischg} \tag{4.25}$$

Hence, the stored energy should be conserved under energy neutral condition and there should be no net discharge of energy store. Having stated the case for required system operation based on the proposed system model, this condition is tested empirically and using simulation. This is done by setting the illumination level (desk lamp) to provide the required I_{reg_out} of 13.1048 mA at the supercapacitor voltage of 2.6V. Figure 4.16 shows the measured and simulated voltage of supercapacitor, under these conditions. It can be observed in Figure 4.16 that net supercapacitor voltage is gradually decreasing over time. The sawtooth pattern is due to charging and discharging of supercapacitor since during load idle state the input power is higher than consumed power and vice versa. The net decrease in voltage indicates that the input power is not sufficient to conserve the stored energy. The model simulation output follows the trend of measured results and the small difference from measured values are due to differences in simulated and actual PV panel current, and modeled and actual efficiency of output regulator. Note that effect of supercapacitor leakage is not shown in simulation results since the exponential leakage model (Section 4.2.5.1) resulted in a steeper fall of supercapacitor voltage than the measured output, indicating that the actual leakage is smaller.

To validate the contributing factors to the net discharge of supercapacitor voltage, the output regulator efficiencies at the given input voltage V_{energy_store} and load demands are considered (Table 4.2). Thus, the required input power to match the load consumption is recalculated by using measured input currents given in Table 4.2 to determine average I_{reg_out} as:

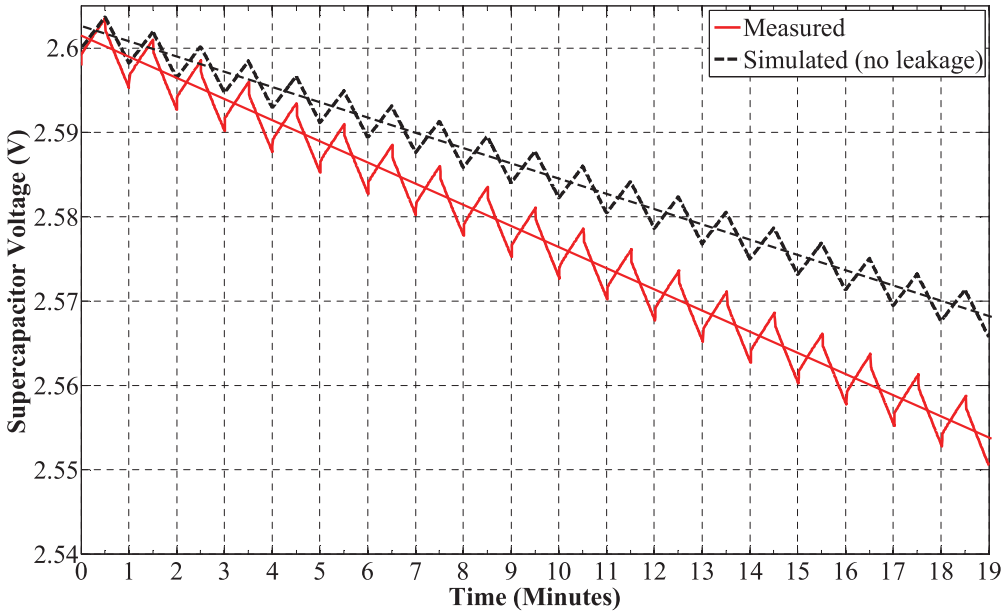

Figure 4.16: Net decrease in supercapacitor voltage shown by the average trend line due to ideal output regulator assumption, indicating that energy-neutral operation is not achieved.

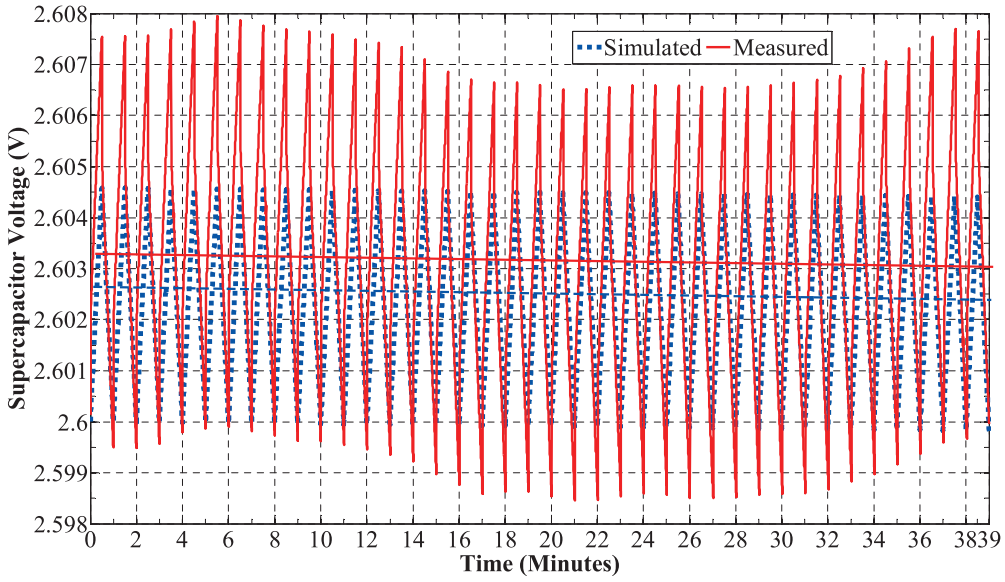

Figure 4.17: No change in net supercapacitor voltage as shown by the average trend line, validating energy neutral operation.

$$I_{reg\_out} = 31.9 \times 0.5 + 1.113 \times 0.5 = 16.5065mA \tag{4.26}$$

To provide this revised I_{reg_out}, the illumination level is increased. The measured and simulated supercapacitor voltage is shown in Figure 4.17. It can be observed that a similar sawtooth trend of supercapacitor voltage as seen in Figure 4.16 is observed according to the two states of workload operation, but there is no net change in supercapacitor voltage over time. This implies that the input power, calculated using revised I_{reg_out} meets the load demand and the energy stored in supercapacitor is conserved. The measured supercapacitor voltage swing is wider than simulated one, however, the scale of voltage on Y-axis indicates that the maximum difference is less than 4mV. Thus, the simulated output trend matches the overall trend, which is the aim of proposed modeling. Supercapacitor leakage is not included for the same reasons as mentioned in the previous case.

In the first case (Figure 4.16) where energy neutral operation is violated, the decreasing supercapacitor voltage will affect both the the overall efficiency of output regulator and the PV panel operating point. Since the PV panel terminal voltage is linked with the energy store voltage, the operating point of the PV panel shifts resulting in change in harvested power. Hence, this case also highlights the interdependence of energy store voltage on both input and output power, which is commonly abstracted in simple system models. Depending on the specific PV panel and supercapacitor, these interdependencies can further increase the mismatch between supply and demand due to the decreasing efficiency of output regulator and decreasing output of PV panel.

It is noted that the exact behaviour of system depends on the property of selected components. The configuration of input regulator dictates how the PV panel output is influenced by the changes in battery voltage. Fixing the PV panel operating point or using MPPT will result in different outcomes under the same conditions. Similarly, the change in output regulator power transfer will also vary with the specific regulator used. Using a battery instead of supercapacitor reduces the voltage swing with changes in stored energy. Nevertheless, some specific relationships according to existing interdependencies need to be taken into account by the energy management to ensure correct energy neutral operation.

4.4 Concluding Remarks

This chapter considered the problem of achieving the desired match between supply and consumption under the non-ideal characteristics or losses of system components. This is addressed by identifying the contribution of individual system component on supply or demand through modeling. The intention is not to propose novel models for different

components, but to identify the characteristics that influence the supply or demand and selection of suitable models that achieve this purpose. The system modeling has been implemented using MATLAB and each system component is modeled using a modular approach by encapsulating functionality within functions or scripts. The simulator uses a specific configuration of an energy harvesting system along with user-defined components data to model the system behaviour. The energy available at a location can be modeled as a series of irradiance values over time. The approach for modeling PV panel requires only four parameters to obtain the IV-curve, which are commonly available in most PV panel datasheets or can be easily determined empirically at a given irradiance level. Modeling of input regulator should consider how it controls the PV panel operating voltage and take into account the efficiency of power transfer of input regulator to determine the actual power delivered from the PV panel. Since the input regulator is an interface between the PV panel and the energy storage, its modeling has to formulate the power transfer relationship depending on the operating point of PV panel and voltage of energy storage. Energy storage is modeled based on losses in energy transfer and terminal voltage characteristics, and leakage. Different approaches are used for supercapacitor and NiMH battery. The modeling of supercapacitor leakage uses an exponential model, which was found to give higher leakage than actually observed. For non-linear characteristics such as battery voltage-capacity profile and regulator efficiency modeling, piecewise linear interpolation is used based on empirical or datasheet provided data. The proposed modeling is validated by comparing the simulated output with measurements from the reference system using an experiment for supply and demand match under fixed conditions of demand. The modeling does not consider the influence of temperature and its accuracy is governed by the accuracy of user data input to the various models. The applicability of this modeling to optimising energy management policy implementation is discussed in the Chapter 5 using case studies of energy management policies. Furthermore, Chapter 6 discusses the application of this model to decide the sizes of PV panel and required energy storage to meet a required demand based on a given profile of energy harvesting source.

Chapter 5

Evaluation and Optimisation of Energy Management Policies

As discussed in Chapter 1, the performance of wireless sensing applications scale with energy consumption [65, 154, 165], with specific gains depending on the application functionality. For example, a higher energy consumption can imply a higher fidelity of data collection or event detection. This can be referred to as the Quality-of-Service (QoS), and ideally maximum QoS is sought but due to fluctuations in harvested-energy, the available energy supply needs to be considered. A harvested-energy management policy adapts the energy budget of the application workload according to energy harvesting supply to achieve perpetual operation while maximising performance. Figure 5.1 depicts the function of a generic energy management policy. The following objectives are common among harvested-energy management policies [65, 154]:

Energy-Neutral Operation Due to the variability of harvested-energy, long-term perpetual operation requires that the energy consumption of the application workload does not exceed the energy harvesting rate. The instantaneous mismatch between supply and demand is smoothed by using energy storage, so that the excess energy is accumulated in energy storage and shortages are overcome from this stored energy. On the other hand, the aim of energy management policies is to actively manage demand-supply match by monitoring the energy resources of the system to ensure long-term perpetual operation.

Maximising Energy Utilisation Since the application's performance is dependent on energy consumption, harvested-energy management policy should maximise energy consumption while ensuring energy neutral operation.

As discussed in Chapter 1 (Section 1.2.3) and illustrated with an example in Chapter 2 (Section 2.2.4), duty cycling the application workload between active and idle states is a

Figure 5.1: Generic functionality of energy management policy.

commonly used technique to minimise application's energy consumption. For example, in an application using duty cycling, 0.6 (or 60%) can be the maximum targeted duty cycle providing maximum QoS while 0.01 (or 1%) is the least tolerable level of application activity below which no QoS is obtained [65, 165]. In this case, a higher duty cycle translates to a higher QoS and the objective of an energy management policy can be to maximise the average QoS level over long-term.

To achieve the objectives stated above, an energy management policy needs to be aware of energy supply and demand. The key question here is, *how does an energy management policy know what is actually available in order to decide what can be spent?*. In this regard, Chapter 4 discussed modeling of the non-ideal characteristics (losses and interdependencies) of system components that influence supply and demand. Some examples of how these non-ideal characteristics of system components can impact energy management are:

- **Supply**: The harvested power from a PV panel for a certain input light intensity is not fixed since it can vary depending on the terminal voltage of the PV panel (operating point). This can have implications on prediction of harvested-energy.
- **Energy storage**: The available stored energy is less than supplied due to the sub-unity efficiency of energy storage or high leakage.
- **Consumption**: The actual energy consumed for a given application demand can vary due to the change in losses based on factors such as varying efficiency of output power regulator.

With few exceptions, harvested-energy management policies in the literature [102, 106, 103, 154] are presented at the algorithmic level and evaluated using system models at a high abstraction level. These simplified system models do not account for losses and their dependency on input/output of components. The goal of energy-neutral operation cannot be achieved unless all non-ideal factors that affect the energy supply and demand are not accounted for. These can differ between different possible energy harvesting and storage subsystem designs (Chapter 2). Figure 5.2 depicts the model of an energy management policy that takes this in to account.

Based on system modeling discussed in Chapter 4, this chapter evaluates harvested-energy management policies to determine if these achieve their objectives on a given

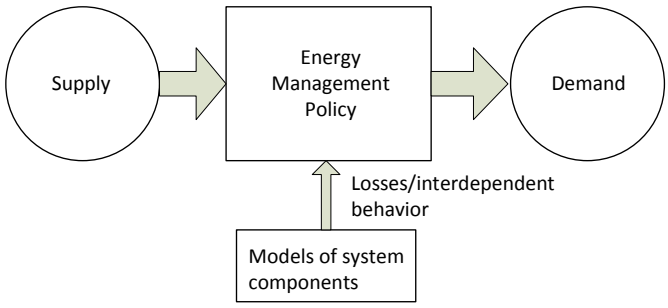

Figure 5.2: Generic function of optimised energy management policy.

energy harvesting system configuration. Each considered policy is first evaluated for non-ideal characteristics that cause deviation from energy-neutral operation and optimised in light of modeled characteristics. The goal of the first case study [65] is energy neutral operation while minimising losses due to battery efficiency. It is shown that these objectives cannot be achieved unless the actual demand is considered. Case 2 considers a supercapacitor leakage minimisation policy [165]. It is shown that other non-ideal characteristics can overshadow leakage consideration and should be taken in to account to maximise allocation of harvested energy. Case 3 considers a policy for time-uniform allocation of harvested-energy [39]. The energy budget allocation of this policy is optimised to meet energy-neutral operation depending on system configuration.

This chapter is organised as follows. Section 5.1 identifies general concepts that are important for understanding evaluation of the case studies. Section 5.2 - 5.4 discusses the three cases, giving the necessary background, system model, evaluation and optimisation results. Section 5.5 concludes the chapter.

5.1 Optimisation Considerations for Energy-Neutral Operation

The previous section discussed the objectives of energy management policies. These objectives can be met by matching the demand with supply over time. However, real systems modeled in Chapter 4 have non-ideal and interdependent components (input conditioning, energy storage and output regulation) with losses that are dependent on energy supply and operating point of components. To achieve energy-neutral operation and maximise energy utilisation, these non-ideal factors and interdependence have to be taken in to account. To generalise the dependence of supply and consumption efficiencies on energy supply and operating state of components, this chapter identifies the following aspects of supply and demand:

Efficiency of replenishing energy This refers to the amount of additional energy required to replenish a certain amount of energy to energy storage. This cost

or additional required energy can be due to efficiency of energy storage and/or harvester. For example, the charging efficiency of energy storage dictates how much extra energy is needed to replenish the energy storage by a given amount. Also, the energy harvested by a PV panel is dependent on its operating point. When connected to an energy storage such as a supercapacitor, replenishing the supercapacitor from a nearly discharged state requires more energy due to less efficient operation of the PV panel. Furthermore, the supercapacitor leakage can also be grouped under this efficiency.

Efficiency of energy consumption This refers to the amount of additional energy required for a given energy demand of application. This can vary due to the efficiency of output regulator being a function of input and output power. Also, complementary to energy storage charging efficiency, energy discharged from energy storage has a higher cost (when it needs to be replenished) rather than energy consumed from output of PV panel.

These efficiencies and their varying nature justify the use of models of system components discussed in Chapter 4 for evaluation and optimisation of harvested-energy management policies, which is the focus of this chapter.

5.2 Case 1: Maximising Energy Allocation Under Energy Storage Losses

5.2.1 Background

The objective of this energy management policy [65] is to maintain energy-neutral operation while maximising the energy allocated to application workload by minimising charge/discharge losses of rechargeable battery. To achieve this, the total consumption budget is determined based on prediction of future energy (Section 3.3.1, Chapter 3). For predicting the harvested-energy, a single day is used as the prediction horizon, by utilising the regularity of daily diurnal cycle of solar energy. Furthermore, the actual harvested-energy is continually monitored to measure errors in prediction and consumption is adjusted accordingly.

This energy management policy serves as a good case for evaluation and optimisation because it needs to account for the relationship between energies harvested, stored and consumed to achieve its target objectives. The system model used for formulating the energy management policy is based on the Heliomote solar energy harvesting wireless sensor node [124], which uses NiMH rechargeable batteries as energy storage. The system configuration is similar to the system described in Chapter 2 (Section 2.3) with

PV panel connected to the NiMH battery using appropriate charging/discharging protection, and the wireless sensor node is supplied a fixed voltage via a boost regulator. For measurement of the voltage of PV panel and the input/output energy of battery, a dedicated battery monitor IC (Maxim DS2438) is used. Although this energy management policy was targeted for a real harvesting system (Heliomote), the supply-demand relationships used to derive the system formulation doesn't consider (or simplify) the non-ideal characteristic of all components in the system. It should be noted that this policy was only evaluated by simulation [65] using measured harvested-energy traces and no validation on an actual system was reported. Furthermore, the following evaluation shows that the selection of harvested-energy measurement approach in [124] cannot correctly measure the harvested-energy, thus resulting in deviation from energy-neutral operation.

5.2.2 System Model

This section discusses the formulation of system model used by Kansal et al. [65] and the next Section presents optimisations based on the modeling discussed in Chapter 4.

This energy management policy aims to maintain energy neutral consumption of harvested energy while maximising energy available for consumption. The formulation of this energy management policy model takes into account the non-ideal energy storage with sub-unity charging (or discharging) efficiency η_{energy_store}. This implies that for every unit of energy charged in requires $\frac{1}{\eta_{energy\_store}}$ of harvested-energy. This is an important consideration because for maintaining energy neutral operation over a given interval (single day), the final battery level should equal the initial value. Thus, any battery energy discharged needs to be restored incurring the cost of battery efficiency. Therefore, to maximise harvested-energy available for consumption, the battery discharge should be minimised. To achieve the required energy allocation, a day is divided into N discrete time slots and estimates of harvested energy in these time slots are obtained using a prediction algorithm (Section 3.3.1). Let $P_s(i)$ be the (predicted) harvested power in time slot i ($1 \leq i \leq N$), $D(i)$ ($D_{min} \leq D(i) \leq D_{max}$) be the duty cycle and P_c be the load power demand in active mode. In a time slot i, if $P_c > P_s(i)$, then the deficit $P_c - P_s(i)$ is supplied by the battery stored energy (see Figure 5.3a). Consuming energy in these slots is less efficient due to costly battery replenishment required. Hence, the objective is to maximise harvested energy consumption during slots when the PV panel output $P_s(i) \geq P_c$ (Figure 5.3b) since the energy consumed doesn't incur the loss of battery efficiency η_{energy_store}.

Using the predicted values, the policy determines those slots in which $P_c > P_s(i)$ and the battery will need to be discharged, called 'dark' slots. When allocating the total harvested-energy budget (in energy neutral manner) these slots have a higher consumption cost. To obtain the power consumption budget of a dark slot, consider that the

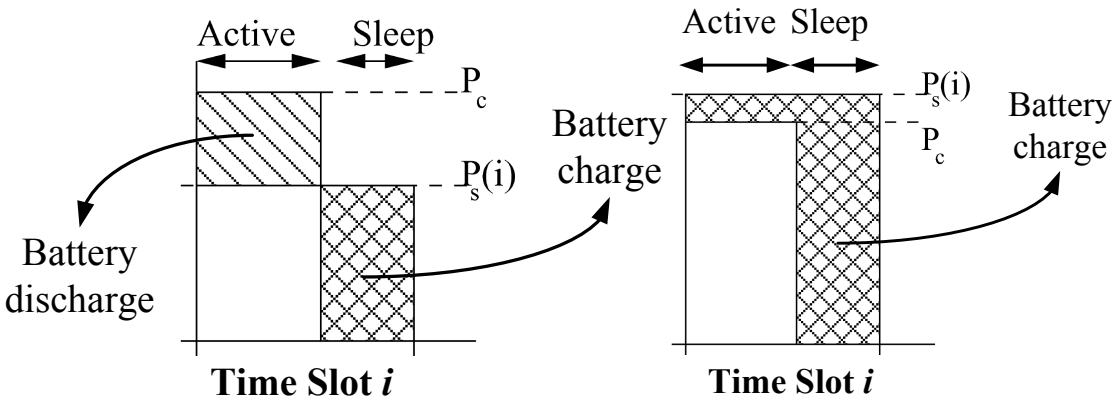

(a) Time slot i with $P_c > P_s(i)$ (dark slot).

(b) Time slot i with $P_s(i) \geq P_c$ (sunny slot).

Figure 5.3: Two types of slots according to the values of P_c and P_s (adapted from [65]).

difference $P_c - P_s(i)$ has to be supplied by the battery, and given that the battery efficiency is η_{energy_store}, this implies that $\frac{P_c - P_s(i)}{\eta_{energy\_store}}$ of energy has to be returned to the battery. Thus, the energy consumption of dark slots if given by:

$$P_{dark} = D(i) \cdot \left[\frac{P_c}{\eta_{energy\_store}} + P_s(i) \left(1 - \frac{1}{\eta_{energy\_store}} \right) \right] \tag{5.1}$$

On the other hand, those slots in which $P_s(i) >= P_c$ are called 'sunny' slots. The energy consumption of these sunny slots is given by:

$$P_{sunny} = D(i) \cdot P_c \tag{5.2}$$

For energy-neutral operation over N slots, the following condition must be satisfied:

$$\sum_{i=1}^{N} P_s(i) = \sum_{i \in sunny} D(i) P_c + \sum_{i \in dark} D(i) \left[\frac{P_c}{\eta_{energy\_store}} + P_s(i) \left(1 - \frac{1}{\eta_{energy\_store}} \right) \right] \tag{5.3}$$

Furthermore, for maximising energy utilisation, the optimisation objective is:

$$max \sum_{i=1}^{N} D(i) \tag{5.4}$$

For a given total harvested-energy budget, this objective can be attained by allocating a higher duty cycles $D(i)$ in sunny slots to consume energy more efficiently. Note that the minimum duty cycle (D_{min}) has to be allocated to dark slots and this is the limiting

factor in minimising battery discharge as it dictates minimum energy that must be consumed in each slot for achieving continuous operation of the workload.

5.2.3 System Model Optimisation

5.2.3.1 Measurement of Harvested-Energy

Since the energy management policy relies on measurement of actual harvested-energy for prediction of future energy, the measurement model used is critical to ensure energy neutral allocation since it affects the accuracy of prediction and prediction error measurement. In the Heliomote system design [124], designed to support implementation of this energy management policy, the harvested power ($P_{harvested}$) is measured as product of PV panel voltage (V_{panel}) and battery current (I_{batt}) using a battery monitor IC [90]:

$$P_{harvested} = V_{panel} \cdot I_{batt} \tag{5.5}$$

Referring to the battery monitor datasheet [90], it is found that the battery monitor measures the difference of charging and discharging battery current ($I_{batt} = I_{chg} - I_{dis\_chg}$). This is not equal to the absolute harvested current output of PV panel I_{panel} (Section 4.2.3) since the power drawn by the node will result in $I_{dis\_chg} > 0$.

$$I_{batt} = I_{chg} - I_{dis\_chg} \tag{5.6}$$

$$I_{panel} \neq I_{batt} \tag{5.7}$$

I_{dis_chg} depends on the activity of the workload, which is not constant as it varies depending on the allocated duty cycle. Furthermore, as given in Section 4.2.4, the harvested power $P_{harvested}$ is the product of battery voltage (V_{batt}) and the input current I_{panel}:

$$P_{harvested} = V_{batt} \cdot I_{panel} \tag{5.8}$$

Since $V_{batt} \neq V_{panel}$ due to the presence of isolation diode or input regulation (Section 4.2.4), using the measurement setup used in [124] (Equation 5.5) will result in an incorrect measurement of harvested energy, causing the energy management policy to deviate from expected outcomes. Hence, based on the correct modeling of interdependency of components it is identified that the correct measurement of harvested-energy requires values V_{batt} and I_{panel}. The I_{panel} can be measured using a PV panel current monitor, as employed in the reference system design discussed in Chapter 2.

5.2.3.2 Efficiency of Output Regulator

This energy management policy is formulated based on a system model that accounts for non-ideal energy storage, however it does not take into account the non-ideal characteristics of the output regulator when transferring power to the workload. As discussed in Section 4.2.6 (Figure 4.14), the efficiency of the output regulator η_{out_reg} is below 100% in practice and it depends on the battery voltage (input voltage of regulator) and output current of the application workload. Therefore, this needs to be accounted for in the system model, otherwise the energy management policy's allocation of total budget will be optimistic, resulting in inability to maintain match between harvested and consumed energy. Furthermore, this also affects the determination of 'sunny' or 'dark' slots based on difference of energy supply and demand (Section 5.2.2). This will cause an eventual depletion of stored battery energy due to a deviation from intended energy neutral operation.

Let η_{out_reg} be the efficiency of the output regulator, which is a function of the energy storage voltage (or stored energy) and the output current (or power) drawn by the workload (Section 4.2.6). Considering the output regulator efficiency, the actual power consumption given the state of battery and workload activity is given by:

$$\acute{P}_c = \frac{P_c}{\eta_{out\_reg}} \tag{5.9}$$

By using $\acute{P}_c$ in Equation 5.3, the correct energy flow from input to output is accounted for. Depending on the actual type of regulator, the efficiency factor η_{out_reg} can be approximated by a constant. However, if this value if smaller than actual efficiency then it will lead to under utilisation of energy and vice versa. For example, the efficiency of output regulator is shown in Table 4.2 (Chapter 4) at different input voltage values, and it can be seen that it also depends on load current.

5.2.4 Empirical Validation

Having identified the potential optimisations in light of the system model, this section presents validation of optimisation in Section 5.2.3.2 using simulation and measurements based on the reference system described in Chapter 2 (Figure 2.14). To achieve this, an experimental setup is selected such that the effect of output regulator loss can be isolated. The aim is to match a fixed application demand with PV panel energy supply and observe the differences when output regulator losses are accounted and vice versa. To simplify harvested-energy prediction, constant input radiation is used. Furthermore, to isolate the influence of output regulator, the supply (lamp distance) is adjusted so that input power is just equal to required load demand and all harvested-energy is allocated

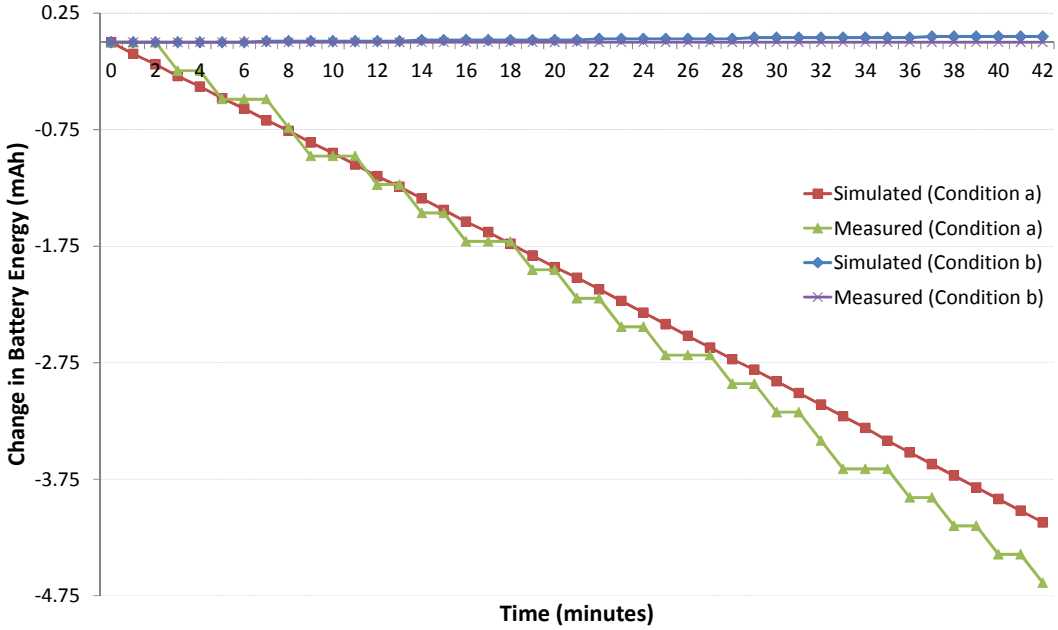

Figure 5.4: Simulated and measured change in battery stored charge for validating energy-neutral operation.

to the load, thus bypassing the influence of battery efficiency (Figure 5.3). Under these conditions, if the supplied energy matches the load power consumption, the battery level should not change appreciably from its initial level at start of experiment. The battery level is monitored under the following two conditions: (a) Output regulator efficiency is not accounted (as in [65]) to calculate the required input power and it is set equal to load power drawn from regulator (3.31V @ 18.88mA = 62.49mW), (b) Output regulator efficiency at given values of load current (18.88mA) and input battery voltage (2.6V) is obtained from the model (Fig. 4.14, 82.47%). This value is used to adjust input PV panel power needed to match supply with consumption.

Fig. 5.4 shows the simulated and measured change in battery charge when input power is not adjusted for regulator efficiency (Condition a) and vice versa (Condition b). The resolution of hardware battery monitor used for measurements is 0.244 mAh. As can be seen, the battery level steadily decreases in Condition 'a' indicating that value of input power (2.6V @ 24.4mA = 63.44mW) is not sufficient to fully support the load consumption and the deficit is being made up by battery energy. On the other hand, Condition 'b' shows a steady battery level when PV panel power (2.6V @ 29.4mA = 76.44mW) is adjusted to account for regulator efficiency. This indicates that the supply is sufficient to meet the load demand. The battery capacity curve for simulation is smoother than measured due to coarser resolution (quantisation effects) of actual battery monitor. The simulated battery charge in Condition 'b' shows a small increase indicating a slight surplus in input energy. Since the resolution of physical battery monitor is less than simulator model resolution, this increase cannot be observed in measured value. It can be seen that the simulator output closely tracks the measured trends. This

Table 5.1: The differences in three system models used for evaluating and optimising case 1.

Characteristic	Model 1	Model 2	Model 3
Harvested Power Measurement	Using Equation 5.5	Same as Model 1	Using Equation 5.8
Output Regulator Model	Ideal output regulator ($\eta_{reg\_out} = 1$)	Based on actual efficiency data (Figure 4.14)	Same as Model 2
Energy Management Policy	Assumes ideal output regulator	Same as Model 1	Uses regulator efficiency values of 60% and 80% for sleep and active power draw

experiment shows that to match workload power consumption with harvested energy supply, the efficiency of output regulator under the operating conditions of input voltage and output current should be factored in.

Note that in this experiment, the measurement of harvested-energy was based on the correct model discussed in Section 5.2.3.1 and the effect of incorrect measurement is not validated for sake of avoiding repetition since it is simple extension of experiment described in this section.

5.2.5 Simulation

In Section 5.2.4, the impact of output regulator efficiency was experimentally validated. In this section, the complete system model is simulated to compare the results of two optimisations identified in Section 5.2.3 with results of original system model in [65]. To achieve this, three variants of system (Table 5.1) are considered for evaluating the policy: Model 1 represents the original system model used in [65], Model 2 represents the system modeling considered in Chapter 4 with no optimisations to policy. Model 3 implements the optimisations discussed in Section 5.2.3: (i) the output regulator efficiency is accounted for, (ii) harvested-energy is correctly measured.

Figure 5.5 shows a comparison of the energy management policy results in terms of average duty cycles allocated and battery capacity at end of a day between the three models given in Table 5.1. As can be seen, the duty cycles allocated by models 1 and 2 are higher than model 3. The reason is that since models 1 and 2 assume an ideal output regulator, the calculated energy demand for a given duty cycle is less than actual energy consumed through the output regulator. Thus, higher duty cycles are allocated. Furthermore, Figure 5.6 shows that the measured harvested energy by models 1 and 2 is higher than model 3 due to the differences in measurement as described in Section 5.2.3.1. The combined impact of measuring higher than actual harvested-energy and

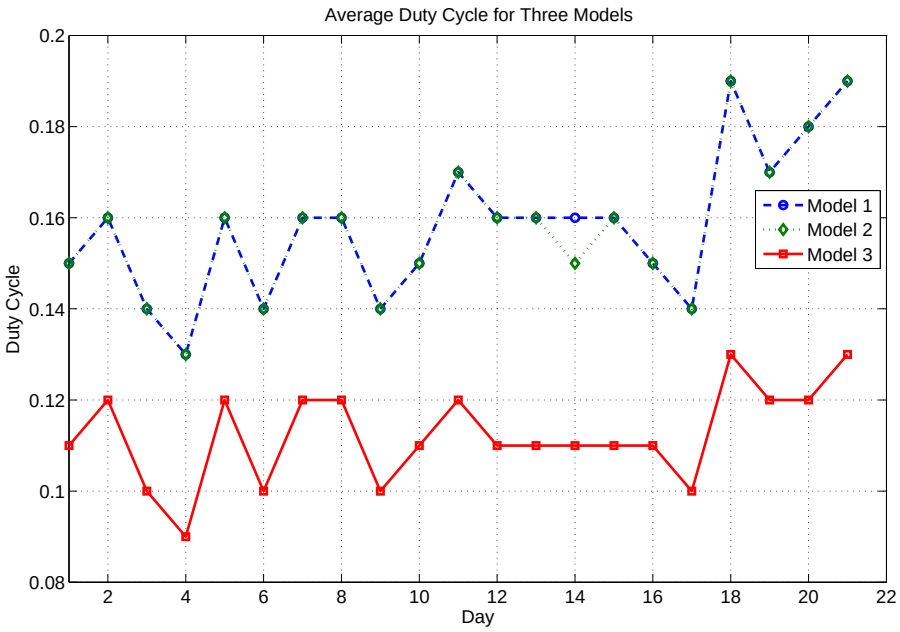

(a) Average duty cycles for each policy model showing that optimised policy allocates lower duty cycles to account for losses.

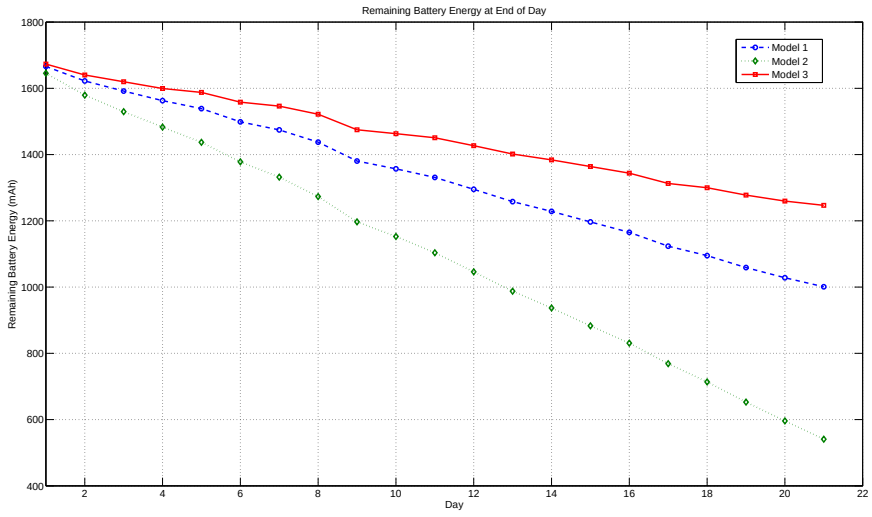

(b) Decrease in battery energy at end of day. The drop in optimised policy model 3 mainly due to prediction errors, while other two models exhibit a sharp drop due to overconsumption.

Figure 5.5: Comparison between results of three models for case 1 with respect to average duty cycle and remaining battery energy.

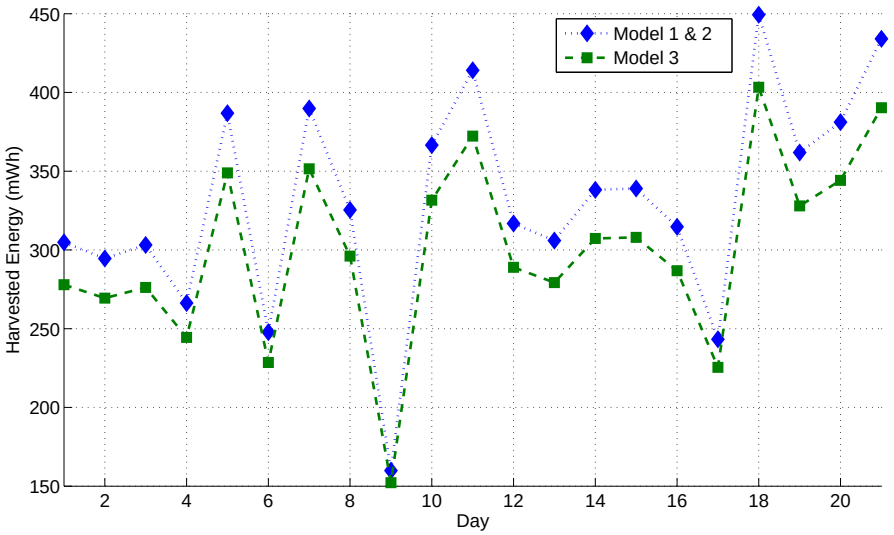

Figure 5.6: Comparison between harvested energy measurement between three models. Models 1 and 2 consistently measure more energy than actually harvested.

assuming an ideal output regulator is that models 1 and 2 allocate higher duty cycles. As a consequence, looking at battery level at end of a day (Figure 5.5b) it is found that battery level for model 2 decreases rapidly indicating that model 2 is using more energy than available and this difference is being made up by battery reserve energy. The same is the case for model 1 but since an ideal regulator is used in system model, the depletion of battery is less than model 1. Note that model 3 displays the least reduction in battery due to correctly measuring the supplied energy and accounting for output regulator efficiency. It should be noted that a common contributing factor to battery depletion among all model variants is the inaccuracy of the harvested-energy prediction algorithm used in [65] (Section 3.3.1), however, this is beyond the focus of this evaluation since this is not related to system components and configuration. These results clearly show that if the energy management policy is not based on the correct model of energy harvesting subsystem, energy-neutral operation cannot be achieved due to the mismatch of supply and demand.

5.3 Case 2: Supercapacitor Leakage-Aware Policy

5.3.1 Background

As discussed in Chapter 4 (Section 4.2.5.1), the modeled self-discharge rate (P_{leak}) of a supercapacitor is non-linear function of voltage, which increases with supercapacitor voltage and vice versa. This energy management policy [165] focuses on this behaviour of supercapacitor leakage and the objective is to minimise the losses due to high leakage and

thus maximise harvested-energy available for utilisation to application workload. This is achieved by increasing the application workload (energy consumption) when leakage is high rather than allowing the supercapacitor to leak energy in the high leakage state. To realise this, the supercapacitor leakage value is determined using a leakage model [165, 131] and based on this value of P_{leak}, the duty cycle D (or energy consumption) is adjusted as:

$$\triangle D_{+} = G \cdot P_{leak} \cdot T_{diff}, T_{diff} \geq 0 \tag{5.10}$$

$$\triangle D_{-} = \frac{G}{P_{leak}} \cdot T_{diff}, T_{diff} < 0 \tag{5.11}$$

$$T_{diff} = T_{actual} - T_{target} \tag{5.12}$$

In Equation 5.10 and 5.11, $\triangle D_{+}$ and $\triangle D_{-}$ are positive and negative adjustments of the duty cycle, respectively, G is constant gain factor and T_{diff} is the difference of the targeted and actual operating lifetime of sensor node based on the currently stored energy in the supercapacitor. Thus, the increase or decrease in energy consumption is influenced by the leakage rate P_{leak}. The energy harvesting system reported in [165] to present the results of this policy has the same configuration as the reference system configuration discussed in Chapter 2 (Figure 2.14), i.e, a PV panel is connected to a supercapacitor via a protection diode and the supercapacitor feeds a boost regulator. This energy management policy has been selected for evaluation since it presents a case where the interdependency between system components as identified in Chapter 4 requires consideration of losses in addition to the supercapacitor leakage to achieve better harvested-energy utilisation. For the given energy harvesting system configuration, these interdependencies are analysed in this case study based on the models of system components discussed in Chapter 4.

5.3.2 System Model Evaluation

Given the reference system configuration (Chapter 2) and its system model (Chapter 4), consider the influence of supercapacitor voltage on losses of components' connected to it, i.e., PV panel and the output regulator (Figure 5.7). As discussed in Section 4.2.3, the harvested-power output from the PV panel is dependent on its terminal voltage V_{panel}:

$$I_{panel} = IV\_curve(V_{panel}) \tag{5.13}$$

$$P_{panel} = V_{panel} \cdot I_{panel} \tag{5.14}$$

For the given system configuration (with no input regulation), V_{panel} is determined as given in Section 4.2.4:

$$V_{panel} = V_{supercap} + V_{forward\_schottky} \tag{5.15}$$

Thus, the voltage of supercapacitor ($V_{supercap}$) determines the harvested-power for a given input light intensity. Referring to the PV panel I-V curve in Figure 4.5, it can be seen that the PV panel power output decreases when V_{panel} shifts from the maximum operating point value.

Now, consider the output voltage regulator connected to the supercapacitor. Its efficiency η_{reg_out} is a non-linear function of the supercapacitor voltage and output current as discussed in Section 4.2.6:

$$\eta_{reg\_out} = f(V_{supercap}, I_{load}) \tag{5.16}$$

$$P_{reg\_out} = \frac{P_{load}}{\eta_{reg\_out}} \tag{5.17}$$

Figure 4.14 shows that the output regulator efficiency for a given load current decreases with decrease in supercapacitor voltage, or in other words, P_{reg_out} increases. Finally, the P_{leak} of supercapacitor is also a function of $V_{supercap}$ as discussed in Section 4.2.5.1:

$$P_{leak} = f(V_{supercap}) \tag{5.18}$$

P_{panel} represents the input while P_{leak} and P_{reg_out} represent the outputs as shown in Figure 5.7. These values of input and output power are dependent on the supercapacitor voltage, in addition to the leakage. Since the energy management policy being evaluated focuses only on change of P_{leak} with supercap voltage, the aim of this section is to consider the changes in P_{panel} and P_{reg_out} to consider the effect of interdependencies. Let ΔP_{leak}, ΔP_{panel}, and ΔP_{reg_out} be the changes in leakage rate, harvested-power and consumed power, respectively, with decrease in supercapacitor voltage while other factors such as input light intensity and load current are kept constant. The net effect P_{net} is given by:

$$P_{net} = \Delta P_{panel} - (\Delta P_{leak} + \Delta P_{reg\_out}) \tag{5.19}$$

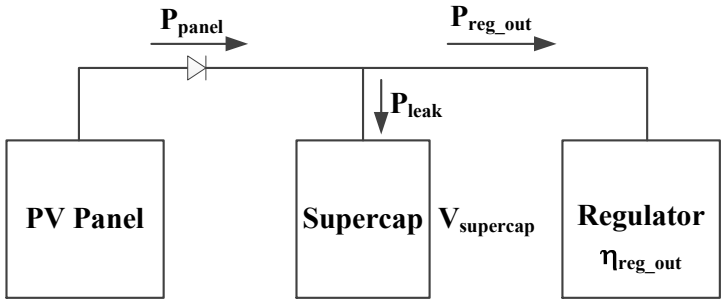

Figure 5.7: Interconnection between the PV panel, supercapacitor and output regulator, showing the interdependency between these system components.

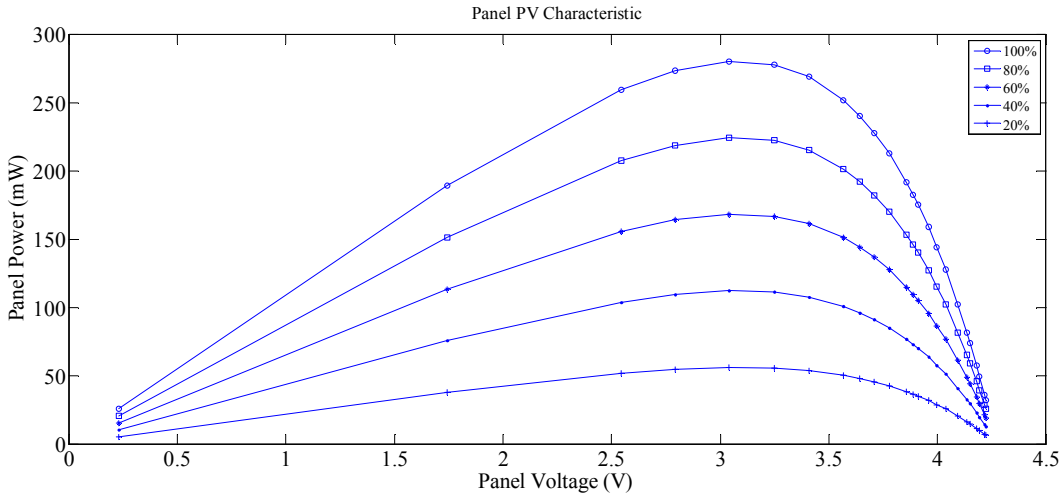

Figure 5.8: P-V curves for different input light intensities.

Thus, a positive P_{net} represents a net gain in energy input with change in supercapacitor voltage and vice versa. Since the objective of this energy management policy is to consume energy while accounting for the leakage rate rather than allowing the supercapacitor to charge up, this may cause the energy harvesting subsystem to operate at a P_{net} value which is negative because reduction in leakage power is accompanied by reduction in energy harvested and decreased output regulator efficiency. This depends on the relative changes and their magnitudes. The next section analyses this using the specific instances of supercapacitor, PV panel and output regulator as modeled in Chapter 4.

5.3.3 Simulation

Figure 5.8 shows the modeled P-V curves of panel at different intensities of light while Figure 5.9 shows the modeled leakage of a 100F supercapacitor [131] based on model in Section 4.2.5.1. The output regulator efficiency change is shown in Figure 4.14a (Chapter 4). Figure 5.10 shows the plots of P_{net} (Equation 5.19) and change in leakage rate ΔP_{leak}, harvested-power ΔP_{panel}, and consumed power ΔP_{reg_out} with decrease in supercapacitor

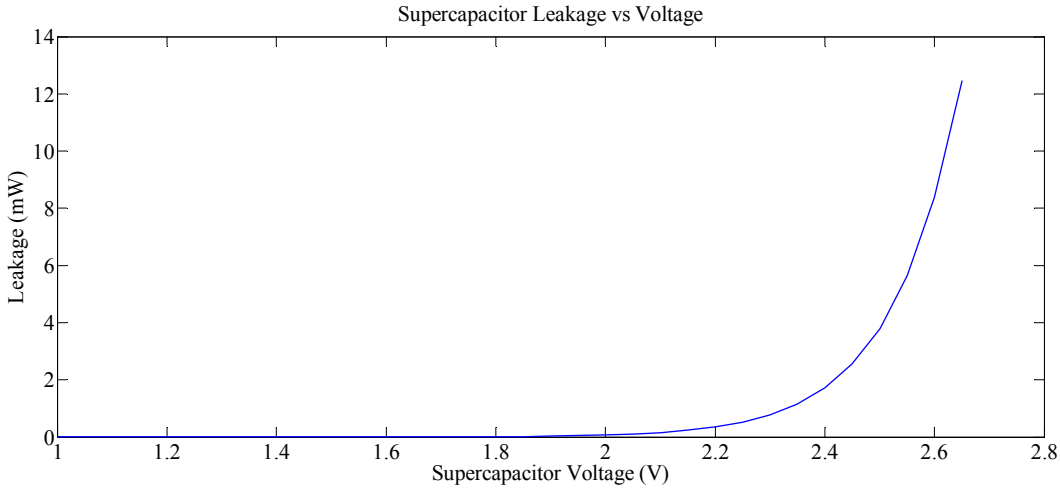

Figure 5.9: Leakage power versus 100F supercapacitor voltage.

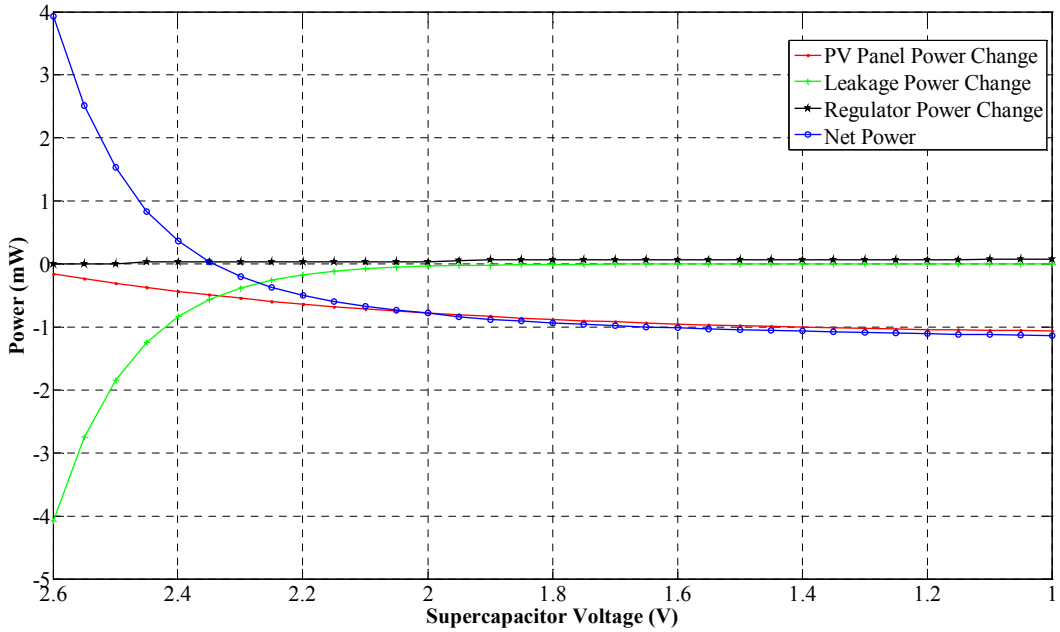

Figure 5.10: Changes in P_{net}, harvested, leakage and regulator power with supercapacitor voltage.

voltage at a fixed input radiation (20% of peak) and workload consumption (10% duty cycle). It can be observed that the a change of supercapacitor voltage from 2.65V to 2.6V, there is a net gain of 4mW due to a larger decrease in supercapacitor leakage power compared to loss in harvested power and output regulator efficiency. Until P_{net} is positive, there is benefit gained from increasing energy consumption and allowing the supercapacitor voltage to drop. However, beyond 2.35V the reductions in leakage are overcome by decrease in harvested power while change in regulator efficiency (around 10%) within this range has very little effect for the given value of the average load current. Figure 5.11 shows the P_{net} plots for different light intensities, indicating that the loss of harvested power dominates P_{net} with increase in input light intensity. This

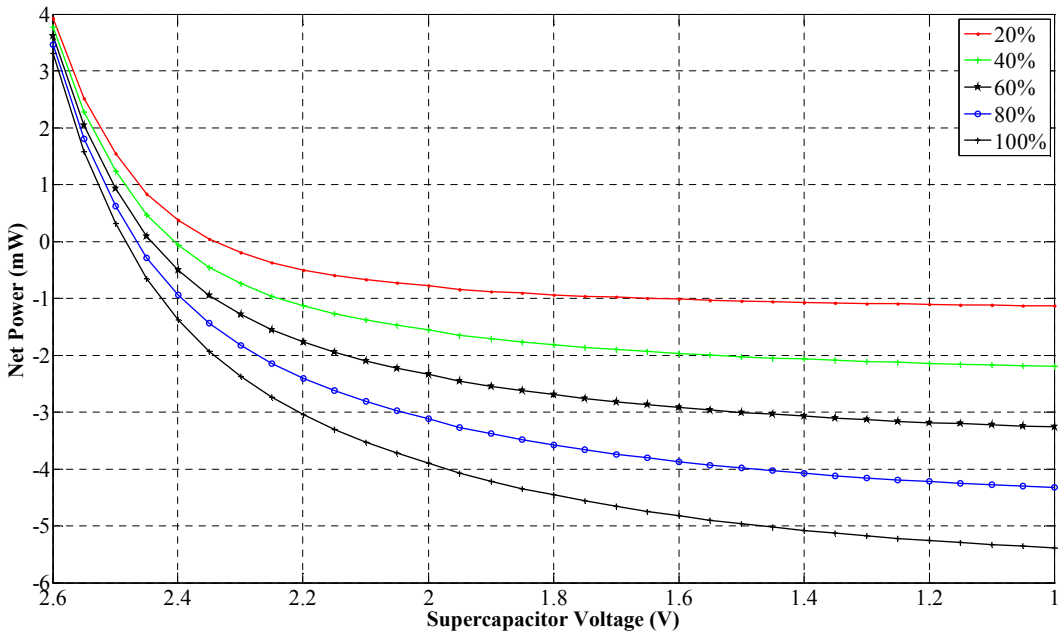

Figure 5.11: Change in P_{net} for different values of input light intensities.

harvested power can be utilised to provide more energy for operation of load and keep the energy storage charged for periods when little or no energy is harvested. Thus, the energy management policy can be optimised to account for this while adapting the load power consumption (duty cycle). To understand how this can be achieved, observe in Figure 5.11, that leakage loss is dominant within a certain voltage range of supercapacitor. Within this range, the leakage loss should be avoided by consuming energy, when $P_{net} > 0$. Outside this high leakage region, the consumption doesn't need to be throttled based on leakage so that system operates near the energy efficient point $P_{net} = 0$. Clearly, the specific values discussed in this section depend on the chosen PV panel, supercapacitor and output regulator, nevertheless, this evaluation shows that considering only leakage power is not optimal and other losses needs to be considered for improved management of harvested energy.

5.4 Case 3: Time-Fair Energy Allocation Policy

5.4.1 Background

For real-world wireless sensor applications using energy harvesting, it is desirable that the harvested-energy should be allocated in a consistent manner over time despite of variability of the harvesting source to maintain consistent workload. The energy management policy considered in this case uses a max-min fair energy allocation policy [39] based on the principle of lexicographic maximisation, borrowed from the area of networks in which it is applied to achieve fair bandwidth allocation [76]. The aim is to allocate

the harvested energy as uniformly as possible with respect to time while maintaining energy neutral operation. The policy uses knowledge of harvested-energy in different time slots (of a day) and calculates the energy consumption budgets for these slot given the knowledge of harvested energy over future time slots and initial stored energy [39]. In [39], the system model used to derive the policy and present numerical evaluation is a simple one with non-ideal characteristic of energy storage and consumption not accounted for. This section discusses the modifications to the system model necessary to achieve time-fair energy allocation while maintaining energy neutral operation using system model discussed in Chapter 4. The next section presents the original system model and energy allocation policy, followed by the proposed modifications.

5.4.2 System Model and Energy Management Policy

Suppose a discrete-time model with time axis divided into K time slots and the energy allocation decision is made at the start of a slot i ($i = \{0, 1, \ldots, K-1\}$). Let the energy storage capacity be denoted by C, the amount of energy stored at start of slot i by $B(i)$ ($0 \leq B(i) \leq C$), and the initial and the final energy levels are denoted by B_0 and B_K, respectively. The energy spending rate is denoted by $s(i)$ and the effective amount of energy a device can harvest from the environment is denoted in by $Q(i)$. Let $\triangle$ be the quantisation factor used to increment energy allocation of a slot. Its value can be decided to achieve a suitable tradeoff between quantisation inaccuracy of using a large $\triangle$ value and computation overhead of using a small $\triangle$ value. The changein energy storage $B(i)$ from slot $i-1$ to i can be expressed as:

$$B(i) = min\{B(i-1) + Q(i-1) - s(i-1), C\} \tag{5.20}$$

Let the total amount of energy the device is allocated be $\hat{Q}$, where $\hat{Q} = \sum_i Q(i) + (B_0 - B_K)$. Given this model formulation, the problem of allocating fair energy consumption to slots with respect to time (time fair lexicographic allocation) is given by: Lexicographically maximise $\tilde{s} = \{s(0), s(1), \ldots, s(K-1)\}$ subject to the following constraints:

$$s(i) \leq B(i) \; \forall \; i \tag{5.21}$$

$$B(i) \leq B(i-1) + Q(i-1) - s(i-1) \; \forall \; i \geq 1 \tag{5.22}$$

$$B(i) \leq C \; \forall \; i \tag{5.23}$$

$$B(0) = B_0; \; B(K) \geq B_K \tag{5.24}$$

$$B(i), \; s(i) \geq 0 \; \forall \; i \tag{5.25}$$

$A_{fix} \leftarrow \varnothing$; $s(i) \leftarrow 0 \ \forall \ i$;
while $\overline{A_{fix}} \neq \varnothing$ **do**
  for $i = 0;\ i \leq K-1;\ i++$; **do**
    if $i \in \overline{A_{fix}}$ **then**
      $\tilde{s}(j) \leftarrow s(j) \ \forall \ j \in [0, K-1]$; $\tilde{s}(i) \leftarrow \tilde{s}(i) + \Delta$;
      $valid \leftarrow$ **check_validity**$(\tilde{s})$;
      if $valid == TRUE$ **then** $s(i) \leftarrow \tilde{s}(i)$;
      else $A_{fix} := A_{fix} \cup i$;
function check_validity$(\tilde{s})$:
$B(i) \leftarrow 0 \ \forall \ i$; $B(0) \leftarrow B_0$; $valid \leftarrow TRUE$;
for $i = 1; i \leq K; i++$; **do**
  $B(i) \leftarrow \min(C,\ B(i-1) + Q(i-1) - \tilde{s}(i-1))$;
  if $\tilde{s}(i) > B(i)$ **then** $valid \leftarrow FALSE$;
if $B_K < B(K)$ **then** $valid \leftarrow FALSE$;
return $valid$

Figure 5.12: The Progressive Filling algorithm for time-fair assignment of harvested-energy [39]

Constraint 5.21 ensures that a node does not spend more energy than it has stored, 5.22 and 5.23 represent the storage evolution dynamics, and 5.24 sets starting storage level to B_0 and ensures that the final storage level is at least B_K.

To solve this lexicographic assignment problem, [39] have proposed a Progressive Filing (PF) algorithm (Figure 5.12), inspired by the algorithms of max-min fair flow control. Let A_{fix} to be the set of time slot indexes for which the lexicographically maximal spending level $s(i)$ has been determined. Starting with $A_{fix} = \emptyset$ and $s(i) \leftarrow 0 \ \forall \ i$, the algorithm iterates through slots 1 to K, increasing the allocation of each slot by $\triangle$. When an increase in allocation $s(i)$ for a slot i is considered, the algorithm verifies (**function check_validity**) that the increase would not result in shortage of energy for other slots (the condition for fair allocation), or lack of final energy B_K (for energy neutrality). If either of these checks fails, the spending level of slot i gets fixed at $s(i)$, and the corresponding slot index i is moved to the set A_{fix}. The progressive filling continues for the slots that are not yet fixed. At the first iteration, since $A_{fix} = \emptyset$, the algorithm considers the entire K slots. With each iteration, at least one spending level value $s(i)$ is determined, and the corresponding index i is moved into the A_{fix} set. In each step of the algorithm, it either increases $s(i)$ by $\triangle$ or fixes the allocation of slot i. The spending level of a slot is increased only when it does not interfere with the spending of slots with lesser spending levels.

5.4.3 Proposed Refinement to the System Model

Based on a practical model of real systems (Chapter 4), two aspects are focused upon to refine the energy management policy: energy storage and energy consumption.

5.4.3.1 Energy Storage Model

The system model considered in Section 5.4.2 does not consider the efficiency of energy storage η_{energy_store} when replenishing the energy storage during the allocation of total energy budget $\hat{Q}$ over K slots. Although this may be a reasonable assumption when using supercapacitors which generally have low losses in charging, in case of rechargeable batteries such as NiMH (Section 4.2.5.2) this is not valid. The consequence of this is that for every unit of energy consumed from the energy storage $\frac{1}{\eta_{energy\_store}}$ units of recharge energy to be replenished. Hence, if the energy storage efficiency is not accounted by the policy in total energy allocation algorithm (Figure 5.12), the energy neutral constraint 5.24 may not be met in a real system since the energy storage will not be replenished to the desired level B_K at the end of slot K, i.e., $B(K) < B_K$.

To account for the energy storage efficiency during energy allocation, we need to consider the case when energy storage is discharged, i.e., $B(i) < B(i-1)$. Considering Equation 5.20, it is clear that this will occur if the spending rate $s(i-1)$ is greater than the harvested-energy $Q(i-1)$. In this case the deficit $s(i-1) - Q(i-1)$ is supplied from the stored energy $B(i-1)$. To account for this in the policy when checking the validity of an energy assignment (**function check_validity**), the energy storage evolution (Equation 5.20) can be modified as:

$$B(i) = min\{B(i-1) - \frac{s(i-1) - Q(i-1)}{\eta_{energy\_store}}, C\} \tag{5.26}$$

Equation 5.26 models the effect of energy storage efficiency as increase in effective energy consumption of a slot in which energy storage is discharged. Hence, in the modified policy Equation 5.26 is used when $s(i-1) > Q(i-1)$ (line 3 of **function check_validity**) to model the change in stored energy.

5.4.3.2 Energy Consumption Model

In a typical system, the allocated energy $s(i)$ is consumed by the workload through an output regulator. As discussed in Section 4.2.6, the output regulator is non-ideal and has a transfer efficiency of η_{reg_out} that must be accounted for during energy transfer to the workload. To account for this during energy allocation, given an energy allocation $s(i)$, the effective energy available to the workload $\acute{s}(i)$ is given by:

$$\acute{s}(i) = \eta_{reg\_out} \cdot s(i) \tag{5.27}$$

Note that as discussed in Section 4.2.6, η_{reg_out} is a function of both energy store voltage input and output power to the workload. Since the energy store voltage is governed

by stored energy $B(i)$, and the workload power is determined by $s(i)$, $\acute{s}(i)$ needs to be determined depending on the state of energy storage and output workload power.

Another issue is the operating range of output regulator depending on the input voltage (of energy storage). For example, the MAX1724 regulator stops working below 0.9V and this defines the V_{min} of energy storage (Section 2.3). This is more important in case of supercapacitors since they can be discharged below this voltage while batteries have a higher voltage when fully depleted. Hence, when considering the total capacity C for energy management policy, the V_{min} determines the actual usable capacity $\acute{C}$ available since the stored energy below V_{min} cannot be used:

$$\acute{C} = C - C_{V_{min}} \tag{5.28}$$

Here $C_{V_{min}}$ is the unusable capacity due to the minimum input voltage V_{min} required by the output regulator.

5.4.4 Simulation

This section presents simulation results of energy management policy using the model of the reference system configuration (Section 2.3) to compare the effect of refinements identified in Section 5.4.3. For modeling the energy source, irradiance data samples from [114] are used. As the policy requires knowledge of input energy $Q(i)$, perfect prediction is assumed to ignore the influence of any prediction errors, because the focus is on the system model refinements discussed in previous section. Thus, based on the reference system design, the harvested input (P_{reg_in}) is assumed to be known to the policy in advance. The discussion of results only focuses on the energy consumption and energy storage aspects of the model. Two cases are considered, depicting the optimised and non-optimised consumption.

We first consider the effect of energy consumption model refinements by considering a system with 100F 2.7V supercapacitor energy storage. Figure 5.13 shows the profile of the harvested-energy over a day given as input to the system (and predicted by the policy). Figure 5.14 shows the initial supercapacitor voltage at the start of day and its changes over time. It is required that energy be allocated in time-fair manner (Figure 5.12) while conserving the initial supercapacitor stored energy at the end of the day. Since V_{min} is 0.9V, the usable capacity $\acute{C}$ of the 100F supercapacitor is calculated accordingly. Based on the given input energy profile, the spending budgets calculated by the policy for each time slot are shown with '+' legend line. These budgets are used to determine the duty cycles for each slot based on the given idle and active power demands of workload. The non-optimised spending represents the 'naive' approach that allocates the spending budget (to calculate the duty cycle) without accounting for efficiency of

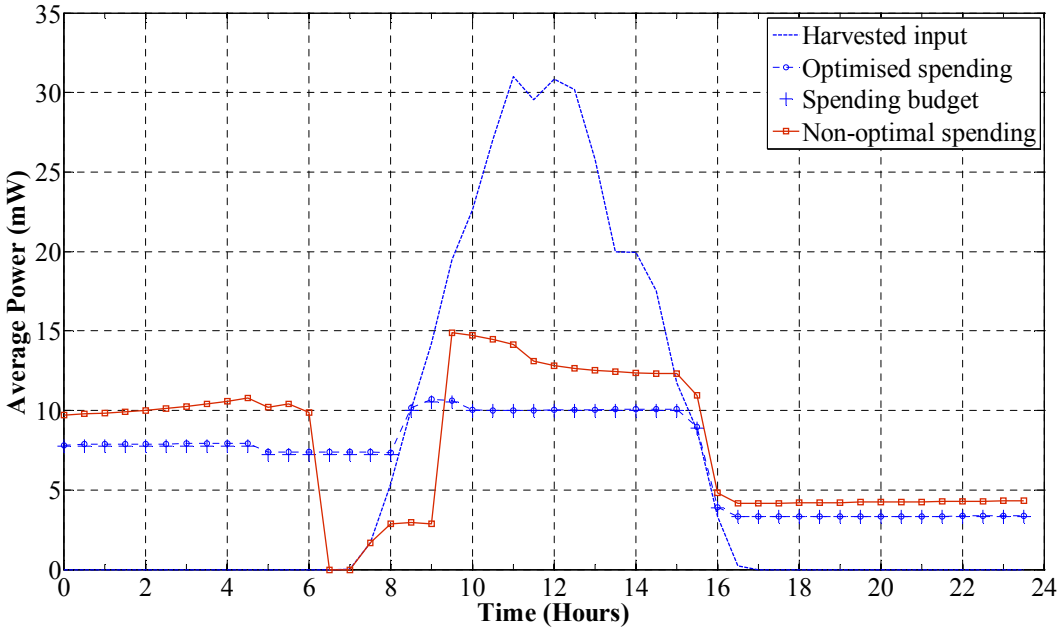

Figure 5.13: Comparison of optimised and non-optimised consumption for a given budget. The non-optimised spending leads to dead-time due to deviation from energy-neutral operation.

output regulator, while the optimised spending follows the changing regulator efficiency to correctly allocate the spending budget. It can be seen in Figure 5.13 that the non-optimised policy over allocates energy, exceeding the actual budget since it has not factored in the losses in output regulator. The excessive energy drawn overly depletes the supercapacitor and its terminal voltage falls below the output regulator operating threshold (0.9V), resulting in unintended shutdown of the system (time 6-8). The system recovers when supercapacitor has replenished sufficient energy to start the output regulator. Furthermore, it can be seen in Figure 5.14 that the stored energy is not conserved at the end of the day for the non-optimised allocation, resulting in deviation from energy neutral operation. It should be noted that the extent of deviation from the desired outcomes depends on the actual values of non-ideal factors such as the output regulator efficiency in this case.

Next, we consider the effect of energy storage efficiency model on the results of the energy management policy. We consider the reference system configuration with 2500mAh NiMH batteries as energy storage ($\eta_{energy\_store} = 66\%$). Figure 5.15 shows the profile of the harvested-energy over a day given as input to the system (and predicted by the policy). Figure 5.16 shows the initial battery stored energy at the start of day and its changes over time. It is required that energy be allocated in time-fair manner (Figure 5.12) while conserving the initial battery stored energy at the end of the day. Based on the given input energy profile, the spending budgets calculated by the policy for each time slot are shown in Figure 5.15. These budgets are used to determine the duty cycles

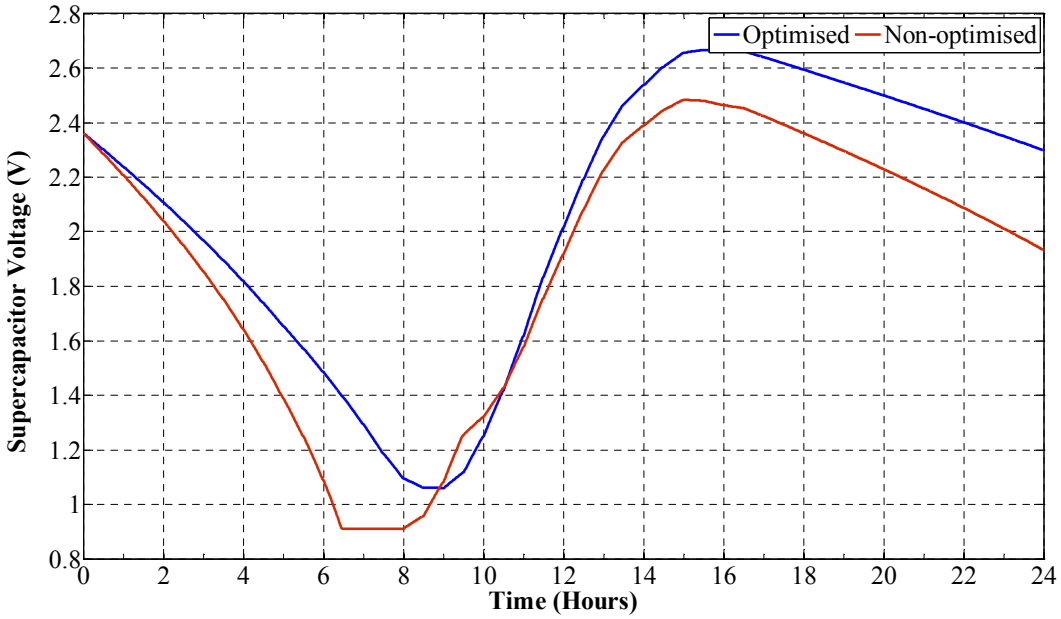

Figure 5.14: Change in net supercapacitor voltage over the day. The non-optimised policy is not able to meet the energy-neutral target for stored energy at the end of day.

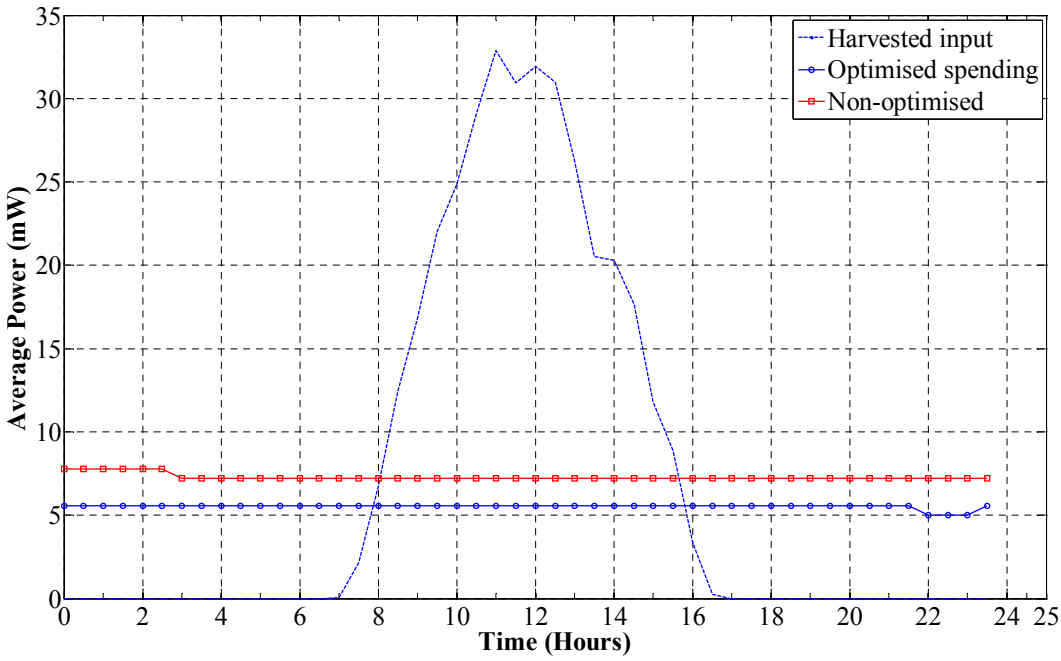

Figure 5.15: Comparison of optimised and non-optimised energy allocations.

for each slot based on the given idle and active power demands of workload. The non-optimised spending represents the 'naive' approach that allocates the spending budget (to calculate the duty cycle) without accounting for efficiency of battery, while the optimised spending uses the refinement presented in Section 5.4.3 to correctly allocate the spending budget. It can be seen in Figure 5.15 that the non-optimised policy over allocates the harvested-energy, by not accounting for the extra energy needed to replenish

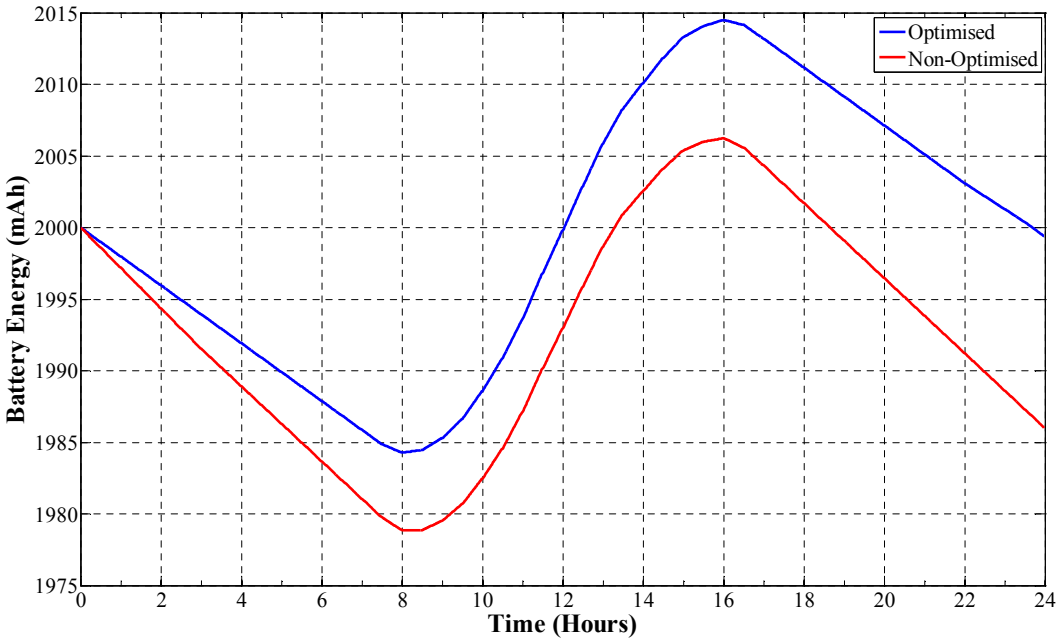

Figure 5.16: Change in net battery capacity over the day. The non-optimised policy overconsumes energy leading to non-conservation of stored energy at end of day.

the battery to the targeted level. The effect of this over allocation of harvested-energy can be seen in Figure 5.16 which shows that the stored energy is not conserved at the end of the day for the non-optimised allocation, resulting in deviation from energy neutral operation. It should be noted that the extent of deviation from the desired outcomes depends on the actual values of non-ideal factors such as the battery efficiency in this case.

5.5 Concluding Remarks

This chapter evaluated and optimised selected harvested-energy management policies based on the knowledge of non-ideal behaviour and interdependencies of system components studied in Chapter 4. It was argued that effective energy management requires consideration of various factors that influence the energy supply and demand for correct allocation of energy budgets. Based on the modeling discussed in Chapter 4, the knowledge of non-ideal characteristics (losses and interdependencies) of various system components is applied to optimise the considered policies to ensure energy-neutral operation and to increase energy utilisation by minimising losses, if possible. The goal of first case study [65] is energy neutral operation while minimising losses due to battery efficiency. It is shown that these objectives cannot be achieved unless the actual demand is not considered. Case 2 considers a supercapacitor leakage minimisation policy [165]. It is shown that other non-ideal characteristics can overshadow leakage consideration

and should be taken in to account to maximise allocation of harvested energy. Case 3 considers a policy for time-uniform allocation of harvested-energy [39]. The energy budget allocation of this policy is optimised to meet energy-neutral operation depending on the system configuration. Although this chapter elaborated these concepts using specific instance of harvesting subsystem and three examples of different energy management policies, optimisation considerations for energy-neutral operation in terms of efficiency of replenishing energy and energy consumption were identified, which are applicable to any energy management policy and configuration of energy harvesting subsystem.

Chapter 6

Energy Management Policy for Low-Variance Energy Allocations

As discussed in Chapters 1 (Section 1.2), many wireless sensor applications are expected to maintain a certain quality-of-service (e.g., data collection rate). An energy harvesting supply should be able to support this required performance (demand) to achieve perpetual operation, while the application's quality-of-service can be adapted depending on the available energy resources using harvested-energy management policies to allocate energy budgets (Chapter 5). Furthermore, achieving consistent application performance is also a desirable feature [154, 140, 103, 39]. For example, it is more useful if the sensor node uses the additional harvested-energy to increase its sampling and communication rate in as uniformly as possible over time instead of sudden bursts of increased activity. Similarly, in times of reduced energy supply the application should gracefully degrade (Section 1.2), instead of abruptly scaling down its activity to the minimum or zero. Furthermore, consistent duty-cycling of wireless radio to sense incoming data or prevent packet collisions is a requirement of network protocols for reliable communications [154]. However, due to the inherent variability of harvested-energy it may not be possible to achieve energy allocations that maintains constant application workload (energy consumption) at all times, while also guaranteeing energy-neutral operation [103]. Figure 6.1 shows an example of low and high variance in allocation of duty cycles (energy consumption) according to variation in harvested-energy over a single day.

Chapter 3 discussed short-term harvested-energy prediction algorithms to manage uncertainty in supply while Chapters 4 and 5 have analysed the impact of non-ideal characteristics of system components on demand and supply. Building upon these aspects, this chapter addresses the above mentioned need for uniform operation of the system under the time-varying energy supply. This can be achieved by allocating energy budgets as uniformly as possible to the application workload. The aim of this chapter is to realise an energy management policy for uniform energy allocation that takes advantage

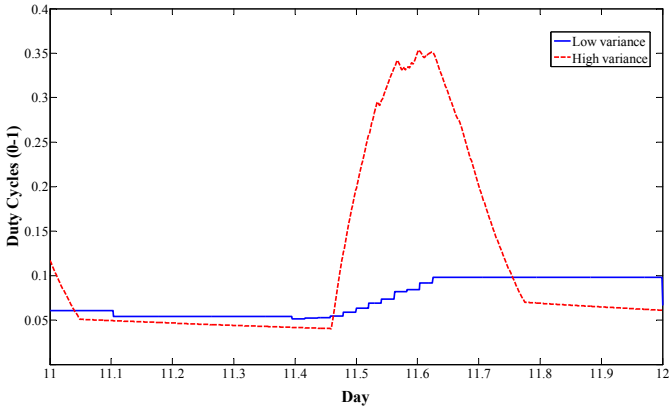

(a) Allocation of cycles.

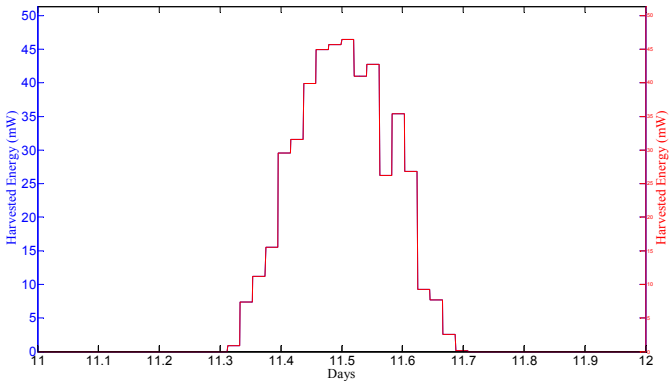

(b) Harvested energy over 48 discrete time slots.

Figure 6.1: Examples of allocation of duty cycles over a single day with low and high variance.

of the knowledge of future harvested-energy by utilising prediction techniques discussed in Chapter 3. The proposed policy is based on two-step predictions of harvested energy; using a low accuracy prediction of multiple time slots in a day and refining these initial estimates using the WCMA algorithm discussed in Chapter 3. Since common sensor nodes are resource (processing, memory and energy) constrained, the policy avoids complex repeated calculations thus minimising the implementation overhead. The results of the proposed policy are compared with other policies and it is shown that proposed policy achieves lower variance in energy budget allocations and lower percentage of dead time of the system, which is important to achieve the goal of perpetual operation. Furthermore, these performance metrics are influenced by size of PV panel and energy storage, which can be considered as fixed input constraints under which the energy management policy operates. Hence, this chapter also considers the influence of these constraints on system dead times and variance of energy allocation.

The chapter is organised as follows. Section 6.1 discusses the performance metrics considered in this chapter. Section 6.2 presented related work and places this work in context. Section 6.3 presents the proposed energy management policy while Section 6.4 presents results and analysis. Section 6.5 concludes the chapter.

6.1 Performance Metrics

This section considers the relationship between application workload demand, energy management policy and size of PV panel and energy storage. The aim is to justify the energy management performance metrics used in this chapter to evaluate the results of proposed policy in Section 6.4. For applications that are powered by energy harvesting, the flexibility permitted in adapting the workload and hence energy consumption can vary. As discussed in Chapter 1 (Section 1.2), if an application must operate at a certain fixed workload (energy demand), clearly it cannot benefit from energy management. In this case, the only solution to ensure uninterrupted workload operation is to size the PV panel and energy storage according to the worst case of energy availability and peak workload demand. Besides this case, if the application's workload can be adapted, the goal of energy management policy is to maintain energy-neutral operation and maximise utilisation of harvested-energy (Chapter 5). Within these objectives, the allocated energy budgets at different time intervals can be determined by different objectives [65, 165] as shown by case studies in Chapter 5. In this chapter, the objective is to minimise the variance of allocated energy budgets under a variable and uncertain supply of harvested-energy. For example, in case of solar energy harvesting systems, the goal can be to achieve as uniform as possible consumption during the whole day rather than having a disproportionate activity during the day (due to higher available energy) as compared to night time. It must be noted that due to the variability of harvested-energy and limited capacity of energy storage, minimising variability of energy budgets while maximising utilisation and avoiding dead times (no operation) can be conflicting objectives. For example, attempting to keep the energy allocation constant under a varying supply can result in wasted energy (poor utilisation) due to saturated storage or suspension of application operation due to depleted stored energy. Since the goal is to operate perpetually, minimising dead times is also an objective. Hence, harvested-energy management considered in this chapter has three metrics:

Average utilisation of harvested-energy should be high to maximise application performance.

Standard deviation of allocated harvested-energy should be low for uniform performance.

Percentage dead time of application workload should be low to meet requirements of near perpetual operation.

As the supply of harvested-energy is variable and not completely predictable, harvested-energy management can aim to achieve these objectives in a best-effort manner. Furthermore, the uniformity of consumption and percentage dead time is also influenced by the size of energy storage with respect to harvested energy. For example, if the capacity

of energy storage is relatively smaller than total harvested-energy during the day, the harvested-energy management has to increase consumption during the day to ensure high utilisation and prevent saturated storage resulting in non-uniform consumption. Furthermore, the maximum energy storage may not be sufficient to sustain operation during night time leading to system dead time. Similarly, during days of extremely low harvested-energy sustaining continuous operation may not be possible and the only way to reduce dead times is to increase the size of PV panel and/or energy storage so that the system is able to harvest and store sufficient energy. Therefore, this chapter also considers the selection of PV panel and energy storage size as a parameter while evaluating results of energy management policy. Selection of size of PV panel and energy storage capacity is commonly termed as dimensioning [10] or capacity planning [146].

6.2 Related Work

6.2.1 Energy Management Policies for Time-Uniform Energy Allocation

The problem of uniform allocation of energy budgets to the application workload under the variability of solar energy harvesting supply has been considered in [154, 103, 39, 113]. Vigorito et al. [154] proposed an adaptive duty cycling algorithm which monitors the changes in stored energy to adapt energy consumption. For minimising the variance of allocated duty cycles, a smoothing filter is used. Moser et al. [103] and Gorlatova et al. [39] assume complete knowledge of variations of energy harvesting supply and propose algorithms to allocate the harvested-energy as uniformly as possible. Noh et al. [113] use prediction to estimate future harvested-energy and solve linear programming problem to allocate energy with the objective of minimising variance. While the first approach [154] assumes no knowledge of energy harvesting source and can be termed as (source) model-free [39], the latter approaches [103, 113, 39] require a model of harvesting source variations.

The energy source model-free algorithm of Vigorito et al. [154] is formulated as a Linear Quadratic (LQ) Tracking closed-loop control problem for duty cycle adaptation. Assuming discrete time steps, the algorithm aims to achieve energy neutral operation by adjusting the energy consumption u (duty cycle) such that deviation of stored energy B_t at time t from a targeted value B^* is minimised over all discrete time-slots N, i.e.:

$$\lim_{N\to\infty} \frac{1}{N} \Sigma_{t=1}^{N} (B_t - B^*)^2 \tag{6.1}$$

$A_{fix} \leftarrow \varnothing$; $s(i) \leftarrow 0 \ \forall \ i$;
while $\overline{A_{fix}} \neq \varnothing$ **do**
  for $i = 0;\ i \leq K-1;\ i++$; **do**
    if $i \in \overline{A_{fix}}$ **then**
      $\tilde{s}(j) \leftarrow s(j) \ \forall \ j \in [0, K-1]$; $\tilde{s}(i) \leftarrow \tilde{s}(i) + \Delta$;
      $valid \leftarrow$ **check_validity**$(\tilde{s})$;
      if $valid == TRUE$ **then** $s(i) \leftarrow \tilde{s}(i)$;
      else $A_{fix} := A_{fix} \cup i$;
function check_validity$(\tilde{s})$:
$B(i) \leftarrow 0 \ \forall \ i$; $B(0) \leftarrow B_0$; $valid \leftarrow TRUE$;
for $i = 1; i \leq K; i++$; **do**
  $B(i) \leftarrow \min(C,\ B(i-1) + Q(i-1) - \tilde{s}(i-1))$;
  if $\tilde{s}(i) > B(i)$ **then** $valid \leftarrow FALSE$;
if $B_K < B(K)$ **then** $valid \leftarrow FALSE$;
return $valid$

Figure 6.2: The Progressive Filling Algorithm (PFA) for assignment of harvested-energy [39].

To minimise the variance, the duty cycle u calculated by the LQ tracking algorithm at each time step is smoothed using exponentially weighted averaging with two parameters α and β as follows:

$$\bar{u}_t = \bar{u}_{t-1} + \alpha(u_t - \bar{u}_{t-1}) \tag{6.2}$$

$$\rho_t = \beta u_t + (1-\beta)\bar{u}_t \tag{6.3}$$

where $\bar{u}_t$ is the exponentially weighted average of calculated duty cycle u, and ρ_t is the final smoothed output which is the weighted combination of u_t and $\bar{u}_t$. While α smooths the output of the algorithm, β is used to select between the contribution of smoothed and non-smoothed output of the algorithm. If α is close to 1 no smoothing occurs while alpha close to zero (not zero) produces maximum smoothing. β determines the contribution of smoothed value to the final duty cycle output. It should be noted that since the objective of the LQ tracking algorithm is to adapt to changes in harvested energy by varying the duty cycle, attempt to smooth these variations by using the two parameters α and β can lead to poor utilisation of harvested-energy and increased dead times of the system due to the reduced responsiveness of the policy output to variations in energy supplied (Section 6.1). This algorithm involves simple computations in each time step and has low implementation and energy consumption overheads. The results of the proposed energy management policy in Section 6.4 are compared with this algorithm using different values of α and β.

Next, energy allocation algorithms that utilise some model of harvesting source to obtain future values of harvested-energy are considered. Among these, the algorithms in [103,

39] allocate the time varying harvested-energy as uniformly as possible by assuming knowledge of future energy supply. The algorithm by Gorlatova et al. [39] is called Progressive Filling Algorithm (PFA), based on the principle of max-min fair allocation of resources. This algorithm (Figure 6.2) was considered in Chapter 5 as case 3 of energy management policy (Section 5.4.2) for optimisation in terms of supply and demand. The input to the algorithms is a profile of harvested energy $Q(i)$ over K discrete time slots in future, an initial value of stored energy B_0, the maximum storage capacity C and the desired value of stored energy at the end of the optimisation interval B_K (for maintaining energy-neutral allocation). The algorithm allocates the harvested energy as uniformly as possible by progressively incrementing the energy allocation of each time slot i by an amount $\triangle$, checking for underflow at every time step while ensuring that at the end of K time slots, the stored energy is equal to B_K. The other algorithm by Moser et al. [103, 104] is called the Recursive-Decomposition algorithm and it requires the same inputs to calculate energy allocations. It is a heuristic that smooths the energy allocations among time slots by averaging the future values of harvested-energy, until an underflow or overflow condition is encountered in some time slot. In this case the previous allocations are adjusted to prevent these, and the algorithm continues from the last slot in the same manner until the condition of stored energy of last time slot slot is met. The overall smoothness of the resulting energy assignments of both these policies are dependent on the size of energy storage used for a given harvested-energy profile. The time complexity of both these algorithms is in the order of $O(K^2)$ but [39] involves simpler operations in each time step. Note that these algorithms determine the optimally uniform allocations and the proof is given [103, 39]. These works [103, 39] do not give any specifics of how the knowledge of future energy can be obtained and how to minimise the impact of errors in prediction of future values. The proposed energy allocation policy is based on the PFA algorithm [39] and addresses the problem of prediction of future values.

Another work that considers minimising the variance of allocated energy is by Noh et al. [113], which formulates a linear programming problem using predicted values of harvested energy in a day. The EWMA prediction algorithm (Section 3.3) is used to predict the values of harvested energy in N discrete time slots of a complete day. Since the error in EWMA prediction is high under highly variable conditions (as discussed in Chapter 3), these predicted values of harvested energy in N future time steps $\tilde{E}_{hrv}^{kmodN}$ are adjusted at each time slot i:

$$\tilde{E}_{hrv}^{k\,mod\,N} = \varphi \bar{E}_{hrv}^{k\,mod\,N}, \forall\, i \leq k < N + i, \; where\, \varphi = \frac{E_{hrv}^{i-1}}{\bar{E}_{hrv}^{i-1}} \tag{6.4}$$

where, φ is the ratio of harvested-energy in previous time slot E_{hrv}^{i-1} and it's historical average $\bar{E}_{hrv}^{i-1}$. Since the adjustment is done at every time step during a day, it requires the linear programming solution to be re-evaluated at each time step. This may be

feasible for the harvesting system considered in [113] which consists of low-end laptop powered by two 105 Watts solar panels, but not for resource constrained sensor nodes powered by small PV panels. The proposed policy also uses two step predictions to refine the initial estimates, however, the optimised prediction algorithm discussed in Chapter 3 is used and the resulting refinement at each time step is carried out using simple calculations as discussed in Section 6.3.

The aim of the energy allocation policy proposed in this chapter is to obtain low-variance energy allocation using simple computations suitable for resource constrained sensor nodes. The proposed policy is based on the Progressive Filling Algorithm as it uses simple computations. An initial prediction of a complete day is used to estimate the energy allocations, which are later refined using the more accurate, one time-slot ahead WCMA prediction algorithm discussed in Chapter 3. The results of the prediction refinements are used to adjust the initial allocations in a low-cost manner that does not use the Progressive Filling Algorithm at each time step. The next section gives the details of the proposed policy.

6.2.2 Dimensioning of Energy Supply and Storage

The determination of the energy supply and storage capacities to ensure perpetual operation has been considered in previous works at different levels of abstraction. Kansal et al. [65] derived a theorem for energy-neutral operation by abstracting the energy supply and workload as functions of their average power (ρ), maximum (σ^h) and minimum (σ^l) fluctuations from the average (burstiness) over some arbitrary operating period. Given an energy storage of maximum capacity C and initial value of stored energy B_0, with efficiency η_{energy_store} and leakage power ρ_{leak}, the theorem states that the energy-neutral operation is guaranteed if:

1. The average power consumption ρ_{load} should not exceed the worst case of average power supply ρ_{supply}, which implies that all supplied energy ρ_{supply} is consumed through the non-ideal energy storage, thus being reduced by η_{energy_store}, in addition to leakage ρ_{leak}:

$$\rho_{load} \leq \eta_{energy\_store} \cdot \rho_{supply} - \rho_{leak} \tag{6.5}$$

2. The required stored energy should be sufficient to cater to the worst case variation in supply σ^l_{supply} and demand σ^h_{load} during any period:

$$\begin{aligned} B_0 &\geq \eta_{energy\_store} \cdot \sigma^l_{supply} + \sigma^h_{load} \\ B &\geq B_0 \end{aligned} \tag{6.6}$$

Although this theorem gives design guidelines that are intuitive, the determination of supply and load are highly abstracted and the calculations of σ^h and σ^l are not well defined, which makes determination of actual sizes of PV panel and energy storage for a given load demand not straightforward. Furthermore, this theorem only explicitly considers the energy storage efficiency and leakage whereas there can be other non-ideal characteristics that influence supply and consumption in typical energy harvesting systems as discussed in Chapters 2 and 4. This chapter presents an intuitive and realistic manner of evaluating the size of PV panel and energy storage capacity based on simulation of a complete model of photovoltaic energy harvesting system. This model of the system discussed in Chapter 4 represents each component in the system, such as PV panel, energy storage and power conditioning, by using parameters that correspond to some chosen instances of these. Given this model of a specific PV harvesting system and model of input supply of energy, the size of PV panel and energy storage is evaluated to determine whether the given load demand is met at all times under modeled harvesting source. This detailed approach is practical since it takes into account a given system configuration and the characteristics of each component on achievable results. A system model based approach to explore the dimensioning of supply and storage is also discussed in [10], but it uses a partial model of the system and the analysis only focuses on fixed demand.

6.3 Proposed Harvested-Energy Allocation Policy

In Section 6.2.1 it was discussed that policies [103, 113, 39] utilising knowledge of harvested-energy over several future time slots, e.g., time slots in a day (24 hours), can achieve more uniform allocation due to the optimal approach to energy distribution [103, 39]. However, for energy harvesting sources such as solar energy, obtaining this knowledge by predicting future energy is a practical consideration in realisation of these policies. The validity of the energy allocations obtained is dependent on the accuracy of predicted values. Errors in prediction can lead to underflow of energy storage due to over utilisation, resulting in unwanted shutdown of system, or in case of under utilisation, less than achievable performance. Furthermore, the prediction based policies require advance knowledge of many time slots (e.g., in a day or more) ahead to smooth the allocated energy across these time slots [103].

In Chapter 3, two low overhead solar energy prediction algorithms were discussed, the Exponentially Weighted Moving Average (EWMA) and the Weather Conditioned Moving Average (WCMA), for predicting the harvested-energy one time-slot ahead using a past history of harvested energies. Accurate prediction of multiple time slots ahead in a day is a more complex problem as discussed in Chapter 3. In this respect the simplistic EWMA approach [65] has been be used in [65, 106, 113] for predicting harvested energies a full day ahead, but the accuracy of this method is only acceptable in consistent

weather conditions. Under sudden fluctuations, such as in case of intermittent cloudy conditions, this method has high prediction error (Chapter 3). The WCMA prediction, on the other hand, predicts more accurately compared to EWMA but only does so for only one time slot ahead.

The aim of this chapter is to realise an energy management policy for uniform energy allocation that takes advantage of the knowledge of future harvested-energy by utilising prediction techniques discussed in Chapter 3. In this regard, the progressive filling algorithm (PFA) is employed to determine estimates over K future time slots of a day. To determine the estimates of harvested energy in each time slot i, a two step approach is used. First, the moving average of every time slot's harvested energies over the past D days are input to the PFA to obtain the initial energy allocations. Since these allocations are based on low-accuracy prediction (using moving average), these are termed as 'unrefined allocations'. These need to be refined to suit the actual harvested-energy during the day as actual measurements of current day's harvested energy are available. One possible approach to this can be to measure the prediction error of a slot when that slot's actual energy has been measured and apply a positive or negative adjustment to the remaining time slots depending on current prediction error [65]. Although this approach helps to correct the energy allocations, it is a reactive approach and the resulting corrections can be slow to prevent under or over utilisation of energy, depending on the difference between the actual and predicted values. The proposed approach is to determine more accurate predicted values of each time slots by using the WCMA prediction algorithm discussed in Chapter 3. However, WCMA prediction only predicts the harvested energy one time slot ahead since it uses some values of current day's harvested energy (Section 3.3.2). Therefore, the issue here is how to use the most recent WCMA prediction to adjust the previously decided energy allocations. One approach can be to use the progressive filling algorithm to reallocate energies for all future time slots every time a refined prediction of next slot is determined. This is costly in terms of computations needed, but it is also important to adjust the energy allocations of all future time slots to enable the system to quickly adjust to the current conditions. The proposed approach is to calculate the difference of the refined and initial prediction of the next time slot, and distribute this difference uniformly across all future time slots. The justification for this approach is that it gradually distributes the predicted deficit or surplus compared to the initial prediction uniformly among all remaining slots, thus gradually adapting to the new predictions over time. Hence, this supports the aim of achieving as uniform as possible allocations under variations and uncertainty of energy supply.

Figure 6.3 gives the pseudo code of the proposed energy allocation policy and the algorithm steps are explained as follow. At start of each day, let $Q_u(i)$ be the initial or unrefined prediction of harvested energies of each time slot i ($i = \{0, 1, \ldots, K-1\}$),

```
For Each Day
    Qu [i] = MovingAverage (i),  0 ≤ i ≤ K-1 // Calculate initial prediction of all slots
    Qr = Qu                                  // Initialise refined estimates
    s  = ProgressiveFillingAlgorithm (Qu)    // Calculate initial allocations
    for j = 0; j ≤ K-1; j++;  do             // For each slot in a day
        if j ∈ day slots; do                 // If next slot has a non-zero average
            // Refine its prediction using WCMA algorithm
            Qr [j] = WCMA_prediction( j)
            // Determine the difference from earlier estimate
            Qdiff = Qr [j] – Qu [j]
            // Determine the adjustment factor for future slots
            Qadj = Qdiff /(K-j)
            // Apply the adjustment to future slots
            s[i] = s[i] + Qadj,  j ≤ i ≤ K-1
```

Figure 6.3: Pseudo code for the proposed energy allocation policy.

which are obtained using moving average of past D days historical values of harvested-energies. Let s be the allocated energies obtained with the Progressive Filling Algorithm based on $Q_u(i)$. For night time slots, these initial predictions will be accurate but for time slots after day rise, more accurate predictions can be obtained using WCMA algorithm discussed in Chapter 3. Suppose that for a slot j after day rise, refined prediction $Q_r(j)$ is obtained using the WCMA prediction. The difference $Q_{diff} = Q_r(j) - Q_u(j)$ between the refined and initial predictions for time slot j is calculated. This is used to calculate the adjustment value $Q_{adj} = \frac{Q_{diff}}{K-j}$ for the next $K - j$ slots. Finally, the allocated energies $s(i)$ for slots $j \leq i \leq K - 1$ are adjusted:

$$s(i) = s(i) + Q_{adj}, \forall j \leq i \leq K - 1 \tag{6.7}$$

It should be noted that this approach is not a substitute for accurate initial predictions but it enables better utilisation of harvested energy while reducing system dead time as compared to the energy allocation based on only initial predictions or model-free approach [154] as shown in the next section.

6.4 Experiments and Analysis

6.4.1 Setup and Methodology

To obtain results of the proposed energy management policy and compare these with other policies, the energy harvesting system configuration described in Chapter 2 (Section 2.3) and modeled in Chapter 4 (Section 4.3) is used. Furthermore, the supply and demand considerations discussed in Chapter 5 for optimised implementation of energy management policies are accounted for. The workload energy consumption is modeled as a duty cycle between 0.0-0.9 with active and idle mode power consumptions as described in Section 4.3. A year long solar energy profile from NREL NWTC data set

[114] is used for modeling the energy harvesting source variations. This energy profile exhibits variability in the form of long-term seasonal and short-term day-to-day fluctuations. The WCMA prediction algorithm uses the optimised parameters determined in Chapter 3. The total number of discrete time slots in a day for energy allocation (K) are set to 48.

First, the proposed approach for evaluating the size of PV panel and energy storage is presented. The aim is to determine if continuous operation can be achieved for a given workload demand and input energy profile. Next, the influence of energy storage capacity on the uniformity of energy allocations is shown, using the progressive filling algorithm and assuming perfect knowledge of harvested-energy variations. Using the sizes of PV panel and energy storage selected using this analysis, the proposed energy allocation policy is evaluated in terms of the three performance metrics discussed in Section 6.1, which are the mean and standard deviation of duty cycles (energy allocation), and percentage of dead times (with zero duty cycle). To show the effectiveness of the energy allocation adjustment method of the proposed policy, two variations of the proposed policy are considered. The first, called '*No Adjustment*', does not adjust the energy allocations obtained using the progressive filling algorithm based on initial predictions. The second, called '*Error Adjustment*,' adjusts the energy allocations based on prediction error observed in the current slot and uniformly distributing the measured error value over remaining slots. These alternate policies are used to show that the adjustment method used in the proposed policy achieves better results. Another policy used for comparison is the model-free approach in [154]. Finally, a '*Perfect knowledge*' policy that uses complete knowledge of harvested-energy profile is also used to compare with results under zero prediction error.

6.4.2 Dimensioning of PV Panel and Energy Storage

This section discusses evaluation of size of PV panel and energy storage based on simulation of system model discussed in Chapter 4 with a given profile of input energy supply. Starting with a given size of PV panel and energy storage, first the case of a fixed workload demand is considered to illustrate how simulation results can be used. Next, the progressive filling algorithm is used for adapting demand with full knowledge of harvested-energy. The aim is to show the effect of energy storage size on the energy allocations when maximum utilisation of harvested-energy is targeted rather than a fixed demand.

Let the reference system configuration with a 100F super capacitor be the base configuration. The 10 days solar radiation profile of NWTC [114] is used as input to the system and the fixed demand is set to 1% duty cycle. Figure 6.4 shows the simulation results with respect to time for 10 days. Both graphs depict the trend of supercapacitor voltage (red) indicating the changes in stored energy, the top graph shows duty cycle

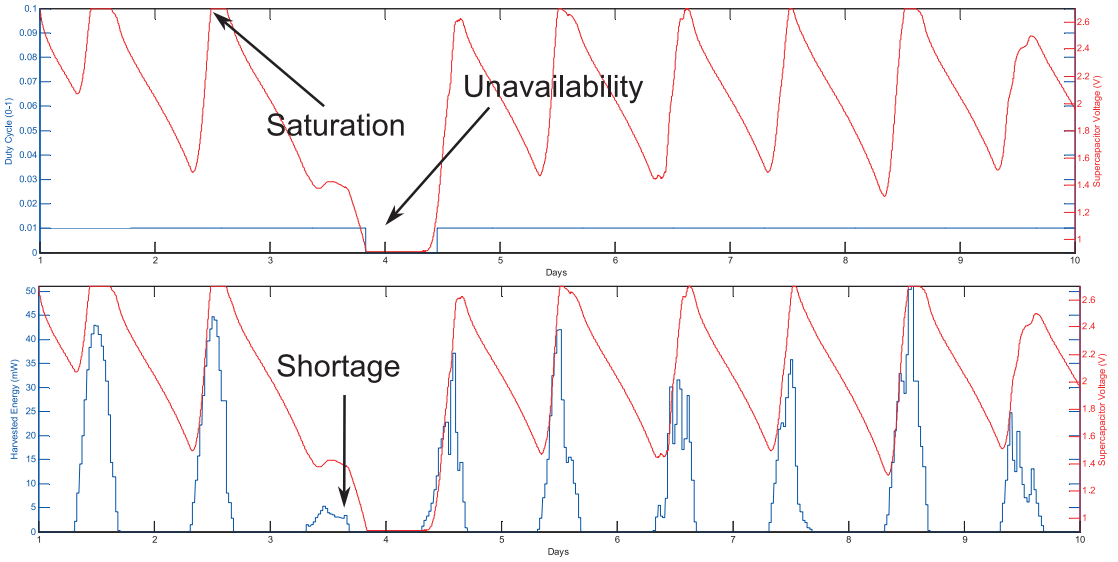

Figure 6.4: Simulation results for 1% duty cycle target using 100F supercapacitor showing the system unavailability during days 3-4 and saturated supercapacitor during day 3.

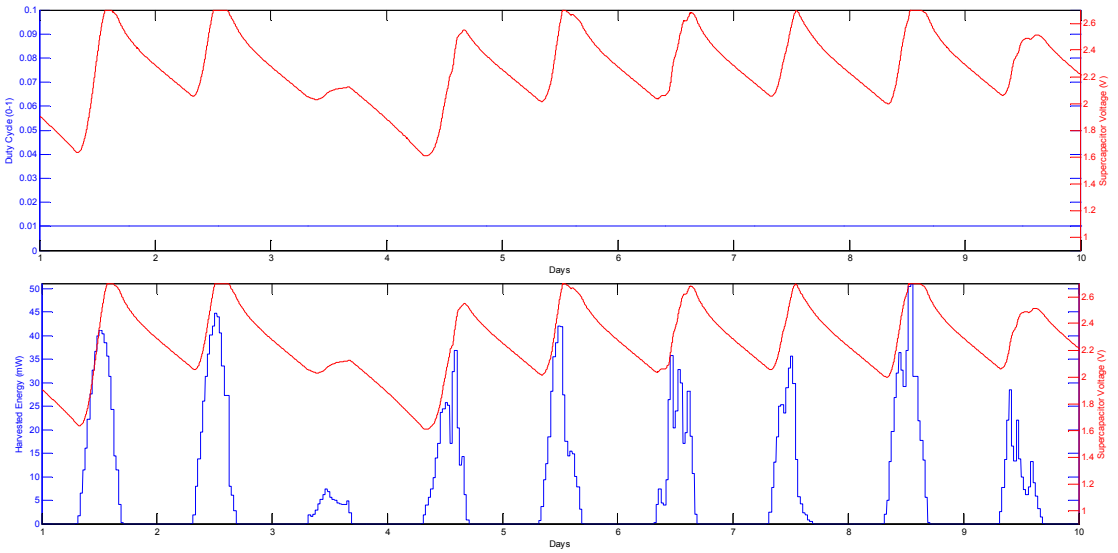

Figure 6.5: Simulation results using 200F supercapacitor and 1% duty cycle indicating that workload is operational continuously.

(blue) while the bottom graph shows the harvested-energy profile (blue) discretised in 48 time slots. It can be observed that system is not able to maintain the required workload demand and there is a period of unavailability at the end of day 3 (labeled on top graph) until the system is able to harvest enough energy to resume operation again. This is due to the depleted energy in the supercapacitor at the end of day 3, since the system harvests significantly less energy in day 3 (labeled on bottom graph) as compared to other days. To enable the system to maintain the given demand in this case, the energy available needs to be increased by increasing the PV panel output and/or the energy storage capacity. To determine which of these components should be adjusted, note that

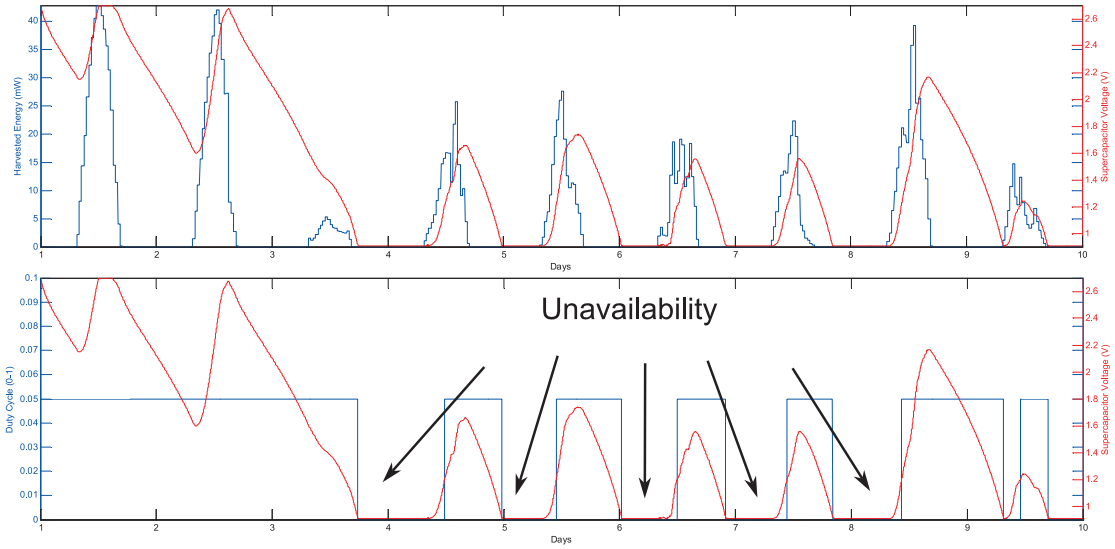

Figure 6.6: Simulation results for 5% duty cycle using 200F supercapacitor indicating periods of system unavailability.

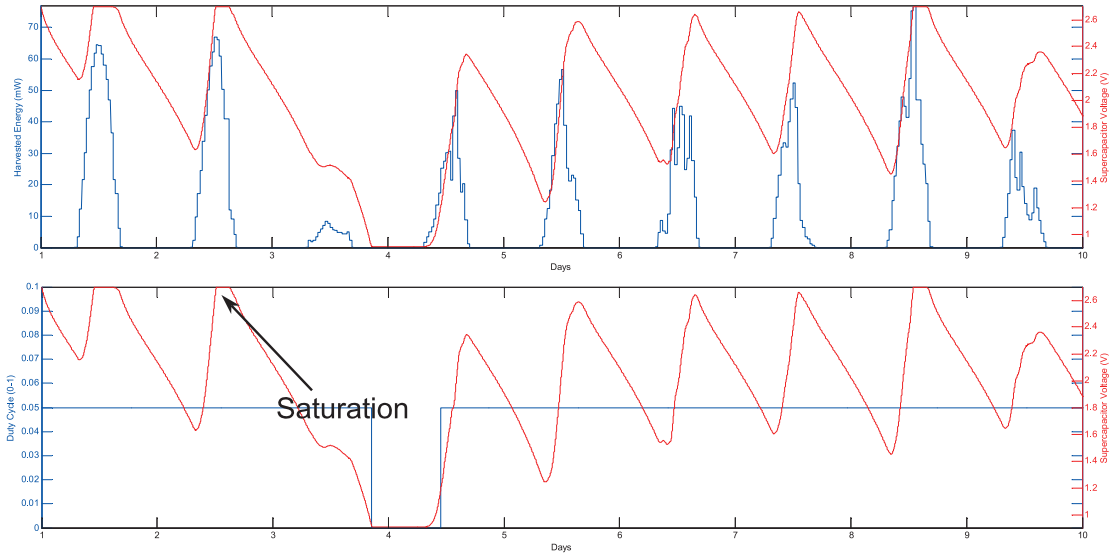

Figure 6.7: Simulation results for 5% duty cycle with 1.5x PV panel indicating improved system availability and saturation of supercapacitor during day 2

during days 1 and 2 the supercapacitor remains fully charged during mid day (labeled on top graph), which indicates that the PV panel is able to harvest more energy than can be stored. Thus, if the capacity of energy storage is increased, then more energy can be captured to be used when the harvested energy is insufficient, i.e., during day 3. Considering a 2x increase in supercapacitor capacity from 100F to 200F, the results of simulation are shown in Figure 6.5. It can be seen that the increased supercapacitor allows more energy to be captured, resulting in less discharge as compared to Figure 6.4. Hence, the system is able to survive the poor supply of harvested energy as encountered during day 3.

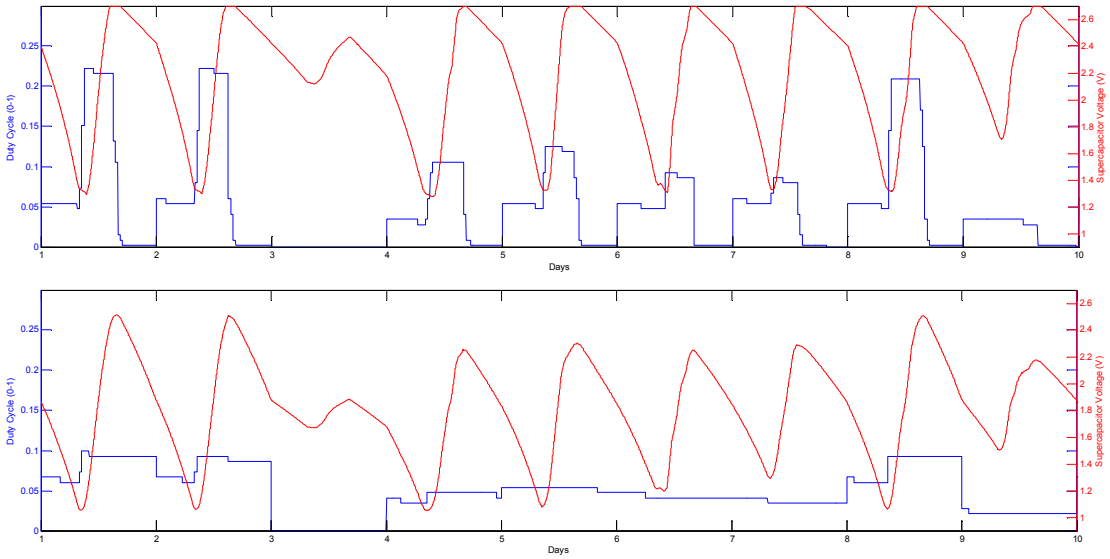

Figure 6.8: Simulation results for maximum energy utilisation using 100F (top) and 200F supercapacitor. There is higher variation in allocations using 100F capacity.

Now consider the case when the desired duty cycle is increased to 5% and the 200F supercapacitor is used as the base system. Figure 6.6 shows the simulation results for the base configuration. It can be observed that due to the increased demand of energy due to the higher duty cycle as compared to previous case, the system is not able to fulfill the required demand at all times from the end of day 2 onwards. In this case, increasing the energy storage cannot benefit since there is clearly shortage of harvested energy as indicated by the supercapacitor voltage trend. Therefore, in this case the system can benefit from an increased supply of harvested energy by selecting a bigger PV panel. Figure 6.7 shows the results if the size of PV increased by 50%, effectively increasing the PV panel output current (Chapter 2, Section 2.2.6). The increased size of panel enables the system to meet the demand, except for day 3. Note that with the increased size of panel, there is saturation of supercapacitor during days 1 and 2, resulting in energy not captured. Thus, the system can now benefit from increase in supercapacitor size to be able to operate continously.

The previous cases illustrated dimensioning using a fixed demand. Now, the maximum energy utilisation is considered using the the Progressive Filling Algorithm. The goal is to consider effect of energy storage size on the uniformity of allocation along with dimensioning of PV panel. The same 10 days profile of input energy is used as before. Figure 6.8 shows simulation results for 100F (top) and 200F (bottom) supercapacitors. Note that the initial value of stored energy at start of day 1 and the targeted stored energy level at the end of each day (for energy neutral allocation) is kept identical for both these cases for a fair comparison. It can be seen that for 100F case (top graph) the allocation has the greater variation due to less capacity to buffer energy during the day, and there a higher energy allocation to utilise the harvested energy. On the other

Table 6.1: Comparisons of proposed policy with other policies according to the three metrics.

Policy	**Mean Duty Cyc**	**Standard Dev.**	**% Dead**
No adjustment (Section 6.4.1)	0.0929	0.0869	31.2%
Error adjustment(Section 6.4.1)	0.0944	0.0989	24.2%
Proposed	0.0964	0.0874	19.4%
LQ [154] ($\alpha = n/a, \beta = 1$)	0.1414	0.2489	1.5%
LQ [154]($\alpha = 0.0005, \beta = 0.75$)	0.1301	0.2340	10.5%
LQ [154]($\alpha = 0.0005, \beta = 0.5$)	0.1246	0.1919	29.4%
LQ [154] ($\alpha = 0.0005, \beta = 0.25$)	0.1151	0.1504	40.1%

hand, the operation has to be suspended near end of day to keep the supercapacitor charged-up to required level of stored energy at the end of day. A drastic improvement in uniformity and system availability is observed if the capacity of supercapacitor is doubled. At the same time more energy is captured since there is no saturation in this case. Note that there is no activity during day 3 since the amount of harvested energy is not enough to meet targeted stored energy level at the end of day 3. This is due to the behaviour of progressive filling algorithm as it prioritises end of day energy conservation while uniformly allocating energy. In this case, the size of PV panel can be increased so that more energy can be harvested during day 3 for system to be operational.

6.4.3 Results of Proposed Policy and Comparison

The previous section discussed the evaluation of PV panel and energy storage sizes using a fixed workload demand and using maximum energy allocation using progressive filling algorithm. Based on these results, the base system configuration with 200F supercapacitor and 1x size the of PV panel is considered to evaluate the proposed energy allocation policy. The duty cycles are set between 0.01 to 0.99 depending on the allocated energy and the efficiency of the output regulator (Chapter 5, Section 5.4.3.2). For model-free LQ tracking policy [154], the targeted stored energy level (B^*) is set at 60% and different values of variance minimisation parameters α and β are tested (see Section 6.2.1 for parameter descriptions).

Table 6.1 shows the results of different policies in terms of the three performance metrics. First consider the top three rows of the table to compare the proposed policy with its two near variants (Section 6.4.1). Note that the proposed policy achieves the highest mean duty cycle and lowest dead time compared to these two variants. The standard deviation of the *No adjustment* policy is slightly lower than the proposed policy, which is explained shortly. It can be seen that in terms energy utilisation (mean duty cycle), the proposed policy is only marginally better, however, in terms of system dead times improvements of 10.8% and 4.8% is significant considering the total evaluation is over 364 days. This shows that the policy is able to adjust to shortages while consuming

Table 6.2: Comparisons with *perfect knowledge* energy allocation policy according to the three metrics.

Policy	**Mean Duty Cyc**	**Standard Dev.**	**% Dead**
LQ [154]($\alpha = n/a, \beta = 1$)	0.1742	0.2903	0.3%
LQ [154]($\alpha = 0.0013, \beta = 0.5$)	0.1705	0.2376	34.99%
LQ [154]($\alpha = 0.0005, \beta = 0.5$)	0.1404	0.2157	23.8%
Proposed	0.1414	0.1267	16.5%
Perfect knowledge (Section 6.4.1)	0.1674	0.1507	5.1%
No adjustment (Section 6.4.1)	0.1345	0.1288	28.2%
Error adjustment (Section 6.4.1)	0.1373	0.1393	22.3%

the available energy better than the other two close variants. Regarding the standard deviation, it should be noted that the design of the proposed policy does not actively minimise the variance but this is inherent in the uniform approach taken to distribute the incoming energy. For to this reason, the higher standard deviation of proposed policy is a by-product of its more responsive energy allocation adjustment property. In light of this reasoning, it can be seen that the proposed policy performs noticeably better than its two close variants in terms of energy utilisation and percentage of dead time.

Next, consider the results of LQ tracking algorithm [154]. It can be seen that this algorithm performs significantly better in terms of both energy utilisation and percentage of dead time, achieving just 1.5% dead time across 364 days. However, note that it has a high deviation of duty cycles, roughly three times that of prediction based policies. Since this algorithm output is parameterised in terms of α and β, which can be used to reduce the variance, three other value combinations these parameters are attempted to reduce the variance. Since β determines the contribution of smoothed duty cycles while α performs the smoothing, a recommended value of α is used [154] while the contribution of smoothed values β is varied from none ($\beta = 1$) to higher. As discussed in [154], as standard deviation decreases, there is a large degradation in dead times and mean duty cycles, since the algorithm becomes unresponsive to changes in supplied energy fluctuations. In the last row of Table 6.1, note that the dead time increases from 1.5% to 40.1% while the variance only decreases by less than half. These results show that the prediction-less policy is better suited to quickly responding to changes in supplied energy and not for minimisation of variability of allocated energy, where the prediction based policies have an inherent advantage.

Table 6.2 shows the comparison of results with Progressive filling algorithm having complete knowledge of harvested-energy profile. A separate set of results are obtained than Table 6.1 because of the changes in the system model needed to model complete knowledge of harvested-energy profile. Recall from Section 4.2.4 that the harvested energy is dependent on the PV panel operating point and hence the supercapacitor voltage for the given system configuration. Since the voltage of the energy storage changes according to the energy consumed from it, the harvested energy is also influenced

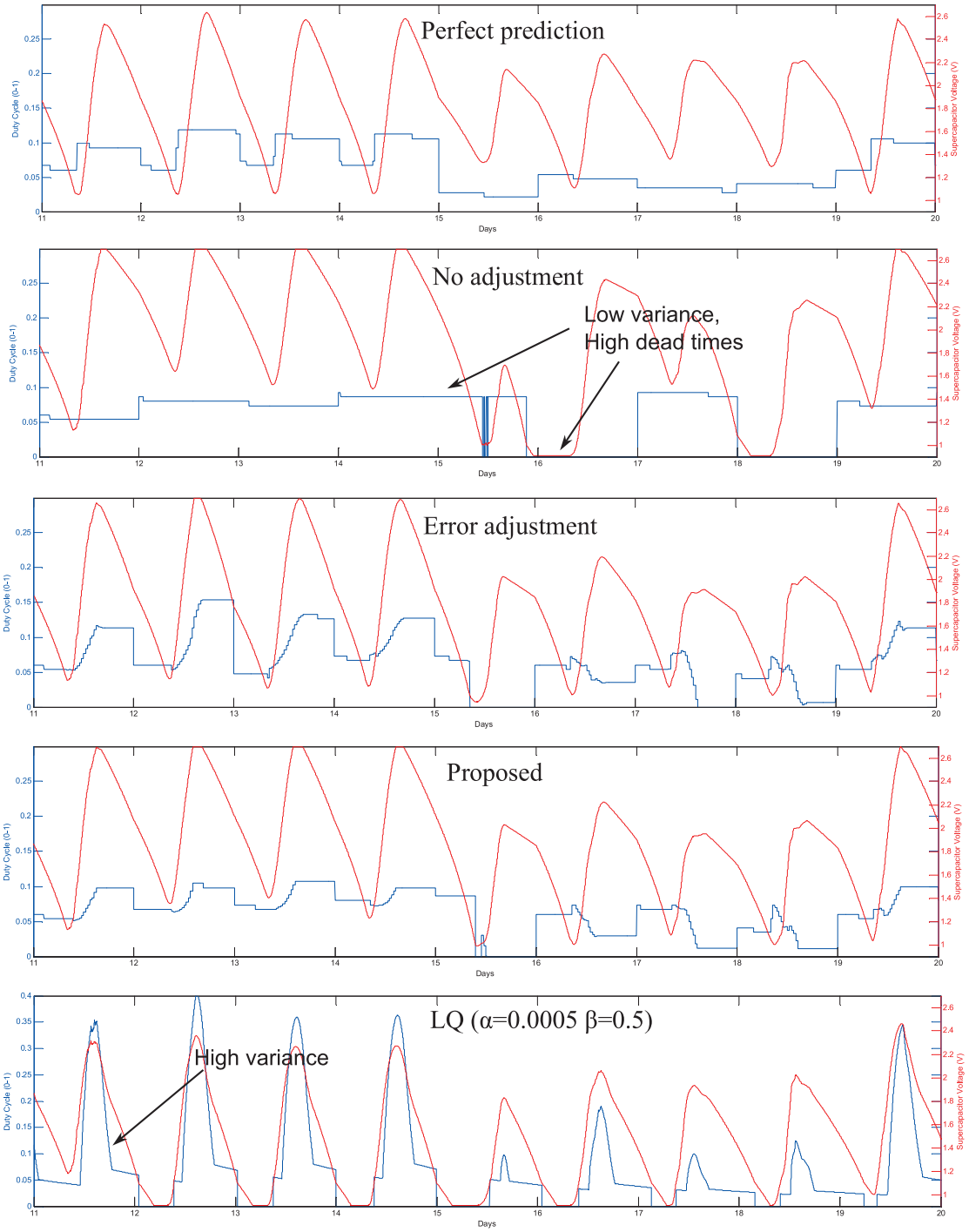

Figure 6.9: Comparison among different policies in terms of variation in allocated duty cycles. The supercapacitor voltage is also shown for indicating changes in stored energy and system dead times.

by these changes. Hence, unless the energy output of the PV panel is decoupled from the voltage of energy storage, it is not possible to determine accurately how much energy will be actually harvested in a given time slot. Hence, to implement perfect knowledge of harvested energy, PV panel voltage and supercapacitor voltage is fixed in the system model and this changes the amount of energy harvested for the same input profile of solar

energy as used in previous results. For this reason, the results of other policies compared in Table 6.1 are also recomputed based on modified system model. Comparing amongst the top 4 rows of Table 6.2, it can be seen that the Perfect prediction policy obtains the highest mean and lowest dead time, followed by the proposed policy. Note that standard deviation of *Perfect knowledge* policy is higher than all prediction based policies, which can be explained in the light of same reasoning as above, referring to the design of the policy. This standard deviation value essentially represents the inherent fluctuation of the harvested supply that cannot be overcome when attempting to allocate energy uniformly even with perfect knowledge of input supply. Also note that the dead time is not zero since the policy design prioritises energy conservation over energy spending when it determines that the harvested energy in any single day is not even enough to maintain the end of day stored energy target. Comparing the results of perfect prediction with LQ tracking algorithm, it can be noticed that the LQ tracking algorithm is adept at tracking the energy supply and maximising consumption but at the cost of very high standard deviation. Comparing the LQ tracking algorithm results in row 3 with the results of proposed policy note that, at similar values of mean duty cycles, the proposed policy performs 30% better in terms of percentage dead times and has 41% lower variability of allocated energy.

To provide insight in the results given in Tables 6.1 and 6.2, and to validate the reasoning above, Figure 6.9 shows a 10 day snapshot of the simulation results of the different prediction based policies, which shows the allocated duty cycles and the changes in supercapacitor voltage over time. It can be observed that the *Perfect knowledge* policy achieves no dead times during this interval as it adapts the consumption according to the available energy. The policy allocates the available energy as uniformly as possible given the the energy storage capacity and variability of harvested energy. Given an initial value of stored energy at the start of the day, the pre-daytime consumption is limited by this, meanwhile the consumption is increased during the rest of the day to utilise the incoming energy in a uniform manner. In case of the *no adjustment* policy, it achieves the lowest variation mainly because of unresponsiveness to variability, resulting in higher dead times. The *error adjustment* policy is able to adapt to the variations compared to no adjustment policy and adjustments, even leading to higher utilisation compared to the proposed policy for instance during the first 4 days of the profile. However, the more drastic adjustments lead to less smooth consumption while dead times are also increased. The LQ tracking policy [154] produces results with high variations in duty cycles, essentially following the change in energy stored in supercapacitor resulting in highly non-uniform consumption. The proposed policy gives the best performance by gradually adjusting to the changes in harvested-energy to minimise the downtime. However, the limitation of inaccuracy of initial prediction is apparent during day 15, during which the proposed policy is not able to adjust to significantly reduced energy supply resulting in dead time of workload during most of the day. As mentioned in Section 6.3, the adaptation approach of the proposed approach cannot completely compensate for

errors in initial predictions but it enables better utilisation of harvested energy while reducing system dead times as compared to the energy allocation based on only initial predictions or model-free LQ tracking approach [154] as shown in Tables 6.1 and 6.2. Further reductions in system dead times can be achieved by using conservative allocations initially during the day until the short-term prediction is able to better estimate the current day harvested-energy.

6.5 Concluding Remarks

This chapter considered the problem of achieving uniform allocation of energy budgets under the variability and uncertainty of energy harvesting supply to achieve uniform performance. Utilising the prediction algorithms discussed in Chapter 3, this chapter proposed a prediction based energy management policy for solar harvested-energy with the objective of achieving low variance of allocated energy. The proposed policy is based on two-step predictions of harvested energy; using a low accuracy prediction of multiple time slots in a day and refining these initial estimates using the WCMA algorithm discussed in Chapter 3. Since common sensor nodes are resource (processing, memory and energy) constrained, the policy avoids complex repeated calculations thus minimising the implementation overhead. The results of the proposed policy are compared with other policies and it is shown that proposed policy achieves lower variance in energy budget allocations and lower percentage of dead time of the system, which is important to achieve the goal of perpetual operation. Furthermore, these performance metrics are influenced by size of PV panel and energy storage, which can considered as fixed input constraints under which the energy management policy operates. Hence, this chapter also considered the influence of these constraints on system dead times and variance of energy allocation.

Chapter 7

Conclusions and Future Work

7.1 Conclusions

Energy harvesting for powering autonomous wireless sensor applications is an attractive solution to meet the goal of perpetual operation. However, the variability and uncertainty of various sources of energy harvesting introduces challenges for design of such system to achieve the desired goal. Many wireless sensor applications' workloads are inherently amenable to being adapted according to the energy resources available and in these cases harvested-energy exploits this flexibility with the goals to maximise utilisation of harvested-energy to achieve maximum achievable performance while at the same time not exceeding the limits of supplied energy to operate perpetually on available supply. These objectives are generally known as maximum performance with energy-neutral operation. Achieving these objectives requires (i) awareness and management of the variability of the energy harvesting source, and (ii) matching the application workload demand with energy supply. This thesis investigates these fundamental design considerations of harvested-energy management. The choice of solar energy harvesting systems is made in this thesis due to the low cost and ubiquity of PV energy harvesting powered wireless sensor applications.

Chapter 1 considers the problem domain of the design of energy harvesting powered wireless sensor applications to motivate the design considerations of harvested-energy management. The contribution of this chapter is to highlight the interplay between various components of the system, including the energy harvesting environment, the wireless sensor application, and harvesting and storage subsystem, to show how the choices of each component influences the selection of other system components. The considerations for effective harvested-energy management are linked to choice of energy harvesting source, applications' characteristics and the design of energy harvesting supply and storage subsystem. This sets the stage for understanding the contributions of this thesis.

Chapter 2 considers the detailed design of photovoltaic energy harvesting supply and storage subsystem and the goal is to consider the general architecture of various possible designs. The contribution of this chapter is to identify the key requirements that influence the choices for various components that constitute the subsystem, such as the need for high efficiency and capability to harvest a desired amount of energy to support the application demand. Furthermore, the detailed behaviour of each component in terms of its non-ideal characteristics, losses and operating interdependency with other components is discussed. The chapter concludes by discussing the design of a reference PV harvesting subsystem and the chosen application platform. This chapter sets the ground to discuss modeling of the non-ideal characteristics of system components in Chapter 4. The reference PV harvesting design is used in Chapter 4 to validate the modeling, and in Chapters 5 and 6 as a specific instance of system model to discuss energy management policies.

Chapter 3 considers the problem of variability of solar energy and discusses prediction of harvested-energy as an approach to manage this. The variability in harvested-energy supply is a challenge in design of energy management due to the difficulty in guaranteeing a match between the system's energy consumption budget and harvester's output at all times. The purpose of harvested-energy prediction is to know how much energy will be harvested in a certain period in future. The amount of solar energy received at different times in a day and across days can vary significantly. To manage this variability, this chapter focuses on effective short-term prediction of solar harvested-energy within a day based on historical data. For the state-of-the-art algorithm with low resource requirements, this chapter targets the problem of determining the prediction algorithm parameters to maximise accuracy across different solar energy harvesting test cases. The contribution of this chapter is selection of an error evaluation function and systematic approach for evaluation of prediction accuracy of solar harvested-energy to determine optimised values of parameters applicable across different profile of input energy. The prediction algorithm with these parameter values is used in Chapter 6 to design energy management policy to achieve low-variance of energy budgets.

Chapter 4 considers modeling of photovoltaic energy harvesting system components with the aim to achieve better correlation between supply and demand. This is addressed by identifying the contribution of individual system component on supply or demand through modeling. The intention is not to propose novel models for different components, but the contribution of this chapter is to model the component characteristics and interdependencies that influence the supply or demand by selection of suitable models that achieve this purpose. The proposed approach to modeling the system and its individual components is validated against empirical measurements using the reference system configuration described in Chapter 2 by considering a scenario of energy-neutral system operation. The utility of this modeling to optimising harvested-energy management policies is discussed in Chapter 5.

Chapter 5 considers the influence of non-ideal system components on the objectives of energy management policy with the aim to optimise energy management policy for these factors. The contribution of this chapter is to evaluate selected harvested-energy management policies to determine if these achieve their objectives on a given energy harvesting system configuration. Each considered policy was first evaluated for non-ideal characteristics that cause deviation from energy-neutral operation and optimised in light of modeled characteristics. The goal of first case study [65] is energy neutral operation while minimising losses due to battery efficiency. It is shown that these objectives cannot be achieved unless the actual demand is not considered. Case 2 considers a supercapacitor leakage minimisation policy [165]. It is shown that other non-ideal characteristics can overshadow leakage consideration and should be taken in to account to maximise allocation of harvested energy. Case 3 considers a policy for time-uniform allocation of harvested-energy [39]. The energy budget allocation of this policy is optimised to meet energy-neutral operation depending on the system configuration.

Chapter 6 considers the problem of achieving uniform allocation of energy budgets under the variability and uncertainty of energy harvesting supply to achieve uniform performance. Utilising the prediction algorithms discussed in Chapter 3, this chapter proposes a prediction based energy management policy for solar harvested-energy with the objective of minimising the variance of allocated energy. The proposed policy is based on two-step predictions of harvested energy; using a low accuracy prediction of multiple time slots in a day and refining these initial estimates using the WCMA algorithm discussed in Chapter 3. Since common sensor nodes are resource (processing, memory and energy) constrained, the policy avoids complex repeated calculations thus minimising the implementation overhead. The results of the proposed policy are compared with other policies and it is shown that proposed policy achieves lower variance in energy budget allocations and lower percentage of dead time of the system, which is important to achieve the goal of perpetual operation. Furthermore, these performance metrics are influenced by size of PV panel and energy storage, which can considered as fixed input constraints under which the energy management policy operates. Hence, this chapter also considers the influence of these constraints on system dead times and variance of energy allocation.

This thesis has investigated fundamental problems common to design of different types energy harvesting powered applications. The contributions of thesis can be summarised in two main aspects: (i) better management of uncertainty of energy supply through improved predictions, and utilising this to achieve low variability in performance of energy harvesting systems, and (ii) optimised energy management policies that achieve better match of application workload demand with energy supply, using system components modeling and practical validations. Although these problems were addressed by considering solar energy harvesting systems and applications, the identification of characteristics of supply, harvesting subsystem and demand are applicable to design

of energy management for other types of harvesting. Clearly, the breadth of different aspects touched upon in this thesis have potential for in-depth exploration. Some directions for such explorations is discussed in the next section.

7.2 Directions for Future work

The central implication of the work undertaken in this thesis is that the objectives of harvested-energy management can only be achieved by considering harvested-energy management and energy harvesting system design in an integrated manner. A variety of harvested-energy management algorithms have been proposed in recent years to suit the needs of individual applications, however, practical realisation of an optimised system needs to take in to account the considerations discussed in this thesis. The fundamental objective is better match of demand and supply and in this regard, there are two key future directions that can be addressed for optimised design of the overall energy harvesting systems.

The first aspect is the design of the energy harvesting supply and storage subsystem. As discussed in Chapter 2 and Chapter 6, given some constraints on size of PV panel and energy storage, it it important to design the energy harvesting supply and storage subsystem that meets the requirements of meeting a certain demand of the application workload. Given a certain energy supply and storage capability of a system, energy management policy attempts to dynamically match demand and supply under variations of harvesting supply. Since the design of PV energy harvesting systems is well understood as discussed in Chapter 2, design automation can be implemented by building upon the system modeling discussed in Chapter 4. This can aid in selection of system components to assist in the system integration stage. Using a given input trace of environmental energy values and an acceptable range of application consumption demand, the performance of the system can be evaluated in terms of whether this demand can be met. The automated tool can make use of library of system component models that incorporate the non-ideal characteristics that influence the supply and demand. A related issue in the systems design is integrating an energy harvesting subsystem from off-the-shelf components to meet the consumption demands of a given application. This is difficult due to the mismatches in component's operating points as discussed in Chapter 2 and careful selection of PV panel, energy storage and power converters is necessary to match the operating requirements. This often results in waste of precious harvested-energy across component interfaces. Off-the-shelf power conditioning solutions are not optimised for low-power energy harvesting supplies and workload demands, resulting in higher losses. Integrated solutions for supply subsystems that have high efficiencies according to the power requirements of low-power energy harvesting can ease the design of energy harvesting systems.

The second aspect is tighter integration of energy management policy with the underlying harvesting subsystem for better demand supply match. As discussed in Chapters 4 and 5, this requires that the energy management policy be aware of supply and demand. This is achieved by using a combination of measurements of voltages/current values and accurate models of system components. Chapter 4 has discussed selection of suitable models to characterise components for their losses in terms of their terminal characteristics. Energy storage devices are complex entities and it has been recently shown [158] that supercapacitors also exhibit non-linearities similar to rechargeable batteries. The outcomes of energy management policies are based on the information available to it regarding energy harvested, currently stored, lost and consumption rate. Consequently, inaccuracies in these measured or modeled values will result in deviation from desired system operation. The problem with off-the-shelf solutions for measuring these variables is that they have a significant operating overhead compared to the workload's demand. Furthermore, they are not designed for measurement ranges and accuracy needed for low-power energy harvesting applications. Hence, suitable low-overhead solutions for measuring the system operating variables can enable implementation of robust energy management.

Appendix A

Reference System Design

A.1 Schematic

A.2 Board Layout

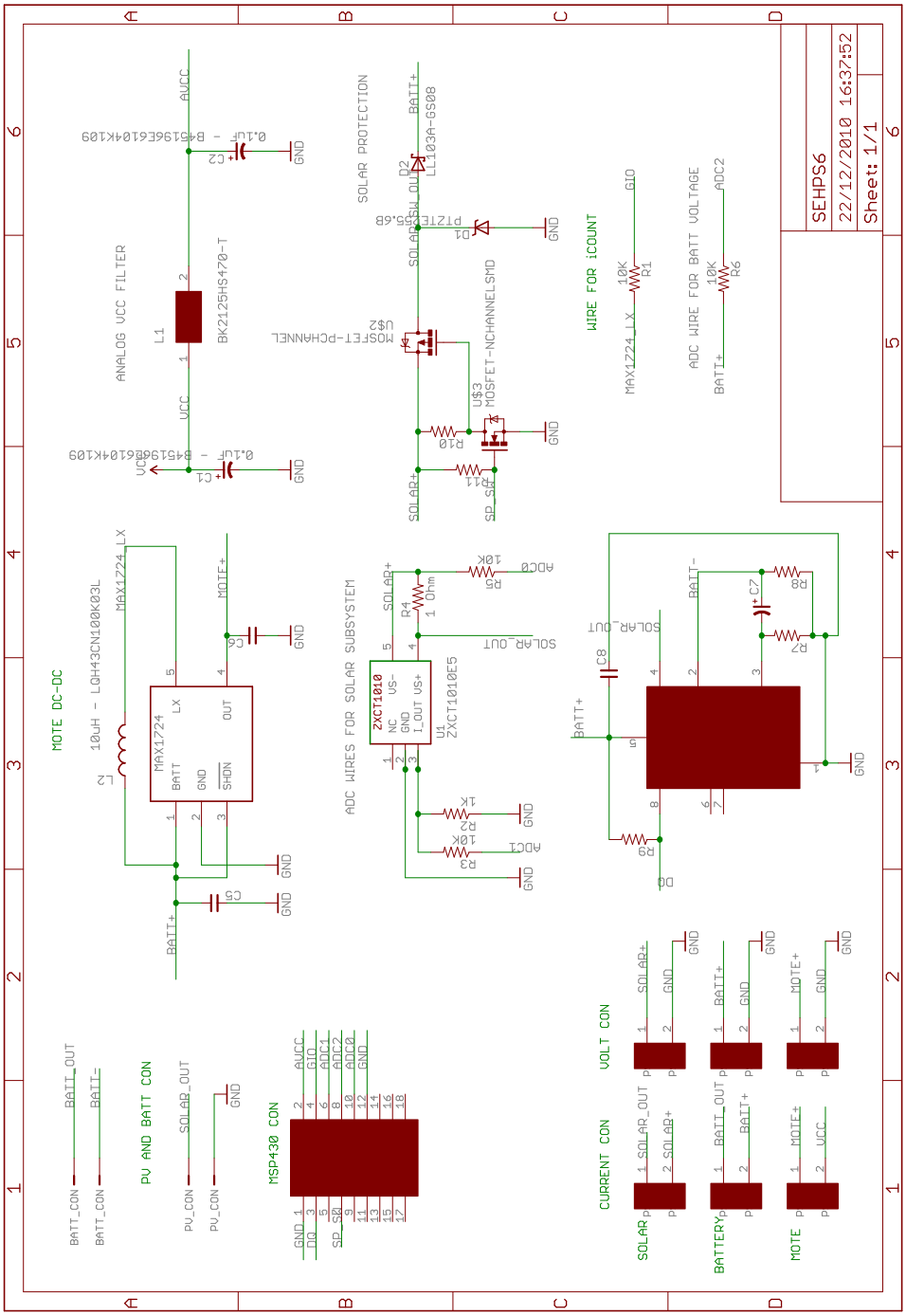

Figure A.1: Schematic of reference PV energy harvesting system.

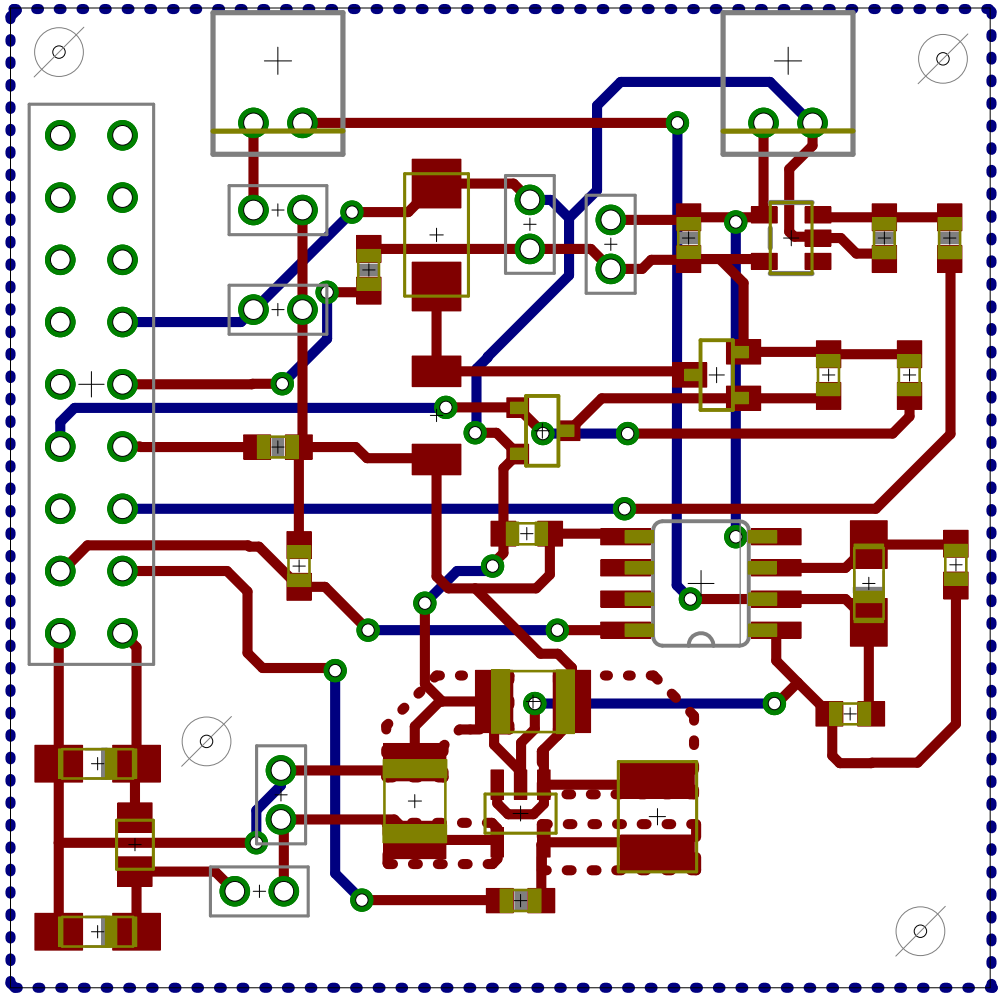

Figure A.2: Two layer board layout of reference PV energy harvesting system.

Appendix B

Other Techniques for Harvested-Energy Prediction

B.1 Long-Term Solar Energy Prediction

Depending upon the requirements of energy management, estimates of energy for the next days may be needed. For instance, [103, 104] presents adaptive energy allocation policies which require knowledge of multiple days to uniformly allocate harvested-energy with respect to time while [65, 39] use knowledge of one day ahead prediction to allocate energy to different slots. The short-term WCMA prediction algorithm (Section 3.3.2) uses the knowledge of current day's energy values to improve prediction of the same day's future slot energy by adjusting the past average based on recent observations. Since the next day's slot values are not known in advance, this principle cannot be used to make predictions for the next day. Note that EWMA (Section 3.3.1) or the moving average step of WCMA (Equation 3.3) estimates the next day's harvested energy in a simple manner, however, the error in this approach can be very high since the next day can be markedly different from the current day. Accurate long-term solar energy prediction based on just currently observed harvested-energy is prone to high error, with exception of continuously clear weather conditions, since other weather effects come in to play such as changing cloud movement and atmospheric turbidity [59]. The aim of this section is to review possible approaches for long-term prediction suitable for energy harvesting wireless nodes.

In [59], a method is discussed for predicting the average energy harvested during a day in future using a k-day history of weather metrics and an astronomical model of a clear day radiation conditions (Section 3.2, Figure 3.2). The weather metrics used are horizontal visibility and cloud cover since these effect the amount of sunlight received during a day and the history of these metrics is commonly available for a given area from weather stations [114]. Horizontal visibility is the distance that can be see horizontally with a

maximum of 10 miles. Cloud cover is the percentage of the sky covered by clouds, and is used to determine the cloudiness of the sky at a particular location. Let the ideal solar energy at time t obtained from astronomical model be $AST(t)$ and the weather factor (horizontal visibility or cloud cover) be $W(t)$, which is a number between 0 and 1. Then the solar energy prediction under the influence of weather factor is given by the following product:

$$RW(n) = W(t) \cdot AST(t) \tag{B.1}$$

To predict the future day's energy value, the first step is to calibrate the values of W(t) based on the different possible values of the weather metric (cloud cover or visibility) and its correlation with historically available data. For example, the different possible values of cloud conditions can be W1=1 (clear), W2=0.8125 (partly cloudy), W3=0.5625 (scatter clouds), W4=0.25 (mostly cloudy) and W5=0 (overcast). For each of these values, calibration factors (c) are derived which determine the correlation with actually observed solar energy. Finally, a k-day history of $RW(n)$ (RW_HIST) is constructed and the future value of $RW(n)$ is obtained using the algorithm given in Figure B.1. The authors in [59] report that using a cloud-based prediction model gave better results than visibility-based model while maintaining a history of 3-7 days. The limitation of this approach is that prediction for a specific time (hour) of the day in future is not possible due to the aggregate historical data used.

The prediction approach presented in [140] relies on availability of weather forecasts of cloud conditions at different times of day. These forecasts are available in increments of three hours for up to 72 hours from national weather service. Similar to the approach described above, the forecasts are assigned a numerical value between 0 and 1. This is multiplied by the value of solar power harvested under ideal conditions to obtain the predicted output. To derive the ideal power model, the power generated on a clear/sunny day (MaxPower) in each months of the year is used to build a model using curve fitting:

$$MaxPower = a \times (Time + b)^2 + c \tag{B.2}$$

Equation B.2 gives the power at different times of a day. The values of a, b and c are determined for the different months of year as shown in Figure B.2. The predicted power is obtained as:

$$Power = MaxPower \times (1 - SkyCondition) \tag{B.3}$$

Require: n: day to estimate solar radiation of
hist: history of solar radiation estimation
k: number of days to look up the history (window size)

1: Evaluate AST(n)
AST(n) ← Estimation of solar radiation using an obstructed astronomical model for day n

2: Evaluation AST_HIST(n) from **hist**
AST_HIST(n) ← $\frac{1}{k}\sum_{i=n-k}^{n-1} AST(i)$

3: Evaluate RW_HIST(n) from **hist**
RW_HIST(n) ← $\frac{1}{k}\sum_{i=n-k}^{n-1} RW(i)$

4: Report RW_PRDT(n) as a solar radiation prediction for day n
RW_PRDT(n) ← AST(n) × (RW_HIST(n) / AST_HIST(n))

5: Evaluate RW(n)
RW(n) ← Estimation of solar radiation using a weather factor for day n

6: Update **hist** with AST(n) and RW(n)

Figure B.1: Algorithm to predict long-term solar harvested-energy using a history of weather effects (from [59]).

This prediction approach is limited by availability of weather forecasts and its accuracy depends on the reliability of weather forecasts and their correlation with ideal power output.

B.2 Generic Prediction Approach for Other Energy Sources

The principle of prediction methods is to utilise some model that captures the correlation between values of data series while smoothing the noise to determine a probable value. For example, using averaging methods such as cumulative average, moving average or weighted average (simple or exponential), a representative value from correlated points can be obtained. However, averaging consecutive values can result in poor accuracy since the data values may have trend or seasonality properties which need to be accounted for [134].

Section 3.3.2 discussed a low overhead prediction method for solar energy that was developed based on the understanding of the solar energy source, i.e., the diurnal cycle, seasonal trend and weather effect fluctuations. By utilising the knowledge of energy

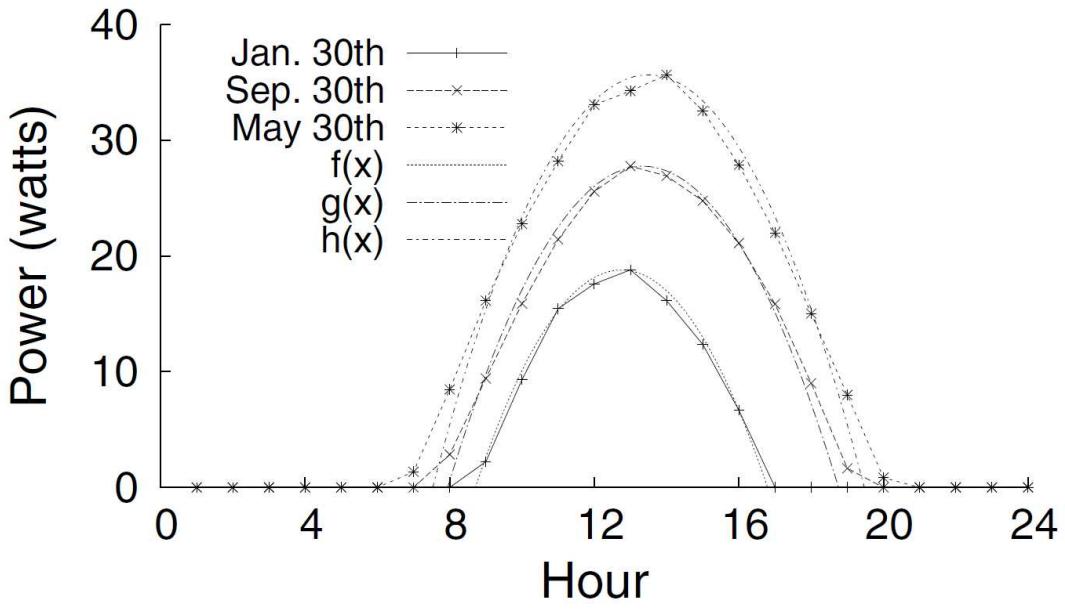

Figure B.2: Profile for solar power harvested on clear and sunny days in January, May, and September, and the quadratic functions f(x), g(x), and h(x) fitted to each profile (Reproduced from [140]).

source behaviour, it is possible to develop to simple prediction methods that achieve reasonable accuracy while being suitable for implementation on resource constrained wireless embedded system. However, other energy sources such as wind and various sources of vibration energy may not exhibit well defined patterns to enable determination of correlation or periodicity, and thus not amenable to building a simple model. In these cases, generic techniques capable of adapting to changes in energy source behaviour can be used. Generic techniques such as neural networks, adaptive filters are more complex in terms of computation and energy consumption depending on whether the training of predictor model is done online or offline, and how the prediction model is adjusted dynamically.

In this section, we discuss a generic prediction method that is inspired by the concept of using prediction to minimise the transfer of sampled data from a wireless sensor to a base station. The original concept is termed as a dual prediction scheme [13], in which both the sensor node a base station use some generic prediction method such as time series prediction or Kalman filter to determine the approximate value of sensed phenomenon. The parameters (or coefficients) of prediction method are determined to minimise the error using a window of past sampled values. As the wireless sensor can compare the sampled value with the predicted value, it can trigger update of the prediction model parameters when the prediction error between the sampled and predicted value exceeds a threshold. In this manner, the generic prediction method used adapts to the variations in source based on monitoring of the error magnitude and triggering a relearning of prediction model parameters.

Table B.1: Results of AR model based wind prediction with different orders and error thresholds for AR parameter update.

Filter order	Error threshold	Average % Error
2	90%	38.88
2	50%	40.86
2	10%	43.12
3	90%	36.79
3	50%	43.59
3	10%	45.43
Persistence	-	34.07

In [13], time series forecasting using AR models is used in which the sampled values of harvested-energy is considered a time series. The prediction at time $t+1$ is obtained by regressing the value X_t of the time series χ_t at time instant t against the elements of the time series at the previous p time instants $(X_{t-1}, X-t-2, \ldots, X_{t-p})$:

$$\hat{X_{t+1}} = \theta_1 X_t + \theta_2 X_{t-1} + \ldots + \theta_p X_{t-p+1} \tag{B.4}$$

where $\theta_1, \theta_1, \ldots, \theta_p)$ are the AR coefficients or parameters and p is the order of the AR model, thus denoted as AR(p). The parameters $\Theta_{AR(p),t} = \theta_1, \theta_2, \ldots, \theta_p$ can be computed by means of Recursive Least Square algorithm, which consists in a computationally thrifty set of equations that allows to recursively update the parameters $\Theta_{AR(p),t}$ as new observations X_t are available.

Figure B.3 shows an example of the use of AR model to predict temperature values. The required prediction accuracy ϵ is set to 0.5 and a autoregressive (AR) model is used. It can be observed that the predicted data are within ± 0.5 of the real data up to the 1261st time step. At time t=1262, the prediction error exceeds the tolerated threshold ϵ and the prediction model is updated to take into account the recent acquired data and from time t=1263 to t=1272, the predicted measurements are again close enough to the real ones. At t=1273, the prediction error exceeds ϵ and the update procedure is repeated again at t=1286.

The limitation of this prediction method is that it works reasonably for sources that remain fairly stable but for highly variable sources, such as wind, the accuracy may be hardly better than using a persistence model. Furthermore, the for highly variable sources, the coefficients may need to change rapidly to keep up with the variations. Table B.1 shows the results of using AR model of orders two and three with different thresholds for recalculation of coefficients. It can seen that best results obtained with error threshold of 90% with AR model of order 2 are worse than using a persistence model, indicating that this approach does not produce useful results with highly variable sources such as wind.

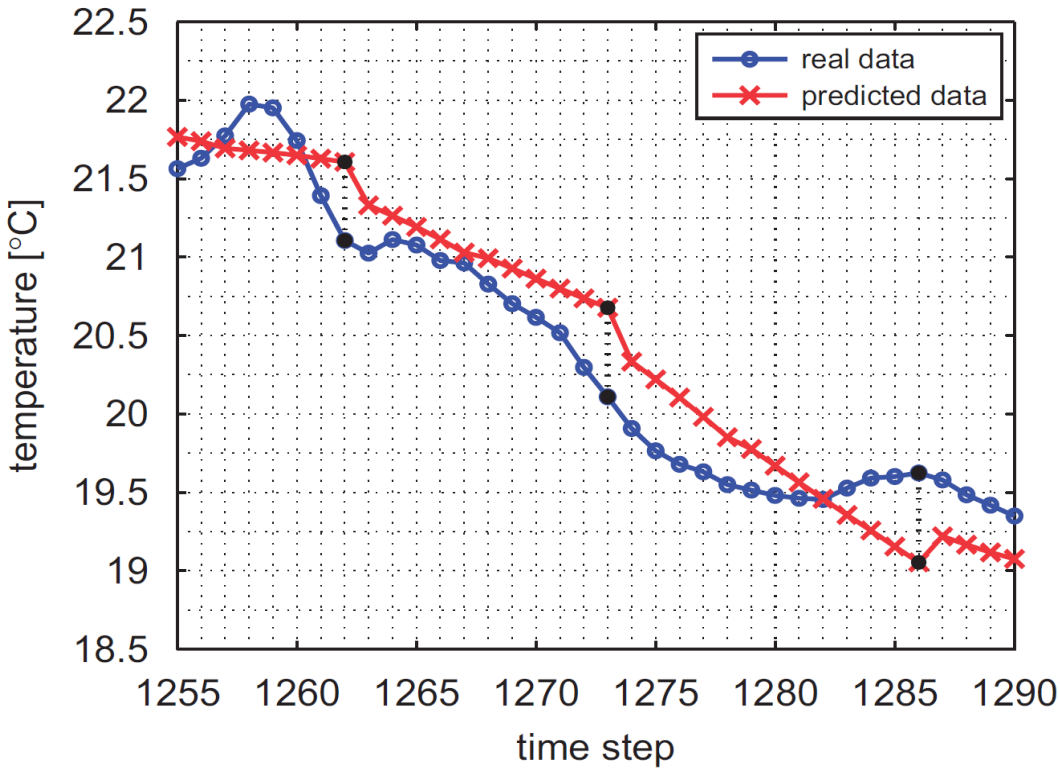

Figure B.3: An example of AR model based prediction with dynamic coefficient update (Reproduced from [13]).

Appendix C

MATLAB Models

C.1 Top-Level System File

```
% Description:
%   Top-level System Simulation File
%
% Parameters:
%   t                 - time vector (array format)
%   radiation_rate    - radiation intensities (array format)
%   supercap_init_mJ  - initial supecap energy level in mJ
%
% Returns: all values are in array format except
%          supercap_energy_final_mJ
%   supercap_energy_final_mJ - final supercap energy level (mJ)
%   radiation_cur - solar panel current with given
%                   radiation condition (mA)
%   radiation_pow - solar panel power with given
%                   radiation condition (mW)
%   net_supercap_energy_mJ - energy that is charged to the supercap (mJ)
%   supercap_energy_mJ - supercap energy level (mJ)
%   panel_vol - solar panel voltage (V)
%   panel_cur - solar panel current at peak radiation (mA)
%   panel_pow - solar panel power at peak radiation (mW)
%   supercap_rel_energy_mJ - relative supercap energy level (percent)
%   supercap_vol - supercap voltage (V)
%   reg_in_pow - output power of input regulator (mW)
%   eff_reg_out - efficiency of output regulator (0 to 1)
%   reg_out_vol - output voltage of output regulator (V)
%   reg_out_pow - output power of output regulator (mW)
%   load_cur - load current draw (mA)
%   load_pow - load power consumption (mW)
%   avail_pow - available power from the solar panel (mW)
%   supercap_draw - supercap power draw (mW)
%   net - net power from solar panel excluding supercap draw (mW)
%   surplus - excess power that is not charged into supercap (mW)
%   is_charging - 1 if being charged, 0 otherwise
%   status_load - 1 if load is operational, 0 otherwise
%   status_reg_out - 1 if output regulator is operational,
%                    0 otherwise
%   supercap_leakage_mJ - energy leak from supercap (mJ)
%
```

```
39  % Author:
40  %   Mustafa Imran Ali - mia08r@ecs.soton.ac.uk
41  %
42  % initializes system-wide variables.
43  % calc_supercap_100F_init();
44  %
45  % % initializes variables
46  % get_HydroSolar_init();
47  % get_current_4V_100mA_panel_init();
48  %
49  % % calculate the size of time vector
50  % N = max(size(t));
51
52  panel_vol = zeros(N,1);         % solar panel
53  panel_cur = zeros(N,1);
54  panel_pow = zeros(N,1);
55  radiation_cur = zeros(N,1);
56  radiation_pow = zeros(N,1);
57  supercap_energy_mJ = zeros(N,1);    % supercapacitor
58  supercap_rel_energy_mJ = zeros(N,1);
59  supercap_vol = zeros(N,1);
60  supercap_lifetime = zeros(N,1);     % supercap lifetimes
61  reg_in_pow = zeros(N,1);        % input regulator
62  eff_reg_out = zeros(N,1);       % output regulator
63  reg_out_vol = zeros(N,1);
64  reg_out_pow = zeros(N,1);
65  load_cur = zeros(N,1);          % load
66  load_pow = zeros(N,1);
67  avail_pow = zeros(N,1);         % system status
68  supercap_draw = zeros(N,1);
69  net = zeros(N,1);
70  net_supercap_energy_mJ = zeros(N,1);
71  surplus = zeros(N,1);
72  is_charging = zeros(N,1);       % 1 if charging, 0 otherwise
73  status_load = zeros(N,1);       % load operational status: 1 or 0
74  status_reg_out = zeros(N,1);    % output regulator status: 1 or 0
75
76  supercap_leakage_mJ = zeros(N,1);
77  running_duty_cycle = zeros(N,1);
78
79  current_duty_cycle = 0; % node duty cycle (1%) *NEW*
80  next_supercap_energy_mJ = supercap_init_mJ;
81
82  for i=1:N,
83
84    supercap_energy_mJ(i,1) = next_supercap_energy_mJ;
85
86    % variables that will be calculated assuming charging mode
87    % or discharging mode.
88
89    supercap_vol_temp = 0;
90    reg_out_vol_temp = 0;
91    eff_reg_out_temp = 0;
92    radiation_cur_temp = 0;
93    radiation_pow_temp = 0;
94
95    supercap_vol_temp = calc_supercap_mJ_to_V(supercap_energy_mJ(i,1), supercap_capacitance);
96
97    % solar panel voltage
98    panel_vol_temp    = supercap_vol_temp + vf_schottky_init;
99
100   % solar panel current
```

```
101   radiation_cur_temp = (interp1(V_panel,I_panel,panel_vol_temp))*1e3;
102   panel_cur_temp = radiation_cur_temp;
103
104   % turn off the Schottky diode if the forward-direction current
105   % is smaller than if_min_mA
106   if (radiation_cur_temp < if_min_mA)
107     panel_vol_temp = 0;
108   end;
109
110   % solar panel output power
111   panel_pow_temp = panel_vol_temp * panel_cur_temp;
112   radiation_pow_temp = panel_vol_temp * radiation_cur_temp;
113
114   % power after Shottky diode and input regulator
115   reg_in_pow_temp = radiation_cur_temp * (panel_vol_temp - vf_schottky_init);
116
117   % override duty cycle calculated if near depletion
118   if supercap_vol_temp < 1.1
119     current_duty_cycle = 0;
120   end
121
122   running_duty_cycle (i,1) = current_duty_cycle;
123
124   % set the load current as the average value. *NEW*
125   load_cur(i,1) = current_duty_cycle * load_active_mA + (1-current_duty_cycle)*load_sleep_
126
127
128   % determine the operating point of MAX1724 output regulator.
129   reg_out_vol_temp = calc_vout_MAX1724(supercap_vol_temp);
130   if current_duty_cycle
131     eff_reg_out_temp = 0.7981;
132   else
133     eff_reg_out_temp = 0.6728;
134   end
135
136   % load seen by output regulator
137   reg_out_pow_temp    = load_cur(i,1) * reg_out_vol_temp / eff_reg_out_temp;
138
139   % available power from the solar panel
140   avail_pow_temp    = max (0, reg_in_pow_temp - reg_out_pow_temp);
141
142   % power discharge from supercap
143   supercap_draw_temp    = max (0, reg_out_pow_temp - reg_in_pow_temp);
144
145   % net power from solar panel excluding load
146   net_temp = avail_pow_temp * eff_supercap - supercap_draw_temp;
147
148   % determine whether it is in discharge or in charge
149   if (net_temp >= 0)
150     is_charging(i,1) = 1;
151   else
152     is_charging(i,1) = 0;
153   end
154
155   % set variables depending on whether in charge or in discharge
156   supercap_vol(i,1)   = supercap_vol_temp;
157   reg_out_vol(i,1)    = reg_out_vol_temp;
158   load_pow(i,1)       = load_cur(i,1) * reg_out_vol(i,1);
159   eff_reg_out(i,1)    = eff_reg_out_temp;
160   reg_out_pow(i,1)    = reg_out_pow_temp;
161   panel_vol(i,1)      = panel_vol_temp;
162   panel_cur(i,1)      = panel_cur_temp;
```

```
163   panel_pow(i,1)      = panel_pow_temp;
164   radiation_cur(i,1)  = radiation_cur_temp;
165   radiation_pow(i,1)  = radiation_pow_temp;
166   reg_in_pow(i,1)     = reg_in_pow_temp;
167   avail_pow(i,1)      = avail_pow_temp;
168   supercap_draw(i,1)  = supercap_draw_temp;
169   net(i,1)            = net_temp;
170
171   % toggle duty cycle
172   current_duty_cycle = ~current_duty_cycle;
173
174   supercap_leakage_mJ(i,1) = min(supercap_max_mJ, ...
175     calc_100F_supercap_leakage_tuh(supercap_energy_mJ(i,1) / 1000, delta_t) * 1000);
176
177   % calculate the supercap energy in the next step
178   % considering leakage
179   next_supercap_energy_mJ = min(supercap_max_mJ, ...
180     supercap_energy_mJ(i,1) ...
181     - supercap_leakage_mJ(i,1) ...
182     + delta_t * 3600 * net(i,1));
183
184   % relative supercap capacity
185   supercap_rel_energy_mJ(i,1) = supercap_energy_mJ(i,1) * 100 / supercap_nominal_max_mJ;
186
187   if (net(i,1) < 0)
188     net_supercap_energy_mJ(i,1) = net(i,1);
189   elseif (supercap_energy_mJ(i,1) < supercap_max_mJ)
190     net_supercap_energy_mJ(i,1) = net(i,1);
191   else
192     net_supercap_energy_mJ(i,1) = 0;
193   end;
194
195   % surplus
196   surplus(i,1) = net(i,1) - net_supercap_energy_mJ(i,1);
197
198   % validating the status of output regulator and mote.
199   status_reg_out(i,1) = is_MAX1724_operational(supercap_vol(i,1), load_cur(i,1));
200   status_load(i,1) = is_TelosB_operational(reg_out_vol(i,1));
201 end;
202
203 duty_cycle_init = current_duty_cycle;
204 supercap_energy_final_mJ = supercap_energy_mJ(N,1);
205 supercap_init_mJ = supercap_energy_mJ(N,1);
206
207 if DEBUG
208   fprintf('%-6.2f,\t  %-6.2f,\t  %-6.2f,\t %-6.2f,\t %-6.2f,\t  %-6.2f,\t%-6.2f,\t\t%-6.2f,\t %-6
209     sum(panel_pow(1:N,1))*delta_t, ...
210     sum(radiation_pow(1:N,1))*delta_t, ...
211     sum(reg_in_pow(1:N,1))*delta_t, ...
212     sum(reg_out_pow(1:N,1))*delta_t, ...
213     sum(load_pow(1:N,1))*delta_t, ...
214     sum(avail_pow(1:N,1))*delta_t, ...
215     sum(supercap_draw(1:N,1))*delta_t, ...
216     sum(net(1:N,1))*delta_t, ...
217     sum(surplus(1:N,1))*delta_t, ...
218     supercap_energy_final_mJ, ...
219     mean(running_duty_cycle (1:N,1)) ...
220     );
221 end
```

C.2 PV Panel Model

```
clear all
clc

%% Information from the MSX-005F solar array datasheet
Iscn = 141e-3;              %Nominal short-circuit current [A]
Vocn = 4.04;              %Nominal array open-circuit voltage [V]
Imp = 115.7e-3;               %Array current @ maximum power point [A]
Vmp = 3.01;               %Array voltage @ maximum power point [V]
Pmax_e = Vmp*Imp;         %Array maximum output peak power [W]
Kv = -16e-3;              %Voltage/temperature coefficient [V/K]
Ki = 0.15e-3;             %Current/temperature coefficient [A/K]
Ns = 8;                  %Nunber of series cells
Gn = 1000;                %Nominal irradiance [W/m^2] @ 25oC
Tn = 25 + 273.15;         %Nominal operating temperature [K]

%% Constants
k = 1.3806503e-23;   %Boltzmann [J/K]
q = 1.60217646e-19;  %Electron charge [C]
a = 1.3;

%% Algorithm parameters
%Increment of Rs
Rsinc = 0.001;
%Initial value of "a"
%a = 1.0;
%Increment of "a"
%ainc = 0.01;
%Maximum tolerable power error
tol = 0.0001;
%Maximum number of iteractions for each value of "a"
nimax = 10000;
%Voltage points in each iteraction
nv = 200;
```

```
%This program evaluates the PV model for any T and G.
%You must run "adjust_model" first.
%%
% Inputs
T = 60;    %Temperature [oC]
G = 880;  %Irradiance [W/m^2]
% Constants
k = 1.3806503e-23;   %Boltzmann [J/K]
q = 1.60217646e-19;  %Electron charge [C]
% Thermal voltages
Vtn = k * Tn / q;    %Thermal junction voltage (nominal)
T = T + 273.15;
Vt = k * T / q;      %Thermal junction voltage (actual temperature)

%% Method of calculating Io
% Chose 1 to use the original method with (T/Tn)^3
% Chose 2 to use the alternative method with KV and KI
method = 1;

%% Calculation of Io (method 1)
%This is the original Io equation generally found in the literature.
%This requires finding the optimal value of Eg.
%See details in:
%"Modeling and circuit-based simulation of photovoltaica arrays"
```

```
if method == 1,
%Calculation of Eg and Io
  Tmax = 75 + 273.15;
  dT_ = Tmax - Tn;
  Isc_ = (  Iscn + Ki*dT_  );
  Voc_ = (  Vocn + Kv*dT_  );
  Vt_ = k * Tmax / q;
  Eg  = log(Isc_*Tn^3/Ion/Tmax^3/(exp(Voc_/a/Ns/k/Tmax*q)-1))*a*k*Tn*Tmax/q/(Tmax-Tn);
  Io  = Ion *(T/Tn)^(3) * exp(  q * Eg/a/ k * (1/Tn-1/T) );
end

%% Calculation of Io (method 2)
%This is the alternative Io equation suggested in:
%"Comprehensive approach to modeling and simulation of photovoltaic arrays"
if method == 2,
  dT = T - Tn;
  Isc_ = (  Iscn + Ki*dT  );
  Voc_ = (  Vocn + Kv*dT  );
  Ipv_ = (Rs+Rp)/Rp * Isc_; %% NEW %% UPDATED ON JUNE/2010 %%
  Io = (Ipv - Voc_/Rp)/(exp(Voc_/Vt/a/Ns)-1); %% NEW %% UPDATED ON JUNE/2010 %%
end

%%  Temperature and irradiation effect on the current
dT = T-Tn;
Ipvn = (Rs+Rp)/Rp * Iscn;         % Nominal light-generated current
Ipv = (Ipvn + Ki*dT) *G/Gn;       % Actual light-generated current
Isc = (Iscn + Ki*dT) *G/Gn;       % Actual short-circuit current

%% Solving the I-V equation for several (V,I) pairs
clear V
clear I
V = 0:Vocn/nv:Vocn;  % Voltage vector
I = zeros(1,size(V,2));    % Current vector

for j = 1 : size(V,2) %Calculates for all voltage values
  % Solves g = I - f(I,V) = 0 with Newton-Raphson
  g(j) = Ipv-Io*(exp((V(j)+I(j)*Rs)/Vt/Ns/a)-1)-(V(j)+I(j)*Rs)/Rp-I(j);
  while (abs(g(j)) > 0.001)
    g(j) = Ipv-Io*(exp((V(j)+I(j)*Rs)/Vt/Ns/a)-1)-(V(j)+I(j)*Rs)/Rp-I(j);
    glin(j) = -Io*Rs/Vt/Ns/a*exp((V(j)+I(j)*Rs)/Vt/Ns/a)-Rs/Rp-1;
    I_(j) = I(j) - g(j)/glin(j);
    I(j) = I_(j);
  end
end

%% I-V and P-V curves
 % I-V curve
 figure(3)
 grid on
 hold on
 title('I-V curve');
 xlabel('V [V]');
 ylabel('I [A]');
 xlim([0 max(V)*1.1]);
 ylim([0 max(I)*1.1]);
 %xlim([0 Vocn]);
 %ylim([0 Iscn*2]);
 plot(V,I,'LineWidth',2,'Color','k') %

 % P-V curve
 figure(4)
 grid on
```

```
 hold on
 title('P-V curve');
 xlabel('V [V]');
 ylabel('P [W]');
 xlim([0 max(V)*1.1]);
 ylim([0 max(V.*I)*1.1]);
 %xlim([0 Vocn]);
 %ylim([0 Iscn*2*Iscn]);
 plot(V,V.*I,'LineWidth',2,'Color','k') %
```

```
% Matlab script for modeling a photovoltaic array
%
% Author: Marcelo Gradella Villalva
% Email: mvillalva@gmail.com
% University of Campinas, Brazil
%
% First version:   May/2009
% Updated:         June/2010
% Current version: March/2011
%
% If you like my work, please cite these two papers:
%
% M. G. Villalva, J. R. Gazoli, E. Ruppert F.
% "Comprehensive approach to modeling and simulation of photovoltaic arrays"
% IEEE Transactions on Power Electronics, 2009
% vol. 25, no. 5, pp. 1198--1208, ISSN 0885-8993
%
% M. G. Villalva, J. R. Gazoli, E. Ruppert F.
% "Modeling and circuit-based simulation of photovoltaica arrays"
% Brazilian Journal of Power Electronics, 2009
% vol. 14, no. 1, pp. 35--45, ISSN 1414-8862
%
% Visit: http://sites.google.com/site/mvillalva/pvmodel

%% Load PV device data
% Uncomment the line corresponding to the desired PV device:
 data_MSX005F_2

%% Adjusting algorithm
plott = 0; %1 = Enables plotting during the algorithm execution
           %0 = Disables plotting
% Reference values of Rs and Rp
Rs_max = (Vocn - Vmp)/ Imp;
Rp_min = Vmp/(Iscn-Imp) - Rs_max;

% Initial guesses of Rp and Rs
Rs = 0;
Rp = Rp_min;

% The model is adjusted at the nominal condition
T = Tn;
G = Gn;
Vtn = k * Tn / q;                    %Thermal junction voltage (nominal)
Vt = k * T / q;                      %Thermal junction voltage (current temperature)
%Ion = Iscn/(exp(Vocn/a/Ns/Vtn)-1);    % Nominal diode saturation current
%Io = Ion;
perror = Inf; %dummy value

% Iterative process for Rs and Rp until Pmax,model = Pmax,experimental
ni = 0;

```

```
52  while (perror>tol) && (Rp > 0) && (ni < nimax)
53    ni = ni + 1;
54  %  Temperature and irradiation effect on the current
55    dT = T-Tn;
56    Ipvn = (Rs+Rp)/Rp * Iscn;         % Nominal light-generated current
57    Ipv = (Ipvn + Ki*dT) *G/Gn;       % Actual light-generated current
58    Isc = (Iscn + Ki*dT) *G/Gn;       % Actual short-circuit current
59    Io = (Ipv - Vocn/Rp)/(exp(Vocn/Vt/a/Ns)-1); %% NEW %% UPDATED ON JUNE/2010 %%
60  % Increments Rs
61    Rs = Rs + Rsinc;
62    Rp_ = Rp;
63    Rp = Vmp*(Vmp+Imp*Rs)/(Vmp*Ipv-Vmp*Io*exp((Vmp+Imp*Rs)/Vt/Ns/a)+Vmp*Io-Pmax_e);
64  % Solving the I-V equation for several (V,I) pairs
65    clear V
66    clear I
67    V = 0:Vocn/nv:Vocn;        % Voltage vector
68    I = zeros(1,size(V,2));    % Current vector
69    for j = 1 : size(V,2) %Calculates for all voltage values
70    % Solves g = I - f(I,V) = 0 with Newton-Raphson
71      g(j) = Ipv-Io*(exp((V(j)+I(j)*Rs)/Vt/Ns/a)-1)-(V(j)+I(j)*Rs)/Rp-I(j);
72      while (abs(g(j)) > 0.001)
73        g(j) = Ipv-Io*(exp((V(j)+I(j)*Rs)/Vt/Ns/a)-1)-(V(j)+I(j)*Rs)/Rp-I(j);
74        glin(j) = -Io*Rs/Vt/Ns/a*exp((V(j)+I(j)*Rs)/Vt/Ns/a)-Rs/Rp-1;
75        I_(j) = I(j) - g(j)/glin(j);
76        I(j) = I_(j);
77      end
78    end % for j = 1 : size(V,2)
79
80    if (plott)
81      %Plots the I-V and P-V curves
82
83      %Current x Voltage
84      figure(1)
85      grid on
86      hold on
87      title('I-V curve - Adjusting Rs and Rp');
88      xlabel('V [V]');
89      ylabel('I [A]');
90      xlim([0 Vocn]);
91      ylim([0 Iscn]);
92
93      %Plots I x V curve
94      plot(V,I,'LineWidth',2,'Color','k')
95
96      %Plots the "remarkable points" on the I x V curve
97      plot([0 Vmp Vocn],[Iscn Imp 0],'o','LineWidth',2,'MarkerSize',5,'Color','k')
98
99      %Power x Voltage
100     figure(2)
101     grid on
102     hold on
103     title('P-V curve - Adjusting peak power');
104     xlabel('V [V]');
105     ylabel('P [W]');
106     xlim([0 Vocn])
107     ylim([0 Vmp*Imp]);
108   end % if(plott)
109
110   % Calculates power using the I-V equation
111   P = (Ipv-Io*(exp((V+I.*Rs)/Vt/Ns/a)-1)-(V+I.*Rs)/Rp).*V;
112
113   Pmax_m = max(P);
```

```
114
115   perror = (Pmax_m-Pmax_e);
116
117   if (plott)
118   %Plots P x V curve
119     plot(V,P,'LineWidth',2,'Color','k')
120
121   %Plots the "remarkable points" on the power curve
122     plot([0 Vmp Vocn],[0 Vmp*Imp 0],'o','LineWidth',2,'MarkerSize',5,'Color','k')
123   end % if (plott)
124 end % while (error>tol)
125
126 if (Rp<0) Rp = Rp_
127 end
128 Ion = Io; %
129
130 %% Outputs
131  % I-V curve
132  figure(3)
133  grid on
134  hold on
135  title('Adjusted I-V curve');
136  xlabel('V [V]');
137  ylabel('I [A]');
138  xlim([0 Vocn*1.1]);
139  ylim([0 Iscn*1.1]);
140  plot(V,I,'LineWidth',2,'Color','k') %
141  plot([0 Vmp Vocn ],[Iscn Imp 0 ],'o','LineWidth',2,'MarkerSize',5,'Color','k')
142
143  % P-V curve
144  figure(4)
145  grid on
146  hold on
147  title('Adjusted P-V curve');
148  xlabel('V [V]');
149  ylabel('P [W]');
150  xlim([0 Vocn*1.1]);
151  ylim([0 Vmp*Imp*1.1]);
152  plot(V,P,'LineWidth',2,'Color','k') %
153  plot([0 Vmp Vocn ],[0 Pmax_e 0 ],'o','LineWidth',2,'MarkerSize',5,'Color','k')
154
155 disp(sprintf('Model info:\n'));
156 disp(sprintf(' Rp_min = %f',Rp_min));
157 disp(sprintf('     Rp = %f',Rp));
158 disp(sprintf(' Rs_max = %f',Rs_max));
159 disp(sprintf('     Rs = %f',Rs));
160 disp(sprintf('      a = %f',a));
161 disp(sprintf('      T = %f',T-273.15));
162 disp(sprintf('      G = %f',G));
163 disp(sprintf(' Pmax,m = %f  (model)',Pmax_m));
164 disp(sprintf(' Pmax,e = %f  (experimental)',Pmax_e));
165 disp(sprintf('    tol = %f',tol));
166 disp(sprintf('P_error = %f',perror));
167 disp(sprintf('    Ipv = %f',Ipv));
168 disp(sprintf('    Isc = %f',Isc));
169 disp(sprintf('    Ion = %g',Ion));
170 disp(sprintf('\n\n'));
171
```

C.3 Supercapacitor Leakage

```
function energy_output = calc_100F_supercap_leakage_tuh(energy_begin, hour_elapsed)
%
% calc_100F_supercap_leakage(energy_begin, hour_elapsed)
%
% Description:
%   Calculates the energy leakage for 100F supercap using model of
%   Christian Renner
%
% Parameters:
%   energy_begin: energy level of the supercap at the beginning (in J)
%   hour_elapsed: hour elapsed since the beginning
%
% Returns:
%   energy_output: energy level of the supercap at the end (in J)
%
% Usage:
%   calc_100F_supercap_leakage(600, 0.25);
%
% Author:
%   Mustafa Imran Ali - mia08r@ecs.soton.ac.uk
%

%capacitance = 100;      % 100 F
capacitance = 200;      % 200 F
%capacitance = 350;      % 350 F
%leak_current_mA = 0.1;  % 0.3 mA
delta_t_sec = 1;        % 1 sec
P0 = 9.3211e-12;        % used with leakage model
alpha = 7.9298;         % for leakage model

cap_energy = energy_begin;
cap_voltage = 0;
cap_leakage = 0;

% converting hour_elapsed in sec
time_end_sec = hour_elapsed * 3600;

% number of for-loop iterations
num_iterations = floor(time_end_sec / delta_t_sec);

% fringe time in case time_end_sec is not multiple of delta_t_sec
time_fringe = time_end_sec - num_iterations * delta_t_sec;

% trivial case when duration is less than or equal to minimum time unit
% no iteration is needed
if (time_end_sec < delta_t_sec)
    cap_voltage = sqrt(2 * cap_energy / capacitance);                   % unit V
    cap_leakage =  P0 * exp(alpha*cap_voltage) * time_end_sec ;         % unit J
    next_cap_energy = cap_energy - cap_leakage;                         % unit J
    cap_energy = max(next_cap_energy, 0);                               % unit J
else
    for i=1:num_iterations,
        cap_voltage = sqrt(2 * cap_energy / capacitance);                   % unit V
        cap_leakage = P0 * exp(alpha*cap_voltage) * delta_t_sec ;           % unit J
        next_cap_energy = cap_energy - cap_leakage;                         % unit J
        cap_energy = max(next_cap_energy, 0);                               % unit J
    end

    if (time_fringe > 0)
```

```
        cap_voltage = sqrt(2 * cap_energy / capacitance);                    % unit V
        cap_leakage = P0 * exp(alpha*cap_voltage) * time_fringe ;            % unit J
        next_cap_energy = cap_energy - cap_leakage;                          % unit J
        cap_energy = max(next_cap_energy, 0);                                % unit J
    end
end

% Total energy leakage
energy_output = energy_begin - cap_energy;

```

C.4 Output Regulator Efficiency

```
function efficiency = calc_efficiency_MAX1724(v_in, i_load)
%
% calc_efficiency_MAX1724(v_in, i_load)
%
% Description:
%   Calculates the power efficiency of MAX1724 using
%   the given parameters.
%
% Parameters:
%   v_in: input voltage
%   i_load: output current draw
%
% Returns:
%   efficiency: efficiency of MAX1724 between 0 and 1
%
% Usage:
%   Eff_2_5V(i,1)   = calc_efficiency_MAX1724(2.5, I_load2_5(i,1));
%
% Author:
%   Jaein Jeong - jaein@eecs.berkeley.edu
%

efficiency = 0;

i_load_1_0 = [
0.010 0.020 0.030 0.040 0.050
0.060 0.070 0.080 0.090 0.100 0.200 0.300 0.400 0.500 0.600 0.700 0.800 0.900 1.000
2.000 3.000 4.000 5.000 6.000 7.000 8.000 9.000 10.000 20.000 30.000 40.000 50.000
];

eff_1_0 = [
0.500 0.553 0.581 0.597 0.606 0.616 0.619 0.622 0.628 0.631 0.641 0.647 0.650 0.653
0.656 0.659 0.663 0.663 0.666 0.675 0.681 0.684 0.688 0.691 0.694 0.694 0.697
0.697 0.700 0.703 0.703 0.703
];

i_load_1_5 = [
0.010 0.020 0.030 0.040 0.050 0.060 0.070 0.080 0.090
0.100 0.200 0.300 0.400 0.500 0.600 0.700 0.800 0.900 1.000 2.000 3.000 4.000 5.000
6.000 7.000 8.000 9.000 10.000 20.000 30.000 40.000 50.000 60.000 70.000 80.000 90.000
];

eff_1_5 = [0.538 0.606 0.634 0.656 0.666 0.672 0.675 0.678 0.681 0.684
0.697 0.703 0.706 0.706 0.709 0.713 0.713 0.716 0.716 0.725 0.728 0.731 0.734
```

```
0.738 0.738 0.741 0.741 0.744 0.747 0.750 0.753 0.756 0.756 0.759 0.763 0.763
];

i_load_2_0 = [
0.010 0.020 0.030 0.040 0.050 0.060 0.070 0.080 0.090 0.100 0.200 0.300 0.400 0.500
0.600 0.700 0.800 0.900 1.000 2.000 3.000 4.000 5.000 6.000 7.000 8.000 9.000
10.000 20.000 30.000 40.000 50.000 60.000 70.000 80.000 90.000 100.000 128.760
];

eff_2_0 = [
0.575 0.644 0.684 0.706 0.719 0.728 0.731 0.734 0.738 0.741
0.753 0.759 0.763 0.766 0.769 0.769 0.769 0.772 0.772 0.778 0.781 0.784 0.784 0.788
0.788 0.788 0.791 0.791 0.794 0.797 0.797 0.800 0.800 0.800 0.803 0.803 0.803 0.806
];

i_load_2_5 = [
0.010 0.020 0.030 0.040 0.050 0.060 0.070 0.080 0.090 0.100 0.200 0.300 0.400 0.500
0.600 0.700 0.800 0.900 1.000 2.000 3.000 4.000 5.000 6.000 7.000 8.000 9.000
10.000 20.000 30.000 40.000 50.000 60.000 70.000 80.000 90.000 100.000 158.760
];

eff_2_5 = [0.613 0.688 0.722 0.741 0.753 0.759 0.766 0.772 0.775 0.778 0.791 0.797
0.800 0.800 0.800 0.803 0.803 0.803 0.806 0.809 0.813 0.816 0.816 0.819 0.819
0.819 0.822 0.822 0.825 0.825 0.828 0.828 0.828 0.831 0.831 0.831 0.834 0.838
];

N = zeros(4,1);
N(1,1) = max(size(i_load_1_0));
N(2,1) = max(size(i_load_1_5));
N(3,1) = max(size(i_load_2_0));
N(4,1) = max(size(i_load_2_5));

vol = zeros(4,1);
vol(1,1) = 1.0;
vol(2,1) = 1.5;
vol(3,1) = 2.0;
vol(4,1) = 2.5;

eff = zeros(4,1);
eff(1,1) = interp1(i_load_1_0, eff_1_0, i_load);
eff(2,1) = interp1(i_load_1_5, eff_1_5, i_load);
eff(3,1) = interp1(i_load_2_0, eff_2_0, i_load);
eff(4,1) = interp1(i_load_2_5, eff_2_5, i_load);

if (i_load < i_load_1_0(1,1))
    eff(1,1) = eff_1_0(1,1);
elseif (i_load > i_load_1_0(N(1,1),1))
    eff(1,1) = eff_1_0(N(1,1),1);
end

if (i_load < i_load_1_5(1,1))
    eff(2,1) = eff_1_5(1,1);
elseif (i_load > i_load_1_5(N(2,1),1))
    eff(2,1) = eff_1_5(N(2,1),1);
end

if (i_load < i_load_2_0(1,1))
    eff(3,1) = eff_2_0(1,1);
elseif (i_load > i_load_2_0(N(3,1),1))
    eff(3,1) = eff_2_0(N(3,1),1);
end

```

```
107 if (i_load < i_load_2_5(1,1))
108     eff(4,1) = eff_2_5(1,1);
109 elseif (i_load > i_load_2_5(N(4,1),1))
110     eff(4,1) = eff_2_5(N(4,1),1);
111 end
112 
113 if (v_in >= 1.0 && v_in < 1.5)
114     if (i_load <= calc_max_iout_MAX1724(1.0))
115         efficiency = interp1(vol, eff, v_in);
116     else
117         error 'Output load is bigger than maximum of MAX1724'
118     end;
119 elseif (v_in >= 1.5 && v_in < 2.0)
120     if (i_load <= calc_max_iout_MAX1724(1.5))
121         efficiency = interp1(vol, eff, v_in);
122     else
123         error 'Output load is bigger than maximum of MAX1724'
124     end;
125 elseif (v_in >= 2.0 && v_in < 2.5)
126     if (i_load <= calc_max_iout_MAX1724(2.0))
127         efficiency = interp1(vol, eff, v_in);
128     else
129         error 'Output load is bigger than maximum of MAX1724'
130     end;
131 elseif (v_in < 1.0)
132     % input voltage of MAX1724 is out of range.
133     % represent it with the closest valid input.
134     if (i_load <= i_load <= calc_max_iout_MAX1724(1.0))
135         efficiency = interp1(vol, eff, 1.0);
136     else
137         error 'Output load is bigger than maximum of MAX1724'
138     end;
139 elseif (v_in >= 2.5)
140     % input voltage of MAX1724 is out of range.
141     % represent it with the closest valid input.
142     if (i_load <= i_load <= calc_max_iout_MAX1724(2.5))
143         efficiency = interp1(vol, eff, 2.5);
144     else
145         error 'Output load is bigger than maximum of MAX1724'
146     end;
147 else
148     error 'Input voltage of MAX1724 is out of range.'
149 end
150 
```

References

[1] AdaptivEnergy. Joule-Thief™ Energy Harvesting Solution Using Ruggedized Laminated Piezo (RLP®), 2011. http://www.adaptivenergy.com/posts/energy-harvesting/.

[2] M. I. Ali, B. M. Al-Hashimi, J. Recas, and D. Atienza. Evaluation and Design Exploration of Solar Harvested-Energy Prediction Algorithm. In *Proceedings of the Conference on Design, Automation and Test in Europe*, pages 142–147, 2010.

[3] C. Alippi, G. Anastasi, M. Di Francesco, and M. Roveri. Energy Management in Wireless Sensor Networks With Energy-Hungry Sensors. *Instrumentation and Measurement Magazine, IEEE*, 12(2):16–23, April 2009.

[4] C. Alippi, G. Anastasi, C. Galperti, F. Mancini, and M. Roveri. Adaptive Sampling for Energy Conservation in Wireless Sensor Networks for Snow Monitoring Applications. In *Mobile Adhoc and Sensor Systems, 2007. MASS 2007. IEEE Internatonal Conference on*, pages 1–6, Oct. 2007.

[5] C. Alippi, R. Camplani, C. Galperti, and M. Roveri. *Recent Advances in Sensing Technology*, (Chapter) From Labs to Real Environments: The Dark Side of WSNs, page 143168. Springer-Verlag Berlin Heidelberg, 2009.

[6] C. Alippi and C. Galperti. An Adaptive System for Optimal Solar Energy Harvesting in Wireless Sensor Network Nodes. *Circuits and Systems I: Regular Papers, IEEE Transactions on*, 55(6):1742–1750, July 2008.

[7] G. Anastasi, M. Conti, M. Di Francesco, and A. Passarella. Energy conservation in wireless sensor networks: A survey. *Ad Hoc Netw.*, 7(3):537–568, 2009.

[8] Energy. Micro. AS. EFM32 Zero Gecko EFM32ZG103 Datasheet, July 2011. http://cdn.energymicro.com/dl/devices/pdf/d0062_efm32zg103_datasheet.pdf.

[9] P. Bacher, H. Madsen, and H. A. Nielsen. Online Short-Term Solar Power Forecasting. *Solar Energy*, 83(10):1772 – 1783, 2009.

[10] S. Bader, T. Scholzel, and B. Oelmann. A Method for Dimensioning Micro-Scale Solar Energy Harvesting Systems Based on Energy Level Simulations. In *Embedded and Ubiquitous Computing (EUC), 2010 IEEE/IFIP 8th International Conference on*, pages 372 –379, dec. 2010.

[11] The Electropaedia - Battery and Energy Technologies. Battery Chargers and Charging Methods. http://www.mpoweruk.com/chargers.htm.

[12] C. Bergonzini, D. Brunelli, and L. Benini. Comparison of Energy Intake Prediction Algorithms for Systems Powered by Photovoltaic Harvesters. *Microelectronics Journal*, 41(11):766 – 777, 2010.

[13] Y.-A. L. Borgne, S. Santini, and G. Bontempi. Adaptive Model Selection for Time Series Prediction in Wireless Sensor Networks. *Signal Processing*, 87(12):3010 – 3020, 2007. Special Section: Information Processing and Data Management in Wireless Sensor Networks.

[14] D. Brunelli, D. Dondi, A. Bertacchini, L. Larcher, P. Pavan, and L. Benini. Photovoltaic Scavenging Systems: Modeling And Optimization. *Microelectronics Journal*, 40(9):1337 – 1344, 2009. Quality in Electronic Design; 2nd IEEE International Workshop on Advances in Sensors and Interfaces; Thermal Investigations of ICs and Systems.

[15] D. Brunelli, C. Moser, L. Thiele, and L. Benini. Design of a Solar-Harvesting Circuit for Batteryless Embedded Systems. *Circuits and Systems I: Regular Papers, IEEE Transactions on*, 56(11):2519 –2528, nov. 2009.

[16] C. Buratti, A. Conti, D. Dardari, and R. Verdone. An Overview on Wireless Sensor Networks Technology and Evolution. *Sensors*, 9(9):6869–6896, 2009.

[17] CAP-XX. Frequently Asked Questions. http://www.cap-xx.com/rethink/resources/faq.htm.

[18] A. Carroll and G. Heiser. An Analysis of Power Consumption in a Smartphone. In *Proceedings of the 2010 USENIX conference on USENIX annual technical conference*, USENIXATC'10, pages 21–21, Berkeley, CA, USA, 2010. USENIX Association.

[19] S. Chalasani and J. Conrad. A Survey of Energy Harvesting Sources for Embedded Systems. In *Southeastcon, 2008. IEEE*, pages 442–447, April 2008.

[20] V. R. Challa, M. G. Prasad, and F. T. Fisher. Towards an Autonomous Self-Tuning Vibration Energy Harvesting Device for Wireless Sensor Network Applications. *Smart Materials and Structures*, 20(2):025004, 2011.

[21] A. Chandrakasan, D. Daly, J. Kwong, and Y. Ramadass. Next Generation Micro-Power Systems. In *VLSI Circuits, 2008 IEEE Symposium on*, pages 2–5, June 2008.

[22] C.-Y. Chen and P. H. Chou. Duracap: A Supercapacitor-Based, Power-Bootstrapping, Maximum Power Point Tracking Energy-Harvesting System. In *Proceedings of the 16th ACM/IEEE international symposium on Low power electronics and design*, ISLPED '10, pages 313–318, New York, NY, USA, 2010. ACM.

[23] M. Chen and G. Rincon-Mora. Accurate Electrical Battery Model Capable of Predicting Runtime and I-V Performance. *Energy Conversion, IEEE Transactions on*, 21(2):504 – 511, june 2006.

[24] P. H. Chou and S. Kim. Techniques for Maximizing Efficiency of Solar Energy Harvesting Systems. In *The Fifth International Conference on Mobile Computing and Ubiquitous Networking (ICMU 2010)*, 2010.

[25] Panasonic. Industrial. Co. Panasonic Gold Cap Electric Double Layer Capacitors. http://panasonic.com/industrial/electronic-components/capacitive-products/gold-cap-electric.aspx.

[26] Digi-Key Corporation. Solar Cell AM 96.7mm x 56.7mm - AM-1816CA - Sensors, Transducers. http://parts.digikey.com/1/parts/1806984-solar-cell-am-96-7mm-x-56-7mm-am-1816ca.html.

[27] M. Corporation. Tmote Sky Datasheet Ultra Low Power IEEE 802.15.4 Compliant Wireless Sensor Module Humidity, Light, and Temperature Sensors With USB (2/6/2006). http://www.sentilla.com/files/pdf/eol/tmote-sky-datasheet.pdf.

[28] Mide Technology Corporation. Piezoelectric Vibration Energy Harvester PEH20w, 2011. http://www.mide.com/products/volture/peh20w.php.

[29] S. Croce, F. Marcelloni, and M. Vecchio. Reducing Power Consumption in Wireless Sensor Networks Using a Novel Approach to Data Aggregation. *The Computer Journal*, page bxm046, 2007.

[30] I. Demirkol, C. Ersoy, and F. Alagoz. MAC Protocols for Wireless Sensor Networks: A Survey. *Communications Magazine, IEEE*, 44(4):115 – 121, april 2006.

[31] D. Dondi, A. Di Pompeo, C. Tenti, and T. Rosing. Shimmer: A Wireless Harvesting Embedded System for Active Ultrasonic Structural Health Monitoring. In *Sensors, 2010 IEEE*, pages 2325 –2328, nov. 2010.

[32] D. Dondi, P. Zappi, and T. Rosing. A Scheduling Algorithm for Consistent Monitoring Results with Solar Powered High-Performance Wireless Embedded Systems. In *Low Power Electronics and Design (ISLPED) 2011 International Symposium on*, pages 259 –264, aug. 2011.

[33] P. Dutta, M. Feldmeier, J. Paradiso, and D. Culler. Energy Metering for Free: Augmenting Switching Regulators for Real-Time Monitoring. In *Information Processing in Sensor Networks, 2008. IPSN '08. International Conference on*, pages 283 –294, April 2008.

[34] P. Dutta, J. Taneja, J. Jeong, X. Jiang, and D. Culler. A Building Block Approach to Sensornet Systems. In *SenSys '08: Proceedings of the 6th ACM conference on Embedded network sensor systems*, pages 267–280, New York, NY, USA, 2008. ACM.

[35] SAMWHA. ELECTRIC. Green-Cap (Electric Double Layer Capacitors) DB. http://www.samwha.com/electric/product/list_pdf1/DB.pdf.

[36] Ferro Solutions, Inc. VEH-360 Electromechanical Vibration Energy Harvester, May 2008. http://www.ferrosi.com/files/VEH360_datasheet.pdf.

[37] J. M. Gilbert and F. Balouchi. Comparison of Energy Harvesting Systems for Wireless Sensor Networks. *International Journal of Automation and Computing*, 5(4):334–347, 2008.

[38] Micropelt GmbH. MPG-D651 MPG-D751 Thin Film Thermogenerators and Sensing Devices Micropelt Datasheet. http://www.micropelt.com/down/datasheet_mpg_d651_d751.pdf.

[39] M. Gorlatova, A. Wallwater, and G. Zussman. Networking Low-Power Energy Harvesting Devices: Measurements and Algorithms. In *INFOCOM, 2011 Proceedings IEEE*, pages 1602 –1610, april 2011.

[40] A. Harb. Energy Harvesting: State-Of-The-Art. *Renewable Energy*, 36(10):2641 – 2654, 2011.

[41] Holistic Energy Harvesting. Vibration Data: Ford Focus Engine. http://www.holistic.ecs.soton.ac.uk/data/focus_engine_plate_2/data.php.

[42] Holistic Energy Harvesting. Vibration Data: Water Pump Motor. http://www.holistic.ecs.soton.ac.uk/data/water_pump/data.php.

[43] M. Healy, T. Newe, and E. Lewis. Wireless Sensor Node Hardware: A Review. In *Sensors, 2008 IEEE*, pages 621–624, Oct. 2008.

[44] M. Hempstead, G.-Y. Wei, and D. Brooks. System Design Considerations for Sensor Network Applications. In *Circuits and Systems, 2008. ISCAS 2008. IEEE International Symposium on*, pages 2566–2569, May 2008.

[45] R. Hernandez, S. Jung, and K. I. Matveev. Acoustic Energy Harvesting From Vortex-Induced Tonal Sound In A Baffled Pipe. *Proceedings of the Institution of Mechanical Engineers, Part C: Journal of Mechanical Engineering Science*, 2011.

[46] F. O. Hocaoglu, mer N. Gerek, and M. Kurban. Hourly Solar Radiation Forecasting Using Optimal Coefficient 2-D Linear Filters And Feed-Forward Neural Networks. *Solar Energy*, 82(8):714 – 726, 2008.

[47] R. J. Hyndman and A. B. Koehler. Another Look At Measures Of Forecast Accuracy. *International Journal of Forecasting*, 22(4):679 – 688, 2006.

[48] Maxim Inc. MAX1722, MAX1723, MAX1724 1.5μA I_Q, Step-Up DC-DC Converters in Thin SOT23-5. http://www.maxim-ic.com/datasheet/index.mvp/id/3024.

[49] Texas Instruments. CC2500 Low Cost, Low-Power 2.4 GHz RF Transceiver Designed for Low-Power Wireless Apps in the 2.4 GHz ISM B. http://www.ti.com/product/cc2500.

[50] Texas Instruments. Cost-Efficient Coulomb Counter For Battery Capacity Monitoring In Embedded Portable Applications. http://www.ti.com/product/bq26231.

[51] Texas Instruments. Dual Sync Step-Down Controller For Low Voltage Power Rails In Embedded Computing. http://www.ti.com/product/tps59124.

[52] Texas Instruments. ez430-RF2500 Development Tool User'S Guide (Rev. E). http://www.ti.com/lit/pdf/slau227.

[53] Texas Instruments. ez430-RF2500-SEH Solar Energy Harvesting Development Kit. http://www.ti.com/tool/ez430-rf2500-seh.

[54] Texas Instruments. MSP430x12x, Mixed Signal Microcontroller (Rev. C). http://focus.ti.com/docs/prod/folders/print/msp430f123.html.

[55] Texas Instruments. MSP430x12x, Mixed Signal Microcontroller (Rev. C). http://focus.ti.com/docs/prod/folders/print/msp430f123.html.

[56] Texas Instruments. TPS61097-33 Low Input Voltage Synchronous Boost Converter With Low-Quiescent Current (Rev. C). http://www.ti.com/lit/gpn/tps61097-33.

[57] Texas Instruments. TPS61221 Low Input Voltage, 0.7V, Boost Converter With 5.5μA Quiescent Current. http://www.ti.com/lit/gpn/tps61221.

[58] ITACA. Part 1: Photovoltaic (PV) Cells. http://www.itacanet.org/a-guide-to-photovoltaic-panels/photovoltaic-pv-cells/.

[59] J. Jeong. *A Practical Theory of Micro-Solar Power Sensor Networks*. PhD thesis, Electrical Engineering and Computer Sciences, University of California at Berkeley, April 2009.

[60] J. Jeong, X. Jiang, and D. Culler. Design And Analysis Of Micro-Solar Power Systems For Wireless Sensor Networks. In *Networked Sensing Systems, 2008. INSS 2008. 5th International Conference on*, pages 181–188, June 2008.

[61] X. Jiang, P. Dutta, D. Culler, and I. Stoica. Micro power meter for energy monitoring of wireless sensor networks at scale. In *Information Processing in Sensor Networks, 2007. IPSN 2007. 6th International Symposium on*, pages 186 –195, April 2007.

[62] X. Jiang, J. Polastre, and D. Culler. Perpetual Environmentally Powered Sensor Networks. In *IPSN '05: Proceedings of the 4th international symposium on Information processing in sensor networks*, page 65, Piscataway, NJ, USA, 2005. IEEE Press.

[63] X. Jiang, J. Taneja, J. Ortiz, A. Tavakoli, P. Dutta, J. Jeong, D. Culler, P. Levis, and S. Shenker. An Architecture For Energy Management In Wireless Sensor Networks. *SIGBED Rev.*, 4(3):31–36, 2007.

[64] P. Juang, H. Oki, Y. Wang, M. Martonosi, L. S. Peh, and D. Rubenstein. Energy-Efficient Computing For Wildlife Tracking: Design Tradeoffs And Early Experiences With Zebranet. In *Proceedings of the 10th international conference on Architectural support for programming languages and operating systems*, ASPLOS-X, pages 96–107, New York, NY, USA, 2002. ACM.

[65] A. Kansal, J. Hsu, S. Zahedi, and M. B. Srivastava. Power Management In Energy Harvesting Sensor Networks. *ACM TECS*, 6(4):32, 2007.

[66] M. Keating, D. Flynn, R. Aitken, A. Gibbons, and K. Shi. *Low Power Methodology Manual: For System-on-Chip Design*. Springer Publishing Company, Incorporated, 2007.

[67] A. Keshavarzian, H. Lee, and L. Venkatraman. Wakeup Scheduling In Wireless Sensor Networks. In *Proceedings of the 7th ACM international symposium on Mobile ad hoc networking and computing*, MobiHoc '06, pages 322–333, New York, NY, USA, 2006. ACM.

[68] S. Kim, S. Pakzad, D. Culler, J. Demmel, G. Fenves, S. Glaser, and M. Turon. Health Monitoring Of Civil Infrastructures Using Wireless Sensor Networks. In *Information Processing in Sensor Networks, 2007. IPSN 2007. 6th International Symposium on*, pages 254 –263, april 2007.

[69] Y. Kim, N. Chang, Y. Wang, and M. Pedram. Maximum Power Transfer Tracking For a Photovoltaic-Supercapacitor Energy System. In *Proceedings of the 16th ACM/IEEE international symposium on Low power electronics and design*, ISLPED '10, pages 307–312, New York, NY, USA, 2010. ACM.

[70] C. Kompis and S. Aliwell. energy harvesting technology to enable remote and wireless sensing. Technical report, Sensors and Instrumentation Knowledge Transfer Network Action Group Report, 2008.

[71] D. Kruger, C. Buschmann, and S. Fischer. Solar powered sensor network design and experimentation. In *Wireless Communication Systems, 2009. ISWCS 2009. 6th International Symposium on*, pages 11 –15, sept. 2009.

[72] D. Kwon, G. Rincon-Mora, and E. Torres. Harvesting ambient kinetic energy with switched-inductor converters. *Circuits and Systems I: Regular Papers, IEEE Transactions on*, 58(7):1551 –1560, july 2011.

[73] Y. Lee, M. Seok, S. Hanson, D. Blaauw, and D. Sylvester. Standby power reduction techniques for ultra-low power processors. In *Solid-State Circuits Conference, 2008. ESSCIRC 2008. 34th European*, pages 186–189, Sept. 2008.

[74] H. Lhermet, C. Condemine, M. Plissonnier, R. Salot, P. Audebert, and M. Rosset. Efficient power management circuit: From thermal energy harvesting to above-ic microbattery energy storage. *Solid-State Circuits, IEEE Journal of*, 43(1):246–255, Jan. 2008.

[75] Y.-S. Lin, S. Hanson, F. Albano, C. Tokunaga, R.-U. Haque, K. Wise, A. Sastry, D. Blaauw, and D. Sylvester. Low-voltage circuit design for widespread sensing applications. In *Circuits and Systems, 2008. ISCAS 2008. IEEE International Symposium on*, pages 2558–2561, May 2008.

[76] R.-S. Liu, K.-W. Fan, Z. Zheng, and P. Sinha. Perpetual and fair data collection for environmental energy harvesting sensor networks. *Networking, IEEE/ACM Transactions on*, 19(4):947 –960, aug. 2011.

[77] R.-S. Liu, P. Sinha, and C. E. Koksal. Joint energy management and resource allocation in rechargeable sensor networks. In *INFOCOM*, pages 902–910, 2010.

[78] S. Liu, J. Lu, Q. Wu, and Q. Qiu. Load-matching adaptive task scheduling for energy efficiency in energy harvesting real-time embedded systems. In *Proceedings of the 16th ACM/IEEE international symposium on Low power electronics and design*, ISLPED '10, pages 325–330, New York, NY, USA, 2010. ACM.

[79] S. Liu, J. Lu, Q. Wu, and Q. Qiu. Harvesting-aware power management for real-time systems with renewable energy. *Very Large Scale Integration (VLSI) Systems, IEEE Transactions on*, PP(99):1 –14, 2011.

[80] S. Liu, Q. Qiu, and Q. Wu. Energy aware dynamic voltage and frequency selection for real-time systems with energy harvesting. In *Design, Automation and Test in Europe, 2008. DATE '08*, pages 236 –241, march 2008.

[81] S. Liu, Q. Wu, and Q. Qiu. An adaptive scheduling and voltage/frequency selection algorithm for real-time energy harvesting systems. In *DAC '09: Proceedings of the 46th Annual Design Automation Conference*, pages 782–787, New York, NY, USA, 2009. ACM.

[82] Perpetuum Ltd. PMG FSH Free-Standing Vibration Energy Harvester Technical Datasheet, May 2010. http://www.perpetuum.com/resources/PMGFSHDatasheet.pdf.

[83] C. Lu, V. Raghunathan, and K. Roy. Maximum power point considerations in micro-scale solar energy harvesting systems. In *Circuits and Systems (ISCAS), Proceedings of 2010 IEEE International Symposium on*, pages 273 –276, 30 2010-june 2 2010.

[84] C. Lu, V. Raghunathan, and K. Roy. Efficient design of micro-scale energy harvesting systems. *IEEE Journal on Emerging and Selected Topics in Circuits and Systems*, 1(3):254 –266, Sept. 2011.

[85] J. Lu, S. Liu, Q. Wu, and Q. Qiu. Accurate modeling and prediction of energy availability in energy harvesting real-time embedded systems. In *International Green Computing Conference 2010, Chicago, IL, USA, 15-18 August 2010*, pages 469–476, 2010.

[86] J. Lu and Q. Qiu. Scheduling and mapping of periodic tasks on multi-core embedded systems with energy harvesting. In *Green Computing Conference and Workshops (IGCC), 2011 International*, pages 1 –6, july 2011.

[87] A. Mainwaring, D. Culler, J. Polastre, R. Szewczyk, and J. Anderson. Wireless sensor networks for habitat monitoring. In *Proceedings of the 1st ACM international workshop on Wireless sensor networks and applications*, WSNA '02, pages 88–97, New York, NY, USA, 2002. ACM.

[88] P. Mannion. Good Vibrations For Energy Harvesting, EE Times Design Article, November 2008. http://eetimes.com/design/microcontroller-mcu/4005859/Good-vibrations-for-energy-harvesting.

[89] F. Marcelloni and M. Vecchio. A Simple Algorithm for Data Compression in Wireless Sensor Networks. *IEEE COMMUNICATIONS LETTERS*, 12(6):411, 2008.

[90] Maxim Inc. DS2438 Smart Battery Monitor. http://www.maxim-ic.com/datasheet/index.mvp/id/2919.

[91] Maxim Inc. Inaccuracies Of Estimating Remaining Cell Capacity With Voltage Measurements Alone, Maxim Inc. Application Note 121, May 2002. http://www.maxim-ic.com/app-notes/index.mvp/id/121.

[92] A. Mellit. Artificial intelligence technique for modelling and forecasting of solar radiation data: A review. *Int. J. Artif. Intell. Soft Comput.*, 1:52–76, November 2008.

[93] A. Mellit, M. Menghanem, and M. Bendekhis. Artificial neural network model for prediction solar radiation data: application for sizing stand-alone photovoltaic power system. In *Power Engineering Society General Meeting, 2005. IEEE*, volume 1, pages 40 – 44, June 2005.

[94] METEOTEST. Meteonorm 7. http://meteonorm.com/download/software/.

[95] Texas Instruments. Michael Day. MSP430 Power Solutions. focus.ti.com/graphics/mcu/ulp/powermanagementsolutionsformsp430.pdf.

[96] Varta Microbattery. Handbook - Rechargeable Ni-MH Button (English) - OEM. http://www.varta-microbattery.com/en/mb_data/documents/sales_literature_varta/HANDBOOK_Rechargeable_Ni-MH_Button_en.pdf.

[97] Varta Microbattery. Rechargeable Lithium Cylindrical. http://www.uk.varta-microbattery.com/en/oempages/product_data/poductdata_types.php?output=typedata&segment=RechLiCyl.

[98] Varta Microbattery. Rechargeable Ni-MH Cylindrical. http://www.uk.varta-microbattery.com/en/oempages/product_data/poductdata_types.php?output=typedata&segment=RechNiMHCyl.

[99] P. Mitcheson, E. Yeatman, G. Rao, A. Holmes, and T. Green. Energy harvesting from human and machine motion for wireless electronic devices. *Proceedings of the IEEE*, 96(9):1457–1486, Sept. 2008.

[100] R. Morais, S. G. Matos, M. A. Fernandes, A. L. Valente, S. F. Soares, P. Ferreira, and M. Reis. Sun, wind and water flow as energy supply for small stationary data acquisition platforms. *Computers and Electronics in Agriculture*, 64(2):120 – 132, 2008.

[101] M. Morales and T. I. Zachery Shivers. Wireless Sensor Monitor Using the ez430-RF2500, Application Report. http://www.ti.com/lit/an/slaa378d/slaa378d.pdf.

[102] C. Moser, D. Brunelli, L. Thiele, and L. Benini. Real-time scheduling for energy harvesting sensor nodes. *Real-Time Systems*, 37:233–260, 2007. 10.1007/s11241-007-9027-0.

[103] C. Moser, J.-J. Chen, and L. Thiele. Reward maximization for embedded systems with renewable energies. In *Embedded and Real-Time Computing Systems and Applications, 2008. RTCSA '08. 14th IEEE International Conference on*, pages 247–256, Aug. 2008.

[104] C. Moser, J.-J. Chen, and L. Thiele. Power management in energy harvesting embedded systems with discrete service levels. In *ISLPED '09: Proceedings of the 14th ACM/IEEE international symposium on Low power electronics and design*, pages 413–418, New York, NY, USA, 2009. ACM.

[105] C. Moser, J.-J. Chen, and L. Thiele. An energy management framework for energy harvesting embedded systems. *J. Emerg. Technol. Comput. Syst.*, 6:7:1–7:21, June 2010.

[106] C. Moser, L. Thiele, D. Brunelli, and L. Benini. Robust and low complexity rate control for solar powered sensors. In *Proc. DATE '08*, pages 230–235, March 2008.

[107] C. Moser, L. Thiele, D. Brunelli, and L. Benini. Adaptive power management for environmentally powered systems. *Computers, IEEE Transactions on*, 59(4):478 –491, april 2010.

[108] T. Muneer. *Solar Radiation and Daylight Models*. Elsevier Butterworth-Heinemann, 2nd edition, 2004.

[109] A. Nahapetian, P. Lombardo, A. Acquaviva, L. Benini, and M. Sarrafzadeh. Dynamic reconfiguration in sensor networks with regenerative energy sources. In *Design, Automation Test in Europe Conference Exhibition, 2007. DATE '07*, pages 1 –6, april 2007.

[110] N. Nandra. Low Power Design for Analog/Mixed-Signal IP, EE Times Design Article, March 2008. http://www.eetimes.com/design/eda-design/4018534/Low-Power-Design-For-Analog-Mixed-Signal-IP.

[111] Ningbo Yongjiang Shenzhou Photovoltaic Co.,Ltd Model no.:SZGD6060-4P. http://www.nbszgd.com/pro_en_67/67840.html.

[112] Ningbo Yongjiang Shenzhou Photovoltaic Co.,Ltd Model no.:SZGD8045-8P. http://www.nbszgd.com/pro_en_67/67969.html.

[113] D. K. Noh, L. Wang, Y. Yang, H. K. Le, and T. Abdelzaher. Minimum variance energy allocation for a solar-powered sensor system. In *DCOSS '09: Proceedings of the 5th IEEE International Conference on Distributed Computing in Sensor Systems*, pages 44–57. Springer-Verlag, 2009.

[114] NREL. Measurement and Instrumentation Data Center (MIDC) Home Page. http://www.nrel.gov/midc/.

[115] Application of Electronic Technique. Application of Electronic Technique. http://group.chinaaet.com/151/8981.

[116] Mindsets online. 90mA Solar Panel/Module. http://www.mindsetsonline.co.uk/product_info.php?products_id=312.

[117] J. A. Paradiso and T. Starner. Energy Scavenging for Mobile and Wireless Electronics. *IEEE Pervasive Computing*, 4(1):18–27, 2005.

[118] C. Park and P. Chou. Ambimax: Autonomous Energy Harvesting Platform for Multi-Supply Wireless Sensor Nodes. In *Sensor and Ad Hoc Communications and Networks, 2006. SECON '06. 2006 3rd Annual IEEE Communications Society on*, volume 1, pages 168–177, Sept. 2006.

[119] J. R. Piorno, C. Bergonzini, D. Atienza, and T. S. Rosing. HOLLOWS: A Power-Aware Task Scheduler for Energy Harvesting Sensor Nodes. *Journal of Intelligent Material Systems and Structures*, 21(13):1317–1335, 2010.

[120] J. Polastre, R. Szewczyk, and D. Culler. Telos: Enabling Ultra-Low Power Wireless Research. In *Information Processing in Sensor Networks, 2005. IPSN 2005. Fourth International Symposium on*, pages 364–369, April 2005.

[121] G. J. Pottie and W. J. Kaiser. Wireless Integrated Network Sensors. *Commun. ACM*, 43(5):51–58, 2000.

[122] S. Priya. Modeling Of Electric Energy Harvesting Using Piezoelectric Windmill. *Applied Physics Letters*, 87(18):184101 –184101–3, oct 2005.

[123] S. Priya, C.-T. Chen, D. Fye, and J. Zahnd. Piezoelectric Windmill: A Novel Solution to Remote Sensing. *Japanese Journal of Applied Physics*, 44:L104–L107, Jan. 2005.

[124] V. Raghunathan, A. Kansal, J. Hsu, J. Friedman, and M. Srivastava. Design Considerations For Solar Energy Harvesting Wireless Embedded Systems. In *Proceedings of the 4th international symposium on Information processing in sensor networks*, IPSN '05, 2005.

[125] A. Rahmati and L. Zhong. Human-Battery Interaction on Mobile Phones. *Pervasive and Mobile Computing*, 5(5):465 – 477, 2009.

[126] Y. Ramadass and A. Chandrakasan. Minimum Energy Tracking Loop With Embedded DCDC Converter Enabling Ultra-Low-Voltage Operation Down to 250 mV in 65 nm CMOS. *Solid-State Circuits, IEEE Journal of*, 43(1):256–265, Jan. 2008.

[127] Y. Ramadass and A. Chandrakasan. A Battery-Less Thermoelectric Energy Harvesting Interface Circuit With 35 mV Startup Voltage. *Solid-State Circuits, IEEE Journal of*, 46(1):333 –341, jan. 2011.

[128] A. Ravinagarajan, D. Dondi, and T. S. Rosing. DVFS Based Task Scheduling in a Harvesting WSN for Structural Health Monitoring. In *Proceedings of the Conference on Design, Automation and Test in Europe*, DATE '10, pages 1518–1523, 3001 Leuven, Belgium, Belgium, 2010. European Design and Automation Association.

[129] J. Recas, C. Bergonzini, D. Atienza, and T. S. Rosing. Prediction And Management In Energy Harvested Wireless Sensor Nodes. In *Proc. VITAE '09*, pages 6–10, May 2009.

[130] G. Reikard. Predicting Solar Radiation At High Resolutions: A Comparison Of Time Series Forecasts. *Solar Energy*, 83(3):342 – 349, 2009.

[131] C. Renner, J. Jessen, and V. Turau. Lifetime Prediction For Supercapacitor-Powered Wireless Sensor Nodes. In *Proceedings of the 8th GI/ITG KuVS Fachgesprch "Drahtlose Sensornetze" (FGSN'09)*, pages 55–58, August 2009.

[132] K. Romer and F. Mattern. The Design Space Of Wireless Sensor Networks. *Wireless Communications, IEEE*, 11(6):54–61, Dec. 2004.

[133] S. Roundy, D. Steingart, L. Frechette, P. Wright, and J. Rabaey. Power Sources For Wireless Sensor Networks. *Berlin, Germany*, pages 1–17, 2004.

[134] E. S. and G. Jr. Exponential Smoothing: The State Of The ArtPart II. *International Journal of Forecasting*, 22(4):637 – 666, 2006.

[135] P. Santi. Topology Control in Wireless Ad Hoc And Sensor Networks. *ACM Comput. Surv.*, 37:164–194, June 2005.

[136] Conrad Electronics SE. RF Development Tool MSP430-RF2500. http://www.conrad.com/RF-DEVELOPMENT-TOOL-MSP430-RF2500.htm?websale7=conrad-int&pi=170231&ci=SHOP_AREA_29142_0214035.

[137] Zetex Semiconductors. ZXCT1010 Enhanced High-Side Current Monitor, July 2007. http://www.diodes.com/zetex/_pdfs/3.0/pdf/ZXCT1010.pdf.

[138] M. Seok, S. Hanson, Y.-S. Lin, Z. Foo, D. Kim, Y. Lee, N. Liu, D. Sylvester, and D. Blaauw. The Phoenix Processor: A 30pW Platform for Sensor Applications. In *VLSI Circuits, 2008 IEEE Symposium on*, pages 188–189, June 2008.

[139] H. Shao, C.-Y. Tsui, and W.-H. Ki. Maximizing The Harvested Energy for Micro-Power Applications Through Efficient MPPT And PMU Design. In *Design Automation Conference (ASP-DAC), 2010 15th Asia and South Pacific*, pages 75 –80, jan. 2010.

[140] N. Sharma, J. Gummeson, D. Irwin, and P. Shenoy. Cloudy Computing: Leveraging Weather Forecasts in Energy Harvesting Sensor Systems. In *Sensor Mesh and Ad Hoc Communications and Networks (SECON), 2010 7th Annual IEEE Communications Society Conference on*, pages 1 –9, June 2010.

[141] F. Simjee and P. Chou. Efficient Charging of Supercapacitors for Extended Lifetime of Wireless Sensor Nodes. *Power Electronics, IEEE Transactions on*, 23(3):1526 –1536, may 2008.

[142] G. Simon, M. Maróti, A. Lédeczi, G. Balogh, B. Kusy, A. Nádas, G. Pap, J. Sallai, and K. Frampton. Sensor Network-Based Countersniper System. In *Proceedings of the 2nd international conference on Embedded networked sensor systems*, SenSys '04, pages 1–12, New York, NY, USA, 2004. ACM.

[143] BP Solar. BP Solar - MSX-005F - Solar Panel. http://www.farnell.com/datasheets/54658.pdf.

[144] J.-H. Su, C.-L. Chien, J.-J. Chen, and C.-M. Wang. Simulink Behavior Models for DC-DC Switching Converter Circuits Using PWM Control ICs. *International Journal of Engineering Education*, 22(2):315–322, 2006.

[145] Y. K. Tan and S. Panda. Self-Autonomous Wireless Sensor Nodes With Wind Energy Harvesting for Remote Sensing of Wind-Driven Wildfire Spread. *Instrumentation and Measurement, IEEE Transactions on*, 60(4):1367 –1377, april 2011.

[146] J. Taneja, J. Jeong, and D. Culler. Design, Modeling, and Capacity Planning for Micro-Solar Power Sensor Networks. In *IPSN '08: Proceedings of the 7th international conference on Information processing in sensor networks*, pages 407–418, Washington, DC, USA, 2008. IEEE Computer Society.

[147] Linear Technology. LTC4080 - 500mA Standalone Li-ion Charger With Integrated 300mA Synchronous Buck. http://www.linear.com/product/LTC4080.

[148] PowerStream Technology. Charging Nickel-Metal-Hydride. http://batteryuniversity.com/learn/article/charging_nickel_metal_hydride.

[149] PowerStream Technology. Lithium-ion Battery Charging Basics. http://www.powerstream.com/li.htm.

[150] PowerStream Technology. NiMH Battery Charging Basics. http://www.powerstream.com/NiMH.htm.

[151] Circuit Celler. Tom Cantrell. Lion King: A Look At "Battery-In-A-Chip" Technology. www.cymbet.com/pdfs/CC-article.pdf.

[152] Battery University. Charging Lithium-ion. http://batteryuniversity.com/learn/article/charging_lithium_ion_batteries.

[153] Varta. Rechargeable Ni-MH Button Battery V150H. http://www.varta-microbattery.com/en/mb_data/documents/ data_sheets/DS55615.PDF.

[154] C. Vigorito, D. Ganesan, and A. Barto. Adaptive Control of Duty Cycling in Energy-Harvesting Wireless Sensor Networks. In *Sensor, Mesh and Ad Hoc Communications and Networks, 2007. SECON '07. 4th Annual IEEE Communications Society Conference on*, pages 21–30, June 2007.

[155] M. Villalva, J. Gazoli, and E. Filho. Comprehensive Approach to Modeling and Simulation of Photovoltaic Arrays. *Power Electronics, IEEE Transactions on*, 24(5):1198–1208, May 2009.

[156] R. Vullers, R. van Schaijk, I. Doms, C. V. Hoof, and R. Mertens. Micropower Energy Harvesting. *Solid-State Electronics*, 53(7):684 – 693, 2009. Papers Selected from the 38th European Solid-State Device Research Conference - ESSDERC'08.

[157] A. Weddell. *A Comprehensive Scheme for Reconfigurable Energy-Aware Wireless Sensor Nodes*. PhD thesis, University of Southampton, May 2010.

[158] A. Weddell, G. Merrett, T. Kazmierski, and B. Al-Hashimi. Accurate Supercapacitor Modeling for Energy-Harvesting Wireless Sensor Nodes. *IEEE Transactions on Circuits and Systems II: Express Briefs (In Press)*, September 2011.

[159] A. S. Weddell, G. V. Merrett, N. R. Harris, and B. M. Al-Hashimi. Energy Harvesting and Management for Wireless Autonomous Sensors. *Measurement + Control*, 41(4):104–108, May 2008.

[160] M. Weiser. The Computer for the 21st Century. *SIGMOBILE Mob. Comput. Commun. Rev.*, 3(3):3–11, 1999.

[161] G. Xing, M. Sha, G. Hackmann, K. Klues, O. Chipara, and C. Lu. Towards Unified Radio Power Management for Wireless Sensor Networks. *Wirel. Commun. Mob. Comput.*, 9(3):313–323, 2009.

[162] J. Yick, B. Mukherjee, and D. Ghosal. Wireless Sensor Network Survey. *Computer Networks*, 52(12):2292 – 2330, 2008.

[163] B. Zhang, R. Simon, and H. Aydin. Harvesting Aware Energy Management for Time Critical Wireless Sensor Networks With Joint Voltage and Modulation Scaling. *Industrial Informatics, IEEE Transactions on*, PP(99):1, 2011.

[164] T. Zhu, Z. Zhong, Y. Gu, T. He, and Z.-L. Zhang. Leakage-Aware Energy Synchronization for Wireless Sensor Networks. In *MobiSys '09: Proceedings of the 7th international conference on Mobile systems, applications, and services*, pages 319–332, New York, NY, USA, 2009. ACM.

[165] T. Zhu, Z. Zhong, T. He, and Z.-L. Zhang. Energy-Synchronized Computing For Sustainable Sensor Networks. *Ad Hoc Networks*, 2010.